Sc

EFFECTS OF HIGH PRESSURE ON ELECTROCHEMICAL PROCESSES

by

John Carleton Currie

A thesis submitted to the School of Graduate Studies in partial fulfillment of the requirements for the degree of Ph.D. in Chemistry

UNIVERSITY OF OTTAWA
OTTAWA, CANADA, 1977

PREFACE

The efficient generation of electrical and thermal energy has become an important scientific, as well as a political, issue in recent years. The development and use of new types of energy sources for supplying large fractions of the population with the necessary energy requirements is expected to occur in the future. However, electrical power sources such as fuel cells, high temperature and seawater-activated batteries have already been used in specialized applications during the past decade.

The development of the seawater-activated battery for use in deep marine environments has led to interest in the pressure-dependent behaviour of this and other types of electrochemical power sources. The evaluation of the electrochemical behaviour of the Pb, $PbCl_2$ electrode (the cathode in the Mg|seawater|$PbCl_2$ battery) as a function of pressure served as a starting point for the high pressure electrochemical studies described in this thesis. Naturally, this led to the evaluation of the behaviour of reversible electrodes for possible use as reference electrodes at elevated pressures. Since volume changes occurring in electrochemical processes can be easily determined from the pressure coefficient of EMF (reversible processes) and of electrochemical rates (activation controlled processes), investigations on several electrode processes of more fundamental interest were initiated.

One of the problems of current interest in fundamental electrochemistry is the mechanism of electron transfer to or from ions and the nature of the associated "solvent reorganisation" which constitute the activation process in such reactions. The study of effects of pressure on such processes provides new information on the activation process through evaluation of the volume change associated with it. This volume change should have different values depending on the mechanism of activation

assumed. The study of the effect of pressure on the $Fe(CN)_6^{3-} + e \longrightarrow Fe(CN)_6^{4-}$ reaction enables useful new information to be obtained on electron transfer in a redox couple, especially on the nature of reorganization of the solvent during the activation process.

Another topic of current interest is the nature of the states of electrochemically deposited atoms in monolayers at electrodes, e.g. H and OH at Pt. A study of the influence of pressure on these processes at Pt and Au enabled the volume changes associated with OH deposition at Pt and Au, and H deposition at Pt to be evaluated.

Most of the work described in this thesis is in course of publication, as indicated in the following list of papers:

1) Significance of Effects of High Pressure on the Kinetics of Electrode Processes: Part I: Applications to Transition States in Hydrogen Evolution Reaction Mechanisms, B.E. Conway and J.C. Currie, J. Electrochem Soc., submitted for publication.
2) Significance of Effects of High Pressure: Part II: The Nature of Solvent Reorganization in the Activation Process of an Electrochemical Redox Reaction, B.E. Conway and J.C. Currie, J. Electrochem. Soc., submitted for publication.
3) Significance of Effects of High Pressure: Part III: Reference Electrodes for High Pressure Studies and their Pressure Coefficients of EMF, B.E. Conway and J.C. Currie, J. Electrochem. Soc., submitted for publication.
4) Temperature and Pressure Effects on Surface Processes at Noble Metal Electrodes: Part II: Volume of Adsorbed H and Oxygen Species at Pt and Au, B.E. Conway and J.C. Currie, J. Chem. Soc., Faraday Trans.I, submitted for publication.

ACKNOWLEDGEMENTS

The author wishes to express sincere gratitude to Professor B.E. Conway under whose direction this work was performed. The keen interest and original contributions of Professor Conway are gratefully acknowledged. The valuable contributions of Dr. H.A. Kozlowska to the development of aspects of the experimental technique of this work are also deeply appreciated.

Previous high pressure work in this Department by Professor Laidler and his co-workers stimulated the present research into effects of high pressure on electrode processes. Grateful acknowledgement is made to Professor Laidler for useful discussions on the significance of volumes of activation in electron transfer processes.

The author also acknowledges the High Pressure Research Laboratory at the National Research Council for the calibration of the Bourdon Gauge and, Master Glassblower, Mr. Egon Kristof for the construction of the high pressure electrochemical cells. Financial assistance from the National Research Council of Canada in the form of a Postgraduate Research Scholarship is also acknowledged.

The author offers special thanks to Mrs. Sandra Childerstone for the typing of the thesis and to Mrs. Linda Blair for her assistance with the typing.

Finally, the author wishes to thank his wife,Janie, for her encouragement, patience and devotion during the preparation of this thesis.

TABLE OF CONTENTS

LIST OF FIGURES

FIGURES

FIGURES

FIGURES

FIGURES

FIGURES PAGE

LIST OF TABLES

LIST OF TABLES

LIST OF TABLES

PAGE

TABLES

ABSTRACT

The significance of effects of pressure on the kinetics and equilibria of chemical processes in the condensed phase has been known since the time of van't Hoff. The use of pressure as an extra variable has become an integral part of kinetic and related studies on reactions over the past 25 years. However, interest in the behaviour of electrochemical processes as a function of pressure is of more recent origin(<10 years); consequently, experimental data are relatively scarce. This thesis describes the pressure dependent behaviour of a variety of electrochemical reactions of fundamental and practical interest.

The pressure coefficient of EMF of several electrochemical cells comprised of two reversible electrodes is evaluated in order to determine their suitability for use as reference electrodes at elevated pressures. The electrochemical cells examined are:

$Pt,H_2|0.5\ M\ H_2SO_4|Pd\text{-}H,Pd$

$Pt,H_2|1.0\ M\ HCl|Pd\text{-}H,Pd$ and

$Pd,Pd\text{-}H|HCl|AgCl,Ag.$

The pressure coefficient of EMF of each electrode cell is converted to the partial molar volume change for the corresponding overall cell reaction. The partial molar volumes of Pd-H,H in Pd and of H_2 itself in solution are also evaluated. The reproducibility of the measured pressure coefficients indicates that the Ag,AgCl and Pd-H,H^+ reference electrodes are the most suitable of those evaluated for use at elevated pressures.

The effects of high hydraulic pressures on the kinetics of electrode reactions are complex because of (a) the variation of reference electrode potentials with pressure so that only an apparent volume of activation can be directly measured experimentally and (b) dependence of coverage by adsorbed intermediates, such as H, with pressure. Methods for dealing with these problems are treated and the significance of measured apparent volumes of activation for the hydrogen evolution reaction is discussed in terms of the nature of the transition state for proton transfer and neutralization. The negative true volumes of activation found for the cathodic H_2 evolution reaction under some conditions are attributed to increasing electrostriction of the proton in the $H_9O_4^+$ complex as the transition state is formed.

New information on the nature of the solvent reorganization process involved in formation of the transition state in an electrochemical redox reaction [the $Fe(CN)_6^{3-}$ /$Fe(CN)_6^{4-}$ couple] is given by studies of the kinetics of this process at high pressures in aqueous solutions at Au. The apparent activation volume is evaluated together with the true volumes of activation for the forward and reverse directions of the redox reaction. By means of calculations of the electrostriction associated with the long-range dielectric polarization in comparison with that associated with ion-solvent interaction in the primary hydration shell, it is shown that the activation process must be mainly (75%) due to short-range solvent reorganization in the primary shell. This is contrary to what has often been assumed in the interpretation of the energy

of activation of ionic redox reactions. The experiments also allow some deduction to be made about the "symmetry" of the transition states in electrochemical reactions in comparison with that in the corresponding homogeneous reactions, in so far as solvent reorganization is concerned.

The multiple states of electrosorbed H and oxygen species at Pt, which arise below monolayer coverage, are of current interest in electrochemical surface science. Experiments on the effects of high hydraulic pressure on H chemisorption and surface oxide formation at Pt electrodes are described. "Clean" electrochemical surface studies can be performed in a shrinkable teflon vessel, under oil, up to several thousand bars. The results of these experiments enable the equilibrium volume changes for electrodeposition of H and surface oxidation of Pt to be evaluated, allowing for the effect of pressure on the potential of the reversible reference electrode used. The volume of electrodeposited H is found to be ca. 5 $cm^3 mol^{-1}$ at Pt, a value substantially larger than that for sorption of H into (α + β) Pd-H but similar to that of H covalently bound in aliphatic hydrocarbon methylene groups.

The pressure effects on surface oxidation arise from (a) the volume change in the surface oxidation reaction itself and (b) the volume change in anion specific adsorption which controls, in part, the potential for onset of surface oxidation of Pt and Au electrodes. Semi-quantitative interpretations of the observed behaviour are offered.

The electrochemical behaviour of the formation and reduction of surface active films such as $PbCl_2$ and $PbSO_4$ which are formed, in part, by a dissolution-precipitation mechanism followed by film growth and passivation are expected to be dependent on pressure.

The formation and reduction of $PbCl_2$ is examined by cyclic voltammetry at 1, 1102 and 2204 bars; the corresponding anodic and cathodic charges, Q_A and Q_C, indicate that pressure reduces the amount of charge required to passivate the Pb surface. This behaviour is related to the presence of solution-soluble Pb complex ions, $PbCl_n^{2-n}$, the partial molar volumes of which are large enough to reduce the solubility of $PbCl_2$ at elevated pressures. This behaviour is confirmed by the decrease of the dependence of the ratio Q_A/Q_C on the cathodic sweep rate at elevated pressures.

Further examination of the electrochemical behaviour of $PbCl_2$ at ambient pressure indicates that more than one type of surface species is present in the passivating film under certain conditions. Rotating disc electrode(RDE) and holding experiments present a complicated picture of the composition of the passivating film. It is postulated that the surface species are either two types of $PbCl_2$ of differing crystal size or a basic Pb salt, in addition to $PbCl_2$.

The effect of pressure on the solubility of $PbCl_2$ in H_2O is examined by conductivity measurements and discussed in terms of the existence of the ion-pair, $PbCl^+$. The pressure coefficient of the molal dissociation constant of $PbCl^+$ and of the solubility product of $PbCl_2$ are evaluated; the results are related to the partial molar volume change for the respective chemical processes. The partial molar volume of $PbCl^+$ is also evaluated.

The electrochemical behaviour of the $Pb,PbSO_4$ electrode at elevated pressures is examined and compared to that of the $Pb,PbCl_2$ electrode. The increase in the amount of charge required to passivate the electrode surface as the pressure is elevated is related to the large increase in the solubility of $PbSO_4$ and to the ability of $PbSO_4$ to form highly supersaturated solutions.

CHAPTER 1

INTRODUCTION

General Introduction

The rates of chemical reactions are a function of concentration, temperature and pressure. The majority of experimental studies has utilized reaction orders and quasi-thermodynamic activation data to characterize the kinetic behaviour of chemical systems of interest. While experiments at high pressures have been known for over 150 years, little work on pressure as a variable in the study of chemical processes in the condensed phase was published until the 1950's. However, the pioneering work of Bridgman[1] led to a basic understanding of the effect of high pressure on the physical properties of matter in addition to improving the state of high pressure technology. The recent generation of interest in pressure as an extra variable in chemical kinetic studies was stimulated by the Discussion of the Faraday Society[2] in 1956 and the publication of Hamann's book "Physico-Chemical Effects of Pressure"[3] (1957). The availability of high pressure equipment at a modest price has expanded the number of research laboratories utilizing pressure as a variable from a handful in 1950 to several hundred at the present time.

The effect of pressure on chemical rate constants[3,4] was originally formulated by van't Hoff in 1901. Evans and Polanyi[5], in 1935, developed this treatment in terms of the "absolute rate theory". The variation of the rate constant with pressure was related to the volume of activation $\Delta V^{\ddagger}$. The significance of $\Delta V^{\ddagger}$ has been discussed by Evans and Polanyi and by Perrin[6] (1938) and, more recently, by Laidler[4,7,8] and by Whalley[9]

in relation to the entropy of activation, $\Delta S^{\ddagger}$.

Research on effects of high pressure on electrode processes is one of the newest aspects of high pressure chemistry. Interest in this approach has grown since the pioneering work of Hills[10,11,12,13,14] and co-workers at mercury electrodes in the 1960's, to include studies at solid electrodes (Heusler[15] et al., Valeriote[16] et al., Conway[17]) and theoretical treatments of $\Delta V^{\ddagger}$ in electrode processes (Barnartt[18], Hills[19], Conway[19], Krishtalik[19], and Parsons[19]).

The variation of the electrochemical rate constant (usually expressed in terms of the exchange of current density i_o,) with pressure is related to the volume of activation in a manner similar to that for chemical reactions in the condensed phase. Pressure effects arise in electrode reactions because there is (a) a finite volume change in the activation process in the kinetics (irreversible process) of the reaction, e.g., the electron transfer step and (b) in any quasi-equilibrium step preceding the rate-determining step. The effect of pressure on the electrode potential of a reversible process is a consequence of the finite equilibrium volume change in the overall reaction.

Application of high pressure to electrochemical systems can provide valuable information hitherto unattainable by other physical methods. Examples of particular interest are as follows:

(i) Electron Transfer Reactions: Recent theories[20,21,22,23] of electron transfer in electrochemical ionic redox reactions have treated the process in terms of either (a) long range fluctuation of Born solvent polarization (polaron model) about the ion, or, (b) short range readjustment of ion-solvent interactions in the primary or inner-coordination sphere about the ion. Both these activation effects have been termed "solvent reorganization" and the reorganization energy is a large contribution to the

total activation energy. A corresponding volume change term must arise, but will be different in models (a) and (b). Hence, the nature of solvent reorganization in the activation process for redox reactions may be elucidated by determining the volume of activation for a simple redox process at an inert electrode interface.

(ii) Atom Transfer Reactions: In atom transfer reactions such as arise in electrochemical gas evolution[13,15], e.g., cathodic hydrogen evolution, metal deposition etc., a different situation arises as one or more charges are annihilated (or created in the reverse reaction). The case of the nature of the transition state of the H_2 evolution reaction is of special interest and will be treated in some detail in Chapter 4.

(iii) Electro-Active Film Formation: A number of electrode reactions exist which involve the transient formation of a sparingly soluble phase, e.g., $PbSO_4$[24,25,26,27] or $PbCl_2$[28,29,30] at a Pb anode. This type of film is believed to be formed in part by a dissolution-precipitation mechanism. This process is related to the solubility product K_{sp} of $PbCl_2$ or $PbSO_4$. The K_{sp} will be affected by pressure in a manner determined by the volume difference between the ions in solution and the solid film. Conductivity measurements provide a convenient method for evaluating the effect of pressure on the solubility of electro-active phases whereas cyclic voltammetry studies are useful in determining the anodic and cathodic charges required for film formation and reduction as a function of pressure.

(iv) Equilibrium Electrode Reactions: The effect of pressure on reversible electrode reactions is based on the finite volume change for the overall equilibrium process. Knowledge of the behaviour of such electrodes at elevated pressures will determine their suitability as reference electrodes in high pressure electrochemical studies. In addition, the EMF pressure

coefficient of an electrochemical cell comprised of two reversible electrodes can provide a convenient method of determining partial molar volume data.

1.2 Basis of Effect of High Pressure

(1) Case of Chemical Processes at Equilibrium in the Condensed Phase

The equilibrium condition in a chemical reaction is characterized by the equilibrium constant K or the corresponding Gibbs free energy, ΔG^o, which are related by

$$\Delta G^o = -RT\ln K$$

However, generally $dG = VdP - SdT$; therefore, for the case of the derivative of K with respect to P,

$$\left(\frac{\partial \Delta G^o}{\partial P}\right)_T = \Delta V \qquad (1.2.1)$$

so that

$$\left(\frac{\partial \ln K}{\partial P}\right)_T = -\frac{\Delta V}{RT} \qquad (1.2.2)$$

where ΔV is the partial molar volume change in the overall reaction. This quantity, ΔV, is the difference between the partial molar volumes of products, V_p and reactants, V_R. The pressure coefficient can therefore be written as

$$\left(\frac{\partial \ln K}{\partial P}\right)_T = -\frac{1}{RT}\left(\Sigma V_p - \Sigma V_R\right) \qquad (1.2.3)$$

(2) Case of Kinetics of Chemical Reactions

While there is no general connection between reaction rates and states of equilibrium, except for special cases represented by Brønsted type linear free energy relations, the rate theory employs the concept of equilibrium between the reactant molecules and activated complexes. The fundamental relationships describing the influence of elevated

pressure on the kinetics of a chemical reaction were initially developed in terms of absolute rate theory by Evans and Polanyi[4,5] in 1935. The rate constant for the general reaction

$$aA + bB \rightarrow X^{\ddagger} \rightarrow lL + mM \qquad (1.2.4(a))$$

is

$$k = \kappa\left(\frac{kT}{h}\right) K^{\ddagger} \qquad (1.2.4(b))$$

where $K^{\ddagger}$ is a quasi-equilibrium constant for the formation of $X^{\ddagger}$ from the reactant species. This equilibrium constant is of a special type since the partition function used to describe the activated complex does not include the vibrational factor for the decomposition of the complex along the reaction coordinate. Making the usual assumption that the transmission coefficient κ is unity and is independent of pressure and temperature, the pressure-coefficient of the natural logarithm of the rate constant can be expressed in terms of the free energy of activation by

$$\left(\frac{\partial \ln k}{\partial P}\right)_T = \left(\frac{\partial \ln K^{\ddagger}}{\partial P}\right)_T = -\frac{1}{RT}\left(\frac{\partial \Delta G^{\ddagger}}{\partial P}\right)_T \qquad (1.2.5)$$

where

$$\left(\frac{\partial \ln K^{\ddagger}}{\partial P}\right)_T = -\frac{\Delta V^{\ddagger}}{RT} \qquad (1.2.6)$$

Then

$$\left(\frac{\partial \ln k}{\partial P}\right)_T = -\frac{\Delta V^{\ddagger}}{RT}$$

The quantity $\Delta V^{\ddagger}$ is known as the volume of activation[3,4] and is the volume change in passing from the initial state to the activated state. If the volume of the activated state is smaller than that of the reactant, the rate of the chemical reaction will be enhanced by pressure and vice-versa for an opposite volume difference.

$\Delta V^{\ddagger}$ is comprised of two main contributions[3]:

(i) a volume change, $\Delta V_1^{\ddagger}$, due to a variation of the local electric charge and its corresponding field as the activated state is being formed. This contribution is particularly important in ionic processes where whole electronic charges are created or destroyed. This volume change arises because of the solvent reorganization associated with changes of the attractive forces between the reactant molecules or ions and the permanent and induced dipoles of the solvent. These effects arise essentially from electrostriction. If the solvent is considered as a continuous dielectric medium, application of the Born theory predicts that the formation of a full electronic charge on a small spherical molecule will result in a volume change of -10 to -20 $cm^3\ mol^{-1}$ for most solvents. This value represents an upper limit, since charges which are commonly developed in transition states are not usually the full electron charge.

(ii) the second contribution, $\Delta V_2^{\ddagger}$, to the overall volume of activation is due to changes in the intrinsic molecular volumes of the reactants as the transition state is being formed. This can be due to changes in interatomic distance, van der Waals radii of reactants and to geometry as the transition state is formed. It is reasonable to assume that a unimolecular dissociation involves a positive volume of activation while, conversely, a bimolecular association is represented by a volume decrease. The volume change for this class of reactions, in simple cases, is generally of the order of 5-10 $cm^3\ mol^{-1}$, numerically. For more complex reactions, $\Delta V_2^{\ddagger}$ is more difficult to estimate.

(3) Case of Electrochemical Processes at Equilibrium

Pressure coefficients for electrochemical reactions at equilibrium arise because of the finite volume change between reactant and product. The equilibrium system normally consists of two reversible electrodes whose EMF is measured as a function of pressure.

The thermodynamic relations for pressure effects on equilibrium electrode processes are similar to those for a chemical reaction. As previously shown,

$$RT\left(\frac{\partial \ln K}{\partial P}\right)_T = -\left(\frac{\partial \Delta G^o}{\partial P}\right)_T = -\Delta V \qquad (1.2.2)$$

For an electrode process, the further relation

$$\Delta G^o = -zFE^o \qquad (1.2.7)$$

is known, so that

$$\left(\frac{\partial E^o}{\partial P}\right)_T = -\frac{\Delta V}{zF} = -\frac{1}{zF}\left(\Sigma V_p - \Sigma V_R\right) \qquad (1.2.8)$$

where V_p and V_R are the partial molar volumes of products and reactants, respectively. Thus, for an electrochemical cell[15,16], e.g.,

$$Pt, H_2 \mid HCl \mid AgCl, Ag,$$

the pressure coefficient of the cell potential can be expressed as

$$\left(\frac{\partial \Delta E}{\partial P}\right)_T = -\frac{1}{zF}\left(V_{Ag} + V_{HCl} - \frac{V_{H_2}}{2} - V_{AgCl}\right)$$

(4) Case of Kinetics of Electrochemical Processes

(i) Analogies between problems arising with temperature and with pressure variation

The treatment of effects of elevated pressures on electrode processes[18,19] can be understood best by first explaining the special

problems that arise in interpretation of effects of temperature changes. Although heats of activation in electrochemical reactions have often been measured, their significance is obscured by the complication that they must be calculated from the measurement of current densities (usually i_o) at constant electrode potential referred to a reversible electrode in the system. However, as the temperature is varied, the real metal-solution potential difference at the reference electrode also varies in a way which is inaccessible to experimental measurement. In the case of the reversible hydrogen electrode, its standard potential is always arbitrarily taken as zero at all temperatures but this does not mean that it does not have a real finite temperature coefficient. Such a temperature coefficient will be that associated with the standard entropy change, ΔS^o, for the half-cell reaction,

$$H_3O^+ + e \rightarrow \frac{1}{2} H_2 + H_2O \qquad (1.2.9)$$

The absolute potential of the reference electrode thus varies with temperature since

$$\left(\frac{\partial E^o}{\partial T}\right)_p = \frac{\Delta S^o}{F} \qquad (1.2.10)$$

for the half-cell. Therefore the heat of activation at constant electrode potential cannot be experimentally evaluated.

Temkin[32] was the first to examine the relation between the true and experimentally accessible apparent heats of activation measured at constant overpotential. More recently, Conway and MacKinnon[33] gave a fuller treatment of the temperature coefficient by including the dependence of the symmetry factor, β, on temperature.

The reaction rate for an electronation process at sufficiently high fields can be expressed as

$$\vec{i} = i_o \exp\left(-\frac{\beta F \eta}{RT}\right) \tag{1.2.11}$$

i_o, the exchange current density, is defined as

$$i_o = zF\,\vec{k}\,C_{A^+} \exp\left(-\frac{\beta F \phi_{rev}}{RT}\right) \tag{1.2.12}$$

where ϕ_{rev} is the metal-solution p.d. when the process is at equilibrium. The chemical rate constant, $\vec{k}$, can be expressed in terms of the free energy of activation, $\Delta G^{o\ddagger}$, in the usual way:

$$\vec{k} = \frac{kT}{h} \exp\left(-\frac{\vec{\Delta G}^{o\ddagger}}{RT}\right) \tag{1.2.13}$$

Therefore,

$$i = zF \frac{kT}{h} \exp\left[-\frac{\vec{\Delta H}^{o\ddagger}}{RT}\right] \exp\left[\frac{\Delta S^{o\ddagger}}{R}\right] C_{A^+} \exp\left[-\frac{\beta F \phi^{o}_{rev}}{RT}\right] \exp\left[-\frac{\beta F \eta}{RT}\right] \tag{1.2.14}$$

Then, neglecting the linear term in T and supposing that $\Delta S^{o\ddagger}$ is independent of T over a reasonable range of T, the natural logarithm of the above expression can be differentiated with respect to T^{-1}, giving, for $\eta = o$

$$\left(\frac{\partial \ln i_o}{\partial (1/T)}\right)_{P,\eta=o} = -\frac{\Delta H^{o\ddagger}}{R} - \frac{\beta F}{RT}\left[\frac{\partial \phi^{o}_{rev}}{\partial (1/T)}\right] - \frac{\beta F \phi^{o}_{rev}}{R}$$

$$= -\frac{\Delta H^{o\ddagger}}{R} + \frac{\beta \Delta G^{o}}{R} + \frac{\beta T \Delta S^{o}}{R}$$

$$= -\frac{\Delta H^{o\ddagger}}{R} + \frac{\beta}{R}\left(\Delta G^{o} + T\Delta S^{o}\right)$$

$$= -\frac{\Delta H^{o\ddagger}}{R} + \frac{\beta \Delta H^{o}}{R}$$

$$= -\frac{1}{R}\left(\Delta H^{o\ddagger} - \beta \Delta H^{o}\right)$$

$$= -\frac{1}{R}\,\Delta W^{o\ddagger} \tag{1.2.15}$$

where $\Delta W^{o\ddagger}$ is an apparent enthalpy of activation which would be measured experimentally. It is seen that $\Delta W^{o\ddagger}$ is comprised of a term $\Delta H^{o\ddagger}$ which is the true enthalpy of activation and β times the enthalpy change ΔH^{o} for the overall reaction in the half-cell (eqn. 1.2.9) which cannot be measured. The true $\Delta H^{o\ddagger}$ can, however, be estimated from $\Delta W^{o\ddagger}$ by a non-thermodynamic calculation of ΔH^{o} utilizing a Born-Haber cycle for the ion-neutralization half-cell reaction. Writing this in a general form[34]

$$\begin{array}{ccccc} A^{z+}_{soln} & + & ze & \xrightarrow{\Delta H^{o}} & A_{soln} \\ \Big\downarrow -\Delta H^{o}_{sAz+} & & \Big\downarrow \Phi_e & & \Big\uparrow -\Delta H_{sub} \\ A^{z+}_{(g)} & + & ze_{(g)} & \xrightarrow{-I_{A\rightarrow A^{z+}}} & A_{(g)} \end{array} \qquad (1.2.16)$$

gives

$$\Delta H^{o} = -\Delta H^{o}_{s,A^{z+}} + z\Phi_e - I_{A\rightarrow A^{z+}} - \Delta H_{sub} \qquad (1.2.17)$$

where $\Delta H^{o}_{s,A^{z+}}$ is the heat of solvation of the A^{z+} ion, $I_{A\rightarrow A^{z+}}$ is the ionization energy of A to A^{z+}, ΔH_{sub} is the heat of sublimation and Φ_e is the electronic work function of the metal A.

We can now proceed to relate this treatment to evaluation of pressure effects on electrode processes which, in the literature, were first incorrectly formulated[13,19].

(4) (ii) Formal Treatment of Pressure Effects on Kinetics of Electrode Processes

The study of electrode processes under the influence of pressure has been rather limited. However, several research groups such as those of Hills[10-14,35], Hamann[3] and Heusler[15] have made important constributions to this field in recent years.

In the case of non-equilibrium electrode processes, the pressure

coefficient of the rate arises because of the volume change occurring in passing from the initial to the transition state of the reaction. As in the case of chemical reactions, the principal derivative for the isothermal pressure coefficient is the ('apparent' - see below) volume of activation. The volume of activation will be determined in part by solvent properties reflected in the electrostriction changes accompanying changes of the charged state of ions, or their neutralization in deposition processes.

The rate of discharge of dissolved ions in a direct electron transfer step depends on several factors. The first is a trivial factor, the ohmic resistivity of the electrolyte, whose contribution is kept negligible by the presence of an excess of inert supporting electrolyte. However, under these conditions, the reaction rate may be solution diffusion-limited depending on the concentration of the reactant. The limiting diffusion current, i_D, will then depend principally on the concentration and on the diffusion coefficient of the reactant species. Therefore

$$RT \left(\frac{\partial \ln i_D}{\partial P}\right)_T = -\Delta V_D^{\ddagger}$$

where $\Delta V_D^{\ddagger}$ is the volume of activation. Then the apparent pressure-dependence of current-density at a given potential will be determined by the pressure dependence of the diffusion rate, i.e., the apparent volume of activation, $\Delta V_D^{\ddagger}$, will be that of the diffusion process for transport of the electroactive species.

The case of greatest interest here is, however, when the charge-transfer process is activation-controlled. Then the pressure coefficient will be determined by the sign and magnitude of volume of activation of the charge-transfer process. In evaluating the effect of pressure on the rate of an activation-controlled electrode process, Conway[19] pointed

out in relation to an erroneous interpretation of pressure effects by Hills[14] that the same kind of difficulty arises in the interpretation of the results as that explained in Section 1.2.4 (i) on the temperature effects and the derivation of heats of activation.

The rate of an electrochemical process such as

$$A^+ + M(e) \rightleftharpoons B \tag{1.2.18}$$

can be expressed (omitting double-layer effects and assuming $\Delta\phi$ to be sufficiently large that the back-reaction can be neglected) as

$$\vec{v} = \frac{kT}{h} C_{A^+} \exp\left(-\frac{\Delta G^{\ddagger}}{RT}\right) \exp\left(-\frac{\beta F \Delta\phi}{RT}\right) \tag{1.2.19}$$

or in terms of current density, i, as

$$\vec{i} = zF\vec{v} = zF\, C_{A^+} \left[\frac{kT}{h} \exp\left(-\frac{\vec{\Delta G}^{\ddagger}}{RT}\right)\right] \exp\left(-\frac{\beta F \Delta\phi}{RT}\right) \tag{1.2.20}$$

where $\vec{\Delta G}^{\ddagger}$ is the free energy activation at zero electrode potential, $\Delta\phi$ is the metal-solution potential difference and β is the symmetry factor. The rate expression can be further simplified if one notes that the terms in the square brackets correspond to the rate constant at zero ϕ; then

$$\vec{i} = zF\, C_{A^+} \vec{k} \exp\left(-\frac{\beta F \Delta\phi}{RT}\right) \tag{1.2.21}$$

where $\Delta\phi$ can be replaced by $\Delta\phi = \eta + \phi_{rev}$ taking η as an overpotential referred to a potential ϕ_{rev}, the reversible potential of the electrode process under examination. If the natural logarithm of equation (1.2.21) is differentiated with respect to pressure at constant absolute electrode potential, then

$$\left(\frac{\partial \ln i}{\partial P}\right)_{\phi} = \frac{\partial \ln \vec{k}}{\partial P} = -\frac{\vec{\Delta V_t}^{\ddagger}}{RT} \tag{1.2.22}$$

where $\vec{\Delta V_t}^{\ddagger}$ is the true volume of activation. However, the condition of constancy of the electrode potential is experimentally impossible to define in the present case, as the pressure is varied. This is a result

of the finite pressure dependence of the reversible potential of the reference electrode, an effect which arises because of the volume change occurring in the half-cell reference electrode reaction. The pressure coefficient of the electrochemical reaction rate must, in practice, be evaluated at constant overpotential or at $\eta = o$ which is a practical, experimentally accessible condition. In kinetic experiments this can be easily achieved at various pressures by maintaining a constant potential with respect to a reference electrode which is the reversible form of the working electrode. However, experiments carried out at constant η or $\eta=o$ do not give the true volume of activation but an apparent value as illustrated in the following manner:

The expression

$$\vec{i} = zF\, C_{A+}\quad \vec{k} \exp\left(-\frac{\beta F \eta}{RT}\right) \exp\left(-\frac{\beta F \phi_{rev}}{RT}\right) \qquad (1.2.23)$$

at the equilibrium potential, ϕ_{rev}, can be written in terms of the exchange current density i_o as

$$i_o = zF\, C_{A+}\ \vec{k} \exp\left(-\frac{\beta F \phi_{rev}}{RT}\right) \qquad (1.2.12)$$

Then differentiating the natural logarithm of equation (1.2.12) with respect to pressure, we obtain

$$\left(\frac{\partial \ln i_o}{\partial P}\right)_{\eta=o,T} = \left(\frac{\partial \ln \vec{k}}{\partial P}\right)_T - \frac{\beta F}{RT}\left(\frac{\partial \phi_{rev}}{\partial P}\right)_T \qquad (1.2.24)$$

and noting that

$$\left(\frac{\partial \ln \vec{k}}{\partial P}\right)_T = -\frac{\Delta V_t^{\ddagger}}{RT} \quad \text{and} \quad \left(\frac{\partial \phi_{rev}}{\partial P}\right)_T = -\frac{\Delta V_o}{F}$$

then

$$\Delta V_a^{\ddagger} = \Delta \vec{V}_t^{\ddagger} - \beta \Delta V_o \qquad (1.2.25(a)$$

Therefore the true volume of activation for the reduction of an ion is given by

$$\Delta\vec{V}_t^{\ddagger} = \Delta V_a^{\ddagger} + \beta\Delta V_o \qquad (1.2.25(b)$$

where $\Delta V_a^{\ddagger}$ is the experimentally measured apparent volume of activation and ΔV_o is the volume change for the equilibrium electrode process being studied. The true volume of activation, $\Delta\vec{V}_t^{\ddagger}$, can thus be determined only if some estimate can be made of the overall volume change, ΔV_o, in the electrode reaction. ΔV_o is not thermodynamically measurable. However, unlike the heat changes in half-cell reactions, discussed earlier, ΔV_o can be quite accurately estimated for a number of processes by non-thermodynamic procedures based on the evaluation of individual partial molar volumes of the respective reactants and products.

As a result of the situation for evaluation of ΔV_o values, and in contrast to the situation with temperature coefficients, the pressure coefficient can generally provide activation (volume) parameters of greater certainty and significance. For the case of the hydrogen evolution reaction, the pressure coefficient is given by

$$RT\left(\frac{\partial \ln i}{\partial P}\right) = -\Delta V_t^{\ddagger} + \left[\frac{\beta}{2} V_{H_2} + \beta V_{H_2O} - \beta V_{H_3O^+}\right]$$

based on the reaction equation

$$H_3O^+ + e = \frac{1}{2} H_2 + H_2O$$

where V_{H_2}, V_{H_2O} and $V_{H_3O^+}$ are the partial molar volumes of the indicated reagents. The value of the partial molar volume of dissolved hydrogen, V_{H_2}, was taken as 25 $cm^3\ mol^{-1}$ ($V_{H_2}^{\infty}$) and the value $V_{H_2O} - V_{H_3O^+} = -V_{H^+}$ which has been estimated by Zana and Yeager[36-38] as 5.4 $cm^3\ mol^{-1}$. Therefore the true volume of activation can be determined quite precisely. For the above reaction, based on Hills' results, Krishtalik[19], following the

correction of the error in Hills' treatment pointed out by Conway[19,39], calculated the true volume of activation as +5.6 $cm^3\ mol^{-1}$.

In summary, the volume of activation for an electrode process differs from that of its chemical counterpart by inclusion of some fraction β of the difference of partial molal volumes of products and reactants in the overall electrode reaction at equilibrium. The effects are precisely analogous to those which arise in the evaluation of the temperature dependence of the rate of an electrochemical reaction.

The final result in the electrochemical case, for the exchange current as a function of pressure is given by

$$\left(\frac{\partial \ln i_o}{\partial P}\right)_{\eta,T} = -\frac{\Delta \vec{V}_t^{\ddagger}}{RT} + \frac{\beta F}{RT}\left(\frac{\partial \phi_{rev}}{\partial P}\right)_T$$

where

$$\Delta \vec{V}_t^{\ddagger} = \Delta V_a^{\ddagger} + \beta \Delta V_o$$

while the pressure effect for the chemical case is represented by

$$\left(\frac{\partial \ln k}{\partial P}\right)_T = -\frac{\Delta V_t^{\ddagger}}{RT}$$

The temperature coefficient of the rate constant of an electrochemical reaction is similarly represented(introducing the linear term in T, in eqn.1.2.15)by

$$\left[\frac{\partial \ln k}{\partial (1/T)}\right]_{\eta,P} = -\frac{1}{R}\left(\Delta H^{o\ddagger} - \beta \Delta H^{o} + RT\right)$$

while the relation for the chemical case is

$$\left[\frac{\partial \ln k}{\partial (1/T)}\right]_{P} = -\left(\frac{\Delta H^{o\ddagger} + RT}{R}\right)$$

It may be noted that the enthalpy of activation $\Delta H^{\ddagger}$ can often be assumed to be almost constant ($\Delta C_p \approx o$) over an appreciable range of temperatures. Then the integrated form of the temperature coefficient can be used to evaluate $\Delta H^{o\ddagger}$:

$$\ln \frac{k_2}{k_1} = \frac{\Delta H^{o\ddagger}}{R} \left(\frac{1}{T_1} - \frac{1}{T_2}\right) + \ln \frac{T_2}{T_1}$$

where k_1, k_2 are values of the rate constant at two particular temperatures, T_1, T_2.

$\Delta V^{\ddagger}$ on the other hand, is usually pressure dependent so that the integrated form of the pressure coefficient is only valid over small intervals of pressure. Therefore

$$\ln \frac{k_2}{k_1} = - \frac{\Delta V^{\ddagger}(P_2 - P_1)}{RT}$$

is normally applicable only when $P_2 - P_1 \leq 100$ bars. The volume of activation should hence be determined by evaluating the slope of the tangent to the lnk vs. pressure curves at a given pressure. The limiting tangent at ambient pressure or $P \rightarrow 0$ is generally the quantity of interest in most high pressure studies.

1.3 Brief Review of Experimental Behaviour of Systems at High Pressures

(1) Chemical Systems

The study of reactions in the condensed phase at elevated pressures has understandably received more attention than any other aspect of high-pressure work. In particular, a wide variety of organic reactions[40,7,8,9] has been examined with reference to mechanistic and synthetic applications. Several important reviews cover this aspect of high pressure research, the most comprehensive being those of Hamann[3] (1957) and le Noble[40] (1967). The first kinetic study at elevated pressure was that of the inversion of sucrose (1892). It was expected that pressure would enhance the rate of inversion in the same manner as does an increase of temperature. The opposite was found to be the case.

This unexpected result, along with engineering problems associated with high pressure experimentation, led to a decline of interest in this field until the 1950's.

During the last 25 years, however, a wide range of organic reactions has been examined at elevated pressures. le Noble has presented an extensive review of this topic with reference to specific reactions. The volume of activation in some cases can provide unqualified evidence of the existence of a particular mechanism, e.g., involving partially charged or ionic intermediates. In addition, if a reaction proceeds in two parallel paths, increase of pressure may retard one in favour of the other, e.g., if the volumes of activation for the two paths are different in sign and magnitude. Such a mechanism will be clearly evident in the shape of the ln k versus P plots which will show a maximum or a minimum. Hamann has classified some simple organic reactions into four types (Table 1.3.1) in order to make predictions of the effects of pressure on the rates of such reactions. The quantities $\Delta V_1^{\ddagger}$ and $\Delta V_2^{\ddagger}$ are predicted only in sign. If the reaction requires the simultaneous formation of one bond and breaking of another, as in the general case of an SN_2 type reaction, then two competing factors are involved in the volume change, the expansion of one of the bonds and the contraction of the other. It appears from numerous examples that the volume change arising from the contraction of the system in the direction of the bond which is being formed, more than balances the volume change associated with the expansion of the other bond. The net result is a negative volume of activation.

In the case where $\Delta V_1^{\ddagger}$, the volume change contribution due to solvent electrostriction, is important, the overall volume change will

TABLE 1.3.1*

THE KINETICS OF CHEMICAL REACTIONS UNDER PRESSURE

The Predicted Effects of Pressure on the Rates of Some Chemical Reactions in Solution

Reaction	Bonds broken	Bonds formed	Changes in number of ionic charges	$\Delta V_2^{\ddagger}$	$\Delta V_1^{\ddagger}$	Expected sign of $\Delta V^{\ddagger}$
Unimolecular dissociations						
(I) $A \rightarrow L + M$	1			+		+
(II) $A \rightarrow L^+ + M^-$	1		increase	+	-	-
Bimolecular associations						
(III) $L + M \rightarrow A$		1		-		-
(IV) $L^+ + M^- \rightarrow A$		1	decrease	-	+	+
Bimolecular exchanges						
(V) $A + BC \rightarrow AB + C$	1	1		-		-
(VI) $A + BC \rightarrow AB^+ + C^-$	1	1	increase	-	-	-
(VII) $A^- + BC \rightarrow AB + C^-$	1	1		-		-
(VIII) $A^- + BC^- \rightarrow AB^- + C^-$	1	1		-	-	-
(IX) $A^{2-} + BC^- \rightarrow AB^{2-} + C^-$	1	1		-	-	-
(X) $A^{2-} + BC \rightarrow AB^- + C^-$	1	1		-	+	+
(XI) $A^- + BC^+ \rightarrow AB + C$	1	1	decrease	-	+	+
(XII) $A^- + BC^{2+} \rightarrow AB^{2+} + C^-$	1	1		-	+	+
Double decompositions						
(XIII) $AB + CD \rightarrow AC + BD$	2	2		-		-
(XIV) $AB + CD \rightarrow AC + B^+ + D^-$	2	1	increase	?	-	-

* From Hamann - "Physico-Chemical Effects of Pressure"[3]

depend markedly on pressure. This is not surprising, since the solvent will be highly compressed at elevated pressures, thus reducing the electrostriction contribution to the total volume of activation. In a case such as this, the volume of activation will tend to become progressively more positive.

(2) Electrochemical Systems

Much of the relatively small amount of work that has hitherto been carried out on the influence of high pressure on electrode processes and on the structure of the double-layer has been provided by Hills[10,11,13] and co-workers. Also, Heusler[15] has studied the rates of hydrogen evolution on copper, silver and gold as a function of pressure. Supporting work on the structure of electrolytic solutions has been provided by Hamann in a larger number of papers and reviews[3,41]. The effects of pressure on ionization equilibria have been studied by Hamann[42], Horne[43] and by Fisher[44-47], with special reference to ion-pair dissociation.

The thermodynamic expressions developed by Hills[13] relating the observed pressure coefficient of rates of electrode processes to the volume of activation were found to be erroneous. The correct relationships were developed by Conway[19], Krishtalik[19] and by Parsons[19]. A more comprehensive treatment was published by Barnartt[18] in terms of a generalized theory. This approach includes complex, higher-order charge-transfer mechanisms which were divided into 4 classes.

(i) Electrochemical Equilibrium Processes. As previously mentioned, the effect on pressure on the equilibrium electromotive force of two reversible half-cell reactions is directly related to the volume change for the overall cell reaction. The earliest study of this kind

was carried out by Hainsworth[48] (1924) on the cell

$$Pt, H_2 \text{ (P bars)} | \text{ 0.1 N HCl} | Hg_2Cl_2, Hg$$

The cell EMF was found to be increased by 100 mV when the pressure applied to the cell by hydrogen was elevated from 1 to 1000 bars.

The variation of the fugacity of hydrogen with pressure was the main contribution to the EMF change. Therefore, thermodynamic data on the variation of the solvent structure with pressure were difficult to obtain in this type of experiment.

In more recent work, the variation of cell EMF with 'hydrostatic' pressure has been used to test the suitability of certain reference electrodes for high-pressure electrode kinetic studies. Hills and Kinnibrugh[13] used the cell

$$Pt, H_2(1 \text{ bar}) | \text{ HCl} | Hg_2Cl_2, Hg$$

in which the electrolyte was pre-saturated with hydrogen at a pressure of 1 bar. The observed cell EMF was a linear function of pressure indicating that the partial molar volumes were constant over the pressure range of 1 to 1500 bars. The observed slope was $8 \times 10^{-6} V \text{ bar}^{-1}$ and this corresponds to a net partial molar volume change of $-7.6 \text{ cm}^3\text{mol}^{-1}$ for the reaction

$$\frac{1}{2} H_2 + \frac{1}{2} Hg_2Cl_2 \longrightarrow Hg + HCl_{aq} \qquad (1.3.1)$$

The pressure coefficient of cell EMF, ΔE, can be expressed in terms of partial molar volumes of the reaction components:

$$\left(\frac{\partial \Delta E}{\partial P}\right) = -\frac{1}{F}\left(V_{HCl} + V_{Hg} - \frac{V}{2} H_2 - \frac{V}{2} Hg_2Cl_2\right) \qquad (1.3.2)$$

This leads to a value of + 15 $cm^3\ mol^{-1}$ for the partial molar volume of hydrogen in 0.1 N HCl. The partial molar volume of hydrogen at infinite dilution, $V_{H_2}^{\infty}$, could not be assessed from Hills' work because the measurements were limited to only one concentration of HCl.

Heusler and Gaiser[15] made a similar study on the cell

$$Pt,\ H_2\ (P = 1\ bar)\ |\ HCl\ |\ AgCl,\ Ag$$

at three concentrations of HCl (0.2 M, 0.4 M and 0.8 M HCl) at pressures up to 2500 bars. The partial molal volume of hydrogen in water, $V_{H_2}^{\infty}$, was determined from the following pressure coefficient:

$$\left(\frac{\partial \Delta E}{\partial P}\right)_T = -\frac{1}{F}\left(V_{AgCl} + \frac{V}{2}H_2 - V_{Ag} - V_{HCl}\right) \qquad (1.3.3)$$

and found to be + 24.5 $cm^3\ mol^{-1}$. This value is in good agreement with the value of 25.2 $cm^3\ mol^{-1}$ obtained by direct measurement utilizing the dilatometer method. Heusler's results show a non-linear variation of EMF with pressure, indicating the partial molar volumes involved in the reaction are pressure sensitive.

Valeriote and Gallup[16] utilized the Ag, AgCl and hydrogen electrodes to monitor the electrochemical behaviour of sea-water activated battery anodes under open-circuit conditions at elevated pressures. The reference electrodes were studied in unbuffered and buffered chloride solutions. In unbuffered solutions, the small variation of EMF of the Ag, AgCl electrode with pressure was due largely to chloride ion activity changes. The large variation of the hydrogen electrode potential was due to changes of hydrogen fugacity. The partial molar volume of hydrogen was not evaluated by these authors but from the data provided for 0.1 M HCl solution, the V_{H_2} can be estimated as $\sim$ 18 $cm^3\ mol^{-1}$.

EMF measurements have been applied to the study of ionic equilibria by Disteche[49,50], utilizing a glass electrode up to 1000 bars. The glass electrode arrangement was initially used to measure the pH of sea water as a function of the ocean depth. Diesteche[49,50] has also shown that ionization constants of weak acids and bases, determined from the glass electrode measurements, agree quite well with those derived from high pressure conductivity data. Hamann has used a similar technique to measure the ionization constant of water up to 1000 bars.

(ii) Electrochemical Kinetic Measurements. The original purpose of Hainsworth's studies on the cell Pt, H_2| HCl| Hg_2Cl_2, Hg was to explain the irreversible overvoltage effects occurring when hydrogen gas is formed from its 'ions'. Although this study did not provide any kinetic information on the origin of the hydrogen "overvoltage"*, it did show quite clearly the effect of dissolved hydrogen on the activity of hydrogen ions. At 1000 bars, the deviation of the cell EMF from ideal behaviour was attributed mainly to the variation of hydrogen fugacity and to a lesser extent, to the decrease in activity of H^+ in the presence of dissolved hydrogen.

The cathodic hydrogen evolution reaction (h.e.r.) has been extensively studied at a variety of metal/solution interfaces, especially platinum, mercury, lead and gold in aqueous media. The major contributors to this field, Schuldiner, Frumkin, Bockris, Parsons and Conway,have postulated two possible mechanisms; other mechanisms involving H_2^+ were proposed by Heyrovsky and by Horiuti but are no longer considered applicable:

* The early work on electrode kinetics treated the phenomena of overvoltage at an electrode as an undesirable feature and therefore sought to determine the origin of this effect in order to remedy the limitations of such an electrode. This attitude applied in particular to the h.e.r. It is now clear that the so-called overvoltage established at any electrode interface is a necessary consequence of a net current being passed.

1. $2M(e) + 2H_3O^+ \rightarrow 2MH + 2H_2O$

$$2MH \rightarrow 2M + H_2$$

or

2. $M(e) + H_3O^+ \rightarrow MH + H_2O$

$$MH + H_3O^+ + M(e) \rightarrow 2M + H_2O + H_2$$

According to Bockris and Reddy[51], the mechanism of the h.e.r. on several metals is known with certainty. On mercury, mechanism (2) occurs with the proton discharge step being rate-determining. Horiuti has, however advocated that the slow step in mechanism (2) is the electrochemical desorption process. In order to characterize further the rate-determining step for the h.e.r. on mercury, Hills[13] evaluated the volume of activation for this reaction by determining the current density as a function of pressure at <u>constant overpotential</u> for the cell

$$Hg \mid 0.1\ M\ HCl \mid 1\ M\ KCl \mid Hg_2Cl_2, Hg$$

The pressure coefficient measured at constant overpotential was erroneously (see p. 13) related to the true volume of activation by the expression

$$\left(\frac{\partial \ln i}{\partial P}\right)_{\eta,T} = -\frac{\Delta V_t^{\ddagger}}{RT}$$

For reasons outlined in section 1.2.4 (ii), the above pressure coefficient can only give the apparent volume of activation:

$$\left(\frac{\partial \ln i}{\partial P}\right)_{\eta,T} = -\frac{\Delta V_a^{\ddagger}}{RT} = -\frac{1}{RT}\left(\Delta V_t^{\ddagger} - \beta \Delta V_o\right)$$

The true volume of activation, $\Delta V_t^{\ddagger}$ can be evaluated if ΔV_o is known for the overall equilibrium reaction. The volume of activation

($\Delta V_a^{\ddagger}$) as determined by Hills was small and negative, viz. -3.4 $cm^3\ mol^{-1}$, and cannot be interpreted in terms of known mechanisms for h.e.r. Krishtalik[19], however, applied the necessary approximate corrections to $\Delta V_a^{\ddagger}$ to give the true volume of activation, $\Delta V_t^{\ddagger}$ = +5.6 $cm^3\ mol^{-1}$. The partial molar volume of the activated complex $V^{\ddagger}$ can then be evaluated from the following expression:

$$V^{\ddagger} = \Delta V_t^{\ddagger} + V_{H^+}$$

$$= +5.6 - 5.4\ cm^3\ mol^{-1}$$

$$= +0.2\ cm^3\ mol^{-1}$$

This unexpectedly small value indicates that the transition state volume is between that of an H atom and a proton. This question will be discussed further in Chapter 4.

Heusler and Gaiser[15] determined the partial molar volume of the transition state, $V^{\ddagger}$, for the hydrogen evolution reaction on silver, gold and copper electrodes at pressures up to 2500 bars. The value of $V^{\ddagger}$ was determined from the experimental apparent volume of activation, $\Delta V_a^{\ddagger}$, utilizing the relationship

$$\Delta V_a^{\ddagger} = \Delta V_t^{\ddagger} - \beta \Delta V_o = V^{\ddagger} - V_{H^+} - \beta \Delta V_o$$

The authors assumed that V_{H^+} was pressure independent and ΔV_o = 1/2 V_{H_2} - V_{H^+} - V_e where V_{H_2} = 15 $cm^3\ mol^{-1}$, V_{H^+} = -5.2 $cm^3\ mol^{-1}$ and V_e = + 3 $cm^3\ Faraday^{-1}$. In acid solutions, in the absence of specific adsorption and at pressures above 500 bars, the volume of activation was independent of pressure, pH value, ionic strength and, surprisingly, electrode material. In the high pressure region, the apparent volume of activation for the h.e.r. at Cu, Ag and Au electrodes in perchloric acid solutions was found to be -12.5 ±1 $cm^3\ mol^{-1}$. This value corresponds

to a true volume of activation of -8 $cm^3\ mol^{-1}$ and a partial molal volume of the transition state of -13.2 $cm^3\ mol^{-1}$.

The authors considered the following mechanism as being operative in all cases considered:

$$H^+ + e \rightarrow H_{ads}$$

$$H^+ + H_{ads} + e \rightarrow H_2$$

The volume of the transition state for each step was assumed to be the same. This assumption was based on the fact that the volume of activation was independent of electrode material and the rates of each step were taken as being equal. On the basis that the proton was a common reactant in both steps, it was assumed by Heusler and Gaiser that the transition state is essentially an 'adsorbed' proton. Further evidence for this assumption is founded on the extrapolated estimate of the partial molar volume of a singly charged, vanishingly small ion being -13.5 $cm^3\ mol^{-1}$. Therefore, the activation process was regarded as involving the transition from the normal solvated state of the proton $H_3O^+ + 4H_2O$ in the bulk solution to a partially desolvated proton in the transition state. The volume decrease of 8 $cm^3\ mol^{-1}$ was attributed to reduction of the 'open-structure' outer hydration shell of the proton, as suggested earlier by Conway[114] in an attempt to interpret Hills' results.

It is indeed surprising that results obtained by two independent researchers on the hydrogen evolution reaction lead to a negative volume of activation for a process which involves a reduction of charge. This is contrary to the usually discussed mechanisms for steps in the h.e.r. reaction and the principles involved in interpretation of $\Delta V^{\ddagger}$ for reactions that involve a change of charge.

While the h.e.r. process has been well characterized in the past (but not at high pressures), the results are often difficult to interpret. The problems associated with the interpretation of the pressure effects on the h.e.r. have made it necessary to examine what determines the process of activation in the fundamental electron transfer step itself. This can be accomplished by studying the pressure dependence of the rates of electron exchange in a simple redox reaction. Hills and Hsieh[52(a),(b)] evaluated the kinetics of the $Fe(CN)_6^{-3}/Fe(CN)_6^{-4}$ system at a platinum electrode as a function of temperature and pressure. The rate constants were evaluated from a.c. impedance measurements utilizing the so-called 'Randles Plot'. The measured apparent volume of activation at 25°C of +8 $cm^3\ mol^{-1}$ was corrected, in this work, by the procedure discussed earlier, to give a true volume of activation of -4.6 $cm^{-3}\ mol^{-1}$ for the process

$$Fe(CN)_6^{-3} + e \rightleftharpoons Fe(CN)_6^{-4}$$

This small negative value of $\Delta V_t^{\ddagger}$ is in accord with the supposition that the mechanics of activation in this electron-transfer reaction is the reorganization of part of the hydration sheath of the ions. This result is consistent with the 'outer-sphere' model for activation in redox reactions and with the greater electrostriction at $Fe(CN)_6^{4-}$ than at $Fe(CN)_6^{3-}$.

Solid electrodes, such as platinum, cause severe limitations in the reliability of the experimental results due to well-known problems of surface contamination and electrochemical deposition of adsorbed hydrogen and oxygen. The potential range at Pt for an oxygen or H-free surface is between +0.40 V and +0.75V versus the normal hydrogen electrode. However, the redox potential for the $Fe(CN)_6^{-3}/Fe(CN)_6^{-4}$ which is ca.

+0.70 V is near enough to the potential region for OH deposition on platinum to cause severe doubts concerning the reliability of the above results. These complications are removed if a gold electrode is used* where the double-layer region with no OH or H species adsorbed extends from +0.05 to +1.35 V in aq. H_2SO_4.

(iii) Electro-active Phases. The generation of anodic films[54] plays an important role in many electrochemical processes of practical interest. Also, the formation of a passivating film on a metal substrate is often used as a means of corrosion protection. The production of electro-active phases such as $Ni(OH)_2$, AgCl, PbO_2, $PbSO_4$ and $PbCl_2$ are of particular significance in the preparation of battery electrodes. The oxidation of lead to various deposited lead species and their subsequent reduction has received considerable attention in the past due to the continued and widespread utilization of the lead-acid battery. More recently, the development of the sea-water activated battery[55] ($Mg \mid Cl^- \mid AgCl$, Ag and $Mg \mid Cl^- \mid PbCl_2$,Pb) has extended this area of research to the Ag, AgCl and Pb, $PbCl_2$ electrodes. The pressure dependence of the sea-water activated battery performance is also of interest, since these battery systems in this respect are often used in deep marine environments. Valeriote and Gallup[16] have recently reported the effects of pressure on the dissolution of Mg and Al in chloride solutions.

(iii-a) The $Pb,PbCl_2$ Electrode. In contrast to the $Pb,PbSO_4$

* Such a system was employed in the present work.

electrode, the Pb, $PbCl_2$ system[56] has received relatively little attention until quite recently. Barradas[28-31] and co-workers have extensively studied the formation and reduction of $PbCl_2$ over a wide range of HCl concentrations, utilizing voltammetric, galvanostatic and potentiostatic transient techniques in conjunction with X-ray diffraction and scanning electron microscopy measurements. A brief summary of their results will now be presented.

The initial process in the anodization of the lead substrate is the almost reversible electrochemical dissolution to Pb^{2+} ions according to the reaction

$$Pb \rightleftharpoons Pb_{aq.}^{2+} + 2e$$

The anodically produced Pb^{++} ions tend to diffuse away from the electrode, but when the diffusion-layer becomes supersaturated with respect to $PbCl_2$, the latter will become precipitated as an insoluble film and grow by a 'dissolution-precipitation' mechanism. However, before passivation occurs, a second type of film begins to grow on top of the original basal layer. Scanning Electron Micrographs show that the basal layer is comprised of a porous structure of small crystal size while the secondary layer is made of larger macroscopic crystals formed by progressive nucleation and growth. This latter film is responsible for the passivation of the electrode surface. The presence of two surface species, (not necessarily the same as described above), was also indicated by electrochemical measurements at rotating disc electrodes. The cyclic voltammetry i-V profiles show two types of cathodic peaks upon reduction of the passivated film. If the voltage is scanned beyond the passivation potential (passivation occurs at -0.470 V vs S.C.E.) in the anodic direction, upon sweep reversal, a cathodic peak

with a shoulder on the anodic side is observed. If the anodic potential limit is extended further, the shoulder becomes the main peak, while the peak of the previous sweep is reduced to a shoulder. It has been postulated that this transformation is the result of a 'reactivation process' occurring at the electrode surface in the transpassive potential region. The basal layer undergoes chemical dissolution to a variety of lead complexes according to the general reaction

$$PbCl_2 + (n-2)Cl^- \rightarrow PbCl_n^{2-n}$$

This allows further electrochemical dissolution of the lead substrate to occur, resulting in a condition of supersaturation near the lead electrode with subsequent nucleation and growth on the outer region of the electrode surface phase.

The mechanism of the anodic layer growth on Pb as postulated by Barradas is thus as follows:

$$Pb \rightleftharpoons Pb_{ads}^{2+} + 2e^-$$

$$Pb_{ads}^{2+} + 2Cl^- \rightleftharpoons (PbCl_2)_{ads}$$

$$(PbCl_2)_{ads} \rightleftharpoons (PbCl_2)_{latt.}$$ -basal layer formation

$$\downarrow (n-2)Cl^-$$ -basal layer dissolution

$$(PbCl_2)_{ads} + (n-2)\,Cl^- \rightleftharpoons (PbCl_n^{(2-n)})\ e.s.$$

$$x(PbCl_n^{2-n})_{e.s.} \rightleftharpoons (PbCl_2)_x + x(n-2)\,Cl^-$$ - formation of critical nuclei for precipitation

$$(PbCl_2)_x + (PbCl_n^{2-n})_{e.s.} \rightleftharpoons (PbCl_2)_{x+1} + (n-2)Cl^- \quad \text{crystal growth}$$

$$x(PbCl_b^{2-n})_{e.s.} \rightleftharpoons (PbCl_n^{2-n}) \quad \text{bulk}$$

where 'ads' indicates attachment of some kind to the electrode surface;

'latt' signifies incorporation into a solid lattice;

'e.s.' implies in solution near the electrode surface;

'bulk' means beyond the diffusion-layer.

The importance of surface and film dissolution processes in the growth of the $PbCl_2$ film suggests that the pressure-dependence of the electrochemical behaviour of this system might provide further information on the nature of the dissolution processes and their role in the anodic film forming process

(iii-b) The Pb, $PbSO_4$ Electrode. The lead electrode in sulfuric acid solutions has been more extensively studied[57,58,59] and many papers have been published, especially with reference to the behaviour of the lead-acid battery. Wynne-Jones[57] and co-workers have established that the reversible cell reaction occurring in the discharge mode of the lead-acid battery is a 'double'-sulphation according to the reaction scheme

$$Pb + PbO_2 + 2H_2SO_4 \rightleftharpoons 2PbSO_4 + 2H_2O$$

Of particular interest in these earlier studies was the conversion of $PbSO_4$ to PbO_2. This process is thought to involve an alkalination condition[59] in the pores of the $PbSO_4$ which results in

the formation of basic lead salts at potentials anodic to the formation of $PbSO_4$. At high enough anodic potentials, the lead salts are completely converted to PbO_2 with simultaneous O_2 evolution. Fleischmann and Thirsk[58] have examined the role of the formation of $PbSO_4$ in the phase change to PbO_2. It is postulated by these authors that the rate of formation of $PbSO_4$ is controlled in part by the rates of nucleation and growth of the film. The lead sulphate deposit grows by ionic transport due to the electric field across the surface layer. At high anodic potentials, regions on the lead sulphate electrode act as centres for the nucleation of PbO_2.

In more recent studies[60-65] the morphology of the deposits on lead have been examined by a variety of optical techniques. The multiphase nature of the lead deposits as a function of anodic potential has, for example, been studied by Ruetschi[64]. However, the main interest in this work has been with the condition of the surface of lead battery plates as a function of anodic potential. The excellent S.E.M. pictures of Weininger[65] on the formation of $PbSO_4$ are of particular interest as they show the morphology of $PbSO_4$ deposits under various conditions.

The main point to be made here is that the majority of electrochemical studies in the past have dealt primarily with the formation and reduction of PbO_2 with minimal attention to the anodic process involved in the lead-acid battery, i.e., $Pb + SO_4^{2-} \rightleftharpoons PbSO_4 + 2e$. A recent series of papers by Archdale and Harrison[24-27] were probably the first in which the fundamental electrochemical processes involved in such a reaction were examined. Although the results are ambiguous, due to the variable nature of the electrode surface, several important conclusions were made. The dissolution reaction of Pb is found to be a reversible two-electron process. At low anodic potentials on an

electropolished surface, the film grows by a solution-precipitation reaction. At higher anodic potentials, a solid-state nucleation and growth process appears to set in. At a mechanically polished surface, only a solid-state process evidently occurs.

In order to provide a comparative study with the Pb, $PbCl_2$ electrode, the behaviour of lead in sulphate solutions has been studied in the present work at elevated pressures as well as at elevated temperatures. Due to the complex nature of the processes involved in film formation, it is difficult to predict a priori the behaviour under such extreme conditions. However, it is expected (a) that at elevated pressures, the rate of Pb dissolution will be enhanced; (b) the solubility of $PbSO_4$ will be increased and (c) the ionic association equilibria in solution will be altered.

1.4 Conductivity Measurements at High Pressures

Studies of various electrode processes at elevated pressures often require knowledge of the conductance behaviour of electrolytes and ion-pair equilibria under corresponding conditions. Since a number of examples of this kind arise in the work to be reported later in this thesis, it will be useful to review the treatment of electrolyte conductivity and ion-pair equilibria at elevated pressures which has already been given in the literature. Conductance information at high pressures is required, for example, in studies of solubility of electrochemically generated phases such as $PbCl_2$, $PbSO_4$, etc. which will be discussed in Chapter 5.

The behaviour of electrolyte solutions under extreme conditions[66] is of fundamental interest in terms of solvent structure, ionic transport properties and ionic equilibria. Applications of pressure-induced effects are of interest in e.g., (a) oceanographic studies of the nature of salt water as a function of the ocean's depth and (b) behaviour of sea-water

batteries at large depths.

(1) Electrolyte Conductivity*

The earliest known conductivity measurements at elevated pressure were reported in 1827 by Colladon and Sturm.[67] The conductivities of NH_4OH and HNO_3 were found to be independent of pressure up to 30 bars. Moderately high pressures (1-3 kbar) were achieved around 1900 and Tammann[67] was able to study conductivity of a wide variety of salts in aqueous solutions at pressures up to 3700 bars, but unfortunately, the conductivity results were recorded in terms of relative resistances. Work in this field did not flourish until the 1950's, when a large number of papers were published by Hamann, Frank, Laidler, Quist and Marshal, and Fisher. Conductivity measurements in non-aqueous media have been published recently, but the results are often difficult to interpret due to the limited knowledge of the physical properties of such solvents at elevated pressures.

The physical properties of water have, however, been well characterized at elevated temperatures and pressures. The effect of pressure on the structure of water at 25°C leads to increased density, dielectric constant and refractive index. The viscosity initially decreases with pressure, exhibiting a slight minimum at approximately 500 bars, but then increases in the manner of a 'normal', unassociated liquid. This minimum is enhanced with decreasing temperature but virtually disappears if the temperature is above 40°C.

Most organic solvents are much more compressible than water and consequently, their physical properties are relatively more affected than water by an increase in pressure. Water exhibits a relative

*The SI convention uses the terms electrolytic and molar conductivity instead of the more familiar specific and equivalent conductivity terminology. In this thesis the original definitions of conductivity are maintained, as otherwise unnecessary complexities arise.

compression of 4% for an increase of pressure from 1 to 1000 bars, while most organic solvents are compressed by 5-8% in this range.

The transport properties of ions are generally characterized by the limiting equivalent conductivity Λ^{∞} of the electrolyte or that of the individual ions, based on Λ and the transference numbers, t_+ or t_-. The equivalent conductivity, Λ, at concentration C, is related to the limiting equivalent conductivity Λ^{∞} by the Kohlrausch equation

$$\Lambda = \Lambda^{\infty} - SC^{1/2} \qquad (1.4.1)$$

or the more complete equations of Fuoss and Onsager[68,69], where S is a function of temperature and pressure. The limiting equivalent conductivity of aqueous KCl[70,71] has been measured up to pressures of 3000 bars by a number of workers with good agreement. Λ^{∞}_{KCl} exhibits a maximum value at approximately 1000 bars and decreases almost linearly with pressure beyond 2000 bars until water freezes out at approximately 10 kbars. This type of behaviour is almost universal for strong electrolytes.

At finite concentrations, interionic forces exist and must be taken into account in analyzing conductivity data in terms of ion transport processes. The Debye-Hückel-Onsager[68,69] theory describes the effect of the ionic atmosphere on the mobility of ions as a result of electrophoretic and relaxation effects. The electrophoretic effect arises because of the tendency of momentum to be[69] transferred between moving ions and the solvent in the ionic atmosphere, thus affecting the motion of the reference ion in the opposite direction. The relaxation contribution is a result of the finite time required for the ionic atmosphere to respond to the motion of a given reference ion. Both effects depend on thesquare-root of ionic strength as expressed in the Debye-Hückel-Onsager

relationship:

$$\Lambda = \Lambda^{\infty} - \left[\frac{2.801 \times 10^{6} \, |z_1 z_2| \, q \, \Lambda^{\infty}}{(\varepsilon T)^{3/2} \, (1 + q^{(1/2)})} + \frac{41.25(|z_1| + |z_2|)}{(\varepsilon T)^{1/2} \, \eta} \right] I^{1/2} \qquad (1.4.2)$$

$$= \Lambda^{\infty} - S \, (I)^{1/2}$$

where ε is the dielectric constant of the solution,

η is the solution viscosity in poise

I is the ionic strength $(1/2 \, \Sigma C_i \, z_i^2)$ in mol l^{-1}

$$q = \frac{|z_1 z_2|}{|z_1| + |z_2|} \cdot \frac{\Lambda_1^{\infty} + \Lambda_2^{\infty}}{|z_2| \, \Lambda_1^{\infty} + |z_1| \Lambda_2^{\infty}} \qquad (1.4.3)$$

The subscripts 1 and 2 represent the cation and anion respectively.

Λ^{∞} is the limiting equivalent conductivity;

Λ_1^{∞} and Λ_2^{∞} are limiting mobilities of cation and anion, and

Λ is the observed equivalent conductivity at ionic strength I.

Since both η and ε increase with increasing hydrostatic pressure, there is a corresponding decrease in the Onsager slopes. Hamann[41] and co-workers confirmed this interpretation for a number of electrolytes in water and methanol at pressures up to 3000 bars. At concentrations greater than 0.01 M, Robinson and Stokes[69] utilize the relationship

$$\Lambda = \Lambda^{\infty} - \frac{(B_1 \, \Lambda^{\infty} + B_2) \, I^{1/2}}{1 + aB(I)^{1/2}} \qquad (1.4.4)$$

where 'a' is an ion-size parameter and B is the parameter in the Debye-Hückel expression for activity coefficients;

$$\log f_{\pm} = - \frac{A\,|z_1 z_2|\,(I)^{1/2}}{1 + aB(I)^{1/2}} \qquad (1.4.5)$$

$$\text{where } A = \frac{1.8246 \times 10^6}{(\varepsilon T)^{3/2}} \text{ mol}^{-1/2} \text{l}^{1/2} \text{ K}^{3/2} \qquad (1.4.6)$$

$$B = \frac{50.29 \times 10^8}{(\varepsilon T)^{1/2}} \text{ cm}^{-1} \text{mol}^{-1/2} \text{l}^{1/2} \text{ K}^{1/2} \qquad (1.4.7)$$

$$\text{Also } B_1 = \frac{2.801 \times 10^6 |\, z_1 z_2 |\, q}{(\varepsilon T)^{3/2}\,(1 + q^{1/2})} \qquad (1.4.8)$$

and

$$B_2 = \frac{41.25(|z_1| + |z_2|)}{\eta(\varepsilon T)^{1/2}} \qquad (1.4.9)$$

This equation was found by Brummer and Gancy [66] to be applicable to a number of salts at moderate concentrations at pressures up to 2000 bars. At high concentrations, the limiting equivalent conductivity decreases almost linearly with pressure and does not exhibit the usual maxima associated with lower electrolyte concentrations. As Hamann [41] explains, this is due to the already viscous nature of the electrolyte at high concentrations and elevation of pressure causes a further increase in the viscosity of the solution.

(2) Ion-Association Equilibria

Fanjung [67] (1894) was the first to observe the effect of pressure on the ionization of weak carboxylic acids in aqueous media. The ionization quotient for acetic acid increased by 12% in the pressure range 1 to 270 bars. The conductivity of weak electrolytes, except at very low concentrations, increases much more rapidly with pressure than that of strong

electrolytes and does not exhibit the maxima typical of strong electrolytes. Since this early work, a wide variety of simple ionization reactions has been studied by volumetric analysis and high pressure measurements. This topic has been recently reviewed by Hamann[41], who compiled an extensive list of volume changes for the ionization of weak electrolytes on a comparative basis. Hamman also recorded the effects of pressure on the dissociation of ion-pairs.

For a 1:1 electrolyte, the Debye-Hückel limiting law can be modified to take into account ion-pairing by writing

$$\log f_{\pm} = \frac{-Az_1z_2[(1-\phi)C]^{1/2}}{1 + aB\,[(1-\phi)C]^{1/2}} \qquad (1.4.10)$$

where ϕ is the fraction of the total number of ions in the form of ion-pairs. Therefore $(1-\phi)C$ is the concentration of free ions. Numerically, in Bjerrum's treatment[68,69,72], $a = \frac{|z_1z_2|e^2}{2\varepsilon KT}$ and is the distance at which the mutual electric potential energy $\frac{|z_1z_2|e^2}{a\varepsilon}$ of the two ions in a pair is equal to 2kT. For a 1:1 electrolyte at 25°C in water, the Bjerrum distance a = 3.57 Å. Thus, at distances of closest approach greater than 3.57 $|z_1z_2|$ Å, ion-pairing is not thermodynamically significant. Fuoss treated ion-pairs as being in physical contact, thus forming a neutral dipole, but solvent-separated pairs in which some solvation shell is maintained are well characterized. Ion-pair formation can be conveniently measured by conductivity methods. The deviations[72-75] of the experimental Onsager slope from the theoretical value were often attributed to ion-pair formation. It is assumed that the ion-pair, for symmetrical electrolytes, is non-conducting and that its activity coefficient in dilute solutions is unity. The free ions can be regarded as obeying Onsager's limiting equation and the Debye-Hückel limiting law. The degree

of dissociation, α, is calculated by an iterative method of approximation, using the Onsager equation, until a constant value of α is obtained. The equation used is of the general form

$$\alpha = \frac{\Lambda}{\Lambda^{\infty} - s(\alpha C)^{1/2}} \qquad (1.4.11)$$

The non-ideal interionic contributions are introduced in the determination of the activity coefficient. The effect of pressure on the dissociation of symmetrical ion pairs has been recently studied by Hamann, Pearce and Strauss[42], and by Fisher[44,46]. Hamann and co-workers studied lanthanum ferricyanide in water at pressures up to 2000 bars. They utilized Kohlrausch's law to evaluate the limiting equivalent conductivity of $LaFe(CN)_6$ at <u>each pressure</u>:

$$\Lambda_p^{\infty}\,[LaFe(CN)_6] = \Lambda_p^{\infty}\,[LaCl_3] + \Lambda_p^{\infty}\,[K_3Fe(CN)_6] - \Lambda_p^{\infty}\,[KCl]$$

The variation of the molal dissociation constant K_m with pressure is represented by

$$\left(\frac{\partial \ln K_m}{\partial P}\right)_T = -\frac{\Delta V}{RT}$$

where ΔV is the partial molar volume change accompanying the ion-pair dissociation process.

The results were analyzed in terms of the theories of Bjerrum and Fuoss. The experimentally obtained volume change $\Delta V^{\infty} = -8.0\ cm^3\ mol^{-1}$,

for the ion-pair dissociation agrees quite well with those predicted by Bjerrum and Fuoss, viz, -6.89 and -8.98 $cm^3\ mol^{-1}$, respectively. The effect of pressure on the dissociation of $MgSO_4$ was evaluated by Fisher[44], using the Kohlrausch equation in the form

$$\Lambda_p^\infty\ [MgSO_4] = \Lambda_p^\infty\ [K_2SO_4] + \Lambda_p^\infty\ [MgCl_2] - \Lambda_p^\infty\ [KCl]$$

The volume change, ΔV^∞, for the ion-pair dissociation at 1 bar. was -7.3 $cm^3\ mol^{-1}$. This value is surprisingly similar to that for $LaFe(CN)_6$. This coincidence was explained by Hamann[41] in terms of Fuoss's theory which predicts a dissociation constant K_m for ion-pairs by utilizing the equation

$$K_m = 3000 \exp \frac{z_1 z_2 e^2}{a\varepsilon kT} \cdot \frac{1}{4\pi\rho Na^3} \qquad (1.4.12)$$

where 'a' is the Fuoss contact distance and ρ is the density of the solvent. Upon differentiation of K_m with respect to pressure and assuming 'a' to be pressure independent, the relation

$$-\left[\frac{\partial(RT\ln K_m)}{\partial P}\right]_T = \Delta V^\infty = \left[\frac{\partial(RT\ln\rho)}{\partial P}\right]_T + \frac{z_1 z_2 e^2 N}{a\varepsilon^2}\left(\frac{\partial\varepsilon}{\partial P}\right)_{\rho,T} \qquad (1.4.13)$$

is obtained. In water at 25°C and 1 bar, equation (1.4.13) becomes

$$\Delta V^\infty = 1.12 + 8.35\ z_1 z_2/a \qquad (1.4.14)$$

If 'a' is determined from the expression for K_m at 1 bar, the ΔV^∞ can be evaluated. The calculated values for $MgSO_4$ and $LaFe(CN)_6$ are -7.4 and -9.0 $cm^3\ mol^{-1}$, respectively. It appears that the greater value of 'a' due to hydration effects for $LaFe(CN)_6$ tends to cancel out the

increased effect of z_1z_2 in the term $8.35 \frac{z_1z_2}{a}$; thus, the ΔV^{∞} values for these two ion pairs are quite similar.

The determination of dissociation constants of unsymmetrical electrolytes by conductivity measurements is often a difficult exercise. This is due to the charged nature of the ion-pair which will, itself, be involved in long-range interionic coulombic interactions. The limiting equivalent conductivity will, in general, be difficult to determine by graphical methods due to the deviations from the Debye-Hückel-Onsager relationship. In the case of symmetrical electrolytes, the Λ^{∞} value can be easily evaluated from Kohlrausch's law. However, in the case of an unsymmetrical electrolyte, an estimate must be made of the mobility of the charged ion-pairs. Davies and Righellato[73], analysed the conductivity data of Noyes and Falk for a number of uni-bivalent salts and found that the Debye-Hückel-Onsager relationship was not strictly obeyed. This deviation was attributed to ion-association. The salt of interest here was lead chloride, which forms $PbCl^+$ ion-pairs at concentrations as low as 10^{-3} mol l^{-1} of $PbCl_2$. The dissociation constant for $PbCl^+$ was determined assuming the ion-pair had a limiting equivalent conductivity of 40 Mhos at 18°C. The value of 40 arises from the fact that in dibasic acid solutions, the intermediate HA^- has a limiting equivalent conductivity of 0.6 that of the acid anion. Thus, $\Lambda^{\infty}_{PbCl^+} = 0.6\ \Lambda^{\infty}_{Cl^-}$ was assumed. The solution was then considered as a mixture of a completely dissociated uni-bivalent salt $PbCl_2$ and a completely dissociated uni-univalent salt $[PbCl^+][Cl^-]$ [74,75,76]. The degree of dissociation α was determined by successive approximations to give the measured equivalent conductivity Λ :

$$2\Lambda = 2(1-\alpha)(\Lambda_{Cl^-} + \Lambda_{Pb^{2+}}) + \alpha(\Lambda_{Cl^-} + \Lambda_{PbCl^+}) \qquad (1.4.15)$$

The existence of the $PbCl^+$ ion-pair was confirmed by observations of Fromherz and Lih[75,76] of ultra-violet absorption bands at 209 and 227 nm, which were attributed to Pb^{+2} and $PbCl^+$, respectively.

The behaviour of unsymmetrical ion-pairs as a function of pressure has been reported by Fisher and Davis[47] for $LaSO_4^+$, and by Fisher and Fox[45] for $NaSO_4^-$. The dissociation constant for $LaSO_4^+$ was calculated from conductivity data by using a mixture rule in which the solution is regarded as a mixture of a 1-2 salt $(LaSO_4)_2SO_4$ at equivalent concentration x and a 3-2 salt $La_2(SO_4)_3$ at an equivalent concentration C-3x. The observed equivalent conductance of the solution is then

$$\Lambda = (x/C)\Lambda_{1,2} + \left[(C-3x)/C\right] \Lambda_{2,3} \qquad (1.4.16)$$

This equation was solved for x by successive approximations of x to give the observed conductivity. The equivalent conductivities $\Lambda_{1,2}$ and $\Lambda_{2,3}$ were determined from the Debye-Hückel-Onsager equation as well as from an extended form of this equation adapted by Davies, Otter and Prue[78] for use at elevated pressures. The limiting equivalent conductivity of $LaSO_4^+$ was estimated as 23.2. This value was chosen because it gave dissociation constants which were virtually independent of concentration. The pressure coefficient of the dissociation constant led to a partial molal volume for $LaSO_4^+$ at 1 bar. in the range -0.9 to +0.2 $cm^3\ mol^{-1}$. Fisher and Fox[45] have studied the pressure dependence of the dissociation constant of the 2-1 ion-pair, $NaSO_4^-$, utilizing the method described above. The solution is assumed to consist of a uni-univalent salt $Na^+\ (NaSO_4)^-$ with an equivalent conductance of Λ_2 and

a uni-bivalent salt Na_2SO_4 with an equivalent conductance Λ_1. The observed equivalent conductivity is expressed as $\Lambda = 0.5\beta\Lambda_2 + (1-\beta)\ \Lambda_1$, where β is the degree of association and Λ is the measured equivalent conductance. The authors estimated the limiting equivalent conductivity of $NaSO_4^-$ to be $0.5\ \Lambda^\infty\ [SO_4^{2-}]$. The volume change for the ion-pair dissociation was calculated at 1 bar to be 8.25 $cm^3\ mol^{-1}$, which gives a partial molar volume of 27.85 $cm^3\ mol^{-1}$ for $NaSO_4^-$.

The method of Fisher has been applied in this work to the conductivity data of $PbCl_2$ solutions at pressures up to 2200 bars. The results and method are discussed in detail in Chapter 5.

CHAPTER 2

EXPERIMENTAL

Introduction

The apparatus necessary for generating moderately high pressure (e.g. < 3000 bars) is available commercially. This equipment can be modified in a simple manner to meet the special experimental requirements of research in electrode processes. For this purpose, the head of the high pressure vessel must be machined to accept a second head, which contains the required electrical connections. The electrochemical cells must be able to respond to changes in volume associated with pressure changes, without breakage and ingress of the pressurizing fluid.

2.1 High Pressure Apparatus

The system consists of a high pressure bomb rated to 10,000 bars* (High Pressure Equipment Co., Inc.). Into the head of the bomb was fitted a second, smaller head which accomodates 5 pairs of electrical connections. In order to prevent trace leakage of the pressurizing fluid around the wires at elevated pressures, a teflon sleeve containing freshly prepared epoxy resin is placed around each pair of electrical leads on the high pressure side of the head. The bomb is then pressurized up to 2500 bars thus forcing the epoxy into any open spaces around the wires. This technique was found to prevent pressure leaks at the weakest spot in the bomb. The pressurizing fluid was di-octyl-sebacate (B.A.S.F.).

---

* The derived unit of pressure in the SI convention is the $N\ m^{-2}$ (or Pa for Pascal); 1 bar = $10^5\ N\ m^{-2}$. In the present work, the more familiar unit, the bar, will be employed as most other comparative data are expressed in this unit.

FIGURE 2.1.1 Photograph of the high pressure apparatus.

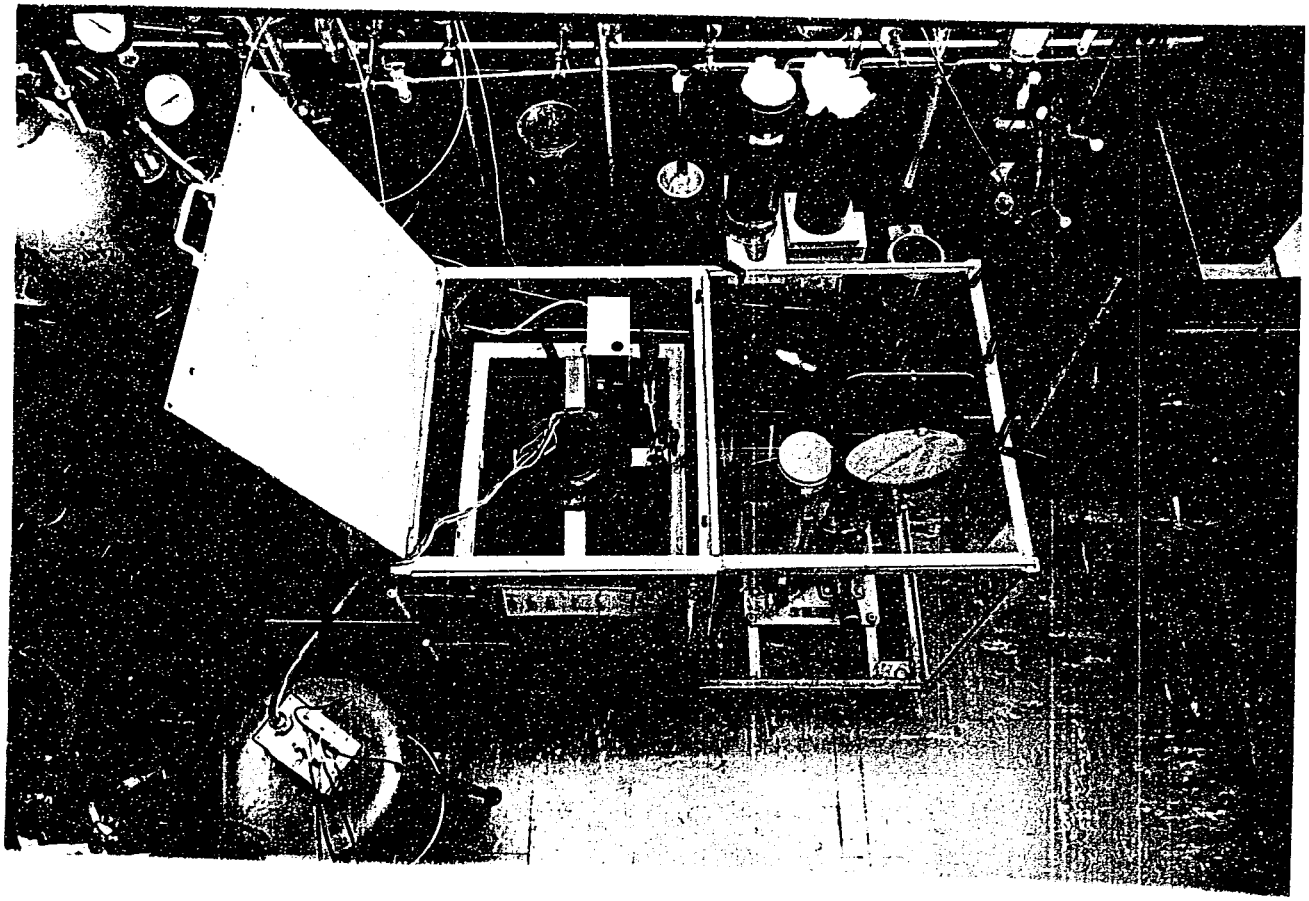

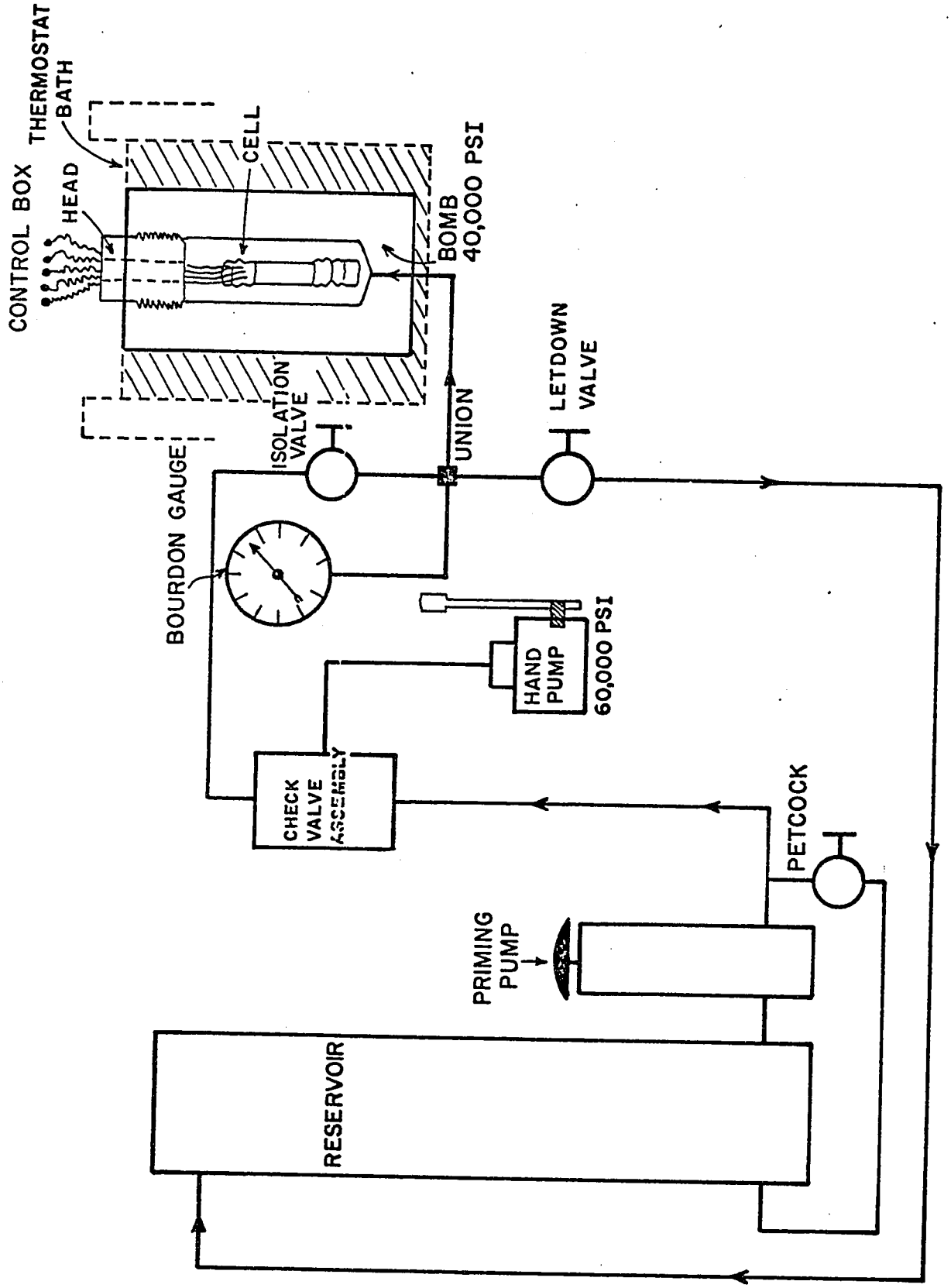

FIGURE 2.1.2 A schematic diagram of the high pressure apparatus.

The bomb is pressurized by means of a hand pump supplied by Pressure Products Industries and thermostated by a large water bath at $24.96^{o}C \pm 0.02^{o}C$. The bath consists of a refrigerator coil thermally opposed by a heater, controlled by a thermo-regulator. The bath is provided with two powerful stirrers. The pressure is monitored by an 8-inch Heise Bourdon gauge, previously calibrated against a pressure-balance apparatus. Calibrations were made at the N.R.C. high-pressure laboratory.

The high pressure apparatus is assembled and enclosed in a specially constructed armoured trolley which provides mobility as well as isolation in the case of an inadvertent pressure release. A general view of the apparatus is shown in Figure 2.1.1. A schematic diagram of the apparatus is shown in Figure 2.1.2.

2.2 Electrochemical Cells for Use at High Pressures

The electrochemical cells are designed to meet the requirements of the individual high pressure experiment. After several designs of high pressure cells proved to be inadequate, the following type was found to be satisfactory. The cell consists of two pyrex end-pieces joined by 2x heat-shrinkable teflon tubing. The top of the cell contains the electrodes varying in number from 2 to 4, depending on the type of system under examination. All the electrode leads are made of platinum wire, which is hammered flat and sealed into the pyrex glass tops of the cells. This type of metal-glass seal was found to withstand repeated elevation of pressure to 2500 bars without development of any leaks or cracks.

The bottom of the cell is a glass cup with a threaded opening for introducing the electrolyte. A screw cap with a teflon plug insert and teflon-covered O-ring was used to make a high pressure seal. Both

the top and bottom of the cell had ridges which allowed a positive teflon-to-glass seal to be made when the two pieces are joined with the shrinkable teflon tubing. This type of cell can easily tolerate a 30% volume change without undue strain being generated.

The cell utilized for high-pressure EMF measurements consists of 3 reversible electrodes, two of which are of the same type. This provides a reliable check on the behaviour of each electrode while in the high-pressure environment. For example, if the cell is Pt, H_2|HCl| Pd-H, Pd, the potential of the palladium-hydrogen electrode can be measured, in turn, against the two Pt, H_2 electrodes. The potential between the two Pt,H_2reference electrodes was also measured periodically. Thus, three EMF measurements are obtained at each pressure. This type of cell is illustrated in Figure 2.2.1.

The cell for electrode kinetic studies at elevated pressures consists of the standard 3-electrode arrangement with the reference electrode, usually palladium, situated in a Luggin capillary adjacent to the working electrode. The counter-electrode is a cylinder of platinum gauze having the standard design used in a.c. impedance measurements. The high pressure cell for electrode kinetic studies of the redox couple $Fe(CN)_6^{-3}/Fe(CN)_6^{-4}$ is illustrated in Figure 2.2.2.

An assortment of high pressure conductivity cells, fabricated from glass or teflon, has been described in the literature. In review articles, Hamann[41] and Horne[43] have critically evaluated the various cell designs. The cell design adopted in this work is based on the requirement that the cell constant remains independent of pressure as pressure is varied [79]. This is achieved by using a concentric electrode arrangement, consisting of a central wire surrounded by a ring. The electrodes were made from platinized platinum. The main body of the cell is made of a

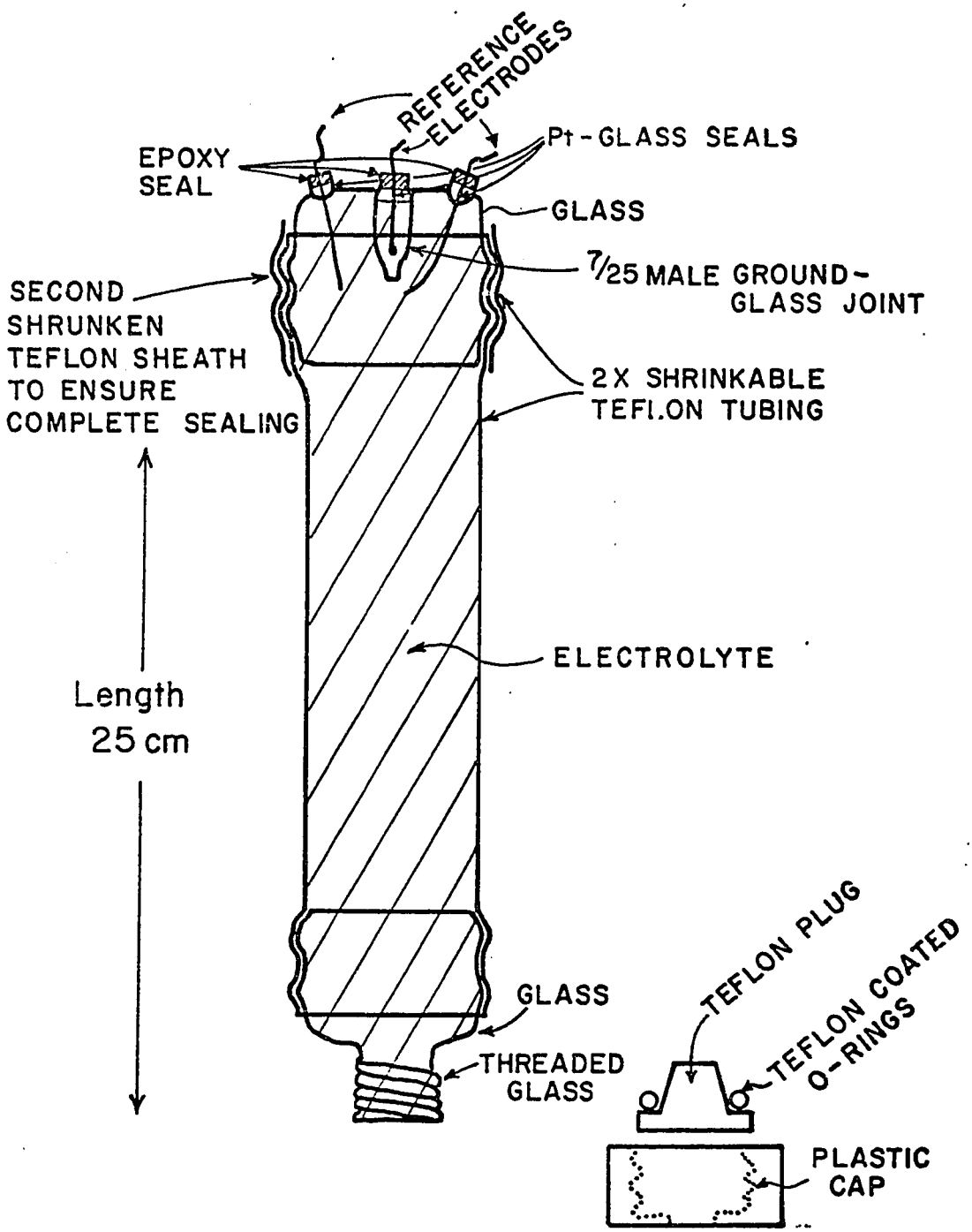

FIGURE 2.2.1 High pressure cell for EMF measurements. The cell is fabricated from heat shrinkable tubing and glass. The cell contains 3 reversible electrodes of which 2 are of the same kind.

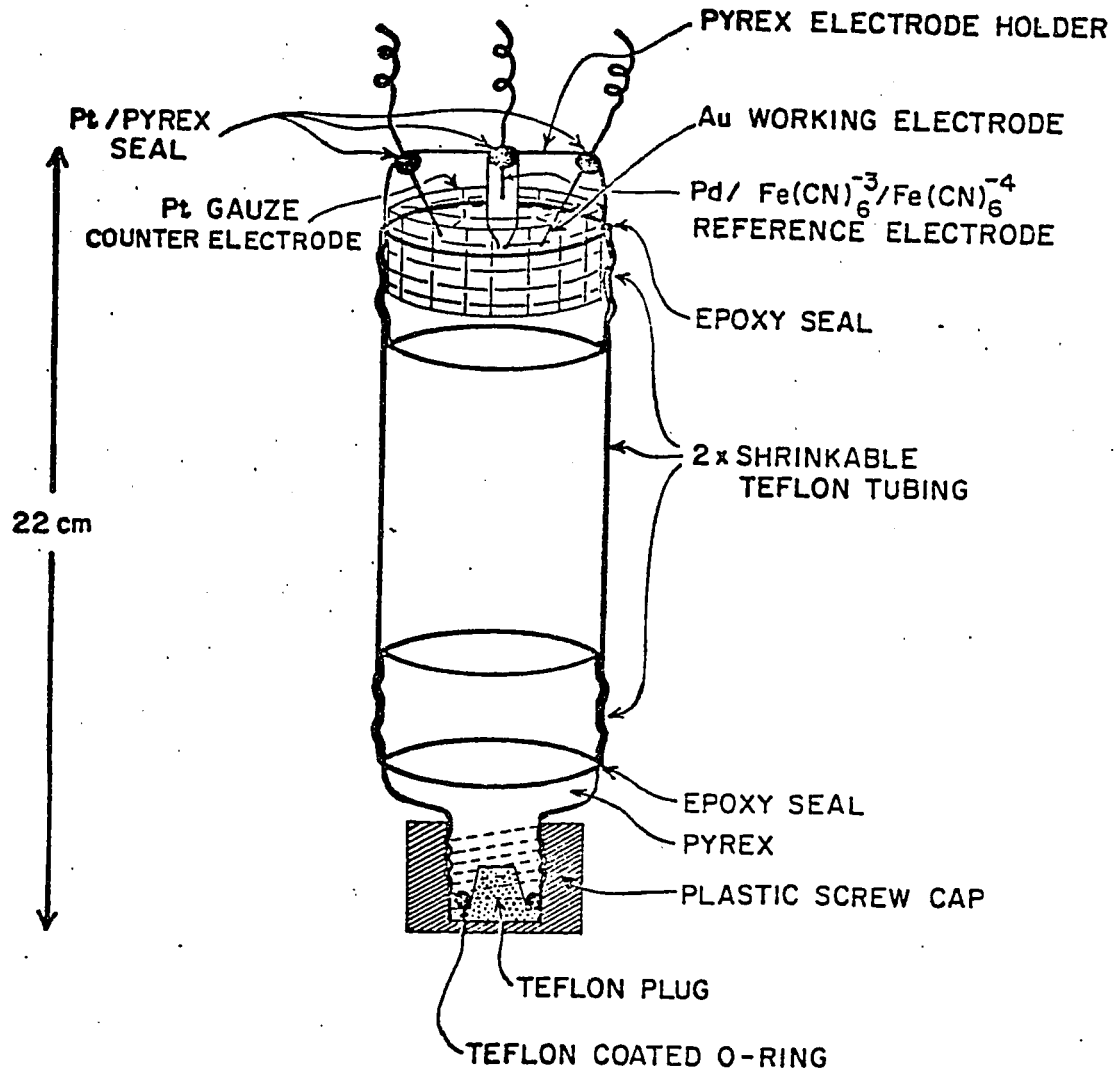

FIGURE 2.2.2 High pressure cell for kinetic measurements. The cell consists of a large cylindrical counter electrode(Pt gauze), a Pt or Au working electrode and a Pd-H,H^+ or Pd/$Fe(CN)_6^{3-}$,$Fe(CN)_6^{4-}$ reference electrode.

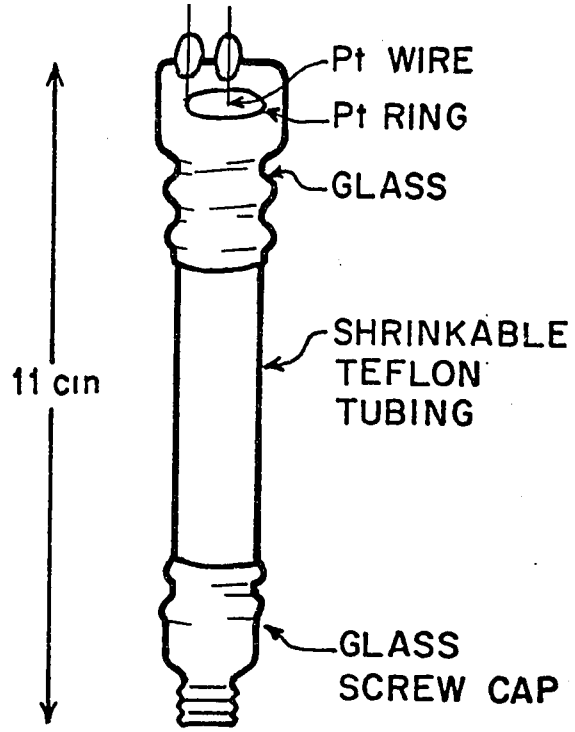

FIGURE 2.2.3 High pressure cell for conductivity measurements. The cell contains 2 platinized platinum electrodes in a concentric arrangement.

FIGURE 2.2.4 Photograph of the conductivity cell for use at elevated pressures.

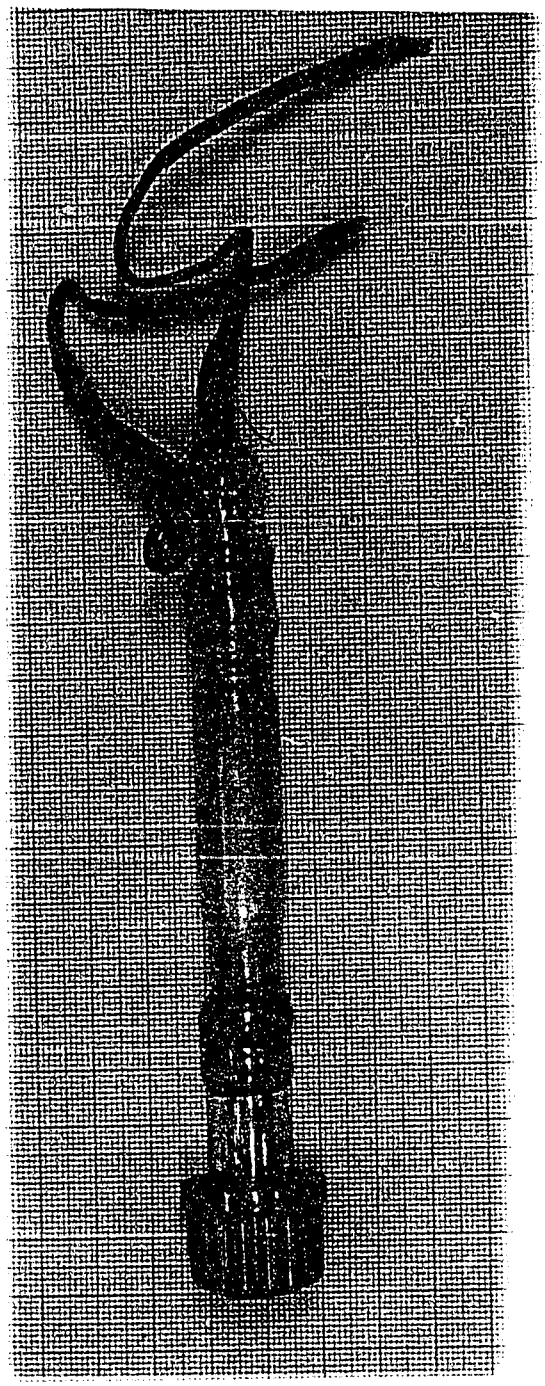

glass top which accommodates the two electrodes and is joined to a glass cap by about 3" of 2x heat-shrinkable teflon tubing. The cell constants were found to be independent of pressure up to 2200 bars. This cell is illustrated in Figures 2.2.3 and 2.2.4.

The study of the electrochemical behaviour of lead electrodes at high pressures presents a problem in the design of the cell. This arises because lead cannot directly be sealed into glass in the same manner as platinum wire. This drawback was overcome by utilizing a cell-top machined from teflon into which three electrode holders could be screwed. This cell was a major improvement over the previously described 3-electrode cells, since the electrodes could be easily interchanged without the manufacture of a new glass cell-top each time. The cell-top was provided with a Pt-gauze counter-electrode, a Pd, Pd-H or Ag, AgCl reference electrode and the lead working electrode. The cell-top is illustrated in Fig. 2.2.5. The remainder of the cell was assembled in the same manner as in the cases of the cells previously described.

2.3. Electrode Preparation

1. Reference Electrodes

Difficulties arise in the choice of reference electrodes for use in high-pressure electrochemistry. Gas electrodes such as the Pt,H_2 system have been studied by Hainsworth and co-workers[48]. The results of their work indicates that a large change in cell EMF arises as a function of pressure which is principally due to the increase of fugacity of the H_2 gas.

However, a Pt, H_2 electrode exerting its own 1 atm. initial pressure of H_2 has been shown by a number of workers to be a suitable reference electrode for high-pressure studies. The Pt, H_2 (1 bar),

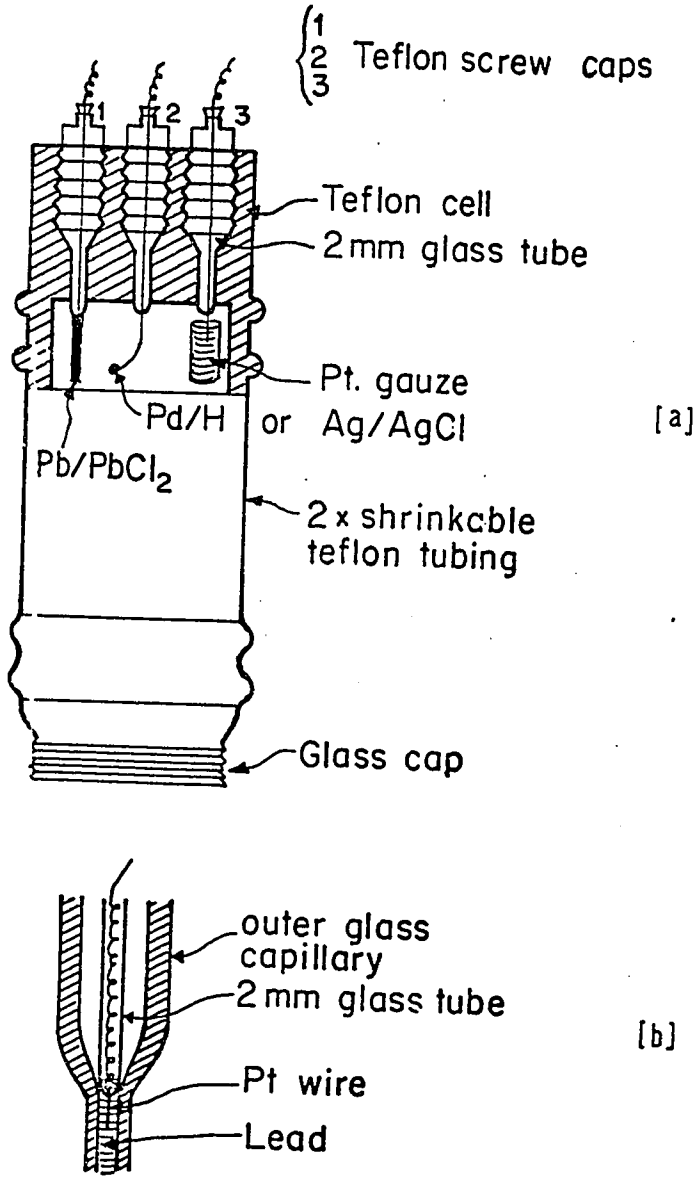

FIGURE 2.2.5 a) High pressure cell (top) for evaluating the electrochemical behaviour of Pb in Cl^- and SO_4^{2-} solutions.

b) Preparation of the Pb electrode for use in the high pressure cell. After the Pb has solidified, the outer glass capillary tube is carefully broken to expose the Pb electrode.

Ag, AgCl and Pd, Pd-H reversible electrodes were chosen as being the most suitable for electrochemical studies at high pressures in the present work.

2.3.1. (i) The Pt, H_2 Electrode

The hydrogen electrode was prepared by cleaning the Pt wire (in the high pressure cell-cap) in warm aqua-regia solution, followed by thorough washing in pyro-distilled water. The high-pressure cell was filled with a platinizing solution containing 3 g of platinum chloride in 100 cm^3 of pyro-distilled water. A second platinum electrode was placed in the cell and was connected through a D.C. power supply to the electrode to be platinized. The current was adjusted to approximately 5 mA cm^{-2}, so that there was only a slight evolution of gas (H_2 and Cl_2); the direction of the current was reversed every minute and the plating was allowed to proceed until a moderately thick coating of greyish-black platinum was obtained. The electrode was then repeatedly washed with tap water, followed by several washings in pyro-distilled water.

2.3.1.(ii) The Pd, Pd-H Electrode

A palladium electrode was built into the high pressure cell by welding a piece of palladium wire to a platinum wire. The platinum was then sealed into the high pressure cell cap. The electrode was cleaned thoroughly with concentrated sulfuric acid and washed with pyro-distilled water. The Pd, Pd-H electrode was prepared by constant current cathodic electrolysis in 0.5 M H_2SO_4. The electrode was oxidized for 1 minute, followed by a 90 second reduction both at a current density of 200 mA cm^{-2}. This cycling procedure was continued for approximately 10 minutes with termination of the electrolysis in the cathodic direction.

The electrode was then washed with pyro-distilled H_2O. This electrode was activated in this manner at the beginning of each experiment.

2.3.1.(iii) The Ag, AgCl Electrode

The silver, silver chloride reference electrode was prepared from a piece of silver wire. The silver was welded to a platinum wire which was then sealed into the high-pressure cell. The electrode was cleaned with concentrated sulfuric acid, followed by repeated washings with pyro-distilled water. Anodic deposition of AgCl on the silver wire was carried out by electrolysis from a 1 M aq. HCl solution at a current density of 1.0 mA cm^{-2} for 30 minutes.

2.3.2 Working Electrodes

(i) Lead Electrodes

This type of electrode was prepared from a spectroscopically-pure rod of lead in the following manner. A small portion of lead was cut from the metal rod and placed in a porcelain crucible which was set up in such a way as to allow a large flame of purified hydrogen gas to be directed onto the top of the metal in the crucible. The crucible was also heated from the bottom by means of a bunsen burner until the metal became molten. The metal remained in the crucible with a brilliant clear liquid surface, like that of mercury, due to the hydrogen flame which served to exclude oxygen and prevent oxidation of the Pb surface. The molten lead was then drawn up into a capillary tube which contained a platinum wire sealed into a smaller diameter capillary.

The molten lead immediately solidifies upon contact with the inner glass tube. The outer tube was carefully broken to provide a cylindrical lead rod of variable length. The electrode was fitted into

a Teflon insert plug and secured in the teflon/glass high pressure cell cap described earlier and shown in Figure 2.2.5 (a). The details of the Pb electrode assembly are shown in Figure 2.2.5 (b).

2.3.2.(ii) Lead Electrode for Rotating Electrode Measurements

In some experiments designed to measure the oxidation/reduction charge balance in the formation and reduction of $PbCl_2$ and $PbSO_4$, where some dissolution of $PbCl_2$ or $PbSO_4$ can occur, it was necessary to establish the extent of loss of Pb ions by means of experiments at a rapidly rotating electrode. For these experiments, the Pb electrode was prepared in a H_2 flame, as described above, by drawing molten Pb up into a capillary tube. The liquid Pb solidified upon contact with the Pt wire lead. The end of the capillary was then cut with a diamond saw and mechanically polished with 3M tungsten carbide followed by diamond grit paper. The electrode was then thoroughly washed with double-distilled H_2O. The area exposed was approximately 0.01 cm^2.

2.3.2.(iii) Gold Electrodes

The gold electrode was built into the high pressure cell by first sealing a length of gold wire to a platinum bead which had previously been sealed into the pyrex cell-cap. The electrode was cleaned in aqua-regia for 1 minute, followed by thorough washing with pyro-distilled water.

2.3.2.(iv) Pt-Gauze Counter Electrode

This type of electrode is made of platinum gauze and is in the form of a large cylinder. The cylinder was of the same diameter as the inside of the high pressure cell so that the counter electrode was securely located. The complete high pressure cell for electrode kinetic

studies is illustrated in Figure 2.2.2.

2.3.3. Solutions*

Pyro-distilled water was used for all solutions and for the re-crystallization of the salts used. The quality of this water has been discussed elsewhere by Conway and co-workers.[80] The use of this type of water is desirable for most surface-electrochemical work (see Section 2.3.3. (vi).

(i) Sulfuric Acid Solutions

H_2SO_4 solutions were utilized in several phases of this work, including equilibrium EMF measurements of the Pt, H_2| 0.5M H_2SO_4|Pd-H, Pd cell and studies on the electrochemical behaviour of lead and platinum in 0.5M H_2SO_4. The acid solutions were made up volumetrically from BDH Aristar H_2SO_4 (a very high purity grade) and pyro-distlled water. The electrochemical purity of these solutions was found to be excellent as indicated by the i-V behaviour of the platinum electrode in a cyclic voltammetry experiment.

2.3.3 (ii) HCl Solutions

The interpretation of electrochemical kinetic and other electrochemical processes at high pressures requires knowledge of the dependence of reference electrode potentials on pressure, as was discussed in Chapter 1. The pressure dependence of the EMF of the cell

Pd, Pd-H|HCl|Ag, AgCl

---

* The derived unit of concentration in the SI convention is mol m^{-3}; however in this thesis M refers to concentration in units of mol dm^{-3}.

was measured in aq. HCl at concentrations of 0.01, 0.25, 0.50, 0.75 and 1.00 M. Hydrochloric acid solutions were prepared volumetrically from BDH Aristar grade HCl and pyro-distilled H_2O.

2.3.3. (iii) K_2SO_4 Solutions

The effect of elevated pressure on the electrode kinetic behaviour of the redox couple $Fe(CN)_6^{-3}/Fe(CN)_6^{-4}$ was studied in 0.5M K_2SO_4 + 0.2M H_2SO_4. The addition of sulfuric acid to the salt solution was to maintain a well-defined pH. This was found to be necessary because of the instability of the working electrode potential due to local changes in pH at the electrode-solution interface. The K_2SO_4 was purified by triple recrystallization in pyro-distilled H_2O. The 0.5M K_2SO_4 solution was prepared volumetrically.

2.3.3. (iv) KCl Solutions

A suitable electrolyte solution was required in the study of the behaviour of $Pb,PbCl_2$ electrodes which are used in sea-water activated batteries (see p.27 , Chapter 1). In order to simplify the sea-water electrolyte system, aq. KCl solution was used whose behaviour as a function of pressure has been well characterized in other published work.

The KCl solutions were prepared volumetrically from 3x re-crystallized KCl and pyro-distilled water. The electrochemical behaviour of lead was studied in 1 M KCl + 0.01 M HCl. The cell constant for the conductivity cells was determined using 0.01 m KCl as a standard solution.

2.3.3 (v) $PbCl_2$ Solutions

An important result of elevated pressure on the behaviour of anodic films of $PbCl_2$ or $PbSO_4$ can be a substantial increase of the solubility of the anodically formed film. This arises because the sums of partial molar volumes of Pb^{2+}, Cl^- or SO_4^{2-} ions are,in general, smaller than the corresponding molar volumes of the solid phases.

The solubility is best measured *in situ* by means of conductivity measurements. Aqueous lead chloride solutions were studied at several concentrations from 0.001M up to the saturation concentration of 0.0388M. The solutions were prepared volumetrically from analytical reagent grade $PbCl_2$ and pyro-distilled H_2O.

2.3.3(vi) Pyro-distilled H_2O

In recent years, both in North America and in Europe[80], it has been found to be increasingly difficult to prepare pure water free from organic, surface-active contaminants by means of distillation, even from alkaline $KMnO_4$.

The organic contaminants now commonly present in many domestic and industrial water supplies are steam-volatile and are hence not removed by distillation. Conway and co-workers[80] have developed a pyro-distillation technique for further purifying regular Barnstead distilled water, which meets the criteria required for use in electrochemical measurements. The principle involved in pyro-distillation is pyrolysis of organic impurities by passage of the steam through a column of silica at 750^{o}C in a stream of oxygen. The hot column contains a 90% Pt/Rh gauze which provides an efficient zone for the catalytic oxidation of organic impurities. The pyro-distillation unit is shown in Figure 2.3.1.

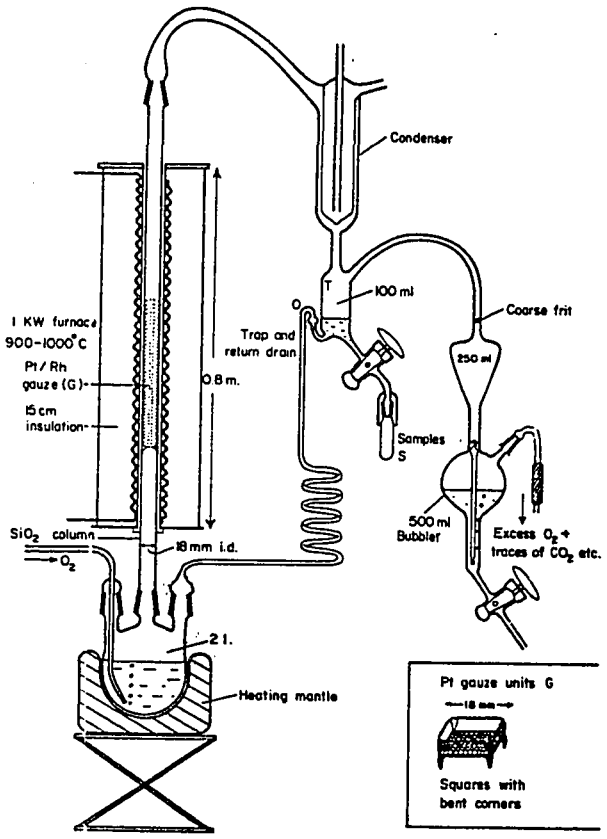

FIGURE 2.3.1 Schematic diagram of the apparatus for the pyrodistillation of water.

Initially, directly-distilled water from a regular aq. $KMnO_4$ still is placed in the boiling pot. The pyro-still was then operated so as to recycle the water through the catalytic furnace for 48 hours with purified O_2 passing through at about 1 $cm^3\ s^{-1}$. The apparatus was provided with a Soxhlet type overflow syphon which returns 100 cm^3 volumes of condensed pyro-distilled H_2O back to the distilling pot every hour. The distillation was continued for 48 hours before the purified H_2O was collected for use in the experiment.

The purity of such water for electrochemical measurements has been discussed by Conway et al.[80] in terms of surface purity and H-adsorption behaviour at Pt in solutions prepared from pyro-distilled H_2O. The specific conductance of this water at ambient pressure was too low to be measured by the a.c. conductivity bridge utilized in this work. The conductivity of pyro-distilled water was consistently less than $10^{-7}\Omega^{-1}cm^{-1}$; therefore a solvent correction was not necessary in the conductance experiments.

2.4 Experimental Procedures

1. Cell Preparation

All electrochemical cells, including those used at ambient and high pressures, were washed in concentrated sulfuric acid for several hours, followed by thorough rinsing in doubly-distilled H_2O. The cells were then filled with pyro-distilled H_2O and allowed to soak overnight. The electrochemical cells for high-pressure measurements were placed in a glove bag which was under a positive pressure of nitrogen. The solutions were degassed (to remove O_2) with pre-purified N_2 in the glove bag. The

cells were then filled with the appropriate solution and allowed to soak for 30 minutes. The cell was then emptied, rinsed a second time and filled with the solution required for the experiment. The cell was then sealed with the lower screw cap.

In the case of equilibrium EMF measurements involving a Pt,H_2 reference electrode, the electrolyte was presaturated with the H_2 gas at ambient pressure. The cell was then filled with electrolyte and H_2 gas was again passed through it for 15 minutes. Several small bubbles of H_2 gas were allowed to remain in the cell after the cell had been sealed, in order to ensure that the Pt,H_2 electrode remained in a well-defined state at elevated pressures.

2.4.2. High Pressure Measurements

(i) General

After the high pressure cells had been removed from the glove bag, the electrical leads of the cell were soldered to those on the interior of the head of the pressure vessel. The electrical connections were then insulated with heat-shrinkable tubing. The electrical connections on the high-pressure side were colour coded to match the electrical leads on the exterior of the head. The electrical leads on the outside of the bomb were plugged into a control box, which was connected to the appropriate monitoring apparatus.

(ii) Equilibrium EMF Measurements

The effect of pressure on the cell EMF of a number of pairs of reversible electrodes was examined in order to obtain reference electrode data for electrodes suitable for use in the high pressure electrode kinetic measurements. The pressure coefficient $(\frac{\partial \Delta E}{\partial P})_T$ was determined for the following couples:

Pd,Pd-H vs. Pt,H_2 (1 bar) in 0.5M aq. H_2SO_4

Pd,Pd-H vs. Pt,H_2 in 1 M aq. HCl

Pd,Pd-H vs. Ag,AgCl in 1.0, 0.75, 0.50, 0.25 and 0.01 M aq. HCl

Pt,H_2 vs. Ag,AgCl in 1 M aq. HCl

The reference electrodes were prepared by well-known electrochemical methods as discussed in the earlier subsection 2.3 on electrode preparation. After the cell had been assembled and connected electrically to the leads in the head of the bomb, it was placed in the high pressure apparatus. The cell was then allowed to come to thermal equilibrium before any EMF measurements were made. The EMF measurements were monitored with a digital voltmeter (Dana Laboratory, Inc. Model 4300). Elevated pressures were then applied only if the cell EMF at ambient pressure varied less than 100 μV during the last 1 hour of the 3 hour equilibration period. If this condition was met, the pressure was slowly increased in increments of 276 bars, up to a maximum of 2210 bars. The appreciable heat of compression which is generated was allowed to dissipate for a period of 2 hours at each pressure before the EMF values were measured. After the maximum pressure had been reached, the system was decompressed in steps of 276 bars, and the EMF values were again measured after the normal equilibration period at each pressure.

The pressure coefficient of EMF, $(\frac{\partial \Delta E}{\partial P})_T$, at 1 bar for each pair of reference electrodes was determined graphically from plots of the measured EMF values vs. pressure.

2.4.2 (iii) Electrode Kinetic Studies at Elevated Pressures

(a) A.C. Impedance Apparatus: The pressure-dependence of the electrochemical rate constant for the redox couple ($Fe(CN)_6^{-3}/Fe(CN)_6^{-4}$)

at equimolar concentrations was evaluated at a gold electrode in 0.5M K_2SO_4 + 0.2M H_2SO_4 solutions. For the study of such fast reactions which proceed under partially diffusion-controlled conditions, it was necessary to utilize a fast transient method or a 'relaxation technique' such as the impedance method. Various procedures can be adopted for the latter measurements, e.g.,

a. use of an a.c.wheatstone bridge

b. use of a phase-sensitive voltmeter circuit (Randles)

c. use of a phase-sensitive lock-in amplifier system

and

d. use of d.c. polarization at a rotating disc electrode.

The a.c. impedance technique is convenient for in situ measurements such as are required in high pressure systems and can be adapted for use with simultaneous potential sweep (cyclic voltammetry) [81, 82] experiments. Such a procedure was used by Conway and Tilak[83] for study of the behaviour of silver oxide electrodes. This technique is a modification of a.c. polarography which provides in-phase and out-of-phase current read-outs for study of fast electrode processes. The method gives impedance information continuously over a range of potentials with the real (ohmic) and imaginary (capacitative) components of the impedance being simultaneously recorded as a function of 'd.c.' potential at various a.c. frequencies.

The system used in the present work was built up from a P.A.R. phase-sensitive amplifier, operating in conjunction with a potentiodynamic sweep apparatus employing a Servomex (LF151) triangular function generator. A.c. modulation signals of 10 mV peak-to-peak amplitude were generated by a Hewlett-Packard oscillator and mixed with the linear potential sweep signal in an operational amplifier (Tektronix

O-type). The phase-sensitive amplifier enabled the current components 0^{o} and 90^{o} out-of-phase with the modulating voltage to be separately recorded; they are equivalent to the reciprocals of the impedance components of the overall equivalent circuit for the working electrode.

A block diagram of the circuit is shown in Figure 2.4.1. The method utilizing phase-sensitive current detection offers some considerable advantages over the standard bridge methods (a) with respect to balancing problems in the presence of a.c. noise and (b) with respect to the continuous read-out as a function of d.c. potential in a potential-sweep scan. Initial a.c. measurements were made with a bridge but severe problems with the balancing were found under low-resistance and high-frequency conditions. The a.c. impedance method with phase-sensitive detection was found to perform quite satisfactorily in the frequency range chosen for this work (25 s^{-1} to 250 s^{-1}).

2.4.2 (iii) (b) Evaluation of the Cell Impedance. The electrochemical cell for high-pressure a.c. impedance measurements consisted of a gold working electrode, a cylindrical platinum gauze counter-electrode and a palladium $Fe(CN)_6^{-4}/Fe(CN)_6^{-3}$ reference electrode. The palladium electrode in the presence of equimolar concentrations of ferro-ferricyanide readily attains the reversible potential of the redox couple. The cell was placed in the bomb and allowed to equilibrate for 1 hour before the first measurements were obtained.

The overall cell impedance was evaluated in terms of the resistance and capacitance components in the following manner. The response of the system to d.c. cyclic voltammetry was first recorded in the form of i-V profiles on a Hewlett-Packard X-Y recorder. The

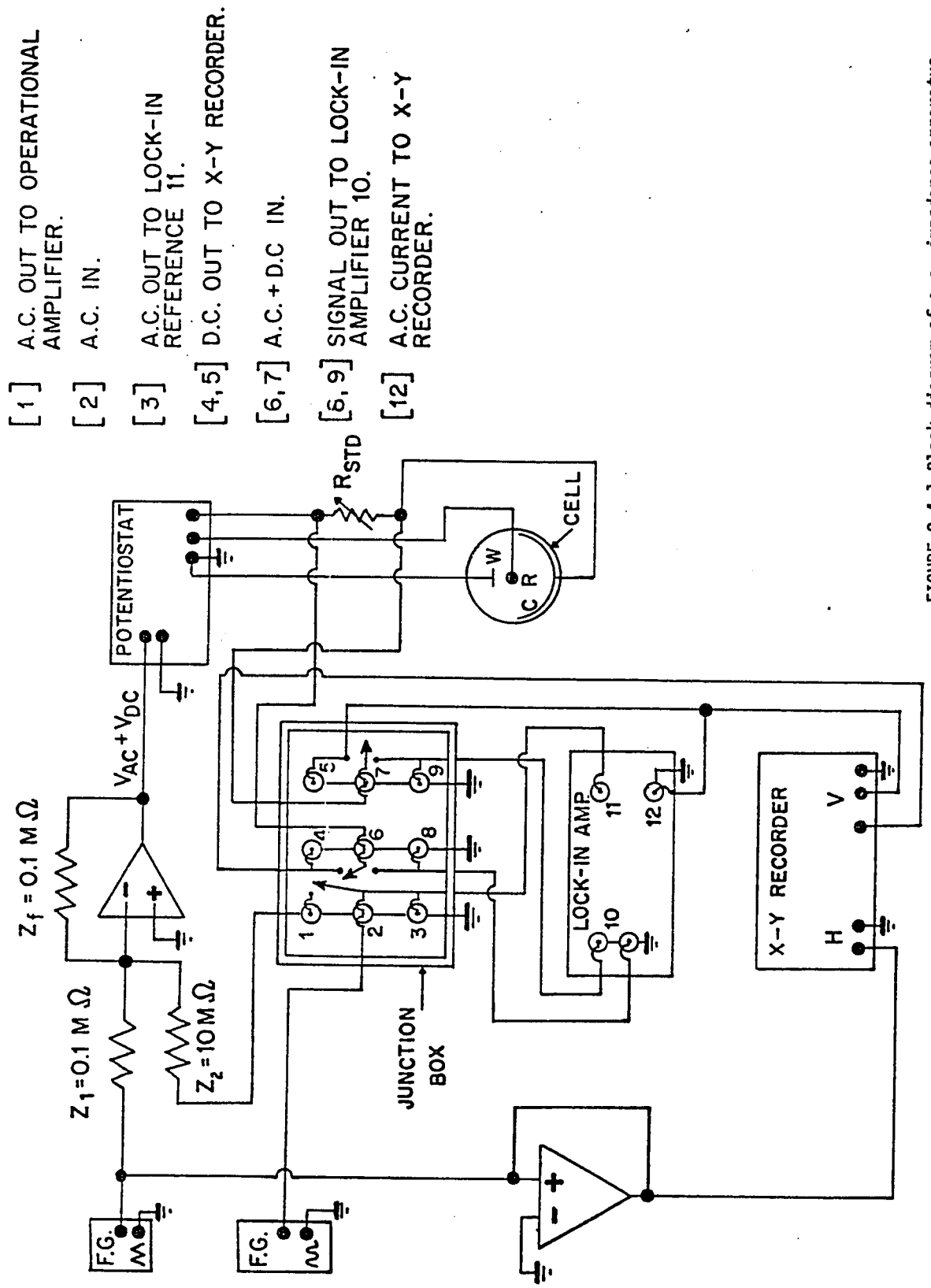

FIGURE 2.4.1 Block diagram of a.c. impedance apparatus.

sweep rate was 20 mV s^{-1} and the potential range scanned was -0.500 V to + 0.200 V vs. Pd, $Fe(CN)_6^{-4}/Fe(CN)_6^{-3}$. A small a.c. signal (10 mV) of fixed frequency was then superimposed on the d.c. signal and the in-phase component of the a.c. current was recorded as a function of 'd.c.' potential. This procedure was repeated for the remaining frequencies with all the i-V profiles being recorded on the same graph paper. The out-of-phase component was evaluated in the same manner. The above procedure was repeated in order to evaluate the reproducibility of the system, which was usually excellent if fresh ferri-ferrocyanide solutions were employed. The a.c. measurements were then performed at pressure intervals of 550 bars up to a maximum pressure of 2200 bars. The cell impedance was also evaluated at several intermediate pressures during decompression of the bomb. At each pressure, time for thermal equilibration was allowed as in the reversible EMF measurements.

It should be noted here that the impedance data was obtained in the form of a.c. current peaks as the 'd.c.' potential was swept through the half-wave potential of the redox system. The out-of-phase component gives the double-layer capacity over the potential range where no redox reaction occurs.

c) Comments on A.C. Measurements

In order to check the reliability of the a.c. measurements, the impedance of an R-C circuit of known resistance and capacitance was measured. This was done by measuring the in-phase ($\phi = 0^o$) and out-of-phase ($\phi = 90^o$) impedance components of a parallel circuit, having a known impedance, as a function of frequency, in the range 25 to 800 s^{-1}. For a given value of R = 100Ω and C = 5 μF it was found that the

measured resistive component was a constant value, 99.3 Ω in the frequency range 25 to 200 s^{-1}. The value of the out-of-phase component, C_p, consistently gave a value higher than the pre-set value of the standard capacitance. However, C_p exhibited a constant value of 5.22 μF between 100 and 400 s^{-1} but at higher and lower frequencies the deviation was as great as 20%. However, when the capacitative impedance and resistance were of comparable values, the error in R and C were less than 2% at all frequencies between 25 and 200 s^{-1}. The out-of-phase and in-phase components of impedance of the electrode solution interface involved in the $Fe(CN)_6^{-3}/Fe(CN)_6^{-4}$ reaction exhibit similar values of impedance as indicated by the height of the respective a.c. voltammograms.

2.4.2 (iv) Electrochemical Behaviour of Pb Electrodes as a Function of Pressure

For studies on the effects of pressure on the processes of formation and reduction of $PbCl_2$ and $PbSO_4$, cyclic voltammetry was used. The electrochemical formation, growth and reduction of the electroactive films of $PbCl_2$ or $PbSO_4$ can be conveniently followed by this technique, as well as the evaluation of anodic/cathodic charge balance in the 'charging'/'discharging' cycle.

In the mechanism of formation of $PbCl_2$ and $PbSO_4$, initial dissolution of Pb^{2+} ions, followed by precipitation and growth of the Pb^{2+} -salt layer is believed to occur. Pressure effects on the charging process will therefore involve any changes of solubility of these materials with pressure. The behaviour of the electrodes during the formation and reduction of the electroactive phases of the Pb salts may therefore be expected to depend on pressure.

2.4.2(iv) (a) Cyclic Voltammetry. Cyclic voltammetry at Pb electrodes was carried out using a Wenking potentiostat and a Tacussel 6STP2 function generator. The i-V(t) profiles were recorded on a Hewlett-Packard X-Y recorder, after conversion of the current to voltage by means of a decade resistance box. The complete electrical circuit utilized in the cyclic voltammetry experiments is shown in Figure 2.4.2.

(b) Pb,$PbCl_2$ Electrodes. The high pressure cell was assembled under a N_2 atmosphere in a glove bag and then placed in the high pressure vessel at which time the necessary electrical connections were made. The electrolyte was 1.0 M KCl + 0.01 M HCl, with a Ag,AgCl reference electrode.

Cyclic voltammetry i-V profiles for formation and reduction of $PbCl_2$ at Pb electrodes were determined at 1, 1100, and 2204 bars. The voltage was scanned between -0.350 and -0.970 V at a fixed anodic sweep rate (11 mV s^{-1}) but at different cathodic sweep rates, 11, 13, 16, 20, 27, 32, 40, 53 and 80 mV s^{-1} for each successive cycle. At each pressure, all i-V profiles were recorded on the same graph paper, as will be illustrated in Figure 5.1.1, Chapter 5.

The results were analyzed in terms of the dependence of charge balance Q_A/Q_C on sweep rate and on hydrostatic pressure. The current maximum and the potential at the current maximum were evaluated as a function of sweep rate at each pressure.

The effect of the anodic potential limit on the charge recoverable in the following cathodic sweep as a function of pressure was examined in the following manner: the applied potential was swept at 16 mV s^{-1} in the anodic direction with sweep reversal occurring at a potential more negative than that of the anodic peak. For each successive cycle, the potential limit in the anodic sweep was made

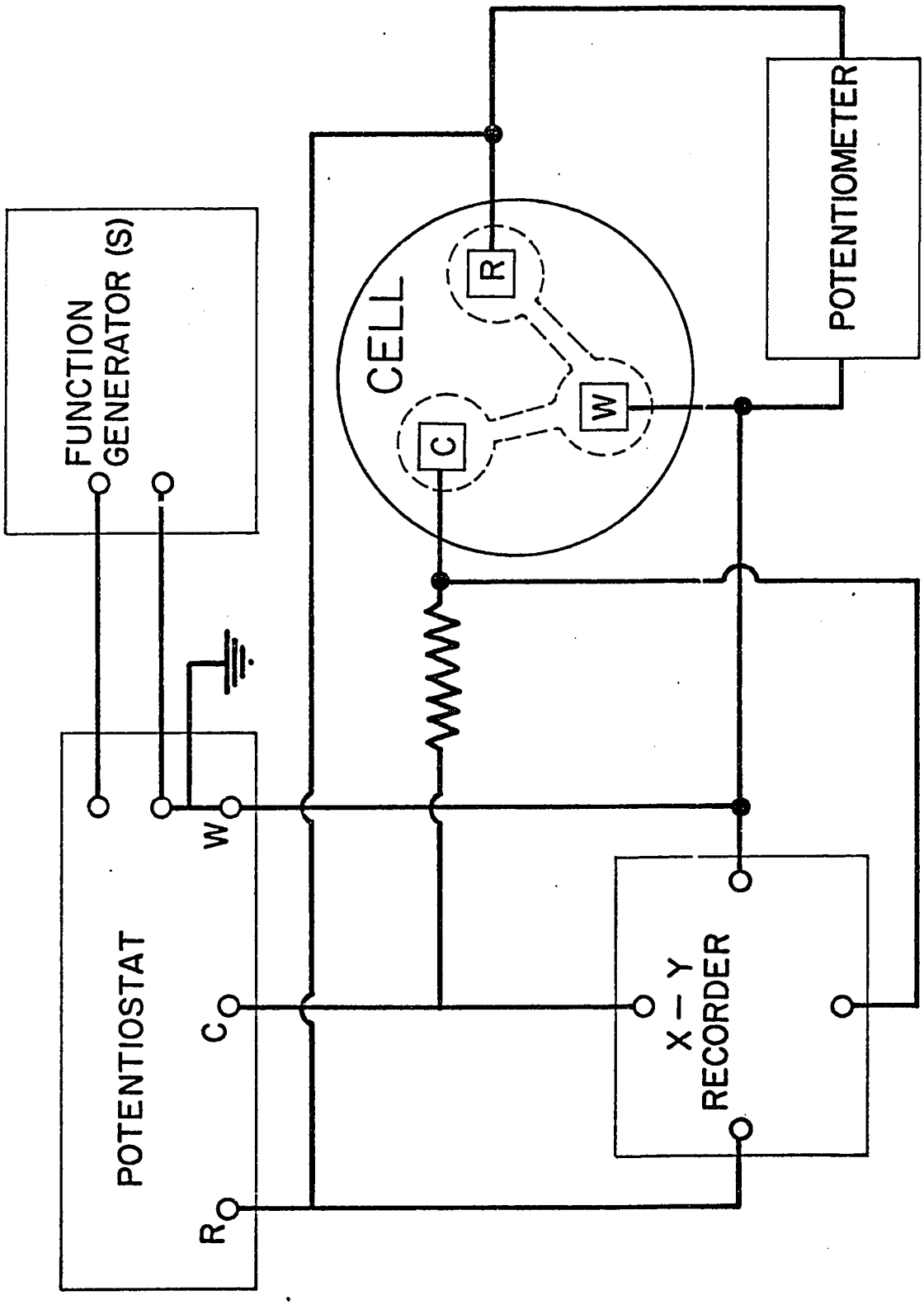

FIGURE 2.4.2 Electrical circuit employed in the cyclic voltammetry experiments.

progressively less negative in steps of 25-40 mV until the potential limit was positive with respect to the passivation peak. All i-V profiles were recorded on the same graph paper as will be illustrated in Figure 5.1.6, Chapter 5. The measurements were repeated in a similar manner at 2200 bars.

(c) Pb,$PbSO_4$ Electrodes. The effect of pressure on the electrochemical behaviour of Pb, $PbSO_4$ in 0.5M H_2SO_4 was examined by cyclic voltammetry in a way similar to that described for the Pb, $PbCl_2$ case above. The potential of the lead electrode was referred to that of the Pd-H,H^+ reference electrode.

2.4.2 (v) Pb Electrode Behaviour at Ambient Pressure

The electrochemical behaviour of $PbCl_2$ and $PbSO_4$ was studied at ambient pressure in order to provide additional information on the processes involved in film formation and reduction. If the electro - chemical behaviour of $PbCl_2$ and $PbSO_4$ electrodes is well characterized at ambient pressure, then the origin of the effect of pressure on these systems may be easier to evaluate.

2.4.2(v)(a) The Pb,$PbCl_2$ System .The $PbCl_2$ electrode was studied by cyclic voltammetry in quiescent solutions and compared to the behaviour of a rotating lead disc electrode (R D E). The R D E experiments provide information on the contribution of solution-soluble species to the processes of film formation and reduction. If the $PbCl_2$ film is sufficiently soluble, the extent of dissolution can be seen by comparison of the charge balance ratio of the respective anodic and

cathodic charges (Q_A/Q_C) at a R D E and in quiescent solutions.

2.4.2 (vi) Conductivity Measurements

The pressure dependent solubility of $PbCl_2$ was determined by conductivity measurements. The high pressure conductivity cells were described earlier in this Chapter. The conductivity bridge (Industrial Instruments, Ltd.) was operated at a frequency of 1000 s^{-1} and calibrated against standard resistances (Leeds and Northrup) at 25.0°C.

(a) Cell Constant The pressure dependence of the cell constant was determined using a 0.01 m KCl standard solution. The conductivity data of Horne[43] for KCl solutions at elevated pressures was used for standardization. The electrolyte was degassed in the glove bag, the conductivity cell was filled with the 0.01 m KCl solution, sealed and then placed in the high pressure vessel. The small size of the conductivity cells permitted more than one cell to be placed in the bomb. This allowed conductivity measurements to be carried out in duplicate.

The conductivity was measured after a 3-hour equilibration period. The pressure was then applied in steps of 550 bars until the maximum pressure of 2204 bars was reached. The conductivity was evaluated at each pressure after the usual 3-hour equilibration period. The same procedure was followed during decompression. If there was a difference of greater than 1% between the results obtained on compression or decompression, then the experiment was repeated. Similarly, if the duplicate cells showed a greater than 1% discrepancy, the run was repeated.

(b) Conductivity Measurements on $PbCl_2$ Solutions. Aqueous lead chloride solutions were studied at a variety of concentrations from 0.001 M up to the saturation concentration of 0.0388 M. Each cell was allowed, as usual, to equilibrate at each pressure before the conductivity was measured. The saturated $PbCl_2$ solutions were mechanically agitated at each pressure by a solenoid device attached to the screwcap of the cell. The cell was then allowed to equilibrate for a further 12 hours at controlled temperature before the conductivity was recorded.

CHAPTER 3

PRESSURE COEFFICIENTS OF EMF OF REVERSIBLE ELECTRODE REACTIONS

The pressure dependence of the potential of a reversible electrode reaction has been shown in Chapter 1 to be related to the volume change occurring in the half-cell reaction. Thus the pressure coefficient of EMF can be written in terms of the appropriate partial molar volumes* as

$$\left(\frac{\partial E}{\partial P}\right)_T = -\frac{1}{zF}\left(\Sigma V_p - \Sigma V_R\right)$$

Since single electrode potentials cannot be experimentally evaluated, the electrochemical cell is comprised of two reversible electrodes, whose EMF is measured as a function of pressure. The evaluation of the behaviour of certain reversible electrodes for possible use as reference electrodes in high pressure electrode kinetic studies was performed by measurements on a combination of two different reversible electrodes (eg. Ag,AgCl and Pt,H_2) in a single high-pressure cell. If the measured cell EMF is reproducible in the ascending and descending modes of compression,then the pressure coefficient of EMF should be correctly given by $-\frac{1}{zF}\left(\Sigma V_p - \Sigma V_R\right)$. Therefore, the partial molar volume of one of the components of the reaction can be evaluated if we have precise knowledge of $\left(\frac{\partial E}{\partial P}\right)_T$ and the partial molar volumes of the remaining constituents of the cell reaction. If the determination of this partial molar volume is consistent with the volumes reported in the literature, then it can be assumed that the two reversible electrodes are functioning in a thermodynamically well defined manner and therefore

* The derived unit of molar volume in the SI convention is $m^3\ mol^{-1}$ however in this thesis cm^3 mol is used to facilitate comparison with existing published data.

can be used as reference electrodes at high pressures.

3.1 The $Pt,H_2|0.5\ M\ H_2SO_4|Pd\text{-}H,\ Pd$ Cell

The EMF data, ΔE, for this particular cell as a function of pressure are listed in Table 3.1.1.

TABLE 3.1.1

EMF DATA FOR THE CELL: $Pt,H_2|0.5\ M\ H_2SO_4\ |\ Pd\text{-}H,\ Pd$

P(bars)	ΔE (compression) (V)	ΔE (decompression) (V)
1	0.0545	0.0531
280	0.0562	0.0557
560	0.0582	0.0581
840	0.0604	0.0604
1120	0.0622	0.0621
1400	0.0640	0.0642
1680	0.0659	0.0662
1960	0.0677	0.0680
2240	0.0694	0.0700
2520	0.0711	0.0711

The variation of cell EMF, ΔE, as a function of pressure is illustrated in Figure 3.1.1. The reversibility of the pressure effects is good with some small degree of hysteresis occurring only with regard to the final readings at low pressure. The slope at 1 bar is 8.6×10^{-6} V bar^{-1}. At pressures above 800 bars, the ΔE vs P plot is linear with a slope of 6.8×10^{-6} V bar^{-1}. The hysteresis is probably due to loss of molecular

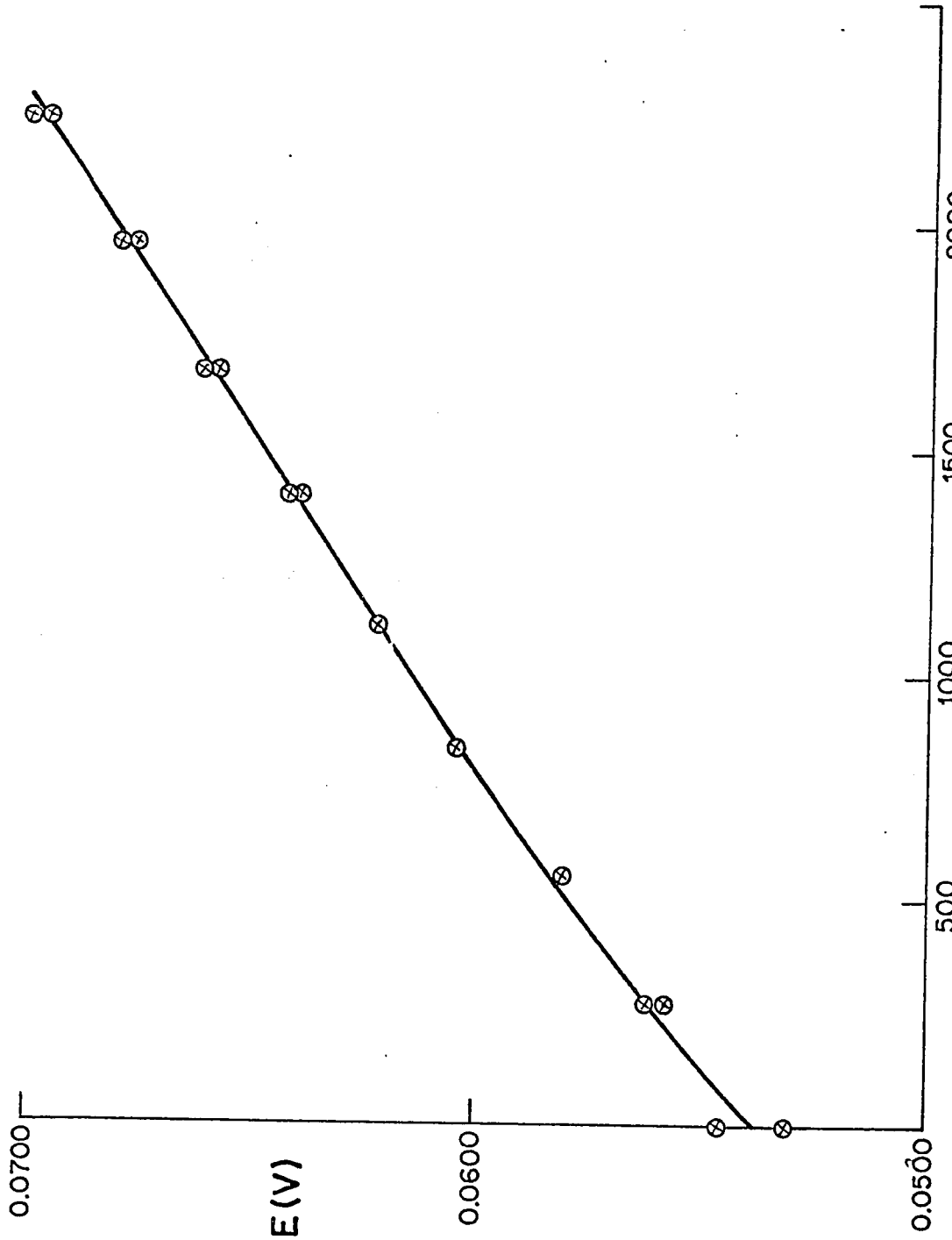

FIGURE 3.1.1 The variation of EMF as a function of pressure for the cell:

$Pt,H_2|$ 0.5M H_2SO_4 | Pd-H,Pd .

hydrogen during the course of the run by diffusion through the Teflon walls of the high-pressure cell (see below).

The pressure coefficient of EMF, $(\frac{\partial \Delta E}{\partial P})_T$ for the cell reaction

$$Pd + 1/2\ H_2 \rightarrow Pd\text{-}H \qquad (3.1.1)$$

is related to accompanying volume change by

$$(\frac{\partial \Delta E}{\partial P})_T = -\frac{1}{zF}(V_{Pd\text{-}H} - V_{Pd} - \frac{V_{H_2}}{2}) \qquad (3.1.2)$$

where $V_{Pd\text{-}H}$ and V_{H_2} are the molar volumes of H_2 and Pd-H. V_{Pd} is the molar volume of Pd. Therefore, at 1 bar, the volume change for reaction (3.1.1) is -8.3 $cm^3\ mol^{-1}$ and at pressures above 800 bars, the volume change is -6.6 $cm^3\ mol^{-1}$. The increase of the reaction volume as the pressure is enhanced is due to the pressure dependence of the partial molar volume of H_2.

Although the molar volumes of H_2 and Pd-H have not been evaluated, it can be concluded that the Pd-H, H^+ electrode provides a stable reference electrode in 0.5M H_2SO_4 at pressures up to 2500 bars. The Pt, H_2 electrode is stable to within 1 mV during the course of the experiment, but the problems associated with a gaseous reference electrode in a plastic or teflon cell are always present.

3.2 The Pt, H_2|1M HCl|Pd-H, Pd Cell

The cell EMF data as a function of pressure are listed in Table 3.2.1 from two separate experiments. The results are also shown graphically in Figure 3.2.1. The behaviour is, as expected, similar to that of the cell described in 3.1.1. The slope at 1 bar, $(\frac{\partial \Delta E}{\partial P})_T$, is 8.4×10^{-6} V bar^{-1}; at pressures above 800 bars the pressure coefficient

is constant at a value of 6.9×10^{-6} V bar^{-1}. The volume change for the reaction

$$Pd + 1/2\ H_2 \rightleftharpoons Pd - H \qquad (3.1.1)$$

is -8.1 $cm^3\ mol^{-1}$ and -6.7 $cm^3\ mol^{-1}$ at 1 bar and above 800 bars, respectively.

The measured cell EMF at 1 bar of 0.0502 V is in excellent agreement with the value of 0.0495 V reported by Schuldiner and co-workers[84]. The value of ΔE measured after the high-pressure readings, 0.0490 V, is 1 mV less than the initial value at 1 bar. This behaviour is quite similar to that for 0.5 M H_2SO_4 (Section 3.1), and therefore can be rationalized in the same manner.

3.3 The Pd, Pd-H|M HCl|AgCl, Ag Cell

The pressure coefficient of EMF for this cell was evaluated at a series of HCl concentrations, 0.01, 0.25, 0.50, 0.75 and 1.0 M HCl, in order to evaluate the behaviour of the Pd-H, H^+ and Ag, AgCl reference electrodes as a function of electrolyte concentration. This cell enables the molar volume of Pd-H to be evaluated at each HCl concentration from the appropriate pressure coefficient of EMF and known molar or partial molar volumes of aq. HCl, AgCl, Ag and Pd.

The experimental EMF data are listed in Table 3.3.1 for each HCl concentration and pressure. The EMF data as a function of pressure are also illustrated in Figure 3.3.1, where $\Delta E_p - \Delta E_1$ values are plotted with respect to pressure. The slopes increase linearly with increasing pressure for the three highest concentrations over the complete pressure range. At 0.01 and 0.25 M, the pressure coefficient decreases (becomes more negative) with increasing pressure up to 500 bars;

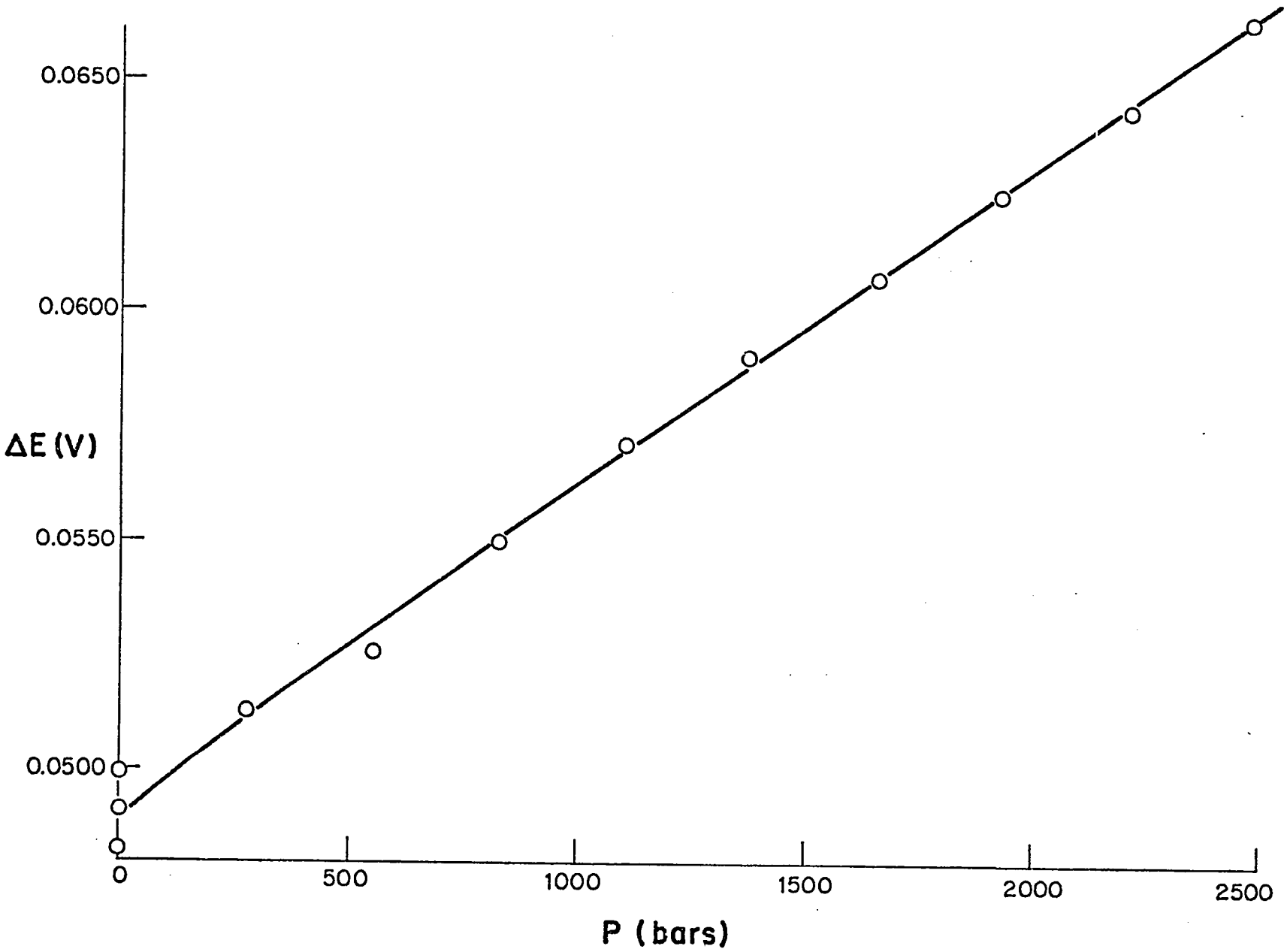

FIGURE 3.2.1 The variation of EMF as a function of pressure for the cell:

Pt,H_2 | 1.0M HCl | Pd-H,Pd .

TABLE 3.2.1

EMF DATA FOR THE CELL: $Pt,H_2|1\ M\ HCl|Pd\text{-}H,Pd$

OBTAINED IN TWO RUNS

P(bars)	ΔE (V)	ΔE (V)
1	0.0503	0.0501
276	0.0512	0.0513
552	0.0525	0.0526
828	0.0550	0.0550
1105	0.0571	0.0571
1376	0.0589	0.0590
1656	0.0607	0.0607
1930	0.0625	0.0625
2210	0.0644	0.0644
2480	0.0663	0.0663
1	0.0492	0.0488

TABLE 3.3.1

EMF DATA FOR THE CELL: Pd, Pd-H|M HCl|AgCl, Ag

	C	C	C	C	C
	0.01(M or mol dm^{-3})	0.25M	0.50M	0.75M	1.0M
P(bars)	ΔE (V)	ΔE (V)	ΔE (V)	ΔE (V)	ΔE (V)
1	0.40084	0.24846	0.21301	0.19210	0.17432
276	0.40064	0.24800	0.21238	0.19142	0.17368
552	0.40025	0.24750	0.21180	0.19069	0.17296
828	0.39978	0.24696	0.21118	0.19004	0.17228
1105	0.39937	0.24641	0.21061	0.18935	0.17162
1376	0.39891	0.24583	0.20994	0.18868	0.17089
1656	0.39842	0.24524	0.20931	0.18800	0.17023
1930	0.39796	0.24468	0.20868	0.18731	0.16952
2210	0.39746	0.24412	0.20806	0.18667	0.16884
1	0.40080	0.24865	0.21314	0.19208	0.17449

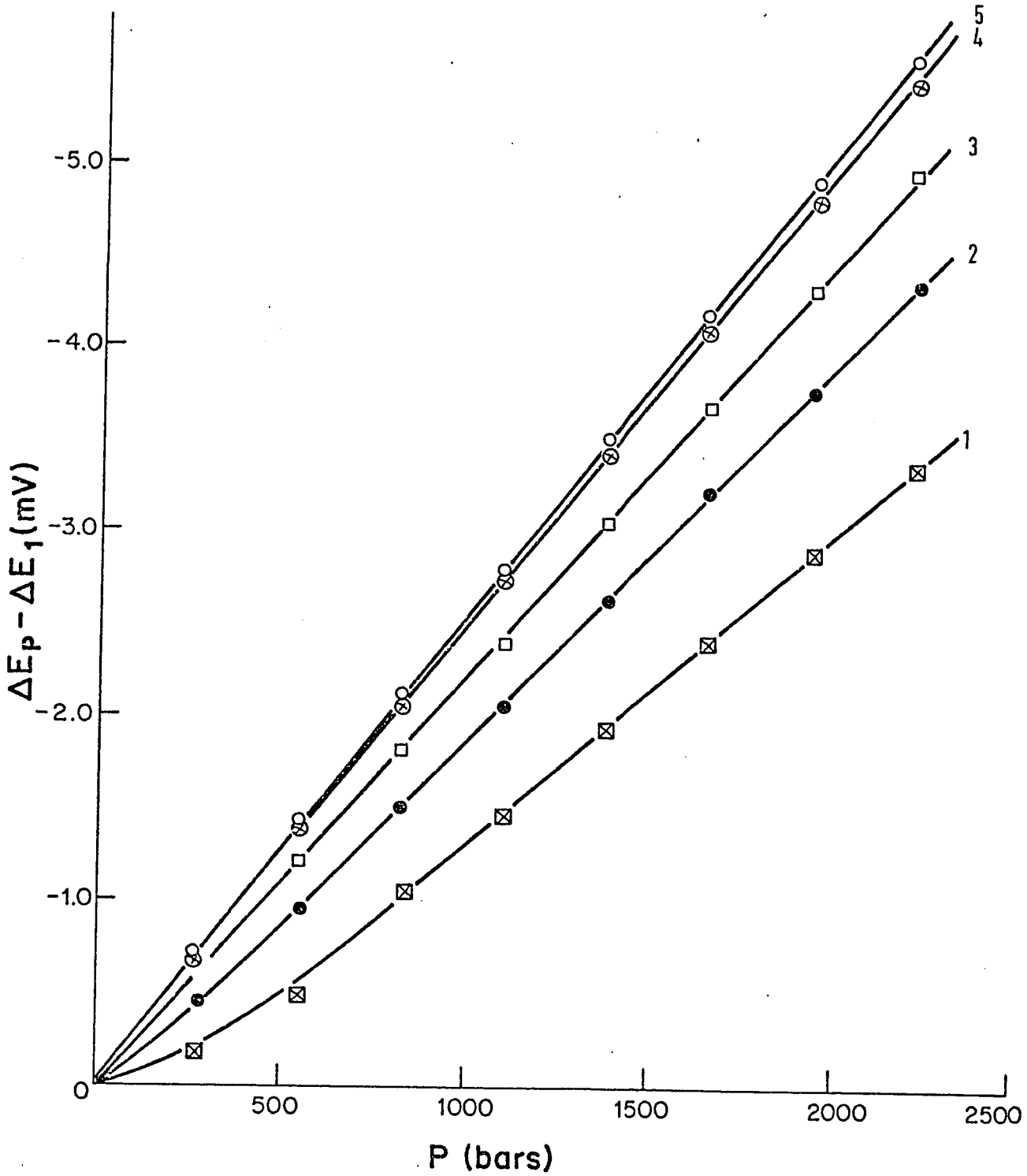

FIGURE 3.3.1 The variation of EMF as a function of pressure relative to the value at 1 bar for the cell:

Pd,Pd-H| HCl |AgCl,Ag

at HCl concentrations: 1) 0.01 M 4) 0.75

2) 0.25 5) 1.00.

3) 0.50

TABLE 3.3.2

PRESSURE COEFFICIENTS OF EMF FOR THE CELL: Pd,Pd-H|M HCl|AgCl, Ag

	P = 1 bar		P ≥ 500 bars	
C(HCl) M	$(\frac{\partial \Delta E}{\partial P})_T$ ($\mu V\ bar^{-1}$)	ΔV_1 ($cm^3 mol^{-1}$)	$(\frac{\partial \Delta E}{\partial P})_T$ ($\mu V\ bar^{-1}$)	ΔV_p ($cm^3 mol^{-1}$)
0.01	-0.50	0.50	-1.70	1.60
0.25	-1.50	1.50	-2.00	2.00
0.50	-2.20	2.10	-2.20	2.10
0.75	-2.48	2.40	-2.48	2.40
1.00	-2.55	2.46	-2.55	2.46

at pressures above 500 bars the pressure coefficient of the EMF is independent of P. The values of $(\frac{\partial E}{\partial P})_T$ at P = 1 bar and P $\geq$ 500 bars are listed in Table 3.3.2. The volume changes at each concentration for the cell reaction

$$Pd\text{-}H + AgCl \rightleftharpoons Pd + Ag + HCl \qquad (3.3.1)$$

are also included in Table 3.3.2.

The pressure coefficient is related to the appropriate volume quantities for the cell reaction 3.3.1 by the equation

$$(\frac{\partial \Delta E}{\partial P})_T = -\frac{1}{F}(V_{Pd} + V_{Ag} + V_{HCl} - V_{Pd\text{-}H} - V_{AgCl}) \qquad (3.3.2)$$

where V_{Pd}, $V_{Pd\text{-}H}$, V_{Ag} and V_{AgCl} are the molar volumes of Pd, Pd-H, Ag and AgCl, respectively. The molar volumes are determined from the appropriate molecular weights and densities of the solid phases. V_{HCl} is the partial molar volume of HCl but for the purpose of this calculation the partial molal volume of HCl at infinite dilution, V^{∞}_{HCl}, is utilized.[110] From the experimentally determined values of $(\frac{\partial \Delta E}{\partial P})$, apparent values of the volume $V_{Pd\text{-}H}$ can be evaluated from equation (3.2.2) for each concentration of HCl employed. The values of $V_{Pd\text{-}H}$ are "apparent" because V_{HCl} in equation (3.3.2) is concentration dependent according to the Debye-Hückel law. Therefore equation (3.3.2) becomes

$$(\frac{\partial \Delta E}{\partial P})_T = -\frac{1}{F}(9.33 + 10.27 + 17.83 - V_{Pd\text{-}H} - 25.78)$$

The apparent values of $V_{Pd\text{-}H}$ calculated from the data for each HCl concentration and equation (3.3.2) are listed in Table 3.3.3. Apparent values of $V_{Pd\text{-}H}$ may be plotted versus $C^{1/2}$ and extrapolated to zero ionic strength of HCl giving a true value of $V_{Pd\text{-}H}$ as shown in Figure 3.3.2. The best-fit straight line by the method of the least squares gives an intercept at C = 0 of $V_{Pd\text{-}H}$ = 11.3 $cm^3\ mol^{-1}$.

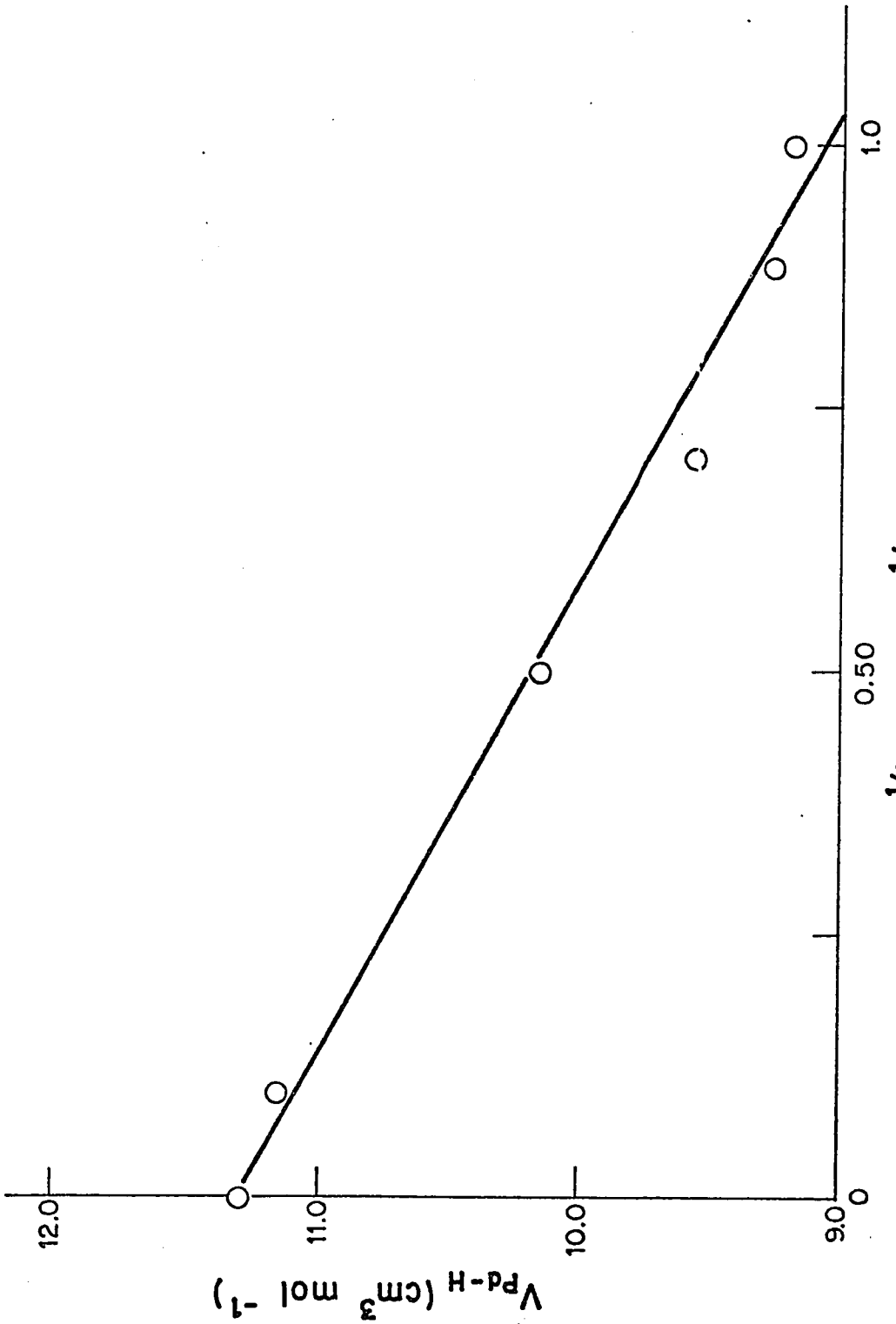

FIGURE 3.3.2 The variation of the molar volume of Pd-H, V_{Pd-H}, with $C_{HCl}^{\frac{1}{2}}$. The best fit straight line is obtained by the method of least squares.

TABLE 3.3.3

APPARENT VALUES OF THE MOLAR VOLUME OF Pd-H

C(M) HCl	V_{Pd-H} (cm^3 mol^{-1})
0	(extrapolated) 11.3
0.01	11.2
0.25	10.2
0.50	9.55
0.75	9.25
1.00	9.19

The EMF data listed in Table 3.3.1 are reproducible over the pressure range 1 to 2210 bars. The maximum variation of ΔE at 1 bar recorded before and after the high pressure measurements was 1.7×10^{-4}V (C = 1.0 M HCl). The minimum variation was 2×10^{-5}V (C = 0.75 M HCl). Therefore the electrodes Pd-H,H^+ and Ag,AgCl can be used as reliable reference electrodes at elevated pressures, with an uncertainty in the measured EMF not greater than 1.7×10^{-4}V.

3.4 The Pt, H_2|1 M HCl|AgCl, Ag Cell.

The EMF of this cell was found to be quite unstable. It was initially thought that a time-dependent mixed-potential was set up at the Ag, AgCl electrode in the presence of H_2. Another possible explanation is that reduction of traces of dissolved Ag^+ by molecular hydrogen occurs at the Pt, H_2 electrode. A separator between the Ag, AgCl and the Pt, H_2 electrodes was therefore introduced in the cell, but

the cell EMF again proved to be unstable. Significant diffusion of H_2 through the Teflon walls of the high-pressure cell appears to be a more realistic explanation for the time-dependent EMF of this cell. Earlier experiments with the Pt,H_2 vs Pd-H, Pd system gave, however, quite stable potentials in the ascending and descending direction of pressure change. In the later experiments, the cells used were made of Teflon from a difference source than that employed in the earlier measurements. Therefore, it seems that the two Teflon samples have a different structure, the most recently obtained being permeable to molecular hydrogen.

Heusler and Gaiser[15] also observed systematic errors of about 2 mV for the equilibrium EMF of the cell Pt, H_2|HCl, NaCl|AgCl, Ag at atmospheric pressure. The errors were attributed to the irreversible reduction of AgCl and to the fact that the H_2 partial pressure was less than 1 bar. The loss of hydrogen was attributed to diffusion through the Teflon cell into the hydraulic oil in the high-pressure vessel. Valeriote and Gallup[16] also observed similar drifts of cell potentials when a hydrogen electrode is used in a Teflon, Lexan or nylon high-pressure cell. The effects were again attributed to diffusion of H_2 through the walls of the cell.

In order to obtain a more reliable estimate of the pressure dependence of EMF of the cell Pt, H_2|HCl|AgCl, Ag, an indirect approach was taken. Two different cell systems were employed:

Pt, H_2|1M HCl|Pd-H, Pd and Ag, AgCl|1M HCl|Pd-H, Pd

The following procedure was adopted to determine the $(\frac{\partial \Delta E}{\partial P})_T$ for the following Pt, H_2|1M HCl|AgCl, Ag system:

Cell 1: $\frac{1}{2} H_2 + AgCl \rightleftharpoons Ag + HCl$ for which (3.4.1)

$$(\frac{\partial \Delta E_1}{\partial P})_T = -\frac{1}{F} (V_{Ag} + V_{HCl} - \frac{V_{H_2}}{2} - V_{AgCl}) \quad (3.4.2)$$

The pressure dependence of the EMF of the following two cells was determined

Cell 2: $Pd\text{-}H + AgCl \rightleftharpoons Ag + HCl + Pd$ for which (3.3.1)

$$(\frac{\partial \Delta E_2}{\partial P})_T = -\frac{1}{F} (V_{Pd} + V_{Ag} + V_{HCl} - V_{Pd\text{-}H} - V_{AgCl}) \quad (3.3.2)$$

Cell 3: $Pd + \frac{1}{2}H_2 \rightleftharpoons Pd\text{-}H$ for which (3.1.1)

$$(\frac{\partial \Delta E_3}{\partial P}) = -\frac{1}{F}(V_{Pd\text{-}H} - \frac{V_{H_2}}{2} - V_{Pd}) \quad (3.1.2)$$

From the three $(\frac{\partial \Delta E}{\partial P})_T$ expressions, it is seen that the required $(\partial \Delta E/\partial P)_T$, value is given by $(\frac{\partial \Delta E_1}{\partial P})_T = (\frac{\partial \Delta E_2}{\partial P})_T + (\frac{\partial \Delta E_3}{\partial P})_T$ in terms of the pressure coefficients of EMF of the cells (2) and (3), so that

$$(\frac{\partial \Delta E_1}{\partial P})_T = -\frac{1}{F} (V_{Ag} + V_{HCl} - V_{AgCl} - \frac{V_{H_2}}{2}) \quad (3.4.2)$$

The pressure coefficients of EMF for cells 1, 2 and 3 and the volume change, ΔV_1, for the cell reaction 3.4.1 are listed in Table 3.4.1. The partial molar volume of H_2 in 1M HCl at P = 1 bar as calculated from equation 3.4.2 is also listed in Table 3.4.1,

TABLE 3.4.1

PRESSURE COEFFICIENTS OF EMF FOR CELLS 1, 2 and 3

P	C(mol dm^{-3} HCl)	$(\frac{\partial \Delta E_1}{\partial P})_T$ ($\mu V\ bar^{-1}$)	$(\frac{\partial \Delta E_2}{\partial P})_T$	$(\frac{\partial \Delta E_3}{\partial P})_T$	ΔV_1 ($cm^3\ mol^{-1}$)	V_{H_2} ($cm^3\ mol^{-1}$)
1 bar	1.0	5.85	8.40	-2.55	-5.65	17.6
> 800 bars	1.0	4.35	6.90	-2.55	-4.20	14.1

3.5 Comments and Discussion on Pressure Coefficients of EMF in relation to Molar Volumes

From the data given above, it is seen that evaluation of the pressure coefficient of EMF for the cell

$$Pd, Pd\text{-}H|M\ HCl|AgCl, Ag$$

provides a convenient method for the determination of the molar volume of Pd-H. The significance of V_{Pd-H} can best be visualized if the processes involved in the Pd-H, H^+ reference electrode reaction are known.

The behaviour of the Pd-H, H^+ reference electrode has been studied by Schuldiner, Hoare and Castellan[84], Flanagan and Lewis[85], and by Aben and Burgers[86] with varying opinions on the actual mechanisms involved in the functioning of such an electrode. However, the mechanism described below appears to be the most consistent with respect to the experimental facts. It is known that a palladium wire charged with hydrogen electrolytically or under a hydrogen atmosphere will achieve a potential of about + 0.050 V with respect to a Pt,H_2 reference electrode. Hydrogen will be absorbed initially by palladium in the α-phase up to a limiting composition of H/Pd = 0.03. Further H absorption produces a second phase, β, with an H/Pd ratio of 0.60. The stable definite electrode potential is due to the simultaneous presence at the electrode surface of the two phases in thermodynamic equilibrium. Electrochemical equilibrium exists between the Pd-H, H^+ electrode and the electrolyte as represented by the equation

$$Pd + H^+ + e \rightleftharpoons Pd\text{-}H$$

The absorption of H into the α phase is known to occur with very little expansion of the Pd lattice; however, the formation of the β phase occurs with considerable increase of the lattice parameters. Values of the latter obtained by Aben and Burgers[86] are listed in Table 3.5.1.

TABLE 3.5.1

LATTICE PARAMETERS FOR THE Pd,Pd-H SYSTEM [86]

α - PHASE	α - PHASE + H	(α + β) PHASE + H
a = 0.3882 nm	a = 0.3886 nm	a_α = 0.3886 nm
		a_β = 0.4017 nm

The value of the measured molar volume of Pd-H is to be associated with the presence of H in the β-phase, since this phase forms with a relatively large expansion of the Pd lattice. Therefore, V_{Pd-H} = 11.3 $cm^3\ mol^{-1}$ is the molar volume of Pd-H when the H/Pd ratio is 0.60 in the β phase. The molar volume of H itself in Pd, V_H, can then be evaluated by taking the difference of V_{Pd-H} and the molar volume of Pd, V_{Pd}. This approach gives a value for V_H = 2.0 $cm^3\ mol^{-1}$ which is the net volume change of palladium upon absorption of 1 mole of H-atoms into a large volume of β-Pd-H.

The quantities V_{Pd-H} and V_H for H in palladium have not been previously reported in the literature, although V_H in pure iron and in Pd-Ag alloys have been evaluated by measuring the uptake of H_2 under uni-axial stress. This type of measurement is based on the fact that when a tensile stress is applied to a metal it causes an increase in the

solubility of H while a compressive stress decreases the quantity of absorbed H-atoms. The change of solubility of H is related to the applied stress by

$$\frac{\partial \ln (C/C_o)}{\partial \sigma} = \frac{V_H}{3RT}$$

where C is the solubility of hydrogen (moles of H/cm^3 substrate) when the applied uniaxial stress is σ and C_o is the solubility when the applied stress is zero. Utilizing this approach, Bockris et al[87] have determined V_H for H in pure Fe as 2.6 cm^3 mol^{-1}. Oriani[88] has determined the value to be 1.90 $cm^3 mol^{-1}$ in a 75% Pd - 25% Ag alloy which is in good agreement with the value obtained in this work, V_H = 2.0 cm^3 mol^{-1}.

The behaviour of the Pd, Pd-H|M HCl|AgCl, Ag cell at pressures up to 2500 bars appears to be sufficiently reliable to equate with certainty F times the pressure coefficient of the cell EMF to the known molar volume differences of the respective components in the cell reaction. This being the case, the Pd-H, H^+ electrode was utilized as a reference electrode in the subsequent high-pressure electrochemical studies in acid media. The Ag, AgCl electrode was adopted for use in Cl^- salt solutions at elevated pressures.

The pressure coefficient of EMF for the electrochemical cell

Pt, H_2|1M HCl|AgCl, Ag

could not be measured experimentally in a reliable manner but could be derived from EMF measurements on the cells

Pt, H_2|1M HCl|Pd-H, Pd

and

Pd, Pd-H|1M HCl|AgCl, Ag.

as described on p. 87-88.

TABLE 3.5.2

PARTIAL MOLAR VOLUMES OF H_2 IN AQ. HCl

C(mol dm^{-3}HCl)	V_{H_2} (cm^3 mol^{-1})				
0	24	-	-	25.2	24
0.02	22.6	-	-	-	-
0.10	-	17.9	15.0	-	-
0.42	20.2	-	-	-	-
0.80	17.7	-	-	-	-
1.00	-	-	-	-	17.6
Reference:	1	2	3	4	5

1. Heusler and Gaiser[15], Pt, H_2|M HCl|AgCl,Ag
2. Valeriote and Gallup[16], Pt,H_2|0.1M HCl|AgCl,Ag
3. Hills and Kinnibrugh[13], Pt,H_2|0.1M HCl|Hg_2Cl_2,Hg
4. Tiepel and Gubbins [53], dilatometer method in aqueous KOH
5. The present work.

The pressure-coefficient of EMF obtained in this manner can be used to determine the partial molar volume of H_2 in 1M HCl.

The partial molar volume of H_2 obtained in the present work is V_{H_2} = 17.6 $cm^3\ mol^{-1}$, and agrees quite well with the value of Heusler et al, V_{H_2} = 17.7 $cm^3\ mol^{-1}$, for 0.80 M HCl. The V_{H_2} values of Heusler and Gaiser[15] are plotted as a function of $C^{1/2}$ in Figure 3.5.1. The best-fit straight line has a slope of -6.3 and gives an intercept $V^{\infty}_{H_2}$ of 24 $cm^3\ mol^{-1}$. The value of V_{H_2} obtained in the present work, is within 0.1 $cm^3\ mol^{-1}$ of the corresponding value of Heusler and Gaiser on their V_{H_2} - $C^{1/2}$ plot at C = 1.0 M HCl. If the slope of Heusler and Gaiser's results is assumed to be correct, then an estimate of $V^{\infty}_{H_2}$ can be made from our single value of V_{H_2} in 1 M HCl using the relationship

$$V_{H_2} = V^{\infty}_{H_2} - 6.3\ (C)^{1/2}$$

This gives $V^{\infty}_{H_2}$ = 24 $cm^3\ mol^{-1}$, which is in excellent agreement with previously reported values of $V^{\infty}_{H_2}$ [53].

Heusler and Gaiser[15] evaluated $V^{\infty}_{H_2}$ as 24 $cm^3\ mol^{-1}$ from the pressure coefficient of EMF of the cell

$$Pt,H_2|M\ HCl|AgCl,Ag$$

Using a similar cell, Valeriote and Gallup's[16] results give a partial molar volume of H_2 in 0.1 M HCl as 17.9 $cm^3\ mol^{-1}$. Hills and Kinnibrugh[13], using the cell

$$Pt,H_2|0.1\ N\ HCl|Hg_2Cl_2,Hg,$$

quote V_{H_2} = 15 $cm^3\ mol^{-1}$ for 0.1 M HCl. For comparison, it is to be noted that Tiepel and Gubbins[53] made a direct evaluation of the partial molar volume of H_2 in pure water by a dilatometer method obtaining a value of $V^{\infty}_{H_2}$ = 25.2 $cm^3\ mol^{-1}$, in good agreement with the extrapolated infinite-dilution value obtained from EMF measurements. Table 3.5.2 summarizes the value of V_{H_2} obtained from the literature and from the present work.

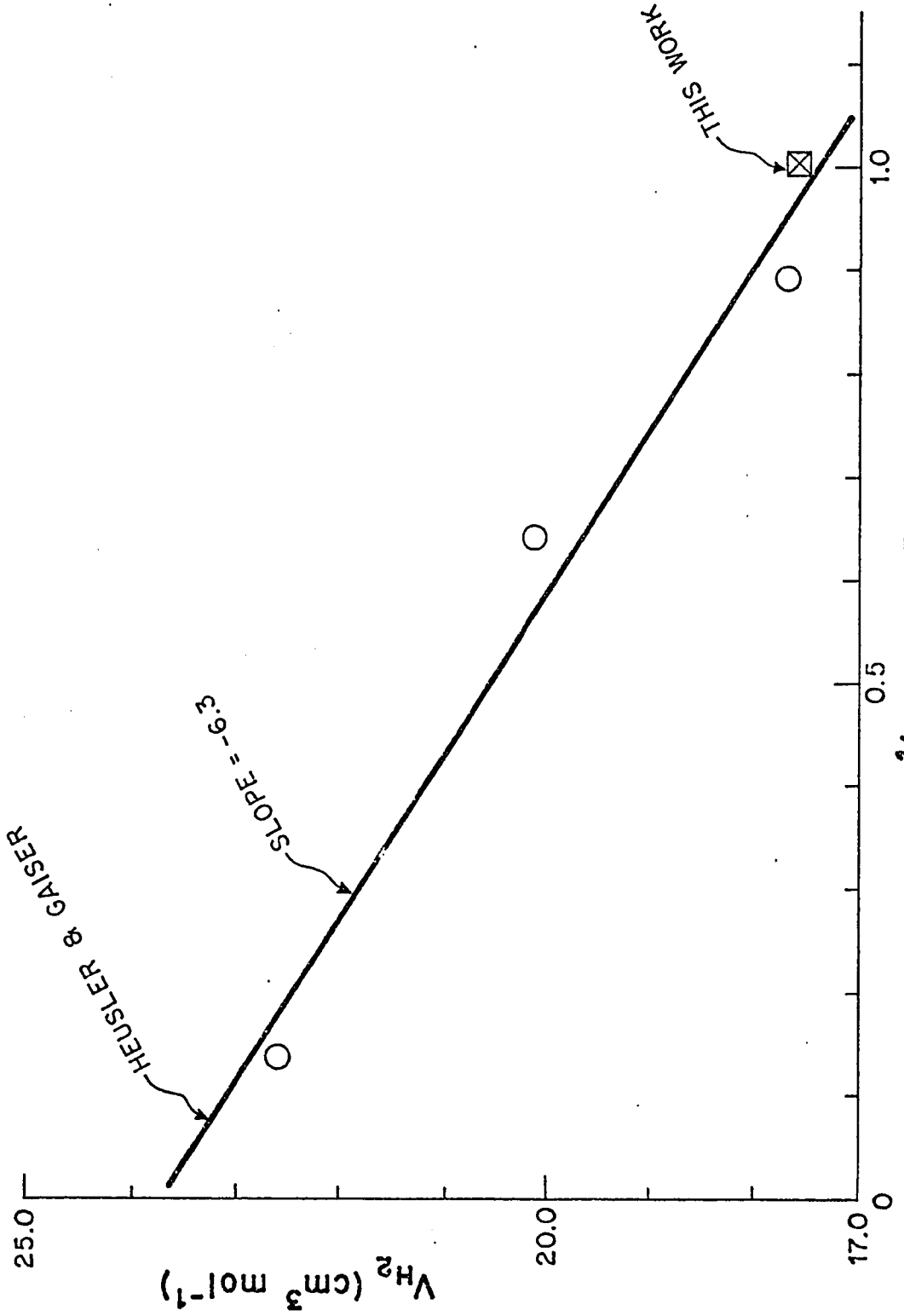

FIGURE 3.5.1 The variation of the partial molar volume of H_2, V_{H_2}, with $C^{\frac{1}{2}}$ from the data of Heusler and Gaiser (Ref.15).

It is seen that introduction of a small molecule such as H_2 into an aqueous solution results in a surprisingly large volume increase ($\sim$ 24 cm^3 mol^{-1}). This observation is consistent with the earlier work of Frank and Evans[89] on the effect of added non-electrolytes on the structure of water. The addition of non-polar gases such as H_2, Ar, He and Rn to aqueous solutions was found by these authors to result in a large decrease in entropy of the system (-105-170 J K^{-1} mol^{-1}). This behaviour was related to the ability of these solutes to promote structure building of water around non-polar solute molecules. The larger solute molecules, such as Rn, will promote a greater degree of structure making. The formation of large aggregates of structured water will result in expansion of the solvent as reflected in the observed apparent or partial molar volume of the solute.

The partial molar volume of H_2 in 1 M aq. HCl at 1 bar is 17.6 cm^3 mol^{-1}; however, as the pressure is increased, V_{H_2} decreases steadily until about 800 bars. Above this pressure, the value of V_{H_2} becomes constant at 14.1 cm^3 mol^{-1}, (Table 3.4.1). The decrease of V_{H_2} with pressure is due to the pressure-induced destruction of part of the expanded water structure. Above 800 bars, the structure promoted by the introduction of H_2 into the aqueous electrolyte has been "melted". This behaviour is analogous to the observations made by Frank and Evans[88] on the increase of entropy with increasing temperature for non-polar gases in water. This variation was attributed to the "melting" of the so-called "iceberg" structures surrounding the solute molecules.

The large concentration dependence of V_{H_2} observed in this work and that of Heusler and Gaiser ($S_v = -6.3$) can be explained in terms of the salting-out effect. In solutions of moderate electrolyte concentration (0.01 → 1M), increasing mole fractions of the solvent will be involved in solvation of the respective ions as their concentration increases. Therefore, a solute molecule such as H_2 when introduced into an ionic solution sees a smaller volume of "free" solvent molecules than would be the case in pure water. The activity coefficient of the H_2 gas is therefore increased to such an extent as to reduce its solubility (salting-out effect). Therefore the volume change accompanying the dissolution of H_2 will be less than the $V^{\infty}_{H_2}$ value due to the finite and positive activity coefficient associated with the decrease in the quantity of H_2 present in solution due to the influence of the ions present.

CHAPTER 4

FUNDAMENTAL ASPECTS OF THE PRESSURE DEPENDENCE OF THE KINETICS OF SELECTED ELECTRODE REACTIONS

General Introduction

Studies on the effects of pressure on condensed-phase chemical reactions[7,8], ionic conductance[43,66] and ionic equilibria[44-47] have produced useful new information on the volume changes which occur in these processes and in the activation process in their kinetics. The method is especially useful for studying reactions in which changes of charge, and corresponding changes of electrostriction, occur, e.g. in reactions where polar transition states are developed or in ionic reactions involving a change of charge.

Electrochemical reactions involving discharge or reduction of cations would normally be expected to have positive volumes of activation due to the elimination, or diminution, of net charge corresponding to a decrease of electrostriction. Because some experimental studies on the cathodic hydrogen evolution reaction reported in recent years give unexpected negative volumes of activation for this process, it is necessary to give a thorough analysis of the significance of the volume quantities normally derived from effects of high pressure on the kinetics of electrode processes. It has been shown (Chapter I) that for several reasons, the pressure derivative of the log of exchange currents (or currents at finite overpotential) do not give a true volume of activation for the electrode process as do measured volumes of activation for homogeneous, non-electrochemical reactions[19].

Applications to electrode processes where generation or annihilation of charge is an essential feature of the reaction, so that pressure effects are of special interest, have received little attention in the past. However, Hills and co-workers[13] and Heusler and Gaiser[15] have made important experimental contributions but the significance of the results was obscured by misinterpretation (as in the former case[13]) and by complications arising from pressure-dependence of coverage, Θ_H, by adsorbed H when Θ_H is significantly greater than 0 at some metals.

In Section 4.1, the significance of effects of high pressure on the kinetics of the hydrogen evolution reaction for several cases will be discussed and the conclusions will be used to clarify conflicting deductions which have hitherto been made regarding the significance of pressure effects on this reaction. The behavior of other types of reactions, e.g. ionic redox processes, will be discussed in Section 4.2 and surface processes at Pt and Au in Section 4.3 of this chapter.

4.1.1 Pressure Effects Arising for Various Reaction Mechanisms of Cathodic H_2 Evolution

The reaction mechanisms considered[90] are

$$H^+ + e + M \underset{k_{-1}}{\overset{k_1}{\rightleftharpoons}} MH_{ads} \qquad \text{I}$$

followed by

$$MH_{ads} + H^+ + e \underset{k_{-2}}{\overset{k_2}{\rightleftharpoons}} H_2 \qquad \text{II}$$

or

$$2MH_{ads} \underset{k_{-3}}{\overset{k_3}{\rightleftharpoons}} H_2 \qquad \text{III}$$

as the desorption pathways. The reaction equations I, II, III, as written above, also serve to define the respective rate constants k_1, k_{-1}, k_2, k_{-2}, k_3 and k_{-3} which will be required in the subsequent discussion.

Case 1

The simplest case arises when a rate-controlling discharge step such as I is involved and the desorption process is fast and irreversible so that coverage by adsorbed H, θ_H, tends to zero

Then $$i_t = 2F\, k_1\, C_{H^+}\, (1-\theta_H) \exp - \beta\phi F/RT \qquad (4.1.1)$$

where i_t is the total current density passing in the rate-determining step plus that in a subsequent desorption step. The potential term ϕ is the metal-solution potential drop. Here, for simplicity, we shall not consider the detailed form of ϕ as determined by double-layer ion-distribution and specific adsorption effects, as the small pressure effects which may arise in the structure of the double-layer will divert attention from the main factors to be developed and discussed in this Section. It is convenient to express ϕ in eqn. (4.1.1) in terms of the experimentally accessible overpotential η, referred to the potential of an electrode in the same solution at which the same overall electrode process, viz.

$$H_3O^+ + e \longrightarrow 1/2\ H_2 + H_2O \qquad \text{IV}$$

is set up, but under equilibrium conditions with a metal-solution p.d of ϕ_{rev}. Then, in the usual way,

$$\phi = \eta + \phi_{rev} \qquad (4.1.2)$$

The pressure derivative of i_t in eqn.(4.1.1) is, then, noting that $\Theta_H \to 0$,

$$\left(\frac{\partial \ln i_t}{\partial P}\right)_{\eta,T} = \left(\frac{\partial \ln k_1}{\partial P}\right) - \beta \left(\frac{\partial \phi_{rev}}{\partial P}\right)_T \qquad (4.1.3)$$

Since $\phi_{rev} = -\Delta G^o_{rev}/zF$ for the electrode process IV at equilibrium and $(\partial \Delta G^o_{rev}/\partial P)_T = \Delta V_o$, the volume change for the overall reaction IV, and because k_1 can be written in terms of the exponential $e^{-\Delta G_1^{\ddagger}/RT}$ it follows that the apparent volume of activation $\Delta V_a^{\ddagger}$ obtained from the experimentally measured $\left(\frac{\partial \ln i_t}{\partial P}\right)_{\eta,T}$ is given (cf. ref. 18,19) by

$$\Delta V_a^{\ddagger} = \Delta V_1^{\ddagger} - \beta \Delta V_o \qquad (4.1.4)$$

Thus, as first pointed out by Conway[39] (cf. refs. 19, 91) the true volume of activation, $\Delta V_1^{\ddagger}$, differs from the apparent value $\Delta V_a^{\ddagger}$ which is the quantity determined by measurements of the change of rate of an electrochemical reaction with pressure at constant η, simply by β times the equilibrium volume change ΔV_o in the overall reaction. Experimentally, it is to be noted that the molar concentration of reactant ions, C_{H^+}, will also increase with pressure*.

It is seen that evaluation of a true volume of activation for an electrode process involves problems similar to those arising[32,33] in evaluation of the activation energy of electrode processes from determinations of the temperature dependence of currents at a given overpotential or

---

* For pressures up to ca. 10^4 bars, the effect of pressure on concentrations in aq. media will be to enhance the rate by ca. 20%. However, this is a trivial effect which can usually be simply allowed for if the compressibility of the solvent or solution is known but in previous work this effect has apparently been neglected.

specifically of the exchange current ($\eta = 0$), as pointed out in ref.39 and p.7.

It is to be noted that the result (4.1.4), derived here for Case 1, is generally applicable to any electron-transfer reaction in which the kinetics are not influenced by a prior or subsequent step, or in which significant coverage of the electrode by an intermediate does not arise so that the pressure-dependence of the coverage Θ by this intermediate need not be considered. When Θ is significant, more complex results arise, and will be treated below.

Case 2. The Mechanism I, II, controlled by the rate constant of the desorption step II

Here significant coverage by adsorbed H can arise so that the pressure-dependence of Θ_H as well as of k_2 and ϕ_{rev} will determine the value of $\Delta V_a^{\neq}$.

For the mechanism I, II, the total current i_t is

$$i_t = i_1 - i_{-1} + i_2 \qquad (4.1.5)$$

In the steady-state $i_2 = i_1 - i_{-1}$, so that

$$i_t = 2i_2 = 2(i_1 - i_{-1}) \qquad (4.1.6)$$

In an analysis previously given by Heusler and Gaiser,[15] i_t was written as $i_t = i_1 + i_2$, i.e., the back reaction in I was evidently neglected. If II is rate-determining, i_{-1} must, however, normally be included in the expression for the total current and it also determines the coverage Θ_H under quasi-equilibrium conditions for step I. In terms of the usual potential-dependence of reaction rate,

$$i_t = 2Fk_2\, C_{H^+}\, \Theta_H \exp(-\beta\phi F/RT) \qquad (4.1.7)$$

where ϕ is the metal-solution p.d. Using eqn. (4.1.2) again to introduce

η and ϕ_{rev}, the pressure-dependence of the current density is given by

$$\left(\frac{\partial \ln i_t}{\partial P}\right)_\eta = \left(\frac{\partial \ln k_2}{\partial P}\right)_T + \left(\frac{\partial \ln \Theta_H}{\partial P}\right)_\eta - \frac{\beta F}{RT}\left(\frac{\partial \phi_{rev}}{\partial P}\right)_T \qquad (4.1.8)$$

at constant η.

Introducing the volume terms that arise from the pressure-dependencies of the k_2 and ϕ_{rev} terms in eqn. (4.1.4), gives an expression for the <u>apparent</u> activation volume $\Delta V_a^{\ddagger}$ as follows:

$$\left(\frac{\partial \ln i_t}{\partial P}\right)_\eta = -\frac{\Delta V_a^{\ddagger}}{RT} = -\frac{\Delta V_2^{\ddagger}}{RT} + \left(\frac{\partial \ln \Theta_H}{\partial P}\right)_\eta + \frac{\beta \Delta V_o}{RT} \qquad (4.1.9)$$

where $\Delta V_2^{\ddagger}$ is the <u>true</u> activation volume of step II while ΔV_o is the volume change <u>per e</u> in the overall reversible reaction of the H_2 electrode

$$\left(H^+ + e \rightleftharpoons \frac{1}{2} H_2\right) \text{ since } \frac{\Delta G^o_{rev}}{zF} = -\phi_{rev}$$

It is seen that the surface coverage factor enters eqn. (4.1.9) when II (or III) is the rate-determining step. The effect of pressure on Θ_H at a given η may be derived from the condition that $i_1 \doteqdot i_{-1}$ when II is rate-controlling, i.e.

$$k_1 C_{H^+} (1-\Theta) \exp(-\beta\phi F/RT) \doteqdot k_{-1}\Theta_H \exp(1-\beta)\ \phi F/RT \qquad (4.1.10)$$

so that in the usual way[34]

$$\Theta_H \doteqdot \frac{K_1 C_{H^+} \exp(-\phi F/RT)}{1 + K_1 C_{H^+} \exp(-\phi F/RT)} \qquad (4.1.11)$$

where K_1, $= k_1/k_{-1}$, is the quasi-equilibrium constant for Step I. Then the pressure-derivative of Θ_H can be written as

$$\frac{1}{\Theta_H}\left(\frac{\partial \Theta_H}{\partial P}\right)_{\eta,T} = \left(\frac{\partial \ln \Theta_H}{\partial P}\right)_{\eta,T} = \left(\frac{\partial \ln K_1}{\partial P}\right)_T - \frac{F}{RT}\left(\frac{\partial \phi_{rev}}{\partial P}\right)_T$$

$$- \frac{1}{1 + K_1 C_{H^+} \exp(-\phi F/RT)} \left[C_{H^+} K_1 \left(-\frac{F}{RT}\right)\exp(-\phi F/RT)\left(\frac{\partial \phi_{rev}}{\partial P}\right)_T + \right.$$

$$\left. C_{H^+} \exp(-\phi F/RT)\left(\partial K_1/\partial P\right)_{T,\eta}\right] \qquad (4.1.12)$$

so that

$$\left(\frac{\partial \ln \Theta_H}{\partial P}\right)_{n,T} = -\frac{\Delta V_1}{RT} + \frac{\Delta V_o}{RT} - \frac{\Theta_H}{RT}(\Delta V_o - \Delta V_1) \qquad (4.1.13)$$

since Θ_H can be written from eqn. (4.1.11) in terms of K_1, C_{H^+} and $\exp(-\phi F/RT)$. With further rearrangements of eqn. (4.1.13),

$$\left(\frac{\partial \ln \Theta_H}{\partial P}\right)_{n,T} = -\frac{\Delta V_1}{RT}(1-\Theta_H) + \frac{\Delta V_o}{RT}(1 - \Theta_H) \qquad (4.1.14)$$

$$= \frac{(1 - \Theta_H)}{RT}(\Delta V_o - \Delta V_1) \qquad (4.1.15)$$

The latter term, $\Delta V_o - \Delta V_1$, it is to be noted, is the volume of adsorption of 1/2 H_2 as H. Then, from eqn. (4.1.9),

$$\Delta V^{\ddagger}_{a,2} = \Delta V^{\ddagger}_2 - \Delta V_o (1 + \beta - \Theta_H) + (1 - \Theta_H)\Delta V_1 \qquad (4.1.16)$$

Under (experimentally inaccessible) conditions of constant ϕ, the true volume of activation for the <u>overall</u> process I, II, with II rate-controlling, would therefore be*

$$\Delta V^{\ddagger}_t = \Delta V^{\ddagger}_2 + (1 - \Theta_H)\Delta V_1 \qquad (4.1.17)$$

so that, with eqn. (4.1.16)

$$\Delta V^{\ddagger}_t = \Delta V^{\ddagger}_{a,2} + \Delta V_o (1 + \beta - \Theta_H) \qquad (4.1.18)$$

---

*In the more complex cases, such as that here where Θ_H can be f(P), $\Delta V^{\ddagger}_t$ can be expressed either in terms of the true $\Delta V^{\ddagger}$ for the rate-determining step or in terms of $\Delta V^{\ddagger}_a$ with ΔV_o and Θ_H.

evaluated at a constant n for a corresponding value of θ_H at the given n. It is thus seen from eqn. (4.1.18) that the true volume of activation differs from the measured apparent value in this case by one term derived from the pressure dependence of θ_H and another from the pressure dependence of ϕ_{rev}. If $\Delta V_2^{\ddagger}$ is desired for step II itself, it is necessary to have information on surface coverage θ_H and the volume change ΔV_1 in step I. ΔV_1 could be obtained in favorable cases from studies[92] of pressure-dependence of underpotential deposition of H, e.g. at Pt, Rh etc. (see Section 4.3)

Two limiting cases can usefully be considered:

(a) if $k_1 >> k_{-1}$, $k_1 >> k_2$, then $\theta_H \to 1$ so that θ_H is pressure independent. Hence

$$\Delta V_{a,2}^{\ddagger} = \Delta V_2^{\ddagger} - \beta \Delta V_o \qquad (4.1.19)$$

(b) $k_{-1} >> k_1$ and $k_{-1} >> k_2$, so that $\theta_H \to 0$ and is f(P), then

$$\Delta V_{a,2}^{\ddagger} = \Delta V_2^{\ddagger} + \Delta V_1 - (1 + \beta)\Delta V_o \qquad (4.1.20)$$

Case 3: Mechanism I, II when I is rate-controlling and II is in quasi-equilibrium as a rapid desorption step.

For some metals, the discharge step I can be rate-controlling but a coverage by H greater than "zero" can be established through step II in quasi-equilibrium. For this case

$$i_t = i_1 + i_2 - i_{-2} \qquad (4.1.21)$$

and since $i_1 = i_2 - i_{-2}$, (4.1.22)

$$i_t = 2 F k_1 C_{H^+} (1-\theta_H) \exp(-\beta\phi F/RT) \qquad (4.1.23)$$

The pressure-coefficient at constant η is then

$$\left(\frac{\partial \ln i_t}{\partial P}\right)_{\eta,T} = \left(\frac{\partial \ln k_1}{\partial P}\right)_T - \frac{\beta F}{RT}\left(\frac{\partial \phi_{rev}}{\partial P}\right)_T + \left(\frac{\partial \ln (1-\Theta_H)}{\partial P}\right)_{\eta,T} \qquad (4.1.24)$$

i.e.

$$-\frac{\Delta V_a^{\ddagger}}{RT} = -\frac{\Delta V_1^{\ddagger}}{RT} + \beta\frac{\Delta V_o}{RT} + \left(\frac{\partial \ln (1-\Theta_H)}{\partial P}\right)_{\eta,T} \qquad (4.1.25)$$

From the condition in eqn. (4.1.22), a steady-state value of Θ_H can be obtained as

$$\Theta_H = \frac{k_1 C_{H^+} + k^*_{-2}\exp(\phi F/RT)}{k_1 C_{H^+} + k_2 C_{H^+} + k^*_{-2}\exp(\phi F/RT)} \qquad (4.1.26)$$

so that

$$1 - \Theta_H = \frac{k_2 C_{H^+}}{k_1 C_{H^+} + k_2 C_{H^+} + k_{-2}\exp(\phi F/RT)} \qquad (4.1.27)$$

Taking logarithms and with further rearrangements, the pressure-derivative of $1 - \Theta_H$ is obtained as

$$\left(\frac{\partial \ln (1-\Theta_H)}{\partial P}\right)_{\eta,T} = \frac{\Delta V_o}{RT} - \frac{\Delta V_2}{RT} - (1-\Theta_H)\left[\frac{\Delta V_o}{RT} - \frac{\Delta V_2}{RT} + \frac{k_1 k_{-2}}{K_2^2}\left(\frac{\Delta V_o}{RT} - \frac{\Delta V_1^{\ddagger}}{RT} + \frac{\Delta V_2^{\ddagger}}{RT}\right)\right] \qquad (4.1.28)$$

Therefore eqn. (4.1.24) becomes

$$\Delta V_a^{\ddagger} = \Delta V_1^{\ddagger} - \Delta V_o(1+\beta) + \Delta V_2 + (1-\Theta_H)\left[\Delta V_o - \Delta V_2 + \frac{k_1 k_{-2}}{k_2^2}(\Delta V_o - \Delta V_1^{\ddagger} + \Delta V_2^{\ddagger})\right] \qquad (4.1.29)$$

The true volume of activation $\Delta V_t^{\ddagger}$ for this case is

$$\Delta V_t^{\ddagger} = \Delta V_1^{\ddagger} + \Delta V_2\Theta_H + K^1\Delta V_2^{\ddagger} - K^1\Delta V_1^{\ddagger} - K^1\Theta_H\Delta V_2^{\ddagger} + K^1\Theta_H\Delta V_1^{\ddagger} \qquad (4.1.30)$$

*P_{H_2} should appear in each of these terms but in general P_{H_2} = 1 bar therefore can be neglected as a pressure dependent term in subsequent derivations.

where $K^1 = \frac{k_1 k_{-2}}{k_2}$. Then eqn. (4.1.30) can be expressed in terms of the experimentally measured volume of activation, $\Delta V_a^{\ddagger}$, and the volume change ΔV_o for the equilibrium reaction IV by

$$\Delta V_t^{\ddagger} = \Delta V_{a,3}^{\ddagger} + \Delta V_o (1 + \beta) - \Delta V_o (1-\theta_H) - \Delta V_o K^1 (1-\theta_H) \qquad (4.1.31)$$

Limiting conditions may also be usefully examined for this mechanism, as for case II considered earlier:

(a) if $k_1 << k_2 >> k_{-2}$, then $\frac{k_1 k_{-2}}{k_2} \to 0$ and $\theta_H \to 0$; then eqn. (4.1.29) can be written as

$$\Delta V_{a,3}^{\ddagger} \equiv \Delta V_1^{\ddagger} - \beta \Delta V_o \qquad (4.1.32)$$

(cf. eqn. 4.1.4)

which is, as expected, simply the result for the discharge step without any equilibrium following step I.

(b) if $k_1 << k_{-2} >> k_2$, then $\theta_H \to 1$ eqn. (4.1.31) reduces to the form

$$\Delta V_{a,3}^{\ddagger} \equiv \Delta V_1^{\ddagger} - \Delta V_o (1 + \beta) + \Delta V_2 \qquad (4.1.33)$$

Therefore the true volume of activation can be written as

$$\Delta V_t^{\ddagger} = \Delta V_1^{\ddagger} + \Delta V_2 = \Delta V_{a,3}^{\ddagger} + (1 + \beta)\Delta V_o \qquad (4.1.34)$$

when $\theta_H = 0$ in (4.1.18) and 1 in eqn. (4.1.31), although of course eqn. (4.1.18) applies when step II is rate-controlling while eqn. (4.1.34) applies when step I is the limiting process.

Case 4: Recombination Step, III, is Rate-Determining

In this case, the reaction is represented by Step I (at quasi-equilibrium) followed by III. This case arises for H_2 evolution at certain noble metals and for Cl_2 evolution on Pt and oxidized Ru surfaces. The total current i_t is given by

$$i_t = i_1 - i_{-1} + i_3 = 2Fk_3\theta_H^2 \tag{4.1.35}$$

where θ_H is given by eqn. (4.1.11) and $\left(\frac{\partial \ln \theta_H}{\partial P}\right)_{\eta,T}$ by eqn. (4.1.15).

Following the procedures used in the previous case, the pressure coefficient $\left(\frac{\partial \ln i_t}{\partial P}\right)_{\eta,T}$ of i_t in eqn. (4.1.35) is

$$\left(\frac{\partial \ln i_t}{\partial P}\right)_{\eta,T} = -\frac{\Delta V_3^{\ddagger}}{RT} + 2\left(\frac{\partial \ln \theta_H}{\partial P}\right)_{\eta,T} = -\frac{V_3^{\ddagger}}{RT} + \frac{2(1-\theta_H)(\Delta V_o - \Delta V_1)}{RT} \tag{4.1.36}$$

Then, the measured apparent volumes of activation, $\Delta V_a^{\ddagger}$, can be represented by

$$\Delta V_{a,4}^{\ddagger} = \Delta V_3^{\ddagger} - 2(1-\theta_H)(\Delta V_o - \Delta V_1) \tag{4.1.37}$$

and the true volume of activation, $\Delta V_t^{\ddagger}$, by

$$\Delta V_t^{\ddagger} = \Delta V_3^{\ddagger} + 2\Delta V_1[1 - \theta_H] = \Delta V_{a,4}^{\ddagger} + 2(1-\theta_H)\Delta V_o \tag{4.1.38}$$

from eqn. (4.1.36) and (4.1.37).

The limiting conditions for case 4, are as follows:

a) $K_1 C_{H^+} \exp(-\frac{\phi F}{RT}) \gg 1$ in eqn. (4.1.11), so that $\theta_H \to 1$, i.e. when the $i \sim \phi$ relation corresponds to a limiting current, as at high overpotentials.

Then

$$\Delta V_t^{\ddagger} = \Delta V_{a,4}^{\ddagger} = \Delta V_3^{\ddagger} \tag{4.1.39}$$

b) $K_1 C_{H^+} \exp\left(-\frac{\phi F}{RT}\right) \ll 1$ in eqn. (4.1.11), so that $\Theta_H \ll 1$ and is potential-dependent. This corresponds to the $i \sim \phi$ relation having a Tafel slope of RT/2F.

Then

$$\Delta V_t^{\ddagger} = \Delta V_{a,4}^{\ddagger} + 2\Delta V_o \tag{4.1.40}$$

where

$$\Delta V_t^{\ddagger} \equiv \Delta V_3^{\ddagger} + 2\Delta V_1$$

Case 5: Coupled Mechanism I, II at high n

Here, the reverse reaction currents for these steps may be considered to be negligible. The total current i_t is given by

$$i_t = i_1 + i_2 = 2Fk_2 C_{H^+} \Theta_H \exp\left(-\beta\phi F/RT\right) \tag{4.1.41}$$

The Θ_H is now determined by a steady-state condition $i_1 = i_2$ rather than by eqn. (4.1.11), so that

$$2Fk_1 C_{H^+} (1-\Theta_H) \exp\left(-\beta\phi F/RT\right) = 2Fk_2 \Theta_H C_{H^+} \exp\left(-\beta\phi F/RT\right) \tag{4.1.42}$$

Hence

$$\Theta_H = k_1/(k_1 + k_2) \tag{4.1.43}$$

From eqn. (4.1.41),

$$\left(\frac{\partial \ln i_t}{\partial P}\right)_{n,T} = -\frac{\Delta V_2^{\ddagger}}{RT} + \left(\frac{\partial \ln \Theta_H}{\partial P}\right)_{n,T} + \frac{\beta\Delta V_o}{RT} \tag{4.1.44}$$

and with $\left(\frac{\partial \ln \Theta_H}{\partial P}\right)_{n,T}$ obtained from eqn. (4.1.43), viz.

$$\left(\frac{\partial \ln \Theta_H}{\partial P}\right)_{n,T} = \frac{1}{\Theta_H}\left(\frac{\partial \Theta_H}{\partial P}\right)_{n,T} = \frac{1}{k_1 (k_1 + k_2)} \left[k_2\left(\frac{dk_1}{dP}\right) - k_1\left(\frac{dk_2}{dP}\right)\right] \qquad (4.1.45)$$

$$= \left[\frac{\Theta_H k_2}{k_1} (\Delta V_2^{\ddagger} - \Delta V_1^{\ddagger})\right]$$

Noting that $k_2/k_1 = (1-\Theta_H)/\Theta_H$ (eqn. (4.1.43), then

$$\left(\frac{\partial \ln \Theta_H}{\partial P}\right)_{n,T} = (1-\Theta_H)\ (\Delta V_2^{\ddagger} - \Delta V_1^{\ddagger}) \qquad (4.1.46)$$

Eqn. (4.1.44) can now be expressed in terms of the apparent volume of activation, $\Delta V_{a,5}^{\ddagger}$ and Θ_H by

$$\Delta V_{a,5}^{\ddagger} \equiv \Theta_H \Delta V_2^{\ddagger} + (1-\Theta_H)\ \Delta V_1^{\ddagger} - \beta \Delta V_o \qquad (4.1.47)$$

The true volume of activation is represented by

$$\Delta V_t^{\ddagger} = \Theta_H \Delta V_2^{\ddagger} + (1-\Theta_H)\Delta V_1^{\ddagger}$$

$$= \Delta V_{a,5}^{\ddagger} + \beta \Delta V_o \qquad (4.1.48)$$

The limiting steady-state cases which arise are

a) If $k_2 >> k_1$, $\Theta_H \to 0$, and

$$\Delta V_{a,5}^{\ddagger} = \Delta V_1^{\ddagger} - \beta \Delta V_o \qquad (4.1.49)$$

which is the same result as that derived for the condition that Step I is rate-determining (i.e. Case I).

b) If $k_1 >> k_2$, $\Theta_H \to 1$ and

$$\Delta V_{a,5}^{\ddagger} = \Delta V_2^{\ddagger} - \beta \Delta V_o \qquad (4.1.50)$$

4.1.2. Discussion of Previously Published Experimental Results

(i) The proton discharge reaction at Hg

Hills and Kinnibrugh's work[13] on the H_2-evolution reaction at Hg gave data* for $(\frac{\partial \ln i}{\partial P})_{\phi \text{ calomel}}$ which they assumed gave the true volume of activation; a negative value of -3.40 cm^3 mol^{-1} was found. As pointed out previously[19,39] this value is, in fact, the apparent volume of activation.

It is generally agreed that the rate-determining step in H_2 evolution at Hg is step I with desorption by II. This is Case I for which $\Delta V_t^{\ddagger} = \Delta V_a^{\ddagger} + \beta \Delta V_o$, where $\Delta V_a^{\ddagger} = -3.4$ cm^3 mol^{-1}, $\Delta V_o = 18$ cm^3 mol^{-1} and $\beta = 0.5$. Hence $\Delta V_t^{\ddagger} = -3.40 + 0.5\ (18) = +5.60$ cm^3 mol^{-1}. $\Delta V_a^{\ddagger}$ was obtained from $\partial \ln i/\partial P$ measured at $P > 250$ bars. It appears that a steeper slope would have been measured if $\partial \ln i/\partial P$ had been derived limitingly at $P = 1$ bar (data at atmospheric pressure were not given). Then $\Delta V_t^{\ddagger}$ could then be appreciably smaller than 5.60 cm^3 mol^{-1}.

4.1.2. (ii) The H_2-evolution reaction at Cu, Ag and Au

In Heusler and Gaiser's treatment[15] of their experimental results, the back reaction of step I was neglected (Case 5 above), i.e. the forward directions of I and II were considered as a coupled mechanism.

For these conditions, the true volume of activation is

---

* Hills and Kinnibrugh's results were obtained from measurements at "constant electrode potential", vs. a calomel reference. They corrected their results to constant overpotential but did not take into account the further correction to constant "metal-solution p.d." which is also required.[39]

$$\Delta V_t^{\ddagger} = \Theta_H \Delta V_2^{\ddagger} + (1-\Theta_H)\Delta V_1^{\ddagger} \qquad (4.1.48)$$

$$= \Delta V_a^{\ddagger} + \beta \Delta V_o$$

The results of Heusler and Gaiser were based on $(\partial \ln i/\partial P)_{n,T}$ evaluated at P > 500 bars where the derivative is independent of P. Under these conditions, ΔV_o for the overall reaction (IV) is 9.7 $cm^3\ mol^{-1}$ based on V_{H_2} = 15.0 $cm^3\ mol^{-1}$ at these pressures and including V_e = 3 cm^3 $Faraday^{-1}$; $V_{H^+}^{\infty}$ was taken[95] as -5.2 $cm^3\ mol^{-1}$. The measured $\Delta V_a^{\ddagger}$ is -12.5 $cm^3\ mol^{-1}$. Therefore $\Delta V_t^{\ddagger}$ = -12.5 + 1/2 (9.7) = -7.6 $cm^3\ mol^{-1}$. There is no evidence for any substantial coverage by chemisorbed H at Cu, Ag or Au at normal overpotentials nor is underpotential deposition observed. Thus, $\Theta_H \simeq 0$ and the true volume of activation can be written as

$$\Delta V_t^{\ddagger} = \Theta_H \Delta V_2^{\ddagger} + (1-\Theta_H)\Delta V_1^{\ddagger} = \Delta V_1^{\ddagger} \qquad (4.1.49)$$

so that

$$\Delta V_1^{\ddagger} = -7.6\ cm^3\ mol^{-1}$$

This negative value is surprising since it might be expected that in the electrochemical reaction when the proton charge is neutralized, a positive volume of activation would arise.

However, if Case 2 (i.e. with quasi-equilibrium in Step I) is examined for the h.e.r., then from eqn. (4.1.18) with $\Theta_H \simeq 0$,

$$\Delta V_t^{\ddagger} = -12.5 + \frac{3}{2}(9.7) = +2\ cm^3\ mol^{-1}.$$

Then the volume of activation for step II, $\Delta V_2^{\ddagger} = 2 - \Delta V_1$ from eqn. (4.1.17), where ΔV_1 is the quasi-equilibrium volume change in Step I. If ΔV_1 is positive and greater than 2 for this case, then $\Delta V_2^{\ddagger}$, the true volume of activation for Step II will be negative.

If case III applied, a complicated expression is generated if $\theta_H > 0$. Thus, combining eqns. (4.1.29) and (4.1.30),

$$\Delta V_t^{\ddagger} = \Delta V_a^{\ddagger} + (1+\beta)\,\Delta V_o - K^1(1-\theta_H)\Delta V_o$$

However, if $\theta_H \to 0$, Case I would be recovered giving

$$\Delta V_t^{\ddagger} = \Delta V_1^{\ddagger} = -7.6 \text{ cm}^3 \text{ mol}^{-1}$$

It is useful to establish the sign of $\Delta V_t^{\ddagger}$ for an appreciable value of θ_H, say 0.5. Then, from eqn. (4.1.50), taking $K^1 = 0$, $\Delta V_t^{\ddagger} = \Delta V_a^{\ddagger} + \Delta V_o = -12.6 + 9.7 = -3 \text{ cm}^3 \text{ mol}^{-1}$. Also with $\beta = 0.5$ and $\theta_H = 0.5$, $\Delta V_t^{\ddagger} = \Delta V_1^{\ddagger} + \frac{\Delta V_2}{2}$. Hence $\Delta V_1^{\ddagger} = -3 - \frac{\Delta V_2}{2}$. But the quantity ΔV_2 which is the equilibrium volume change in the process $MH_{ads} + H^+ + e\ (M) \rightleftharpoons H_2$ (step II) is expected to be positive. Hence $\Delta V_1^{\ddagger}$ will be negative for intermediate coverages of the metal.

The above discussion shows, surprisingly, that negative values of the true volume of activation of the h.e.r. arise at certain metals. A summary of the $\Delta V_t^{\ddagger}$ and $\Delta V_a^{\ddagger}$ values for various conditions is given in Table 4.1.1.

4.1.2 (iii) Significance of negative or small positive values of $\Delta V_t^{\ddagger}$

On the basis of their original uncorrected results, it was concluded by Hills and Kinnibrugh[13] and by Hills[91] that the observed negative volume of activation (really $\Delta V_{a,1}^{\ddagger}$) indicated electrochemical

TABLE 4.1.1

Relation Between True ($\Delta V_t^{\ddagger}$) and Apparent ($\Delta V_a^{\ddagger}$) Volumes of Activation for Various Mechanisms or Conditions in the Hydrogen Evolution Reaction

Case	Rate-Determining Step or Condition	$\Delta V^{\ddagger}$ Relation	Observed or Derived Values of $\Delta V^{\ddagger}$ ($cm^3\ mol^{-1}$) for constant n
1	H_3O^+ discharge step I; $\theta_H \ll 1$	$\Delta V_1^{\ddagger} = \Delta V_a^{\ddagger} + \beta\Delta V_o$	$\Delta V_a^{\ddagger}$ = -3.4 (Hg) $\Delta V_t^{\ddagger}$ = +5.6 (Hg)
2 limiting cases.	Desorption of H in Step II; $\theta_H > 0$ and potential and pressure dependent $\theta_H \to 1$ $\theta_H \ll 1$	$\Delta V_t^{\ddagger} = \Delta V_a^{\ddagger} + (1+\beta-\theta_H)\,\Delta V_o$ $= V_2^{\ddagger} + (1-\theta_H)\,\Delta V_1$ $\Delta V_a^{\ddagger} = \Delta V_2 - \beta\Delta V_o$ $\Delta V_a^{\ddagger} = \Delta V_1 - (1+\beta)\Delta V_o + \Delta V_2^{\ddagger}$	$\Delta V_a^{\ddagger}$ = - 12.5 (Cu, Ag, Au) $\Delta V_t^{\ddagger}$ = + 2 (Cu, Ag, Au) for $\theta_H \ll 1$
3 limiting cases	Step I, with θ_H determined by quasi-equilibrium in Step II $\theta_H \to 1$ $\theta_H \ll 1$	$\Delta V_t = \Delta V_a^{\ddagger} + [1 + \beta - (1-\theta_H)]\Delta V_o - K'(1-\theta_H)\Delta V_o$ $\Delta V_a^{\ddagger} = \Delta V_1^{\ddagger} - (1+\beta)\Delta V_o + \Delta V_2$ or $\Delta V_t^{\ddagger} = \Delta V_1^{\ddagger} + \Delta V_2 = \Delta V_a^{\ddagger} + (1+\beta)\Delta V_o$ $\Delta V_a^{\ddagger} = \Delta V_1^{\ddagger} - \beta\Delta V_o$	$\Delta V_a^{\ddagger}$ = -12.5 (Cu, Ag, Au) $\Delta V_t^{\ddagger} = \Delta V_1^{\ddagger}$ = -7.6 (Cu, Ag, Au)
4 limiting cases	Recombination Step III $\theta_H \to 1$ $\theta_H \ll 1$	$\Delta V_t^{\ddagger} = \Delta V_3^{\ddagger} + 2\Delta V_1\,(1-\theta_H)$ $= \Delta V_a^{\ddagger} + 2\,(1-\theta_H)\,\Delta V_o$ or $\Delta V_a^{\ddagger} = \Delta V_3^{\ddagger} - 2(1-\theta_H)\,(\Delta V_o - \Delta V_1)$ $\Delta V_t^{\ddagger} = \Delta V_a^{\ddagger} = \Delta V_3^{\ddagger}$ $\Delta V_t^{\ddagger} = \Delta V_a^{\ddagger} + 2\Delta V_o\ (\equiv \Delta V_3^{\ddagger})$	
5 limiting cases	Coupled I, II; high n $\theta_H \to 1$ $\theta_H \ll 1$	$\Delta V_t^{\ddagger} = \theta_H\Delta V_2^{\ddagger} + (1-\theta_H)\Delta V_1^{\ddagger}$ $= \Delta V_a^{\ddagger} + \beta\Delta V_o$ $\Delta V_a^{\ddagger} = \Delta V_2^{\ddagger} - \beta\Delta V_o$ $\Delta V_a = \Delta V_1^{\ddagger} - \beta\Delta V_o$	$\Delta V_a^{\ddagger}$ = - 12.5 (Cu, Ag, Au) $\Delta V_t^{\ddagger}$ = - 7.6 (Cu, Ag, Au)

* This type of relation also applies to any simple discharge step, e.g. as in an ionic redox reaction.

formation of the hydrated electron as the primary step in the h.e.r. at Hg. Various objections to this mechanism, apart from those connected with the difference between $\Delta V_1^{\ddagger}$ and $\Delta V_{a,1}^{\ddagger}$, were, however, pointed out by Conway et al[93].

It is very difficult to see how a negative value of the true volume of activation can arise in the discharge of a cation, here H_3O^+. It will be shown[92] in Section 4.2 that the true volume of activation for an ionic redox reaction

$$Fe(CN)_6^{4-} \longrightarrow Fe(CN)_6^{3-} + e$$

does have the expected sign (positive for the direction written above). Hence, it may be suggested that the anomalous behaviour of H_3O^+ arises from the special nature of the hydrated proton in solution. Thus, good evidence exists[94,95] that H^+_{aq} exists as the $H_9O_4^+$ ion in which the proton charge is decentralized by joint proton tunneling between 4 H_2O molecules + H^+ and delocalized at any momentarily existing H_3O^+ center. The transition state for classical proton transfer must presumably arise by a reorganization of the $H_9O_4^+$ aq complex; if the activation process involves localization of the proton on one of the H_2O molecules in $H_9O_4^+$ in the double-layer to produce an excited state to which electron transfer occurs by the usual radiationless transfer (Fig. 4.1.1), then it can be seen that a negative volume of activation could arise since more electrostriction could be temporarily developed in the double-layer at the localized proton state than in the initial $H_9O_4^+$ ion in which proton charge-density is diffused. That the proton in water has an unusually large partial molal volume is indicated when the volume of ionization of water is compared with that for NH_3 aq. in the processes:

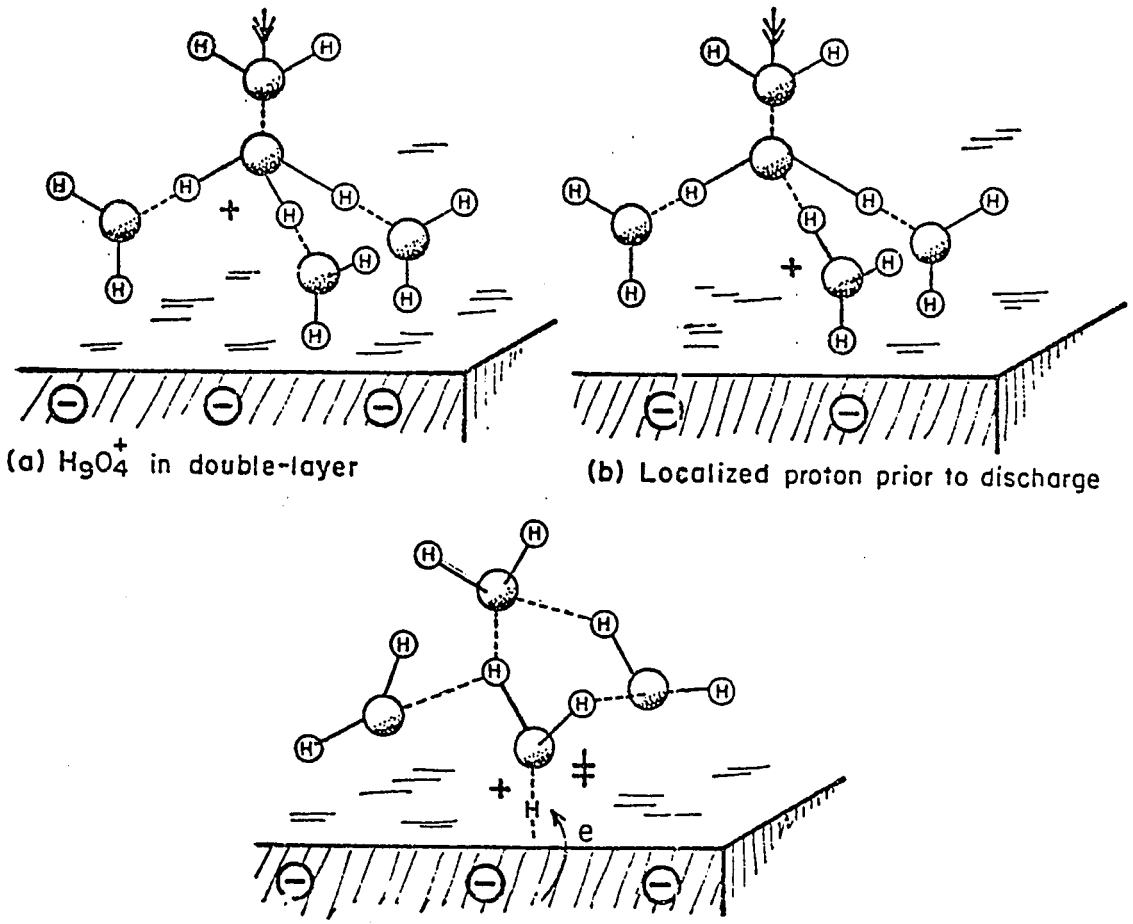

FIGURE 4.1.1 Configurations of the hydrated proton, as $H_9O_4^+ + 1\ H_2O$ in the double-layer in the course of the activation process in the electrochemical proton discharge(schematic).

$$H_2O + H_2O \longrightarrow "H_3O^+" + OH^- \qquad \Delta V^\infty = -21.8;\ -22.1\ cm^3\ mol^{-1}$$

and

$$H_2O + NH_3 \longrightarrow NH_4^+ + OH^- \qquad \Delta V^\infty = -28.9;\ -28.5\ cm^3\ mol^{-1}$$

in which NH_3 is isoelectronic with H_2O and NH_4^+ with "H_3O^+". (The first values of ΔV^∞ are derived from pressure effects on the ionization constant and the second from volumetric measurements; data are from ref. 96). Assuming that the difference of intrinsic volume of NH_4^+ and "H_3O^+" would be close to the corresponding difference between NH_3 and H_2O, it seems reasonable to conclude that the electrostriction at "H_3O^+" is ca. 6.5 - 7 $cm^3\ mol^{-1}$ smaller than at the isoelectronic NH_4^+ ion. This is consistent with diffusion of the proton charge in $H_9O_4^+$ which does not occur in the hydrated NH_4^+ ion. The difference of 6.5 - 7 $cm^3\ mol^{-1}$ is of the correct magnitude to account for the negative $\Delta V_t^{\neq}$ values.

While the volume of activation for H_2-evolution from H^+_{aq} exhibits unusual behaviour, that for ionic redox reactions should help to elucidate the nature of the activation process involving solvent reorganization in redox reactions. In particular, the question arises whether short-range reorganization of the hydration shell is involved or whether fluctuations of the long-range dielectric polarization are mainly operative. These questions will be dealt with in Section 4.2 on the $Fe(CN)_6^{3-}$ redox reaction.

4.2 The Nature of Solvent Reorganization in the Activation Process of an Electrochemical Redox Reaction.

In Section 4.1, some of the general problems of interpretation of effects of pressure on the kinetics of electrode reactions were discussed and exemplified with respect to the hydrogen evolution reaction. It was shown that investigations of pressure effects on the latter reaction are complicated by (a) the mechanism having more than one step; (b) the consequent adsorption of an intermediate H and (c) the unusual properties of the hydrated proton, referred to in Section 4.1, as well as the general point that reference electrode potentials required in all measurements are themselves pressure-dependent.[39]

It is therefore desirable to examine pressure effects on a simpler reaction where only an electron-transfer step is involved, e.g. as in a redox reaction. Hitherto, studies of electrochemical redox reactions have been concerned with (a) evaluation of absolute values of standard electrochemical rate constants[97,98]; (b) their comparison with values for corresponding homogeneous solution reactions[20] and (c) the role of the substrate metal[99] (its work-function and the state of its surface) in determining the rate constant.

In this section, pressure effects on the $Fe(CN)_6^{3-} + e \rightleftharpoons Fe(CN)_6^{4-}$ reaction at a gold electrode are reported. This type of reaction is of special interest with regard to current theories of electron transfer[20-24] where the reorganization of the initial state is involved in the activation process for electron transfer. One of the questions involved is the extent to which the activation process involves long-range solvent polarization fluctuations[20,21] around the initial state ion, or more specific

short-range changes of hydration shell configuration or inner coordination shell reorganization [23,100,101]. It may be expected that study of pressure effects on the kinetics of a simple electrochemical redox reaction may provide a means of distinguishing these effects, e.g. in terms of the anticipated changes of electrostriction involved in the reorganization process. Examination of the effect of pressure on the kinetics of a redox reaction thus provides a further dimension from which new data of a useful kind can be derived. Previous high-pressure work on a redox reaction has been restricted to a report of values of $\Delta V_t^{\ddagger}$ for the ferro-ferricyanide reaction in a review[52(b)] but no experimental details or commentary on the data have been published. The results quoted are quite inconsistent with the known electrostrictions at the two ions in this reaction.

A second point, of general interest, is whether a chemically symmetrical reaction such as the ferro-ferricyanide one behaves in a kinetically symmetrical way (symmetry factor $\beta = 0.5$) when established at an electrode.

4.2.1 Results

The kinetics of the $Fe(CN)_6^{3-} + e \rightleftharpoons Fe(CN)_6^{4-}$ reaction were studied at a gold electrode. The latter was chosen as the substrate metal because it is known to have a wide range of potentials over which neither H nor O-species are chemisorbed (under-potentially deposited). The exchange rate constants for the ferro-ferricyanide reaction are relatively large[97], so that a non-steady state method is required for their proper evaluation. In the present work, the kinetics of the reaction were studied by a.c. impedance measurements based on well-known principles[102,103] which lead to evaluation of the reaction resistance and hence the exchange current density i_0. From this the standard rate constant can be obtained

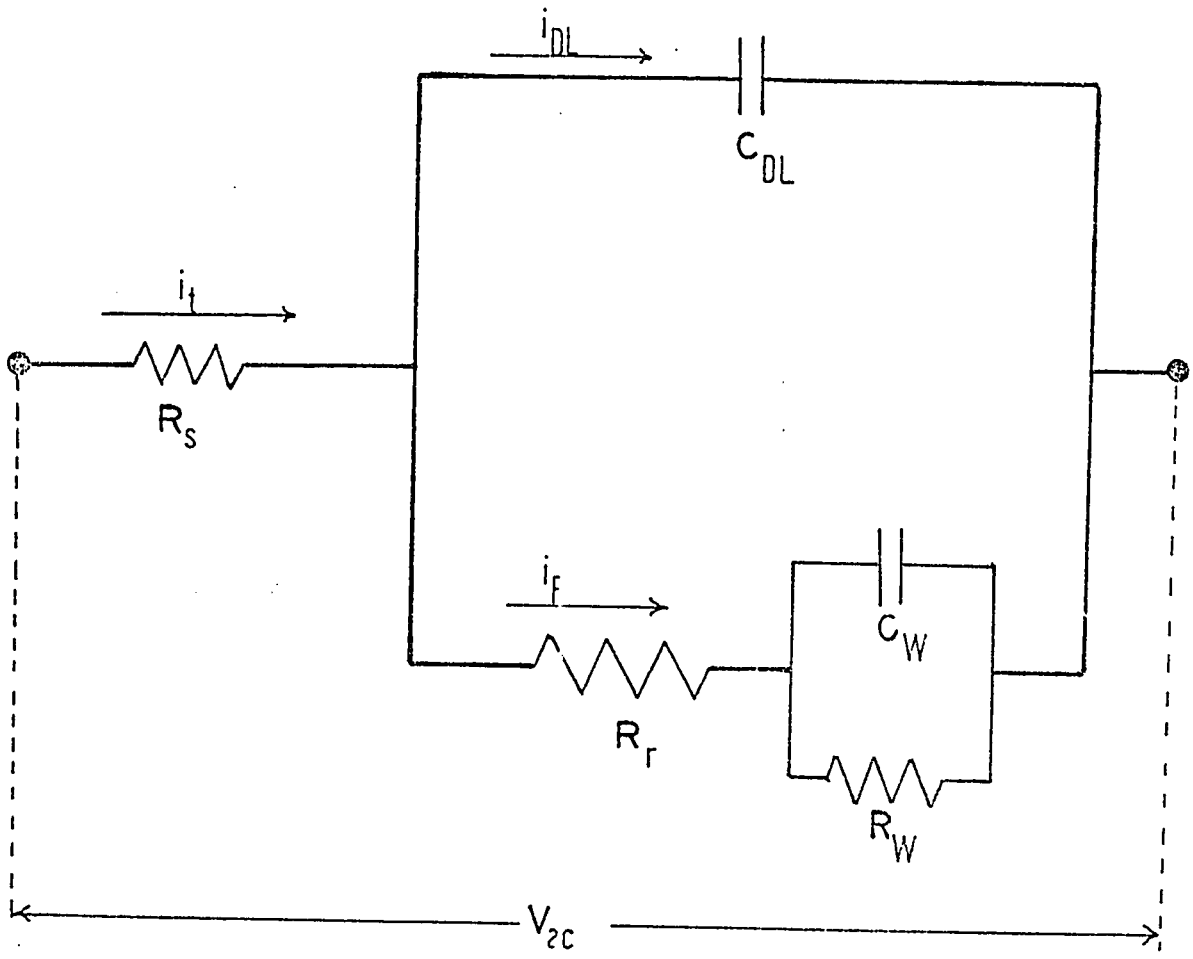

FIGURE 4.2.1 The equivalent electrical circuit of the electrode-solution interface in terms of the double-layer capacity, C_{DL}, reaction resistance, R_r, solution resistance, R_s, and the Warburg impedance, R_W and $\frac{1}{\omega C_W}$.

knowing the concentrations of the reactant species.

The faradaic impedance determined by phase-sensitive a.c.[104-106] voltammetry (Chapter 2) at phase angles $\phi = 0$ and $\phi = 90^{o}$ gives, respectively, the ohmic and capacitative components of the impedance. The faradaic impedance is comprised of a reaction resistance, R_r, in series with a complex component called the Warburg impedance[107,108] (Fig. 4.2.1). This latter component arises from diffusional transport of the reacting ions in response to the electrode reaction, the rate of which is periodic on account of the a.c. driving potential. The Warburg impedance has a phase-angle of 45^{o} at all frequencies. In parallel with the above two impedance components is the double-layer capacity. The resistance due to the supporting electrolyte and the electrode material is also in series with the parallel components of the faradaic impedance. In the case where the electrode and electrolyte are highly conductive, the solution resistance will be small and can normally be neglected.

The equivalent circuit for the electrode-solution interface is represented in the usual way as shown in Fig. 4.2.1. In order to determine the faradaic impedance[108], the equivalent circuit must be simplified by first eliminating the non-faradaic components such as C_{DL} and R_S. If it is found necessary to evaluate R_S, this must be done by separately determining[105] the ohmic component R_S of impedance at a phase-angle $\phi = 0^{o}$ in the supporting electrolyte. In this work, R_S has been neglected because of its small contribution to the overall impedance. In addition, we are interested in the derivative $\left(\frac{\partial \ln i_o}{\partial P}\right)_{\eta}$ so that the absolute values of i_o, while important, are of less significance than the variation of $\ln i_o$ with pressure.

The double-layer capacity can be evaluated simultaneously with the capacitative component ($\frac{1}{\omega C_{F,s}}$) of the faradaic impedance. The capacitative impedance was determined at a phase-angle $\phi = 90^{o}$, from the a.c. voltammograms shown in Fig. 4.2.2(a) at 1 bar pressure where the concentrations of both $Fe(CN)_6^{-4}$ and $Fe(CN)_6^{-3}$ are 5×10^{-3} M. The a.c. frequency range was 25 to 250 s^{-1}. The i_{AC}-V_{DC} profiles show a base-line current in the double-layer region (at Au) due to the capacitance of the double-layer. The magnitude of the double-layer charging current is $(\omega C_{DL})\ V_{AC}$. In the potential region of the $E_{1/2}$ for the reaction

$$Fe(CN)_6^{-3} + e \longrightarrow Fe(CN)_6^{-4}$$

the a.c. current, i_{AC}, exhibits a maximum as a result of the above faradaic process[87]. The ohmic component of the faradaic impedance is measured at a phase-angle $\phi = 0$. The a.c. voltammograms for the in-phase (ohmic) component of the faradaic impedance are shown in Fig. 4.2.2(b) at 1 bar pressure. The a.c. current-potential (i-V) profiles at elevated pressures, although not illustrated, are similar in shape to those for the 1 bar case.

The double-layer capacitance is evaluated at each frequency and subtracted from the total measured capacity to give the faradaic component. The ohmic component is also calculated at each frequency from the in-phase ($\phi = 0$) voltammograms. These components of impedance must be converted to their values in a <u>series</u> circuit by a vector diagram or by means of the following equivalence expressions:

$$R_{F,s} = \frac{(X_{F,p})^2 \times R_{F,p}}{(X_{F,p})^2 + (R_{F,p})^2} \quad ;$$

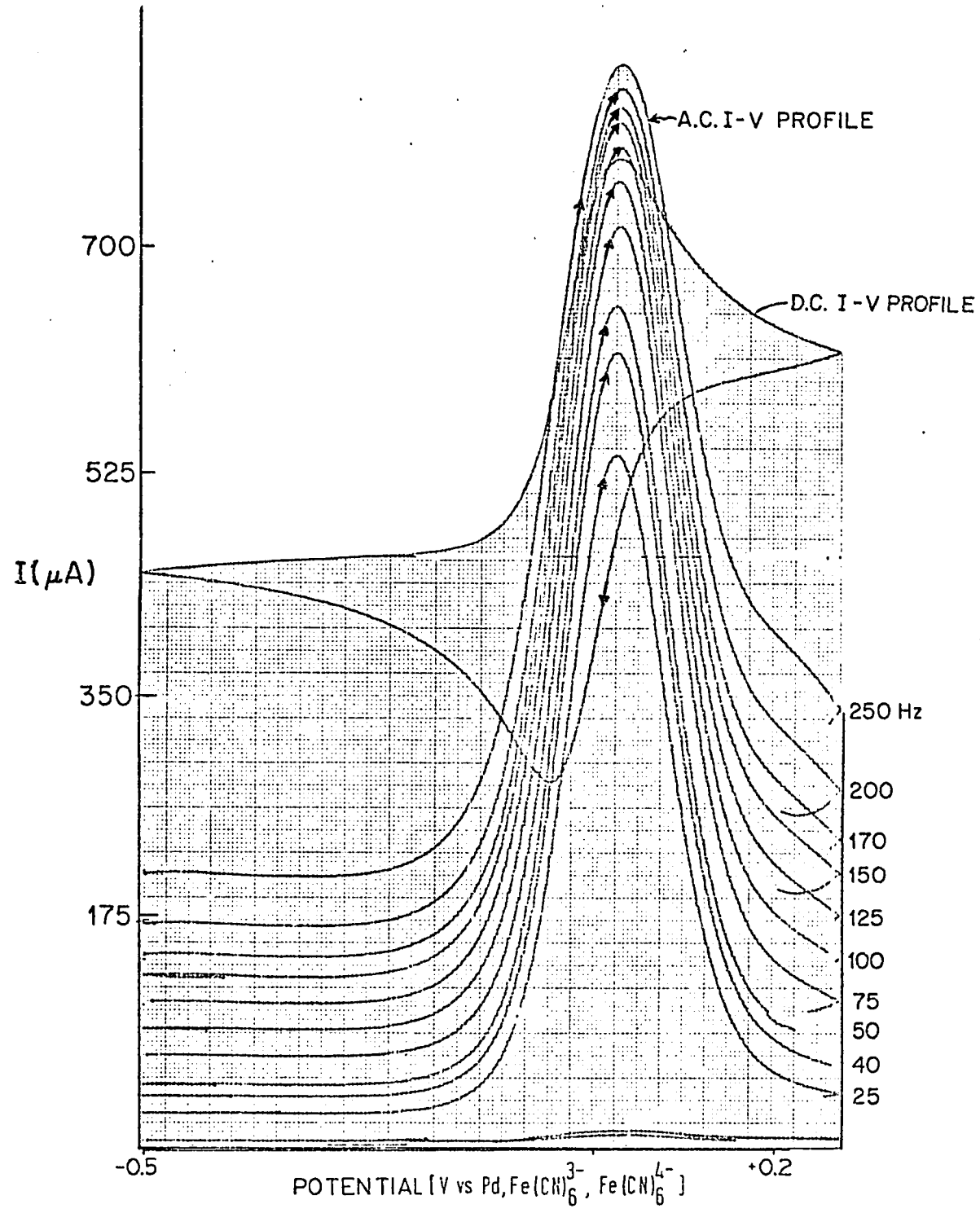

FIGURE 4.2.2 a) A.c. voltammograms for the redox couple $Fe(CN)_6^{3-}$ / $Fe(CN)_6^{4-}$ at phase angle $\phi=90^0$ at various a.c. frequencies. P=1 bar, s=20 mV s^{-1}.

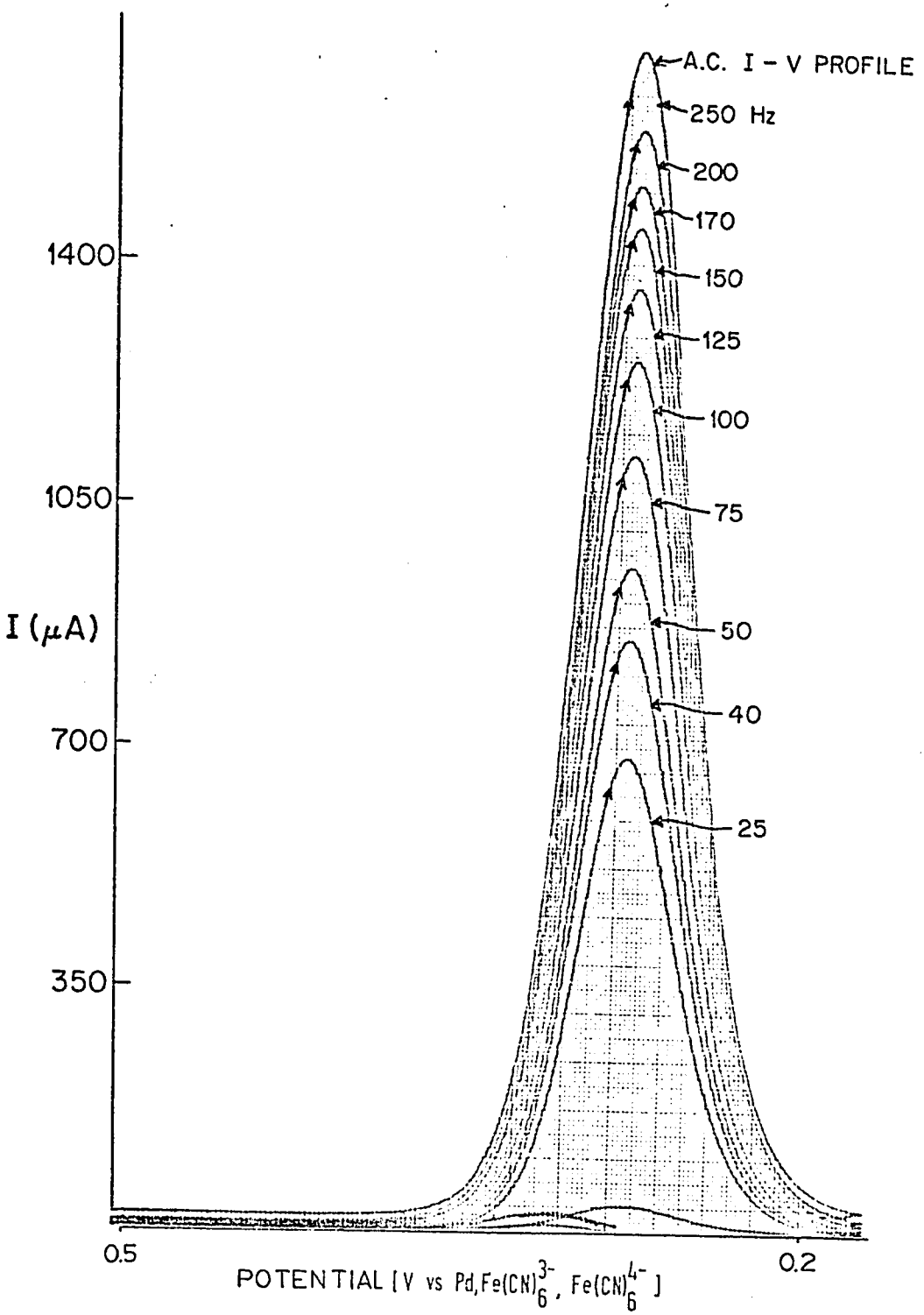

FIGURE 4.2.2 b) Same as in figure 4.2.2 a) but $\phi=0^{o}$.

TABLE 4.2.1

Impedance Data for Redox Reaction $Fe(CN)_6^{-4}/Fe(CN)_6^{-3}$ at Au in 0.5M K_2SO_4 + 0.2M H_2SO_4

Pressure (bars)	1	550	1100	1650	2204
$\omega x10^{-3}$(rad s^{-1})	$R_{F,s}$	$R_{F,s}$	$R_{F,s}$	$R_{F,s}$	$R_{F,s}$
1.571	5.304 Ω	5.216 Ω	5.329 Ω	5.288 Ω	5.316 Ω
1.257	5.514	5.468	5.552	5.529	5.533
1.068	5.554	5.627	5.661	5.648	5.688
0.9425	5.833	5.756	5.837	5.849	5.832
0.7854	6.027	5.995	6.056	6.055	6.028
0.6283	6.368	6.316	6.334	6.300	6.336
0.4712	6.817	6.764	6.884	6.822	6.793
0.3142	7.578	7.533	7.581	7.571	7.522
0.2513	8.168	8.044	8.149	8.116	8.086
0.1571	9.526	9.442	9.484	9.413	9.356
$\omega x10^{-3}$(rad s^{-1})	$X_{F,s}$	$X_{F,s}$	$X_{F,s}$	$X_{F,s}$	$X_{F,s}$
1.571	2.003 Ω	1.870 Ω	1.965 Ω	1.929 Ω	1.895 Ω
1.257	2.299	2.170	2.250	2.228	2.178
1.068	2.633	2.361	2.412	2.383	2.386
0.9425	2.710	2.536	2.625	2.615	2.536
0.7854	2.970	2.830	2.884	2.833	2.808
0.6283	3.425	3.249	3.248	3.167	3.191
0.4712	4.009	3.784	3.949	3.798	3.752
0.3142	4.905	4.678	4.779	4.703	4.657
0.2513	5.683	5.369	5.449	5.370	5.300
0.1571	7.365	6.877	7.008	6.787	6.918

$$X_{F,s} = \frac{(R_{F,p})^2 \times X_{F,p}}{(X_{F,p})^2 + (R_{F,p})^2}$$

where $X_{F,p}$ and $X_{F,s}$ are the parallel and series capacitative components of the impedance, $1/\omega C_{F,p}$ and $1/\omega C_{F,s}$ respectively. $R_{F,p}$ and $R_{F,s}$ are the parallel and series ohmic components of the faradaic impedance. It is convenient to calculate $R_{F,s}$ and $X_{F,s}$ from the experimental data by means of a HP 25 programmable scientific calculator. The numerical values of $R_{F,s}$ and $X_{F,s}$ as a function of ω and P are listed in Table 4.2.1.

4.2.1 (i) The Impedance Behaviour

Analysis of the a.c. impedance was made in the usual way[107] by means of Randles plots[102] in which the "series" faradaic resistance $R_{F,s}$ and the diffusional capacitance ($1/\omega C_{F,s}$) contributions are plotted as a function of $\omega^{-1/2}$ after separation of the double-layer capacity determined in experiments in the absence of the redox couple. The double-layer capacity was also determined from the results at $\phi = 90^{o}$ at potentials well away from the half-wave potentials, i.e. where the Warburg diffusional capacitance is negligible. The faradaic reaction resistance, R_r, was then evaluated by extrapolation of the Randles plots to infinite frequency, as shown in Fig. (4.2.3), giving

$$R_r = RT/zFi_o \qquad (4.2.1)$$

where the exchange current i_o is related to the standard electrochemical rate constant $\bar{k}^{o}$ by

$$i_o = zF\bar{k}^{o}CA \qquad (4.2.2)$$

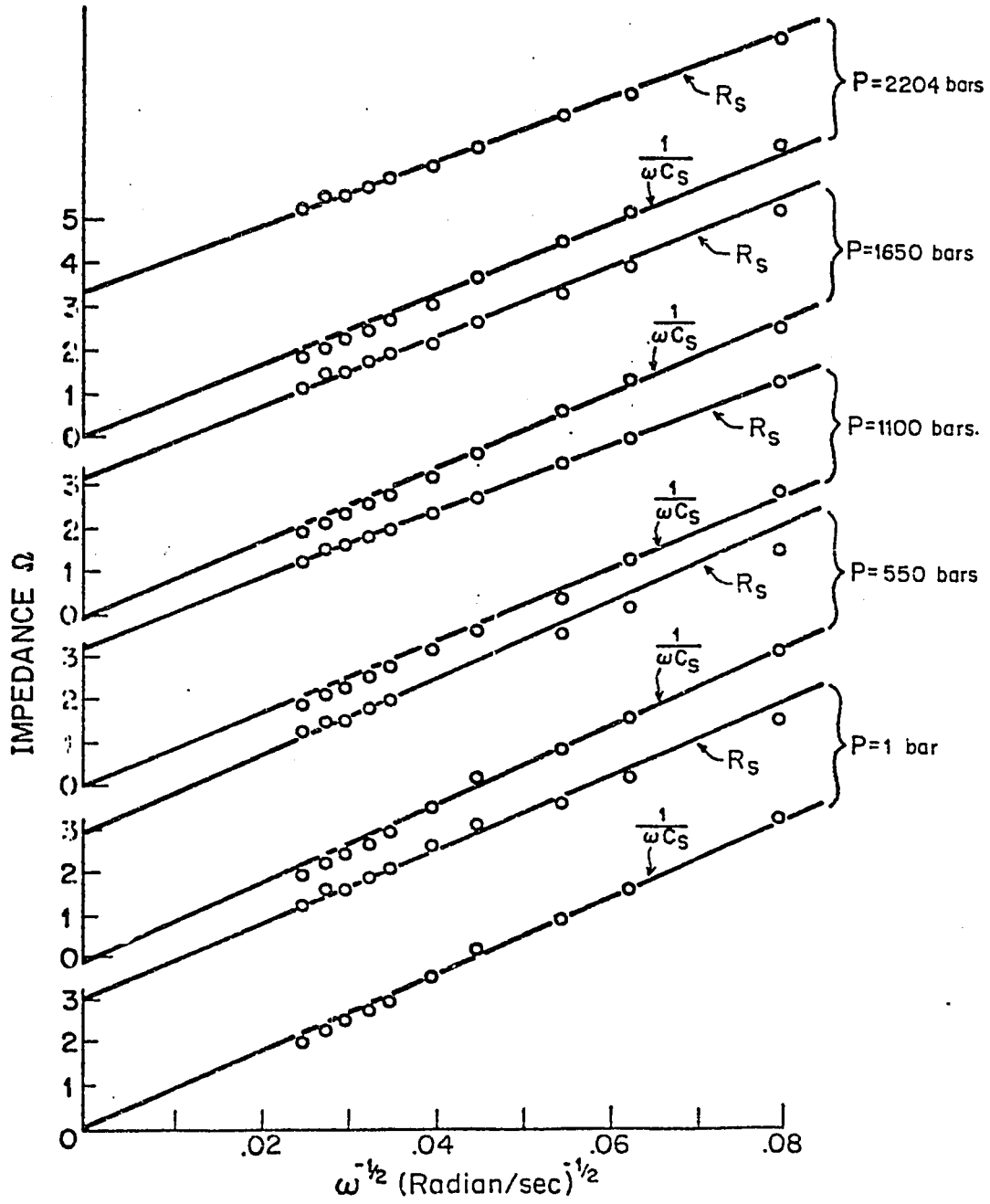

FIGURE 4.2.3 Randles plots for the impedance behaviour of the $Fe(CN)_6^{3-}$ / $Fe(CN)_6^{4-}$ redox reaction at Au at 298K. P=1,550,1100,1650 and 2204 bars.

and A is the electrode area, z is the number of electrons (z = 1 here) in the exchange reaction and C the concentration in mol cm^{-3} of the reactant species. The measured "a.c.", currents were evaluated for unit area of the substrate metal and, for high pressures, corrections were made to the ambient pressure concentration using the known compressibility of the solutions.[41]

A test of the satisfactory operation of the electronic measurement system is that the $R_{F,s}$ and $1/\omega\ C_{F,s}$ quantities should give parallel lines in a plot against $\omega^{-1/2}$ and the $1/\omega\ C_{F,s}$ relation should pass through the origin.

Figure (4.2.3) shows the results at pressures 1, 550, 1100, 1650 and 2204 bars. The plots of $R_{F,s}$ and $1/\omega\ C_{F,s}$ versus $\omega^{-1/2}$ at each pressure are satisfactorily parallel, with the out-of-phase component passing through the origin as required from the treatment of Randles[102]:

$$\frac{1}{\omega C_{F,s}} = \frac{RT}{z^2F^2AC}\left[\frac{2}{\omega D}\right]^{1/2} \qquad (4.2.3)$$

where A is the area of the electrode, C the bulk concentration of the 'depolarizer', i.e., $Fe(CN)_6^{-4}/Fe(CN)_6^{-3}$ and D the mean diffusion coefficient of the redox couple ions.

The intercept of the in-phase component line is related to the heterogeneous rate constant $\bar{k}^o$ by the following relation:

$$R_{F,s} = \frac{RT}{z^2F^2AC}\left[\left[\frac{2}{\omega D}\right]^{1/2} + \frac{1}{\bar{k}^o}\right] \qquad (4.2.4)$$

At $\omega^{-1/2} = 0$, the faradaic resistance becomes the reaction resistance, R_r, as represented by the equation

$$R_r = \frac{RT}{z^2F^2AC}\left(\frac{l}{k^o}\right) = \frac{RT}{zFi_o} \qquad (4.2.5.\ \text{cf. } 4.2.1)$$

The numerical results are recorded in Table 4.2.2. The results are fitted to a second-order polynomial of the form

$$\ln i_o = a + bP + cP^2$$

and plotted as $\ln i_o$ vs P as in Fig. (4.2.4). Also included are the error limits of the best-fit data. The limiting slope $\left(\frac{\partial \ln i_o}{\partial P}\right)_{\eta=0}$ at $P \to 0$ bars is evaluated from the coefficient b as $(-7.47 \pm 0.4) \times 10^{-5}$ bar^{-1}. The significance of this finite, rather than zero, value for $(\partial \ln i_o/\partial P)_{\eta = o}$ for the symmetry of the activation process will be discussed later.

4.2.1 (ii) Relation to Volumes of Activation

The pressure coefficient derived above is related to the apparent (see ref. 39) volume of activation $\Delta V_a^{\ddagger}$ given by

$$\left(\frac{\partial \ln i_o}{\partial P}\right)_{\eta=0} = \frac{\Delta V_a^{\ddagger}}{RT} = -\ 7.47 \times 10^{-5}\ bar^{-1} \qquad (4.2.6)$$

Hence

$$\Delta V_a^{\ddagger} = 1.9 \pm 0.1\ cm^3\ mol^{-1} \qquad (4.2.7)$$

for the ferri/ferrocyanide couple at its equilibrium potential.

TABLE 4.2.2

Impedance and kinetic results for the $Fe(CN)_6^{3-}/Fe(CN)_6^{4-}$ couple at a gold electrode at 25°C as a function of pressure

Pressure (bars)	R_r (Ω)	$i_o \times 10^2$ (A cm^{-2})	ln i_o	$\bar{k}^o \times 10^2$ * ($cm\ s^{-1}$)
1	3.24	1.13	-4.481	2.34
550	3.35	1.11	-4.514	2.30
1100	3.51	1.05	-4.561	2.18
1650	3.58	1.02	-4.581	2.11
2204	3.70	0.99	-4.614	2.05
Initial slope $(\partial \ln i_o/\partial P)_{P\to 0\ bar}$ = -7.47×10^{-5} bar^{-1}				

* Derived from i_o values after allowance for pressure-dependent concentration of reactant ions.

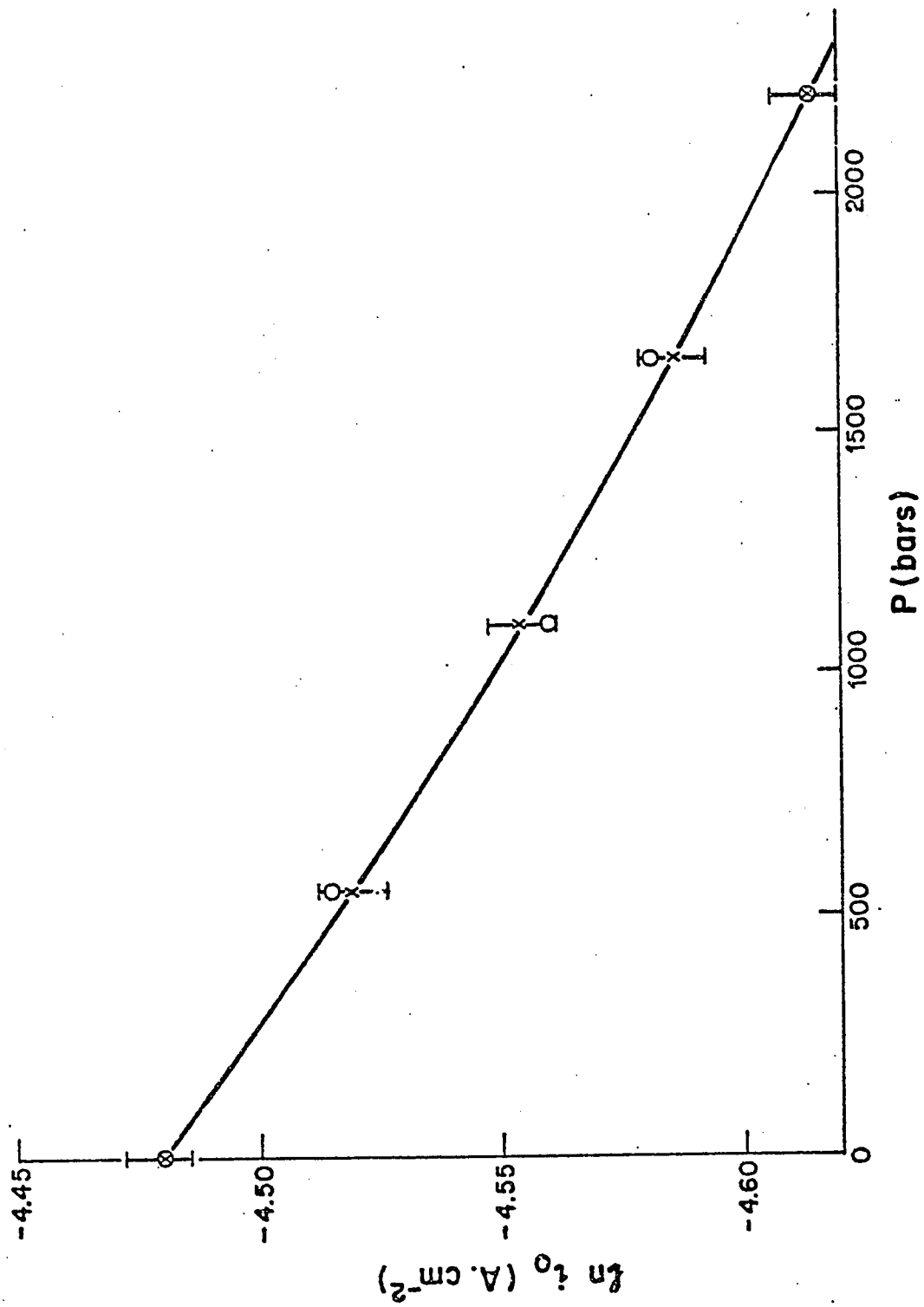

FIGURE 4.2.4 Plot of ln i_o against pressure for the $Fe(CN)_6^{3-}/Fe(CN)_6^{4-}$ redox reaction at Au at 298 K.

4.2.2 Discussion

(i) Significance of the Kinetic Data Derived from the a.c. Impedance Measurements

The reaction resistance determined gives the exchange current density, i_o, as indicated by eqn (4.2.1). It is thus the i_o values which are obtained in an electrochemical experiment as a function of pressure or, through eqn. (4.2.2), the standard electrochemical rate constants $\bar{k}^o$.

In terms of the metal-solution p.d. at the reversible potential ϕ_{rev} (for which i_o is evaluated), or the standard reversible potential ϕ^o_{rev},

$$i_o = zF \vec{k} C_o \exp(-\beta\phi^o_{rev}F/RT) = zF \overleftarrow{k} C_R \exp (1-\beta)\phi^o_{rev}F/RT \qquad (4.2.8)$$

for oxidized O and reduced R species at concentrations C_0 and C_R, respectively. Thus, $\frac{i_o}{zFC_0}$ or i_o/zFC_R measures the electrochemical (i.e. for the metal-solution p.d. ϕ_{rev}) rate constant. For standard conditions

$$\vec{k} \exp(-\beta\phi^o_{rev} F/RT) = \overleftarrow{k} \exp(1-\beta)\phi^o_{rev} F/RT \qquad (4.2.9)$$

i.e. when $C_0 = C_R$ (or more exactly $a_0 = a_R$). The values of $\vec{k}$ or $\overleftarrow{k}$, or their pressure coefficients, can only be obtained, respectively, from an absolute knowledge of ϕ_{rev} or its pressure coefficient. Knowledge of ϕ_{rev} is always quite inexact but it is clear that true values of $\partial \ln \overleftarrow{k}/\partial P$ or $\partial \ln \vec{k}/\partial P$ can be known if the more accessible pressure coefficient of ϕ_{rev} is available, as is usually the case. This, of course, is related to the volume change in the overall reversible reaction, ΔV_o.

Thus,

$$\left(\frac{\partial \ln \vec{k}}{\partial P}\right)_{\eta=0,T} - \frac{\beta F}{RT}\left(\frac{\partial \phi^{o}_{rev}}{\partial P}\right)_{T} = \left(\frac{\partial \ln \overleftarrow{k}}{\partial P}\right)_{\eta=0,T} + \frac{(1-\beta)F}{RT}\left(\frac{\partial \phi^{o}_{rev}}{\partial P}\right)_{T} \quad (4.2.10a)$$

or

$$\left(\frac{\partial \ln \vec{k}}{\partial P}\right)_{\eta=0,T} = \left(\frac{\partial \ln \overleftarrow{k}}{\partial P}\right)_{\eta=0,T} + \frac{F}{RT}\left(\frac{\partial \phi^{o}_{rev}}{\partial P}\right) \quad (4.2.10b)$$

Noting the relations previously obtained (Chapter 1) for the $\partial \ln k/\partial P$ derivatives in terms of the volumes of activation, and the relation between ϕ^{o}_{rev} and ΔG^{o} for the reversible reaction ($-zF\phi^{o}_{rev} = \Delta G^{o}$), we have

$$\frac{\Delta \vec{V}_t^{\ddagger}}{RT} = \frac{\Delta \overleftarrow{V}_t^{\ddagger}}{RT} + \frac{\Delta V_o}{RT} \quad (4.2.11)$$

or

$$\Delta V_o = \Delta \vec{V}_t^{\ddagger} - \Delta \overleftarrow{V}_t^{\ddagger} \quad (4.2.12)$$

as may be seen intuitively in terms of changes of free energy and volume along the reaction coordinate. The relations between $\Delta \vec{V}_t^{\ddagger}$, $\Delta \overleftarrow{V}_t^{\ddagger}$ and ΔV_o are illustrated schematically in Fig. (4.2.5(a)) for a general case. Normally, for an ionic redox reaction, $V^{\ddagger}$ will be expected to lie between V_o and V_R, where the V terms denote the partial molar quantities.

It is seen that the pressure coefficient of $\ln i_o$, which we have derived in the present experimental work, gives the <u>equal</u> volume changes, $\Delta V_a^{\ddagger}$, corresponding to

$$-\frac{\Delta V_a^{\ddagger}}{RT} = \left(\frac{\partial \ln \vec{k}}{\partial P}\right)_{\eta=0,T} - \frac{\beta F}{RT}\left(\frac{\partial \phi^{o}_{rev}}{\partial P}\right)_{T} \text{ or } \left(\frac{\partial \ln \overleftarrow{k}}{\partial P}\right)_{\eta=0,T} + \frac{(1-\beta)F}{RT}\left(\frac{\partial \phi^{o}_{rev}}{P}\right)_{T} \quad (4.2.13)$$

since, at the reversible potential, the electrochemical free energies of the reactant and product species are at identical levels.

It also follows from eqns. (4.2.10a) or (4.2.10b), or eqn. (4.2.13), that

$$\Delta V_a^{\ddagger} = \Delta \vec{V}_t^{\ddagger} - \beta \Delta V_o = \Delta \overleftarrow{V}_t^{\ddagger} + (1-\beta)\ \Delta V_o \qquad (4.2.14)$$

so that $\Delta V_a^{\ddagger} = 0$ for a symmetrical reaction ($\beta = 0.5$).

This corresponds to the situation illustrated schematically in Fig. 4.2.5(b) for volume changes at the reversible potential.

Since a relatively accurate non-thermodynamic estimate can usually be made of the volume change ΔV_o for the overall reaction, both $\vec{V}_t^{\ddagger}$ and $\overleftarrow{V}_t^{\ddagger}$ can be separately evaluated from $\Delta V_a^{\ddagger}$ derived from $(\partial \ln i_o/\partial P)_T$.

A relation obtainable from eqn. (4.3.14) is

$$2\Delta V_a^{\ddagger} = \Delta \vec{V}_t^{\ddagger} + \Delta \overleftarrow{V}_t^{\ddagger} + (1-2\beta)\ \Delta V_o \qquad (4.2.15)$$

giving

$$(1-2\beta) = [2\Delta V_a^{\ddagger} - (\Delta \vec{V}_t^{\ddagger} + \Delta \overleftarrow{V}_t^{\ddagger})]/\ \Delta V_o \qquad (4.2.16)$$

which would enable β to be evaluated if $\Delta \vec{V}_t^{\ddagger}$ and $\Delta \overleftarrow{V}_t^{\ddagger}$, or their sum, were independently available. A symmetrical transition state, $\beta = 1/2$, corresponds, of course, to $V_a^{\ddagger} = 1/2(\Delta \vec{V}_t^{\ddagger} + \Delta \overleftarrow{V}_t^{\ddagger}) = 0$. Unfortunately, it is clear from the foregoing that $\Delta \vec{V}_t^{\ddagger}$ and $\Delta \overleftarrow{V}_t^{\ddagger}$ can be evaluated through eqn. (4.2.14) from the measured $\Delta V_a^{\ddagger}$ and a non-thermodynamic value of ΔV_o only by choosing a reasonable value for β which would be presumed to be 1/2 for a "symmetrical" redox reaction.

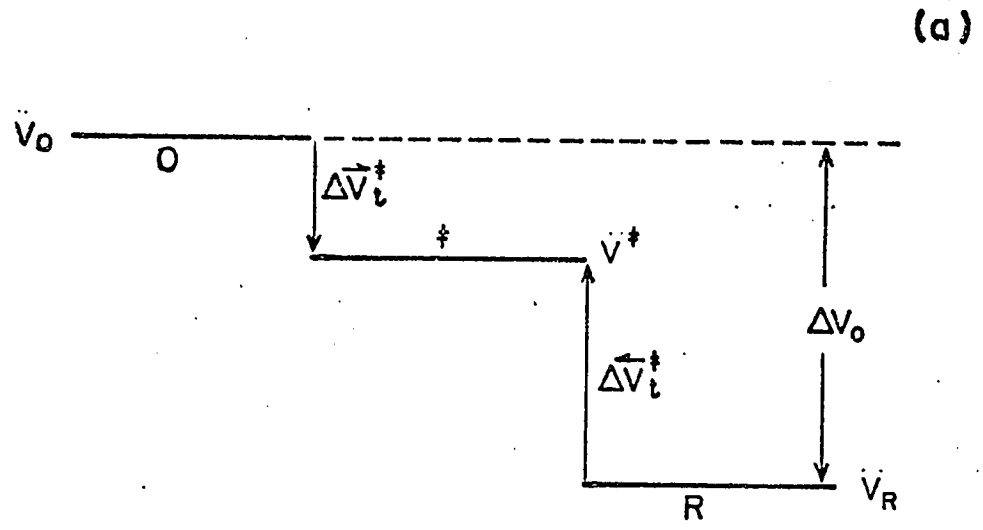

General Case $O + ze \longrightarrow R$
(Hypothetical $\phi = o$)

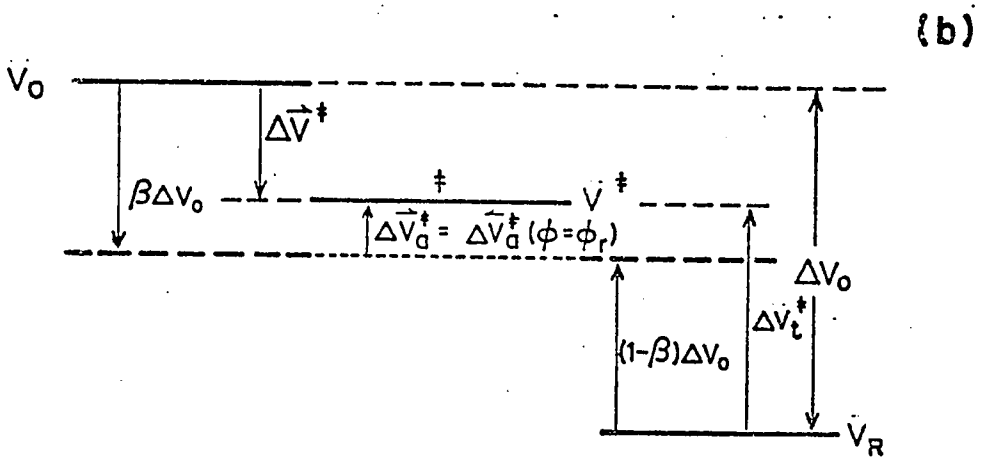

General Case $O + ze \longrightarrow R$
($\phi = \phi_r$, at equilibrium)

FIGURE 4.2.5 Schematic relations between the true and apparent volumes of activation for the backward and forward directions of a general electron transfer reaction at ϕ=0 (hypothetical) and $\phi=\phi_{rev}$, i.e. at equilibrium, and the overall partial molar volume difference ΔV_o, between products and reactants. $V^{\ddagger}$ is the partial molar volume of the transition state.

4.2.2 (ii) Applications to the Results for the $Fe(CN)_6^{3-}/Fe(CN)_6^{4-}$ Couple

In order to interpret the solvent reorganization behaviour in this reaction, we require the change of electrostriction volume between the initial state and the transition state. The apparent volume of activation, $\Delta V_a^{\ddagger}$, is available from the measurement of $\left(\frac{\partial \ln i_o}{\partial P}\right)_T$. Hence we first require ΔV_o (eqn. 4.2.14) for the reaction $Fe(CN)_6^{3-} + e \rightarrow Fe(CN)_6^{4-}$.

For the systems studied here, the individual partial molar volumes for the ions of the couple are[109,110]

$$V^{\infty}_{Fe(CN)_6^{4-}} = 95.6 \text{ and } V^{\infty}_{Fe(CN)_6^{3-}} = 137.0 \text{ cm}^3 \text{ mol}^{-1}$$

These values are based on the well established individual ionic volume of the proton ($V^{\infty}_{H^+} = -5.4$ cm^3 mol^{-1}) derived in at least two ways which give concordant results as discussed in previously published literature[36-38,111]. The volume of the electron V_e in the half-cell redox reaction should be taken into account. It is difficult to find a reliable value for this term but Heusler and Gaiser[15] have suggested a value of 3 cm^3 Faraday^{-1} in a metal in their work on the H_2 - evolution reaction. Using this value,

$$\Delta V_o = V^{\infty}_{Fe(CN)_6^{4-}} - V^{\infty}_{Fe(CN)_6^{3-}} - V_e = -44.4 \text{ cm}^3 \text{ mol}^{-1}$$

Then, following eqn. (4.2.14), the true volumes of activation for the forward and backward directions of the reaction can be calculated from the common apparent volume of activation, $\Delta V_a^{\ddagger} = 1.9$ cm^3 mol^{-1} (eqn. 4.2.7). Thus, for the reaction written in the direction $Fe(CN)_6^{3-} + e \rightarrow Fe(CN)_6^{4-}$,

$$\Delta\vec{V}_t^{\ddagger} = 1.9 + 1/2(-44.4) = -20.3 \text{ cm}^3 \text{ mol}^{-1} \qquad (4.2.17a)$$

and

$$\Delta\overleftarrow{V}_t^{\ddagger} = 1.9 - 1/2(-44.4) = 24.1 \text{ cm}^3 \text{ mol}^{-1} \qquad (4.2.17b)$$

assuming β for this reaction can be taken (see below and ref. 21) as 1/2. The partial molar volume of the transition state, $V^{\ddagger}$, is estimated from the relationship

$$V^{\ddagger} = V^{\infty}_{Fe(CN)_6^{3-}} + V_e + \Delta V_t^{\ddagger} = 119.7 \text{ cm}^3 \text{ mol}^{-1} \qquad (4.2.18)$$

As in Fig. 4.2.5a, the changes of volume in the system as it passes from its initial state, through the transition state, to the final state can be represented schematically as shown in Fig. 4.2.6.

While the main changes in volume of conjugate ions in a redox couple are associated with the difference of electrostriction between the pair of ions, significant effects which must be considered can also arise from the change of ionic radius or ligand-to-metal bond length [112,113]. Thus, in an isoelectronic series, e.g. Na^+, Ne and F^-, changes of charge produce appreciable changes, Δr, of radii, from 0.95, through 1.1 to 1.36Å, respectively, for these three elements. Similarly, for Pb^{4+} to Pb^{2+}, the difference of radii is 0.36 Å for 2e. It is more difficult to judge the effects of change of charge in $Fe(CN)_6^{3-}/Fe(CN)_6^{4-}$ because it is a complex ion with some charge delocalization[114]. Based on the above figures for simple ions, a reasonable estimate of Δr would be 0.1 Å per electron. However, recent crystallographic data[115,116] on $Fe(CN)_6^{3-}$ and $Fe(CN)_6^{4-}$ (as their acids or salts) indicate, in fact, that there is very little difference in radius of these two ions and M.O. calculations[114] show that the effective charges on Fe are almost identical. Thus the total Fe-to-N

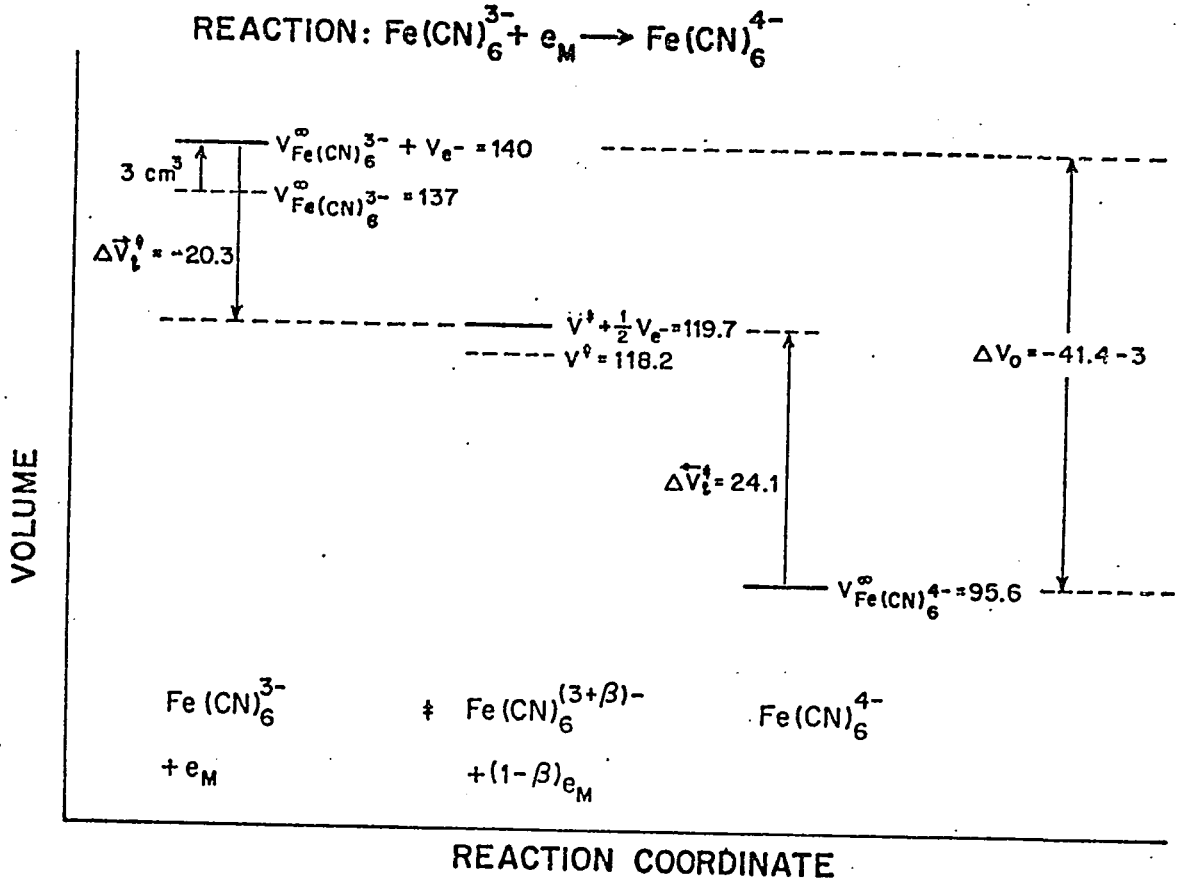

FIGURE 4.2.6 Schematic relation for the volume changes in the $Fe(CN)_6^{3-} + e \longrightarrow Fe(CN)_6^{4-}$ reaction showing the true volumes of activation in relation to the partial molar volumes of the initial, final and transition state (=). All volume data are in $cm^3\ mole^{-1}$.

length is 3.07 Å in La $Fe(CN)_6 . 5H_2O$[115] and 3.04 Å in $H_4 [Fe(CN)_6]$[116], the value for the 4-ion being surprisingly the smaller of the two. This is consistent with a difference of 0.1 Å taken by Mathieson[117] in that direction. The similar sizes of the two ions of the couple is also borne out by the similarilty of their ionic mobilities[118-120] at infinite dilution which indicates they have almost the same Stokes hydration radii.

Bearing in mind that it has been assumed that $\beta = 0.5$ for the $Fe(CN)_6^{3-}/Fe(CN)_6^{4-}$ system, then the transition state for an adiabatic electron transfer (cf.[21]) should bear a charge of -3.5e. Taking the radius of $Fe(CN)_6^{3-}$ as 3.31 Å[117], an intrinsic volume of 91 $cm^3\ mol^{-1}$ is calculated. With $\Delta r = -0.03$ Å per e[115,116], the intrinsic volume of the transition state ion (charge -3.5e) would be 90 $cm^3\ mol^{-1}$, i.e. 1 $cm^3\ mol^{-1}$ smaller than the initial state ion. Therefore the volume change due to solvent reorganization ($\Delta\vec{V}^{\ddagger}_{t,r}$) will be somewhat less than $\Delta\vec{V}^{\ddagger}_{t}$ and takes the value -20.3 + 1 in $cm^3\ mol^{-1}$, i.e. -19.3 $cm^3\ mol^{-1}$, since $\Delta\vec{V}^{\ddagger}_{t}$ measures the total of all volume contributions associated with the formation of the transition state. Correspondingly $\Delta\overleftarrow{V}^{\ddagger}_{t,r}$ will be 23.1 $cm^3\ mol^{-1}$.

The main point to be emphasized is that these figures of -19.3 and 23.1 $cm^3\ mol^{-1}$ are relatively large volume changes and are associated mainly with the change of electrostriction about the ion since the small change of intrinsic volume has been allowed for. It is to be noted that the $\Delta\vec{V}^{\ddagger}_{t}$ differ significantly, but by a small amount, from half the volume change, ΔV_o, in the overall reaction. This behaviour originates from the fact that $\Delta V^{\ddagger}_{a}$ differs significantly from zero. The significance of the volume changes in Fig. 4.2.6 for the "symmetry" of the reaction will be examined later.

From the above data and Fig. 4.2.6 it is seen that the total volume of activation, less the contribution associated with "(1/2)e" that

remains in the metal, is -18.8 $cm^3\ mol^{-1}$. This is the volume change associated with solvent reorganization about the ion (including any contribution locally in the double-layer) plus the change of intrinsic volume of the ion in the activation process in which (1/2)e is transferred. Therefore the solvent electrostriction volume change in the activation process is -18.8 -(-1) $cm^3\ mol^{-1}$ = -17.8 $cm^3\ mol^{-1}$ for the forward direction of the reaction and 21.6 $cm^3\ mol^{-1}$ for the backward direction. This is to be compared with the solvent electrostriction change in the overall reaction which is -41.4-(-2) = -39.4 $cm^3\ mol^{-1}$. Although the numerical value of the volume of activation depends on the effective volume of the electron, it is to be noted that the evaluation of the solvent electrostriction volume from $\Delta V_a^{\ddagger}$ is independent of the value assigned to V_e. Values of the electrostriction volumes* derived for the present case are illustrated in Fig. 4.2.7.

4.2.2 (iii) Electrostriction Change and the Nature of the Activation Process

The electrostriction contributions, ΔV_{el}, to the volumes of activation derived above are quite large. In related theoretical considerations[99,100], it has been pointed out that there are difficulties in accepting the view[20-22] that the solvent reorganization process is associated only with organized fluctuations of long-range (Born) dielectric

* The ions of the ferro-ferricyanide couple exhibit unusual partial molal volume behaviour[117] as there is evidently an appreciable structure-forming volume in $Fe(CN)_6^{3-}$ aq. like that for R_4N^+ ions[111]. There is, however, the expected large electrostriction increase (-39.4 $cm^3\ mol^{-1}$) in going from the 3- to the 4- ion (Fig. 4.2.7).

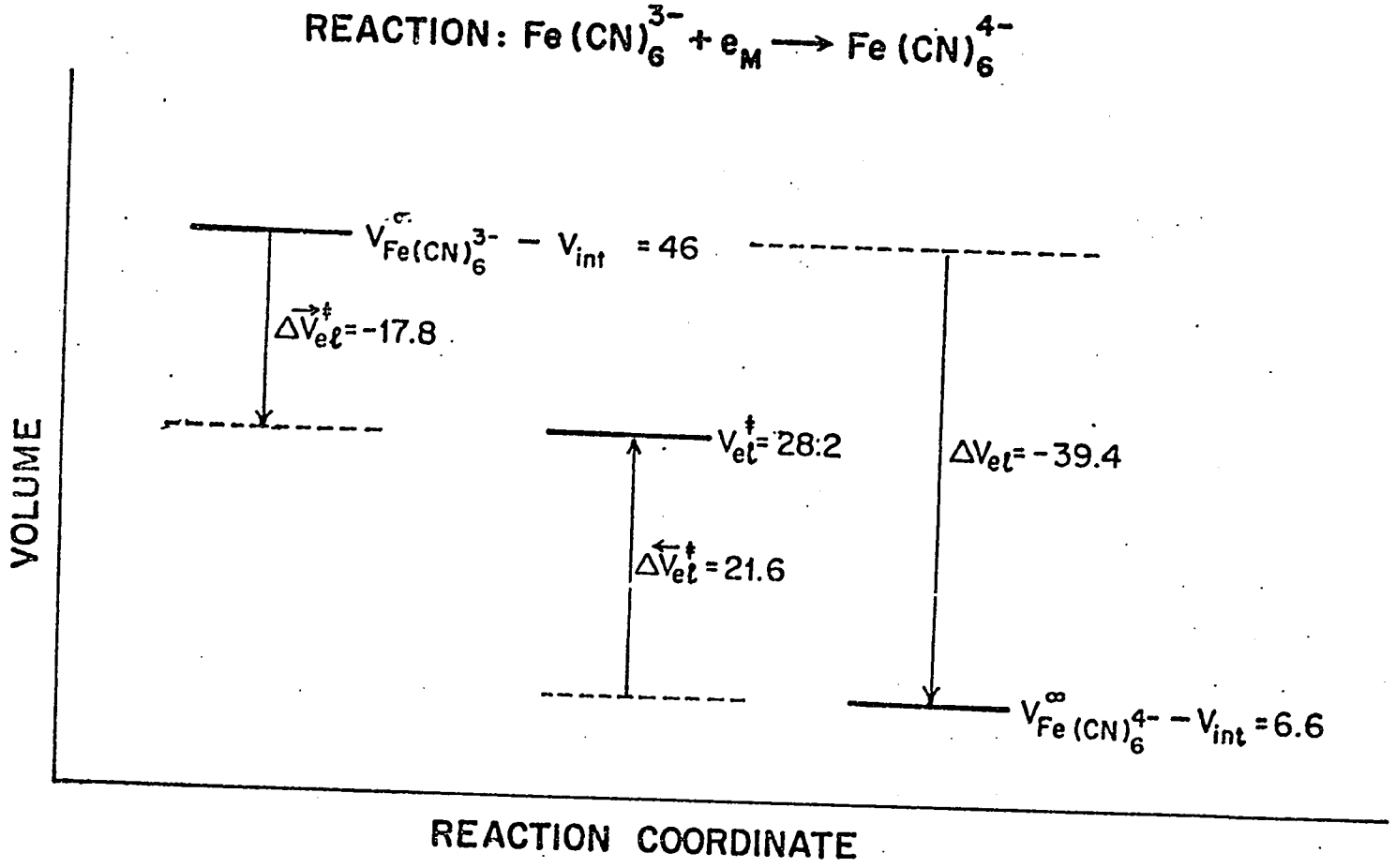

FIGURE 4.2.7 Schematic relation for the electrostriction volume changes in the $Fe(CN)_6^{3-}$ reaction, i.e. after the intrinsic volumes of the ions and the e volume have been subtracted out.

polarization. The quantum-mechanical objections to primary hydration sphere reorganization being involved in the activation process on the basis that the $h\nu$ values for the modes involved are much larger than kT are invalidated by the known[121] important contributions which such solvation-sphere modes make to the heat capacities of solvated ions in aqueous media at ordinary temperatures. Sufficient low-frequency vibration and intermolecular modes are available.

It is therefore important to attempt to estimate the relative contributions to the electrostriction, ΔV_{el}, at an ion in water from successive spherical annular elements of the solvent out from the periphery of the ion; especially the contribution to ΔV_{el} from the solvent volume within 3-4 $\overset{o}{A}$ from the ion in comparison with that further out, viz. 5-50 $\overset{o}{A}$, will be of interest.

The specific compressibility γ is given by

$$\gamma = -\frac{1}{V}\left(\frac{dV}{dP}\right) \tag{4.2.19}$$

and the electrostrictive pressure P by

$$P = \varepsilon_r E^2/8\pi = (ze)^2/8\pi\varepsilon_r r^4 \tag{4.2.20}$$

where E is the field $ze/\varepsilon_r r^2$ due to the ion in the dielectric taking into account the fact that the relative permittivity, ε_r, is a function of r, the distance from the ion.

Then, from eqn. (4.2.20)

$$\frac{dP}{dr} = -\left[(ze)^2/2\pi\varepsilon_r r^5\right] - \frac{(ze)^2}{\varepsilon_r^2\, 8\pi r^4}\left(\frac{d\varepsilon_r}{dr}\right) \tag{4.2.21}$$

The relative volume change dV in a spherical volume element $4\pi r^2$. dr about the ion will be given by eqn. (4.2.19) as

$$dV = -\gamma\, 4\pi r^2 . dr . dP \qquad (4.2.22)$$

Then, introducing dP as f(r.dr) from eqn.(4.2.21),

$$dV = \frac{2\gamma(ze)^2}{\varepsilon_r\, r^3}\, dr.dr + \frac{\gamma(ze)^2}{2r^2\, \varepsilon_r^2}\, dr.d\varepsilon_r \qquad (4.2.23)$$

from which changes of volume due to electrostrictive tension in successive annular elements of volume can be calculated by integration. In eqn. (4.2.23), it is to be expected[122] that γ as well as ε will be a function of r. Hence integration of eqn. (4.2.23) with both γ and ε as a function of r is obviously difficult but another approach may be made using the calculations previously published[122] from this Laboratory, based on empirical equations for pressure and field effects on ε, and the thermodynamic theory of electrostriction given by Frank[123].

It is convenient to consider the permittivity near an ion in terms of a step-function[124] related to the semi-empirical expression[125] for the differential dielectric constant ε_d as f(E):

$$\varepsilon_d = [(\varepsilon_o - n_o^2)/(1 + bE^2)] + n_o^2 \qquad (4.2.24)$$

where n_o^2 is the square of the refractive index and ε_o is the static, zero-field dielectric constant; b is a coefficient related to field-dependence of ε_d derived in Booth's theory[126]. Two cases of interest arise in electrostriction theory[122]: when $bE^2 \ll 1$ and $bE^2 \gg 1$, i.e. for low and high fields.

The high-field approximation gives[122] for the relative volumes of normal (v_o) and electrostricted (v) water

$$\log v_o/_v = G \log (KE^2 + 1) \qquad (4.2.25)$$

where

$$G = D/(1-C) = 0.1469$$

and

$$K = C(1-C)n_o^2/8\pi\beta D = 1.102 \times 10^{-11}$$

and β, C and D are known empirical constants[122] determining the pressure-dependence of n_o^2 and ε.

The following model of the hydration of the $Fe(CN)_6^{3-}$ and $Fe(CN)_6^{4-}$ ions will be considered: eight hydration shell water molecules can be accomodated in the faces of the octahedral 6CN/Fe arrangement and will be firmly bound electrostatically; another shell, one H_2O molecule in thickness, is also firmly associated ($\varepsilon \to n_o^2$) with the complex further out. Both types of ions presumably will have a similar inner layer of the 8 water molecules. This model seems reasonable since the two kinds of ions have 3 and 4 times the charge of a simple ion like Na^+ but have a hydration radius about twice as great so that, although the field is 2 1/2 times smaller <u>per charge</u>, the net electrostrictive field near the periphery of both ions will be larger than that near a small univalent ion.

Under low-field conditions, <u>beyond</u> the primary hydration shell, the equation for dV can be analytically integrated since ε can then be assumed[124] to be almost independent of E as can γ. Then eqn (4.2.23) can be integrated to give the electrostriction volume

$$\Delta V_{el} = \int_{r_h}^{\infty} dV = \int_{r_h}^{\infty} \int_{r_h}^{\infty} \frac{2(ze)^2\gamma}{\varepsilon r^3} \, dr. \, dr$$

$$= \frac{(ze)^2\gamma}{\varepsilon} \left[\frac{1}{r}\right]_{r_h}^{\infty} \qquad (4.2.26)$$

where r_h is the radius of the outer periphery of the primary hydration shell. Taking $\gamma = 4.57 \times 10^{-11}$ cm^2 dyn^{-1} for water and $r_h = 6.09$ Å (where $r_i = 3.31$ Å) for $Fe(CN)_6^{3-}$ and 6.06 Å for $Fe(CN)_6^{4-}$ ($r_i = 3.28$ Å), enables the "Born" electrostriction volume, ΔV_{el}, arising <u>beyond</u> the primary hydration shells of these ions to be evaluated as

$$\Delta V_{el,\ Fe(CN)_6^{3-}} = -12.0;\ \Delta V_{el,Fe(CN)_6^{4-}} = -21.0 \text{ cm}^3 \text{ mol}^{-1} \qquad (4.2.27)$$

The relative contributions to the ΔV_{el} in annular volume elements of increasing thicknesses over the first 50 Å from the periphery of the primary hydration shells of the ions can be evaluated from eqn. (4.2.27) using successively different integration limits and are shown in Fig. 4.2.8. The total difference of the long-range electrostriction, which corresponds to the figures in eqn. (4.2.27) with ∞ taken as the upper limit in the integrals of eqn. (4.2.26), is -9 cm^3 mol^{-1}, i.e. -4.5 cm^3 mol^{-1} for the electrostriction change upon activation ($\beta = 1/2$). It is important to note that this is only <u>ca.</u> 25% of the total real volume of activation.

The primary hydration shell volume differences $\delta\Delta V_{el,1}$ in $Fe(CN)_6^{3-}$ and $Fe(CN)_6^{4-}$ are evaluated using eqn. (4.2.25) assuming the field E is given by $E = (ze)^2/\varepsilon(r_h')^2$ where r_h' is the mean radius of the hydration shell (i.e. $r_h' = r_i + 1/2\ d_{H_2O}$ where r_i is the ionic radius and d the diameter (=1.39 Å) of a water molecule; also r_h' is related to r_h in eqn. (4.2.26) by $r_h' = r_h - 1/2\ d_{H_2O}$). ε for the primary hydration shell is taken as 2 (cf. refs. 124,125 and 126). The volume differences will depend (a) on the ionic radii taken for the ions themselves and (b) on the field E in the primary shell.

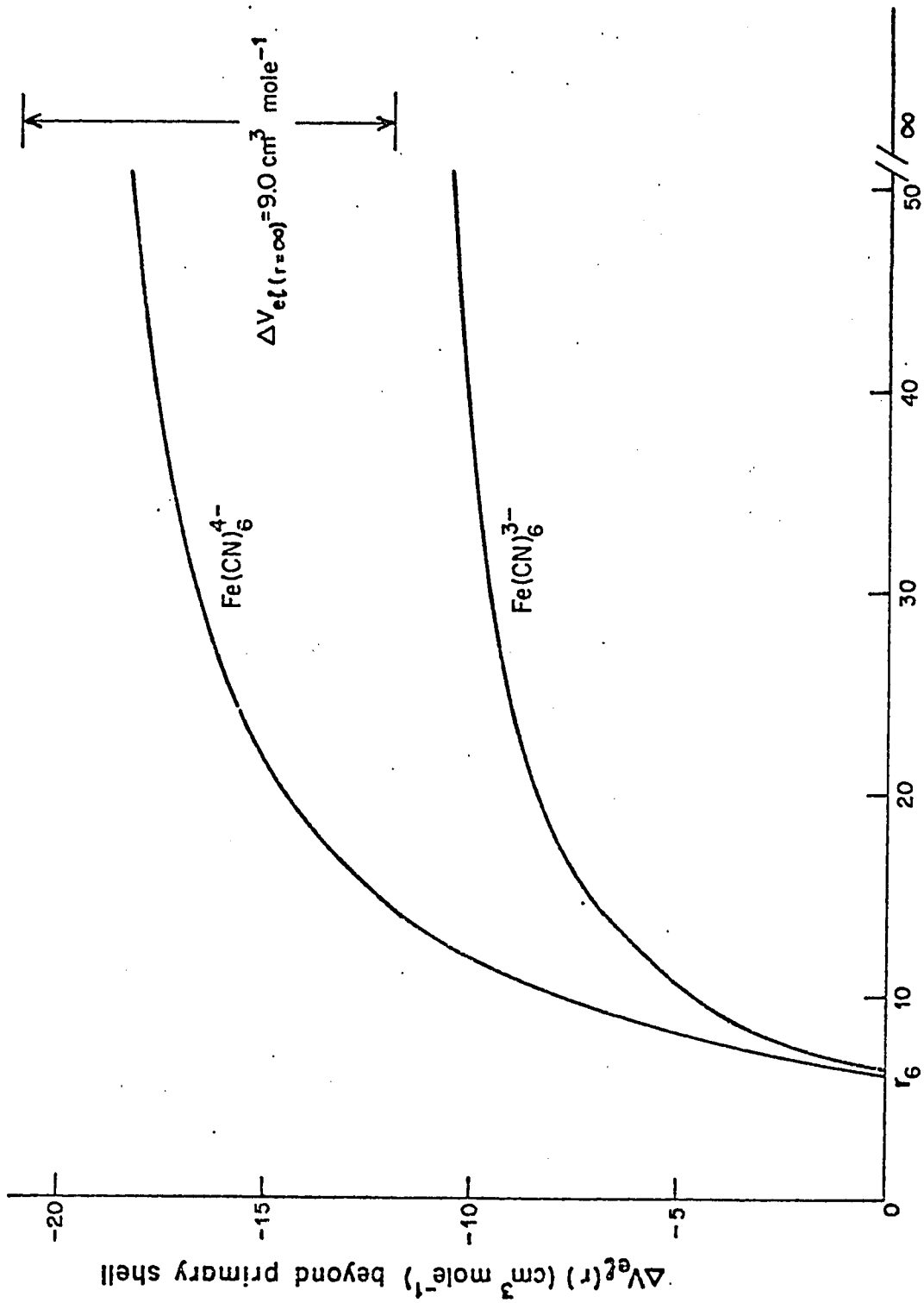

FIGURE 4.2.8 Calculated Born polarization electrostriction volume changes ΔV_{el} (from eqn. 4.2.26) beyond the primary hydration shells as a function of distance r from the periphery of those shells at $Fe(CN)_6^{4-}$ and $Fe(CN)_6^{3-}$ ions.

In order to try to make an objective evaluation of the electrostriction, we have made several estimates of the primary shell contribution to ΔV_{el} based on one assumed and various available values of the differences of ionic radii. The volumes of the primary hydration shells are calculated, the field is estimated as above and then application of eqn. (4.2.25) gives the compression ratio[123] v/v_o to be applied to these volumes for the two ions; hence $\Delta V_{el,1}$ is evaluated. The results of these calculations are given in Table 4.2.3. Calculations of this kind have been given in ref. 122 where the uncertainties were examined. However, here, differences in volumes are involved so the reliability of their evaluation may be better than that in calculations for individual ions.

4.2.3 Relation to Theories of Electron Transfer

(i) Evidence for Reorganisation in the Primary Hydration Shell

The experimental value for the overall volume change in the reaction (4.2.8)(-44.4 $cm^3\ mol^{-1}$) when corrected for the change of intrinsic volume of the ion and for the finite volume of the electron gives an electrostriction volume change of -39.4 $cm^3\ mol^{-1}$. This agrees best with the total electrostriction change (-40 $cm^3\ mol^{-1}$) calculated for the case where there is a small contraction of ionic radius from $Fe(CN)_6^{3-}$ to $Fe(CN)_6^{4-}$ as indicated by the X-ray diffraction results (Table 4.2.3). Other assignments of ionic radii differences, except that where $r_{Fe(CN)_6^{4-}} > r_{Fe(CN)_6^{3-}}$, give the right order of magnitude but not such good agreement with experiment. It can be concluded from these calculations that the main contribution (ca. 75%) to ΔV_{el} arises from changes in primary hydration shell volume and only ca. 25% from volume changes due to long-range polarization (Fig. 4.2.8). The latter calculations

TABLE 4.2.3

Electrostriction Volume Difference in Primary Hydration Shells of $Fe(CN)_6^{3-}$ and $Fe(CN)_6^{4-}$ Ions in Water for Various Assumed Radii

Ion	Ionic Radii (Å)	Hydration Shell volumes ($cm^3\ mol^{-1}$)	Field in shell (e.s.u.)	Electrostriction factor ν_o/ν from eqn. (4.2.25)	Electrostriction volume difference $\Delta V_{el,1}$ ($cm^3\ mol^{-1}$)	Total electrostriction volume difference: primary shell + Born electrostriction beyond.
$Fe(CN)_6^{3-}$	3.31*	484	3.3×10^5	1.12	-22	-31
$Fe(CN)_6^{4-}$	3.31*	484	4.4×10^5	1.18		
$Fe(CN)_6^{3-}$	3.31*	484	3.3×10^5	1.12	-31	-40 (in best agreement with expt.)
$Fe(CN)_6^{4-}$	3.28≠	478	4.48×10^5	1.19		
$Fe(CN)_6^{3-}$	3.31*	484	3.3×10^5	1.12	-42	-51
$Fe(CN)_6^{4-}$	3.21	464	4.6×10^5	1.19		
$Fe(CN)_6^{3-}$	3.31 +	484	3.3×10^5	1.12	∿ - 1	∿ -10
$Fe(CN)_6^{4-}$	3.41 +	504	4.23×10^5	1.17		
$Fe(CN)_6^{3-}$	3.28[x]	478	3.35×10^5	1.13	-41	-50
$Fe(CN)_6^{4-}$	3.18[x]	458	4.65×10^5	1.20		

* From Mathieson[1] based on space-filling models with $V = 2.52\ r^3 = 91\ cm^3\ mol^{-1}$

x Based on emprical relations for effective ionic radii [127].

≠ Difference based on x-ray diffraction data on the solid salts [115, 116].

\+ Based on an assumption (see text) that $\Delta_r = 0.1$A increase per e added.

are relatively reliable since they depend on near normal values of ε and γ.

It has been shown above that the activation volume $\Delta V_t^{\ddagger}$ for the forward direction of the reaction is about 40% of the total volume change. Hence the activation volume involves a contribution of about 40% of 9.0 $cm^3\ mol^{-1}$ in the long-range polarization effect plus about 40% of 30.4 $cm^3\ mol^{-1}$ for the primary hydration shell volume change, assuming[21] in an adiabatic reaction there is a progressive change of electron charge density as the transition state configuration is developed from the initial state.

These results lead to the important conclusion that the activation process is associated mostly with a change of state of the primary hydration shell of the reactant ion rather than with fluctuations in the long-range polarization co-sphere of the ion. The latter effect has formed the basis of most theories of the activation process in redox reactions. Were it the main factor, as implied with respect to energies of activation, only a small volume of activation calculated from β times the result given by eqn. (4.2.26) would be observed; it is much smaller than that found experimentally.

4.2.3 (ii) Symmetry of the Transition States

For a homogeneous reaction between ferri and ferro-cyanide, the transition state must be a symmetrical complex between the ions with each having an intermediate charge -3.5e. While the overall equilibrium in a redox couple established at an electrode, referred to some other reference electrode, will be identical with that in the corresponding homogeneous reaction, a symmetrical transfer of charge

will not necessarily occur in the transition states involved in the electrochemical reactions

$$Fe(CN)_6^{3-} + e_M \longrightarrow Fe(CN)_6^{4-} \qquad (4.2.28)$$

or

$$Fe(CN)_6^{4-} \longrightarrow Fe(CN)_6^{3-} + e_M \qquad (4.2.29)$$

which occur at an electrode as distinct events at a common potential. The reason is that the ferri and ferro-cyanide ions will probably not interact with the electrode in the same way (cf. ref. 99) nor is this interaction likely to be negligible; for example, at Pt and Au, even simple ions such as SO_4^{2-} and ClO_4^- are quite strongly adsorbed. This situation means, of course, that β need not necessarily be exactly 0.5. This does not involve any conflict with the principle of microscopic reversibility, of course, since the equilibrium condition will always involve electrode potential terms in both $\exp(-\beta\phi_{r_{ev}}F/RT)$ and $\exp(1-\beta)\phi_{r_{ev}}F/RT$ in the usual way where $\phi_{r_{ev}}$ is the metal/solution p.d. at equilibrium.

The present experimental results, treated in the first approximation with the assumption that $\beta = 0.5$ (cf. ref. 21), show that the activation process, from the point of view of the volume changes involved, is, in fact, not "symmetrical" since the $\Delta\vec{V}_t^{\ddagger}$ is appreciably less than the $\Delta\overleftarrow{V}_t^{\ddagger}$. This result arises principally from the experimental fact that $\Delta V_a^{\ddagger}$ is not zero (see eqns. 4.2.7 and 4.2.14). From the point of view of solvent reorganization in the activation process,[20,21] this means that the hydration shell configurations of the transition states in eqns. (4.2.28) and 4.2.29) are not symmetrical with respect to those of reactant and product ions as would be the case in the corresponding homogeneous reaction. Presumably this could be due to different adsorption of

$Fe(CN)_6^{3-}$ and $Fe(CN)_6^{4-}$ anions at Au, i.e. different interactions of the two ions with the Au surface and with adsorbed water in the inner Helmholtz layer[128]. It is of interest to note that the asymmetry is less at higher pressures since $\Delta V_a^{\ddagger}$ decreases with pressure (Fig. 4.2.2).

If, in eqn. (4.2.14) a value of β were sought that gave equal numerical values for $\Delta\vec{V}_t^{\ddagger}$ and $\Delta\overleftarrow{V}_t^{\ddagger}$, it would not be 0.5, again indicating asymmetry in the activation processes for the forward and backward directions of the redox reaction at the electrode surface. It is to be noted that values of β for this reaction, differing significantly from 0.5, have been reported in the literature[97].

4.3 Pressure Effects on Surface Processes at Noble Metal Electrodes

4.3.1 Introduction

Monolayer electrodeposition processes at electrodes are characterized by the development of multiple states of chemisorption below monolayer coverage. These states, which are also observed on well characterized single-crystal surfaces, are of great interest in surface science[129,130]. They appear to be a general result of the surface-structural and electronic properties of the substrate metal since they are observed in under-potential deposition of H and metal atoms at noble metal cathodes, and of OH and O species at anodes. While electrochemical methods such as cyclic voltammetry and the modulated potentiodynamic linear sweep technique[131] give excellent resolution of the multiple states and enable their relative free energies of binding to be evaluated with an accuracy of ca. 1600 J mol^{-1}, it is desirable to evaluate other aspects of the behaviour of the electrochemical adsorption process. The use of high-pressure techniques enables the volume changes, ΔV_{ads}, in the deposition processes to be evaluated according to the relations

$$\Delta G_{ads} = - zFE_{ads}$$

and

$$\left(\frac{\partial \Delta G_{ads}}{\partial P}\right)_T = - zF \left(\frac{\partial E_{ads}}{\partial P}\right)_T$$

$$= \Delta V_{ads}$$

where ΔG_{ads} is the free energy of adsorption in the electrodeposition process in the monolayer and E_{ads} is the potential for adsorption into a particular state, relative to the potential of some reference electrode. Since the individual partial molar volume of the H^+ in water is quite well established, evaluation of ΔV_{ads} enables the volumes of deposited H and OH at Pt to be estimated and hence some information on their state at the surface to be derived. In evaluating ΔV_{ads}, attention must be paid (see below) to the pressure-dependence of the potential of the reference electrode to which E_{ads} values are referred.

Corresponding studies over a range of temperatures are also important as these give values for the standard entropies of adsorption in the various states. Relations between ΔV and ΔS quantities are also of interest, especially for processes in the water medium, where solvent-structure effects determine connections between ΔV and ΔS due to electrostriction changes (Hepler's relation[132]).

The electrochemical surface processes which will be considered are:

$$H_3O^+ + Pt + e \rightarrow PtH_{ads} \text{ (in 4-5 states)} + H_2O$$

and

$$H_2O + Pt \rightarrow PtOH \text{ (in various states)} + H^+ + e$$

$$\downarrow$$

$$PtO + H^+ + e$$

(cf. ref. 133) together with the similar processes involved at a gold anode.

RESULTS

4.3.2 Pt in 0.5 M H_2SO_4

The electrochemical surface processes which occur at Pt in 0.5 M H_2SO_4 were examined by cyclic voltammetry in the range of potentials from those where H_2 evolution commences (+ 0.025V vs Pd-H/H^+) in a N_2-saturated solution to where O_2 evolution becomes significant ($\sim$ 1.300V vs Pd-H/H^+) at pressures up to 2204 bars. The behaviour at pressures of 1 and 2204 bars is illustrated in Fig. 4.3.1.

The effects shown in Fig. 4.3.1, although small, are entirely significant as (a) the peak potentials move reproducibly in both directions with increase or decrease of pressure and (b) the pressure effects on the H-peak potentials in a given experiment relative to the pressure effect on the surface oxidation current profile, is such as to cause a small but significant convergence of the surface oxidation profile towards that for H oxidation.

The i-V profiles shown in Fig. 4.3.1 are those obtained directly in the experiment, with the potential scale referred to the potential of a reversible Pd-H,H^+ electrode in the same solution in the cell within the bomb, i.e. against a reference electrode whose own potential will be changing with pressure. In order to evaluate the true effects of pressure on the surface processes at Pt and Au, it is necessary[39] to evaluate the volume change in the reference electrode reaction at equilibrium. This is equivalent to correcting for the pressure-dependence of the reference electrode potential which arises because of the normally finite volume change in the electrode reaction. The pressure coefficient of the electrode potential of the Pd-H,H^+ half-cell[134] is determined by the volume difference

$$\Delta V = V_e + V^{\infty}_{H^+} + V_{Pd} - V_{Pd\text{-}H} \quad . \qquad (4.3.1$$

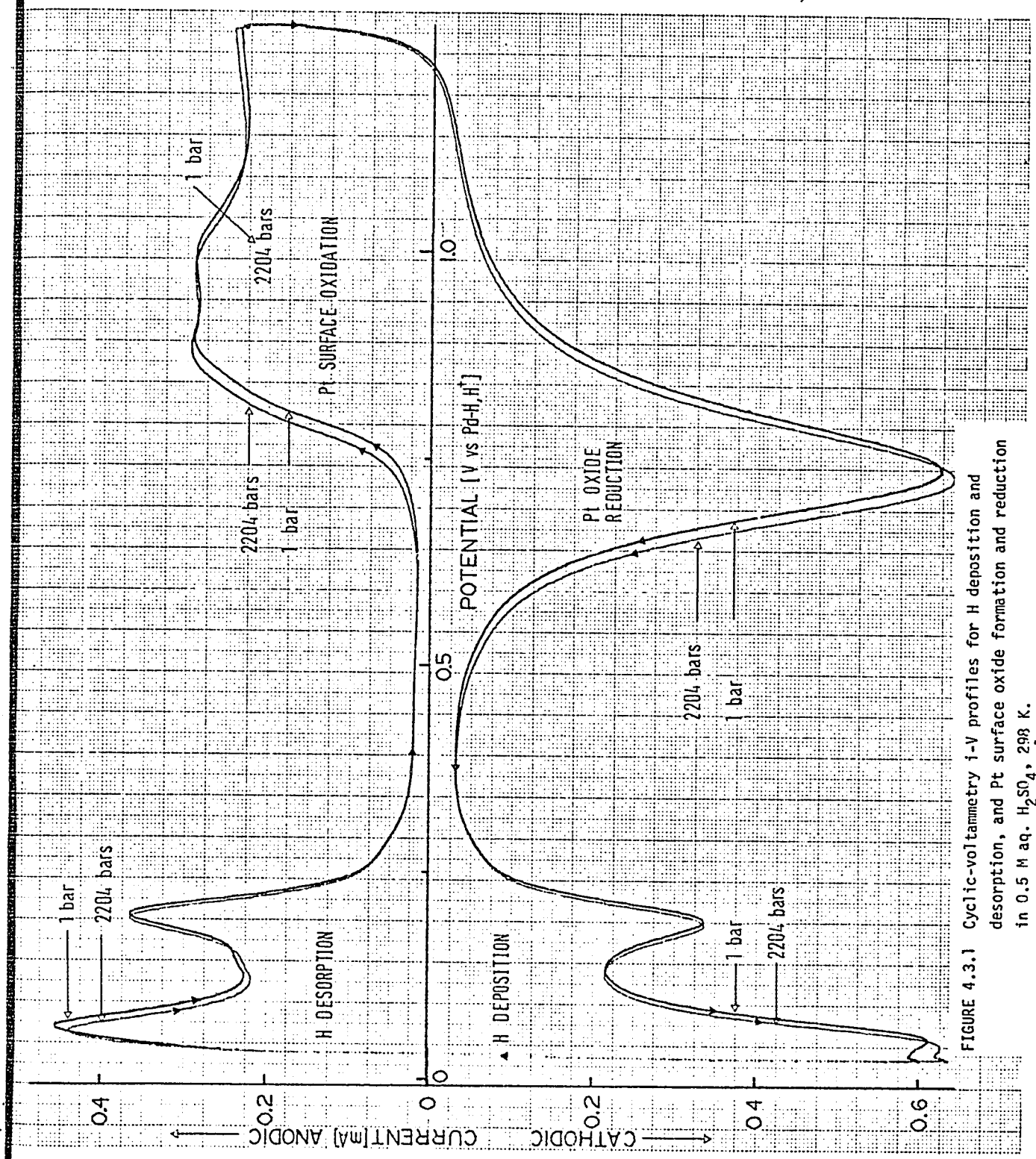

FIGURE 4.3.1 Cyclic-voltammetry i-V profiles for H deposition and desorption, and Pt surface oxide formation and reduction in 0.5 M aq. H_2SO_4, 298 K.
Sweep - rate 50 mV s^{-1}. P=1 and 2204 bars.

$V^{\infty}_{H^+}$ is quite reliably known, V_e has been estimated[15] as 3 cm^3 $Faraday^{-1}$, V_{Pd} = 9.3 cm^3 mol^{-1} and V_{Pd-H} has been evaluated in this work as 11.3 cm^3 mol^{-1}.

4.3.3 Volume of Adsorbed H at the Pt Electrode

If the peak potentials for underpotential deposition of H at Pt are referred to the potential scale of the Pd-H,H^+ electrode in the same solution at any pressure, then the resulting dependence of peak potential on pressure corresponds to the volume difference determined[35] by the two reactions

$$Pt + H^+ + e \rightleftharpoons Pt\,H_{ads} \qquad (4.3.2)$$

and

$$Pd + H^+ + e \rightleftharpoons Pd\text{-}H_{abs}, \qquad (4.3.3)$$

i.e. by the volume of transfer of H in the process

$$Pt + Pd\text{-}H_{abs} \rightleftharpoons Pt\text{-}H_{ads} + Pd \qquad (4.3.4)$$

corresponding to the difference of reactions (4.3.2) and (4.3.3). It is to be noted that process 4.3.4 is independent of pH and electrons and hence evaluation of the volume change requires no knowledge of the properties of H^+ and e other than those involved in the evaluation of $V_{Pd\text{-}H_{abs}}$ described earlier.

The shift of H peak potentials, ΔE, from P = 1 to P = 2204 bars is observed to be -7 ± 2mV (Fig. 4.3.1) so that

$$(\partial \Delta E/\partial P)_T = -3.2 \pm 1\ \mu V\ bar^{-1} \qquad (4.3.5)$$

and the corresponding volume change for reaction 4.3.4 is 3.1 ± 0.9 cm^3 mol^{-1}. The volume change for reaction 4.3.4 can be written in terms

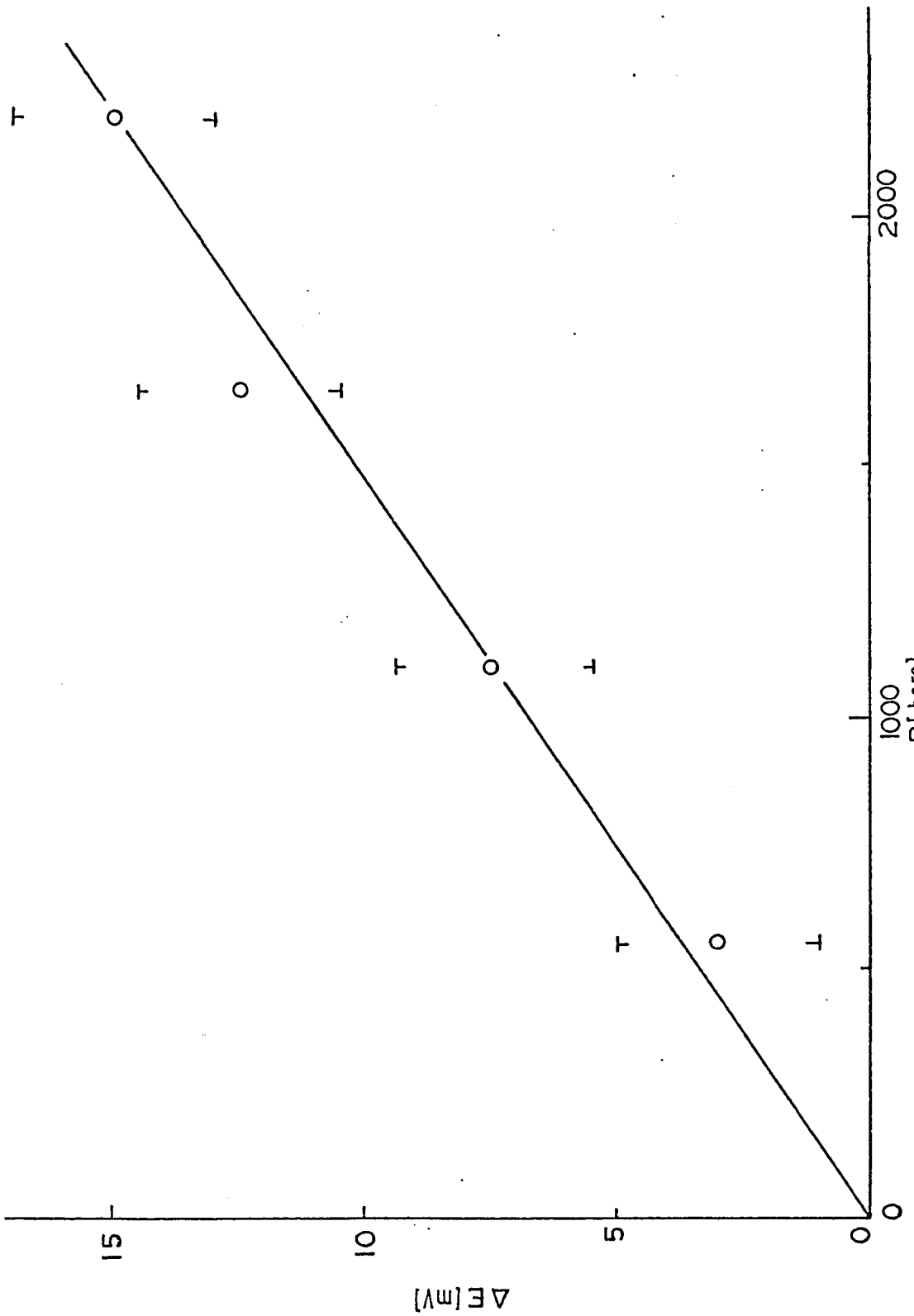

FIGURE 4.3.2 The effect of pressure on the potential for onset of Pt surface oxidation in 0.5 M H_2SO_4 . The potential shift, ΔE, is taken as E_1-E_p, where E is determined from the potential at 1/2 the current maximum of the first Pt oxidation peak.

of the molar volumes of Pt, Pd-H_{abs}, Pt-H_{ads} and Pd as follows

$$\Delta V = V_{Pt\text{-}H_{ads}} + V_{Pd} - V_{Pt} - V_{Pd\text{-}H_{abs}} \qquad (4.3.6)$$

$$= 3.1 \pm 0.9 \text{ cm}^3 \text{ mol}^{-1}$$

The molar volumes of Pd and Pt are readily calculated from the known densities and molecular weights of the elements assuming that the Pt metal atoms retain almost the same volume in the metal surface as in the bulk, and $V_{Pd\text{-}H_{abs}}$ was evaluated as described earlier as 11.3 cm^3 mol^{-1}. Therefore the molar volume of Pt-H_{ads}, $V_{Pt\text{-}H_{ads}}$, can be determined as

$$V_{Pt\text{-}H_{ads}} = \Delta V + V_{Pd\text{-}H_{abs}} + V_{Pt} - V_{Pd} \qquad (4.3.7)$$

Then, from eqn. (4.3.6),

$$V_{Pt\text{-}H_{ads}} = 3.1 + 11.3 + 9.1 - 9.3$$
$$= 14.2 \pm 0.9 \text{ cm}^3 \text{ mol}^{-1} \qquad (4.3.8)$$

The molar volume of H electrodeposited on Pt is therefore

$$V_H = V_{Pt\text{-}H_{ads}} - V_{Pt} = 5.1 \pm 0.9 \text{ cm}^3 \text{ mol}^{-1}$$

It is of interest that this volume is close to the value of 5.5 cm^3 mol^{-1} for covalently bonded H on aliphatic methylene groups as evaluated from additivity measurements[153] on molar volumes of organic substances at corresponding temperatures. It is significantly smaller than the volume of H in Pd, viz. 2 cm^3 mol^{-1} evaluated in Chapter 3, corresponding to the well known partially protonic state of H in Pd. The relatively larger volume of H chemisorbed on Pt is consistent with (a) the electrosorption valency factor γ evaluated by Schultze[136] as near 1

for electrodeposited H on Pt, i.e. H is virtually a neutral atom and (b) the lack of significant repulsive energy between chemisorbed H atoms (i.e. they are "atoms" rather than "partial ions") in the 4 or 5 states of electrodeposited H as indicated by the half-widths of the pseudo-capacitance peaks[154].

It is also to be noted that the effect of pressure on all the resolved states of chemisorbed H is, within experimental error, the same (Fig. 4.3.1).

4.3.4 Volume Changes Resulting from Surface Oxidation of Pt

The most obvious effect of pressure on the shape of the current-potential profiles occurs in the Pt surface oxidation region (Fig. 4.3.1). The potential for the initiation of Pt oxidation is shifted to less positive potentials in the anodic sweep as the pressure is increased. Although small, this effect is significant for the present study since it arises only on account of the change of pressure. Impurity effects are an unlikely (cf. ref 80) reason for the effect since (a) the shift is to less positive values and (b) the effect is reversible with respect to increase or decrease of pressure.

The process responsible for this shift must occur with a negative volume change since the initial stage of surface oxidation of platinum forming OH on Pt is evidently favoured by an increase of pressure.

The anodic i-V profile is known[133] to correspond to a fast surface oxidation process since its s_o value[137] is large, i.e. the value of sweep rate beyond which polarization in the anodic process becomes significant. Hence shifts of charging currents in the anodic profile of Fig. 4.3.1 correspond to shifts of potentials for almost equilibrium coverages[133] with change of pressure. The initial stage of surface oxidation of Pt has been shown[133] to be the almost reversible formation of

electrodeposited OH species on the Pt surface according to the reaction (in acid media)

$$Pt + H_2O \rightleftharpoons Pt\text{-}OH_{ads} + H^+ + e \qquad (4.3.9)$$

The shift of potential, ΔE, for initiation of surface oxidation of Pt at 1 and 2204 bars can also be evaluated from Fig. 4.3.1 as $\Delta E = 15 \pm 2$ mV. A plot of potentials for initial surface oxidation vs. pressure for five pressures is given in Fig. 4.3.2. The pressure coefficient of ΔE is then

$$\left(\frac{\partial \Delta E}{\partial P}\right)_T = 6.8 \pm 1 \ \mu V \ bar^{-1} \qquad (4.3.10)$$

Experimentally the potential scale for onset of Pt surface oxidation is referred to the potential of the $Pd\text{-}H_{abs}, H^+$ electrode in the same solution, viz,

$$Pd\text{-}H_{abs} \rightleftharpoons Pd + H^+ + e \qquad (4.3.11)$$

Combination of reactions (4.3.9) and (4.3.11) is equivalent to the process

$$Pt + H_2O + Pd \rightleftharpoons Pt\,OH_{ads} + Pd\text{-}H_{abs} \qquad (4.3.12)$$

the free energy of which corresponds to the potentials for surface oxidation of Pt measured on the $Pd\text{-}H_{abs}$, H^+ scale.

The directly measured pressure coefficient of ΔE gives from eqn. (4.3.10) $\Delta V = -6.6 \pm 0.9$ cm^3 mol^{-1}. The volume change, ΔV, will be determined in part by the volume of formation of Pt-OH, $V_{Pt\text{-}OH}$, plus any other volume contribution due to desorption of anions, to be denoted by V_-. Then $V_{Pt\text{-}OH} + V_-$ is evaluated from

$$\Delta V = -6.6 = V_{Pt\text{-}OH} + V_- + V_{Pd\text{-}H_{abs}} - V_{Pd} - V_{Pt} - V_{H_2O} \qquad (4.3.13)$$

which gives $V_{Pt\text{-}OH} + V_- = 18.5 \pm 0.9$ cm^3 mol^{-1}, taking $V_{Pt} = 9.1$, $V_{H_2O} = 18$ and $V_{Pd} = 9.3$ cm^3 mol^{-1} from the known densities, together with $V_{Pd\text{-}H_{abs}} = 11.3$ cm^3 mol^{-1} determined in the present work. The volume of adsorbed OH, V_{OH}, together with V_-, will be given by

$$V_- + V_{OH} = V_{Pt\text{-}OH} + V_- - V_{Pt}$$

$$= 9.4 \pm 0.9 \text{ cm}^3 \text{ mol}^{-1}$$

This is a minimum value based on the assumption that the volume of Pt as the substrate atom for OH chemisorption retains its metallic volume upon deposition of an OH species. A Pt atom on which an OH is chemically bound may be expected to have a somewhat smaller volume than a regular metallic Pt atom due to overlap of van der Waals envelopes when two atoms are chemically bonded.

An estimate of V_{OH} is difficult to make reliably but two approaches give some idea of an appropriate value:

(a) OH is isoelectronic with F. Hence an estimate of the volume of bound OH may be obtained from that of F derived from half the molar volume of F_2. Dividing half the molecular weight of F_2 by its density in the liquid state near its freezing point gives

$$V_F \simeq V_{OH} = 17 \text{ cm}^3 \text{ mol}^{-1}$$

This volume is also the same as that of Ne under similar conditions.

(b) Taking the known covalent bond distance O to H (0.096 nm) and the van der Waals radius of H (0.1 nm), and allowing rotation of the OH group around an O to Pt bond, gives a volume of revolution of 17.3 cm^3 mol^{-1}, in good agreement with the volume derived by analogy to 1/2 F_2.

Then, since $V_{OH} + V_- = 9.4 \pm 0.9$ cm^3 mol^{-1}, it is seen that approximately -8 cm^3 mol^{-1} can be attributed to anion desorption as surface oxidation of Pt commences. The significance of this result will be discussed

in section 4.3.6.

4.3.5 Surface Oxidation of Au in 0.5 M K_2SO_4 + 0.01 M H_2SO_4

The electrochemical behaviour of Au in 0.5 M K_2SO_4 + 0.01 M H_2SO_4 was also studied in a similar manner to that of Pt; the i-V profiles for surface oxidation of Au (at which no underpotential deposition of H occurs) at 1 and 2200 bars are illustrated in Figure 4.3.3. The shift of potential for the onset of oxidation is 20 ± 2 mV vs. Pd-H_{abs}/H^+ electrode over the pressure range 1 to 2200 bars. The pressure coefficient is hence

$$(\partial\Delta E/\partial P)_T = 9.1 \pm 1\ \mu V\ bar^{-1} \qquad (4.3.14)$$

The corresponding volume change is $\Delta V = -8.8 \pm 0.9\ cm^3\ mol^{-1}$. Proceeding as is the case of Pt surface oxidation, the volume $V_{Au\text{-}OH} + V_-$ for the initial, almost reversible stage of surface oxidation of Au according to the process

$$Au + H_2O \rightleftharpoons Au\text{-}OH + H^+ + e \qquad (4.3.15$$

is found to be $7.2 \pm 0.9\ cm^3\ mol^{-1}$. Assuming that the volume of bound OH at Au at low coverage is similar to that at Pt, viz. $17\ cm^3\ mol^{-1}$, V_- is evaluated as $-9.8\ cm^3\ mol^{-1}$ for the volume associated with anion desorption.

4.3.6 Significance of Pressure Effects on Anion Adsorption

On whatever basis an assignment of the volume of bound OH at Pt or Au is made, the apparent volume of deposition of OH on Au is appreciably smaller than that on Pt. It is suggested that this is a measure of the greater relative importance of anion desorption in the process of surface oxidation at Au than at Pt. This is supported by the observations of Ho, Conway

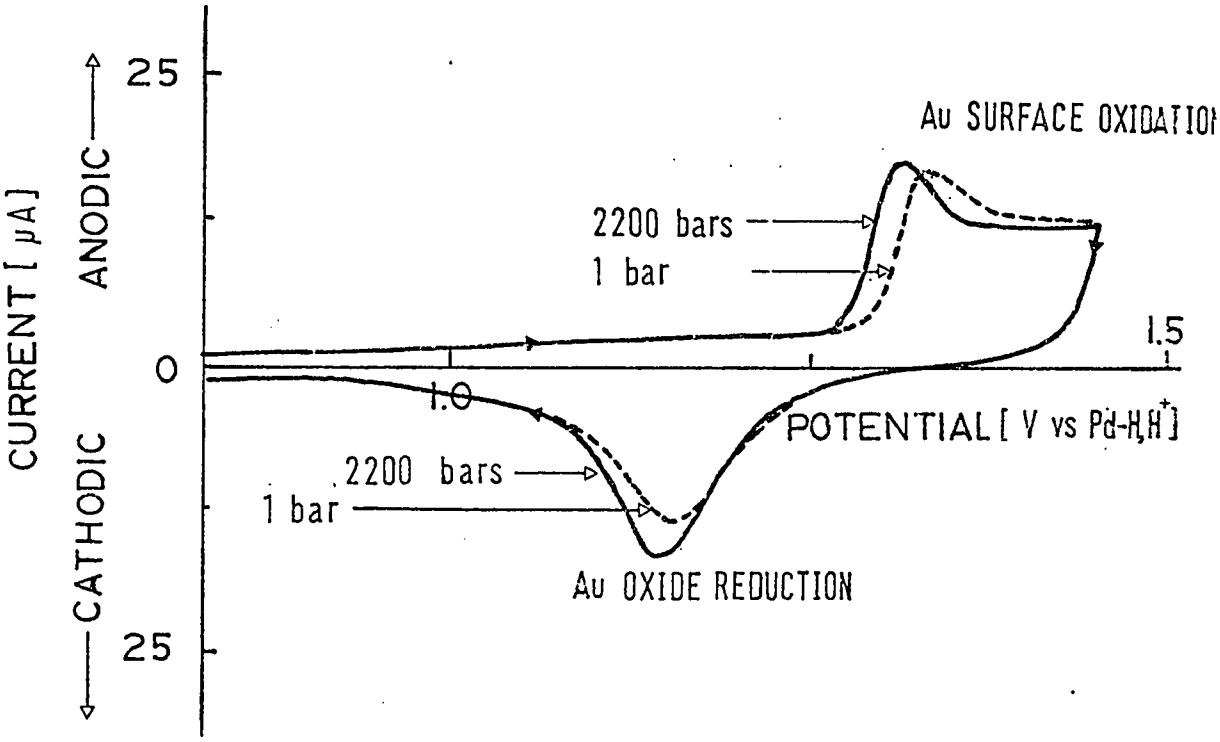

FIGURE 4.3.3 Cyclic-voltammetry i-V profiles for surface oxide formation and reduction at Au in 0.5M K_2SO_4+ 0.01M H_2SO_4 at 1 and 2200 bars,298 K; sweep-rate is 20mV s^{-1}.

and Angerstein-Kozlowska[138] who found appreciable SO_4^{2-} (or HSO_4^-) adsorption effects on the initial stages of surface oxidation of Au (see Figure 4.3.5). Thus, in 1N aq. $HClO_4$, surface oxidation of Au commences at approximately 1.30 V (vs. Pt,H_2) while the addition of small amounts (10^{-4}M) of SO_4^{2-} leads to a displacement of the potential for initial oxidation of the gold surface to + 1.40 V. The effects are larger than those at Pt (Fig.4.3.4). Hence the adsorption of SO_4^{2-} or HSO_4^- ions appears to be stronger on Au than on Pt which is consistent with the larger relative shifts of potential, ΔE, with pressure in the former case. Thus experimentally, at Pt, it is found[135] at ambient pressure that significant shifts of potential for onset of surface oxidation arise only with relatively large changes of SO_4^{2-} concentration.

The process of adsorption of SO_4^{2-} or HSO_4^- on the electrode surface probably takes place with a volume increase due to partial desolvation of the anion and to the removal of oriented water molecules previously existing at the surface of the electrode. If this is the case, then pressure will have the effect of diminishing the extent of anion adsorption at a given potential which will be manifested by a contribution to the shift of the potential for the onset of Pt surface oxidation.

With regard to the direction of pressure effects on the adsorption of SO_4^{2-}, it is to be noted that specific adsorption of an anion at a positively charged electrode at which water is oriented in the Helmholtz layer has some of the characteristics of an "ion-pair" formation process. It is known[44,46] that ion-pairing, e.g. of the contact or solvent-shared type, is associated with a positive volume change but smaller than that which would arise if complete loss of electrostriction occurred. Examples are afforded by $MnSO_4$ and $MgSO_4$ which have ion-pair association volumes of 7.4 and 7.3 $cm^3\ mol^{-1}$ in aq. solutions. Hence, by analogy with

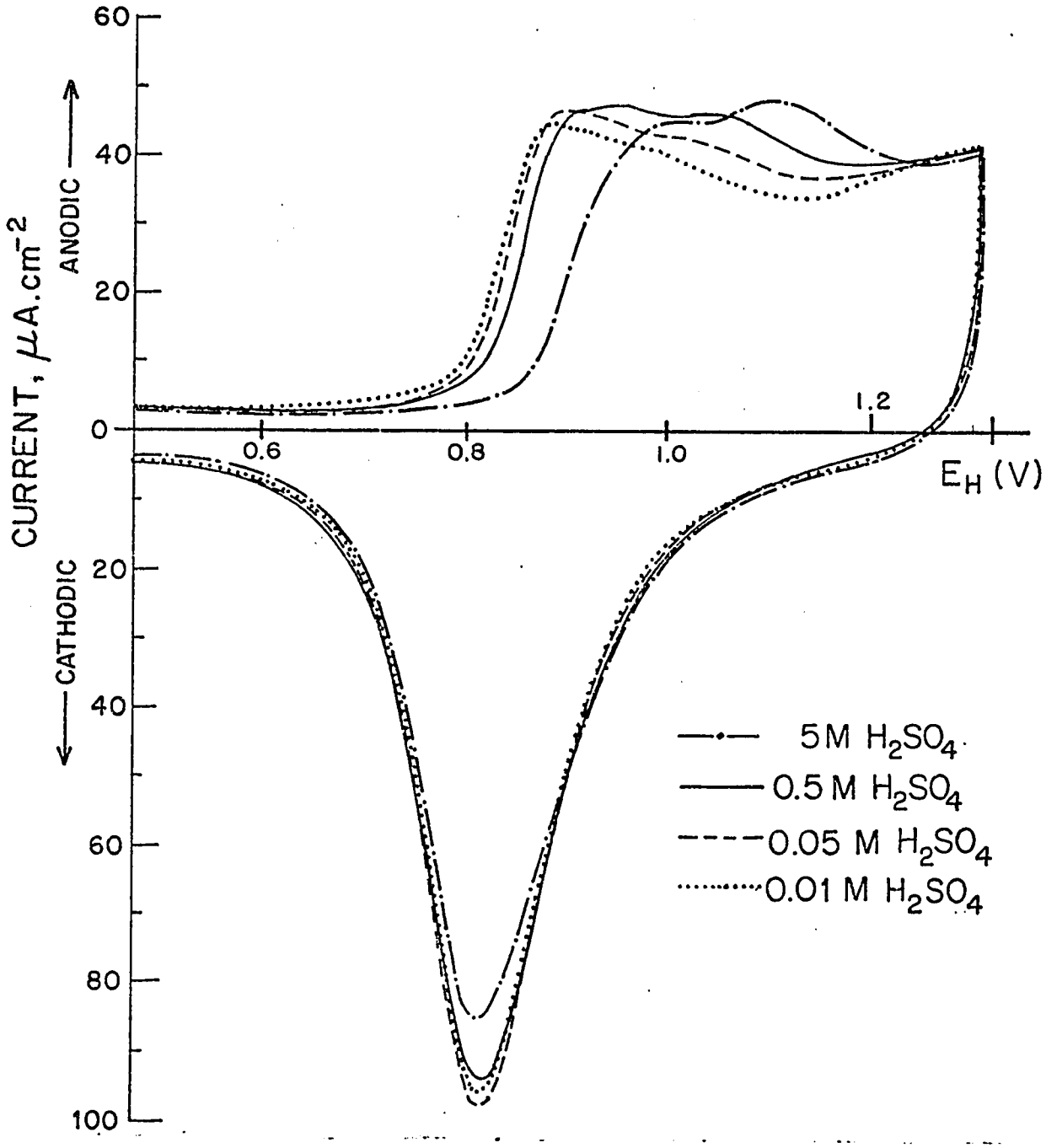

FIGURE 4.3.4 Effect of concentration of H_2SO_4 on initiation of anodic surface oxidation of Pt at 298 K. , sweep - rate 50 mV s^{-1} (From W.B.A. Sharp, Ph. D. thesis, University of Ottawa, 1976).

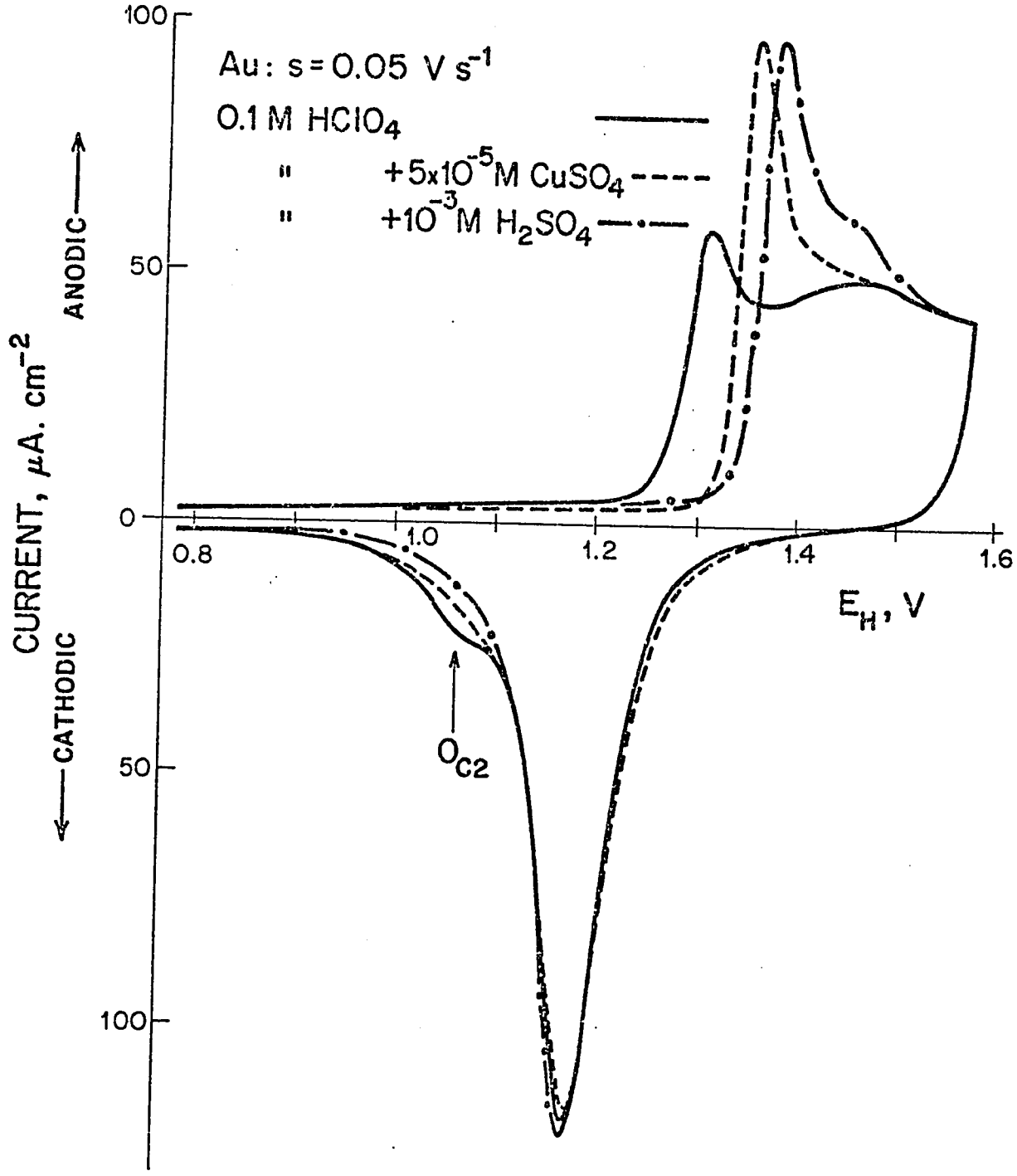

FIGURE 4.3.5 Effect of added SO_4^{2-} ion on the potential for onset of surface oxidation of Au in 0.1 M $HClO_4$ at 298 K. The sweep-rate is 50 mV s^{-1}.

such ion-pairing processes, pressure will tend to decrease the extent of association of SO_4^{2-} ion with positively charged metal surfaces. An increase of applied pressure thus tends to cause a reduction of the extent of anion adsorption at Pt or Au electrodes resulting in a shift of potential for initial surface oxidation of these metals to less positive values, as observed. The effect is larger at Au than at Pt.

4.3.7 Conclusions

The interpretation of the high pressure results for surface processes must remain somewhat tentative owing to the paucity of data for such systems. However, the current-potential profiles (Figures 4.3.1 and 4.3.3) show that reliable electrochemical measurements on surface processes can be achieved at elevated pressures without contamination due to leakage of fluid into the high-pressure cell. In fact, the high pressure electrochemical cells can be maintained at 2204 bars for several days without significant variation of the shape of the current-potential profiles.

The measurements then allow information to be obtained about the volumes of adsorbed species. The volume of H electrodeposited at Pt is appreciably larger than that of H in Pd ($\alpha + \beta$), but is similar to that of H covalently bound,e.g. in aliphatic hydrocarbon $\geq CH_2$ groups.

Pressure effects on surface oxidation of Pt and Au are due to the finite volume change in the oxidation process itself and to pressure-induced desorption of adsorbed anions. Useful analogies to pressure effects on ion-pair dissociation can be made.

CHAPTER 5

ELECTROCHEMICAL BEHAVIOUR OF ELECTROACTIVE SURFACE FILMS AT ELEVATED PRESSURES

5.1 The Pb, $PbCl_2$ Electrode at Elevated Pressures

5.1.1 Current-Potential Profiles

The lead chloride system was studied by cyclic voltammetry in the potential range for oxidation of the lead substrate and subsequent reduction of $PbCl_2$ in 1 M KCl + 0.01 M HCl. Figures 5.1.1 and 5.1.2 show typical cyclic voltammetry current-potential (i-V) profiles for the formation and reduction of $PbCl_2$ at Pb at pressures of 1 and 2204 bars for a series of cathodic sweep-rates following application of an anodic sweep at a common fixed sweep-rate of 11 mV s^{-1}. The charges Q_A and Q_C involved in these anodic and cathodic sweeps were obtained by integration of the area between the respective i-V profiles and the zero-current base-line. They correspond to the charges for formation and reduction of $PbCl_2$ films on Pb.

The shape of the i-V profiles for the generation and removal of $PbCl_2$ arises in the following way. As the potential is scanned in the anodic direction, a potential is reached at which the anodic dissolution of the lead substrate is initiated. This process can be represented by the half-cell reaction

$$Pb \rightleftharpoons Pb^{2+} + 2e$$

where Pb^{2+} represents a species generated initially in the solution at the Pb surface. However, the lead species in solution will most likely be in the form of higher chloride complexes ($PbCl_n^{2-n}$) depending upon the supporting electrolyte composition and concentration. As the potential is made more anodic, the solution adjacent to the electrode surface becomes supersatura-

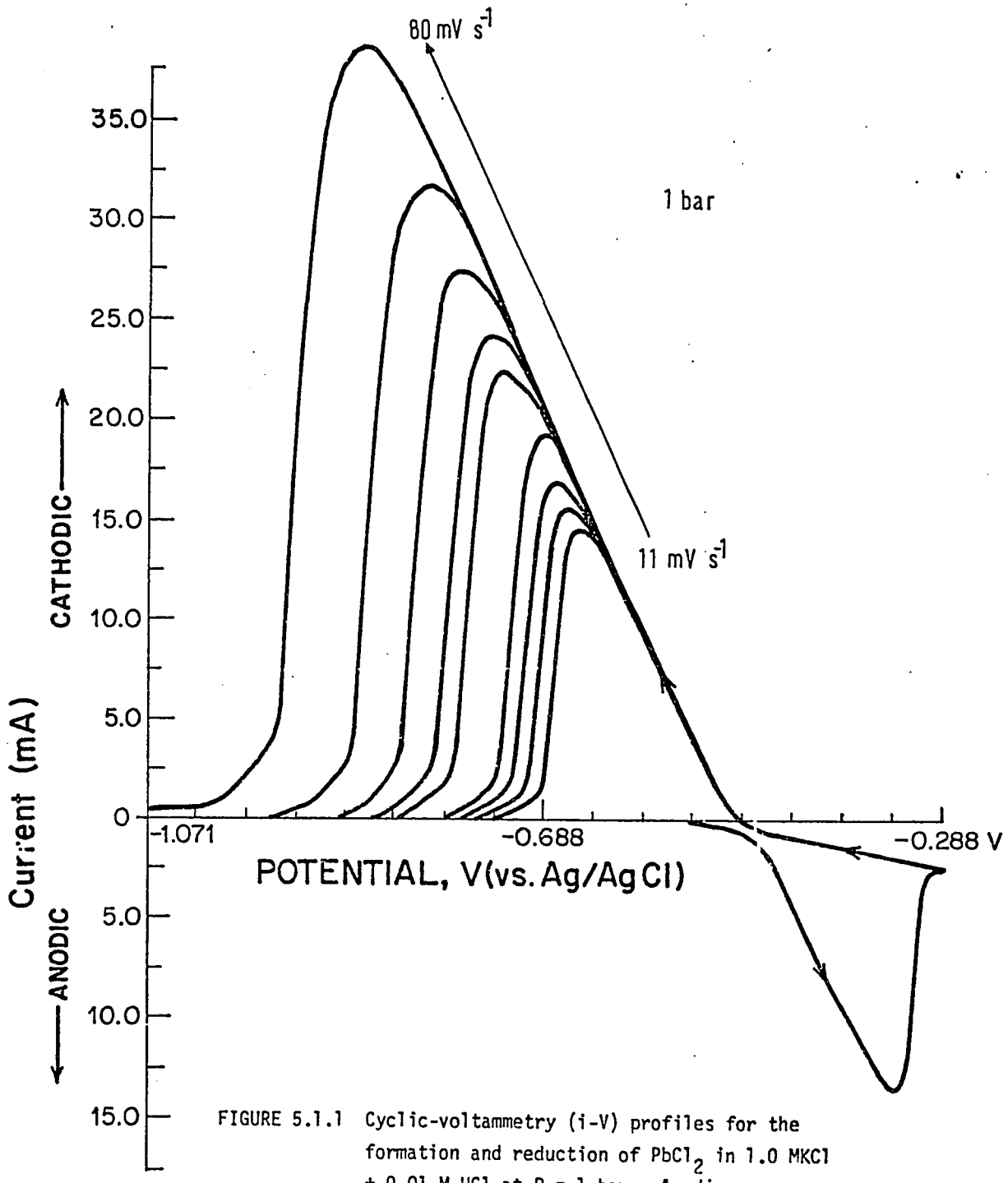

FIGURE 5.1.1 Cyclic-voltammetry (i-V) profiles for the formation and reduction of $PbCl_2$ in 1.0 MKCl + 0.01 M HCl at P = 1 bar. Anodic sweep rate, s_A, is 11 mV s^{-1}. The cathodic sweep rates, s_C, are 11, 13, 16, 20, 27, 32, 40, 53 and 80 mV s^{-1}.

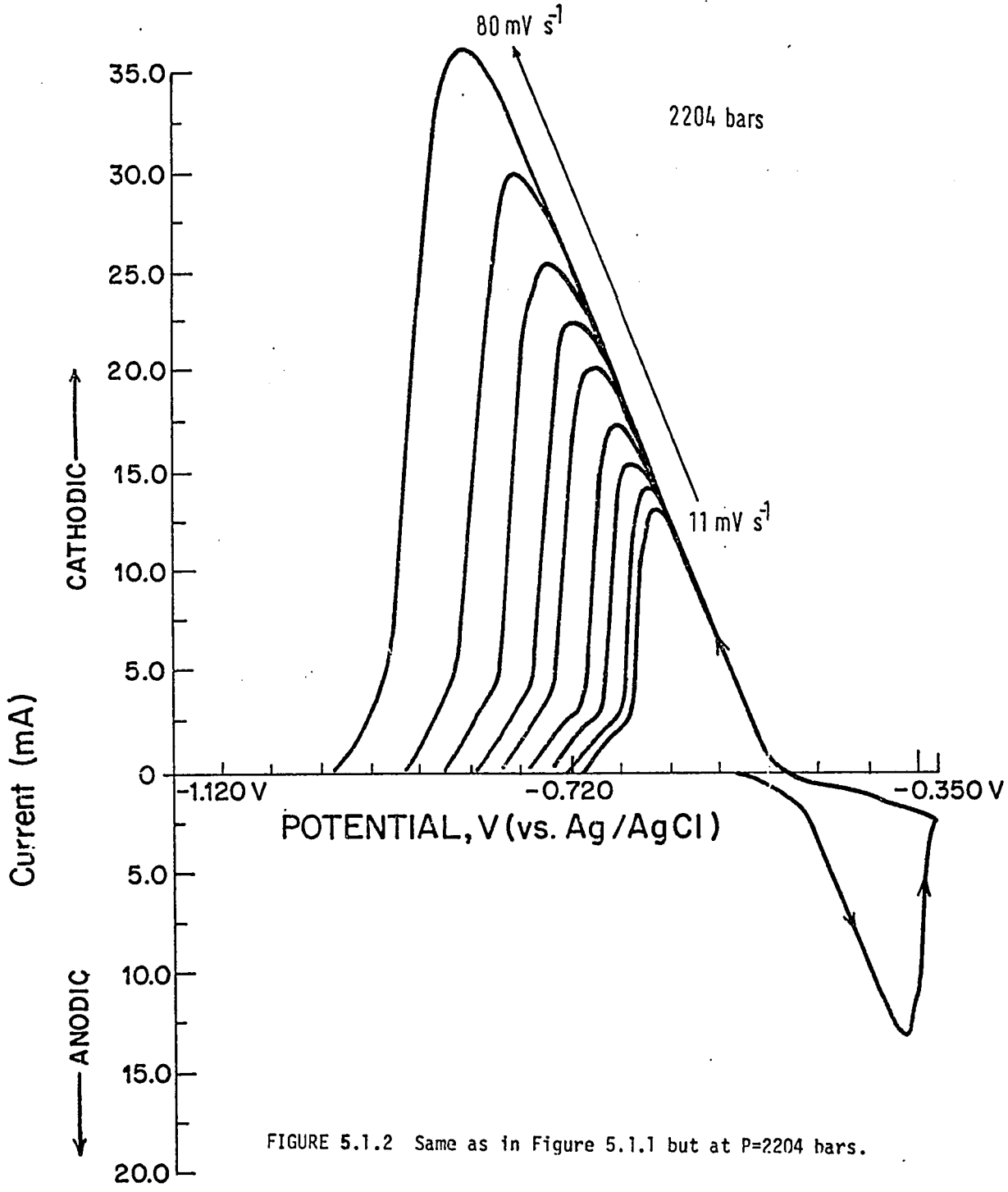

FIGURE 5.1.2 Same as in Figure 5.1.1 but at P=2204 bars.

ted with respect to solution-soluble lead species, resulting in the formation of $PbCl_2$ nuclei and deposition of $PbCl_2$ on the electrode surface.[28-31] This process occurs simultaneously with the anodic dissolution process during the rising portion of the anodic i-V profile. At the peak of the i-V profile, the Pb substrate becomes passivated, resulting in a sharp drop in the current. Upon sweep reversal, virtually no current passes until the potential is cathodic to the lead dissolution potential, i.e., the reversible potential for Pb, Pb^{++} in the solution. It is of interest that the initial rising part of the i-V profile on the cathodic side is almost linear over an extended potential range. However, at the peak of the cathodic i-V profile, the current drops sharply as a result of consumption of the $PbCl_2$ film formed on the previous anodic sweep. The linear form of the initial parts of both the anodic and cathodic i-V profiles suggests a predominantly ohmic behaviour of the oxidized surface on account of the presence of a resistive film. The inverse of the slope of the i-V profile can therefore be characterized by an electrochemical resistance $R_o = dE/di$. The effect of an ohmic potential-drop component, due to the resistance in the pores of the film, in relation to the effect of the normal exponential dependence of current on potential on the shape of the i-V profiles is illustrated schematically in Figure 5.1.3 . If the slope of the linear regions of the i-V profiles is attributed mainly to the ohmic polarization contribution, then the following values for $dE/di = R_o$ are obtained from the i-V profiles at each pressure.

P (bars)	R_o (Ohm)
1	9.07
1102	8.25
2204	7.96

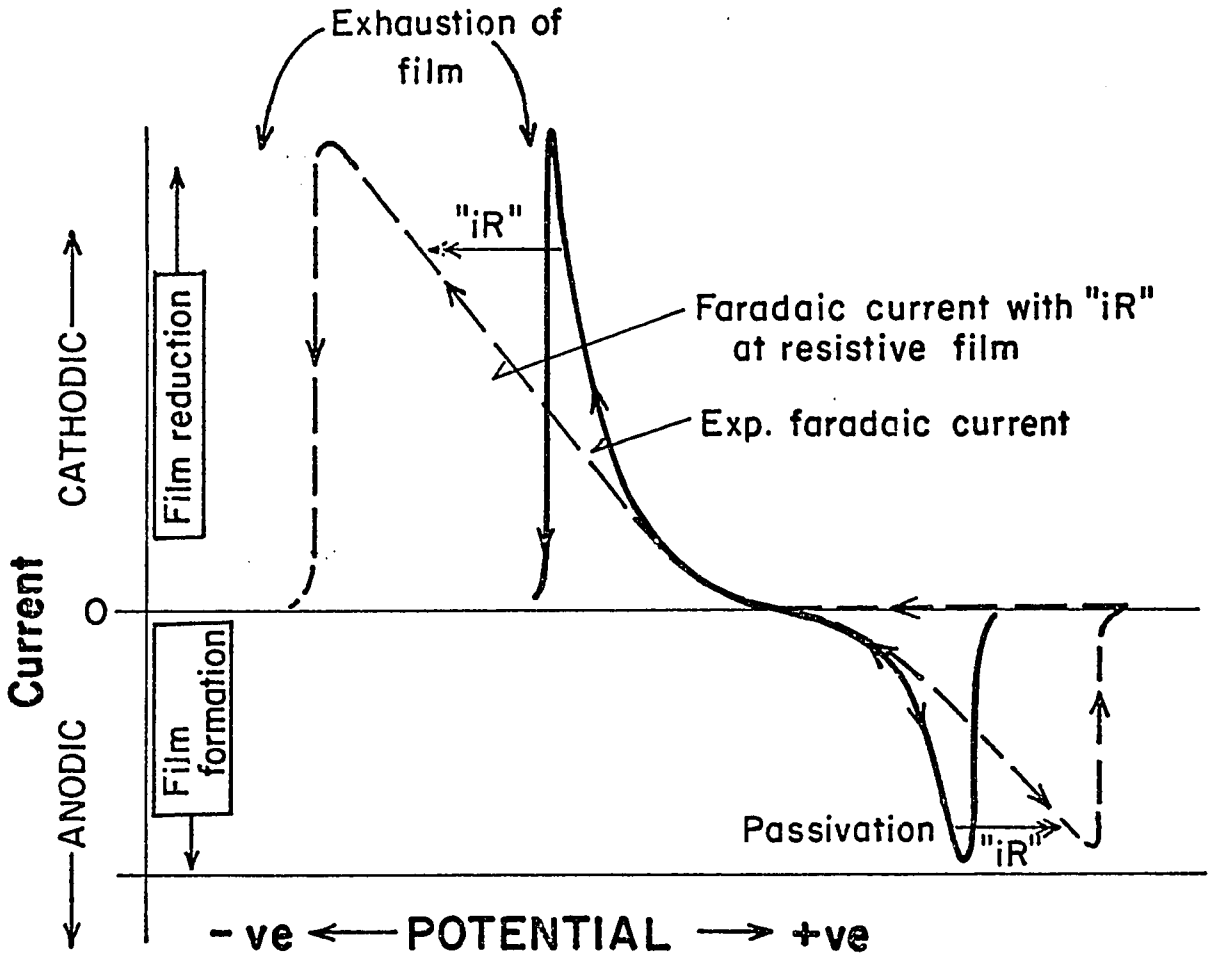

FIGURE 5.1.3 Schematic illustration of ohmic resistance effects in a film formed and reduced in a potentiodynamic sweep.

The observed pressure dependence of this effective resistance may be related to an increase in the specific conductivity of the electrolyte in the pores of the $PbCl_2$ film. It is known that the specific conductivity of KCl solutions is enhanced with application of hydrostatic pressure (see section 5.2.1).

The anodic/cathodic charge ratio, Q_A/Q_C, recorded in Table 5.1.1 measures the charge balance between the anodic and cathodic processes. The significance of the charge balance ratio, Q_A/Q_C, in the general case of film formation and reduction can be directly interpreted in terms of the formation of solution-soluble electro-active species. A ratio Q_A/Q_C = 1.0 indicates that the anodic charge required for the process of film formation is completely recovered during the reduction reaction. A value of Q_A/Q_C in excess of unity signifies that less charge is recovered in the cathodic sweep than is passed in the previous anodic one. This charge imbalance is normally the result of a chemical dissolution process involving the electro-active phase and the supporting electrolyte. This process produces electroactive solution-soluble complex species which may not be completely reduced during the cathodic direction of the cyclic voltammogram due to their diffusion away from the electrode. The dissolution process may also occur in the trans-passive region during the anodic as well as the cathodic sweep (prior to film consumption). The case where Q_A/Q_C is less than unity is less common than the above two situations. This type of behaviour may be the result of two electrochemical processes occurring in the cathodic potential region, such as some H_2 evolution in parallel with film reduction.

The results in Table 5.1.1 indicate that the charge balance ratio, Q_A/Q_C, is slightly in excess of unity. The values of Q_A/Q_C show a small dependence on the cathodic sweep-rate. This behaviour indicates that the chemical dissolution of the $PbCl_2$ film results in a decrease of approximately

10% in the recoverable charge ($Q_A/Q_C \simeq 1.10$).

The slight increase of Q_A/Q_C with increasing cathodic sweep-rate is consistent with the reduction of a small amount of anodically formed lead complexes that have diffused into the bulk of solution. However, solution-soluble species may be present in the pores of the $PbCl_2$ film as well so that the quantity of these complexes, measured on reduction, will not depend on the cathodic sweep-rate.

The variation of Q_A/Q_C with $s_C^{1/2}$ (cathodic sweep-rate) at P = 1, 1102, and 2204 bars is illustrated in Figure 5.1.4. Although there is considerable scatter of the Q_A/Q_C data, the best-fit straight lines indicate that elevated pressures tend to reduce the magnitude of Q_A/Q_C as well as its dependence on the cathodic sweep-rate. A similar trend is observed if the cathodic peak current, i_P,is plotted as a function of the square-root of cathodic sweep rate. Figure 5.1.5 indicates that the data for i_P are linear in $s_C^{1/2}$ over the range of sweep-rates studied (0.011 to 0.080 $V\ s^{-1}$) and the respective slopes are independent of pressure. The decrease in the cathodic peak current at a given sweep-rate as the pressure is increased is related to the fact that less anodic charge is required to passivate the electrode at elevated than at ambient pressures. Table 5.1.2 lists the relative anodic values of the anodic charge Q_A^P at pressure P to that Q_A^1 at P = 1 bars and the corresponding ratio Q_C^P/Q_C^1 for cathodic charges at each pressure. The charge ratios measure the relative effect of pressure on the charges passed in the anodic and cathodic sweeps. At 1102 bars the Q_A^P/Q_A^1 becomes decreased by 22% from the ambient pressure value. Further increase of pressure to 2204 bars results in an additional decrease of about 7%. The variation of Q_C^P/Q_C^1 with pressure is similar to that in the anodic case.

TABLE 5.1.1

CHARGE BALANCE DATA (Q_A/Q_C) FOR THE Pb, $PbCl_2$ ELECTRODE IN 1M KCl + 0.01 M HCl AS A FUNCTION OF CATHODIC SWEEP RATE AT 1, 1102 and 2204 BARS

s_C(mV s^{-1})	$Q_A(s_A = 11)$(mC)	Q_C(mC)	Q_A/Q_C
P = 1 bar			
11	156	145	1.08
13	156	146	1.07
16	156	139	1.12
20	156	143	1.09
27	156	145	1.08
32	156	138	1.13
40	156	140	1.11
53	156	142	1.10
80	156	132	1.18
P = 1102 bars			
11	121	111	1.09
13	121	110	1.10
16	121	112	1.08
20	121	111	1.09
27	121	110	1.10
32	121	110	1.10
40	121	108	1.12
53	121	108	1.12
80	121	103	1.17
P = 2204 bars			
11	111	103	1.08
13	111	101	1.10
16	111	107	1.04
20	111	105	1.06
27	111	105	1.06
32	111	105	1.06
40	111	106	1.05
53	111	105	1.06
80	111	102	1.09

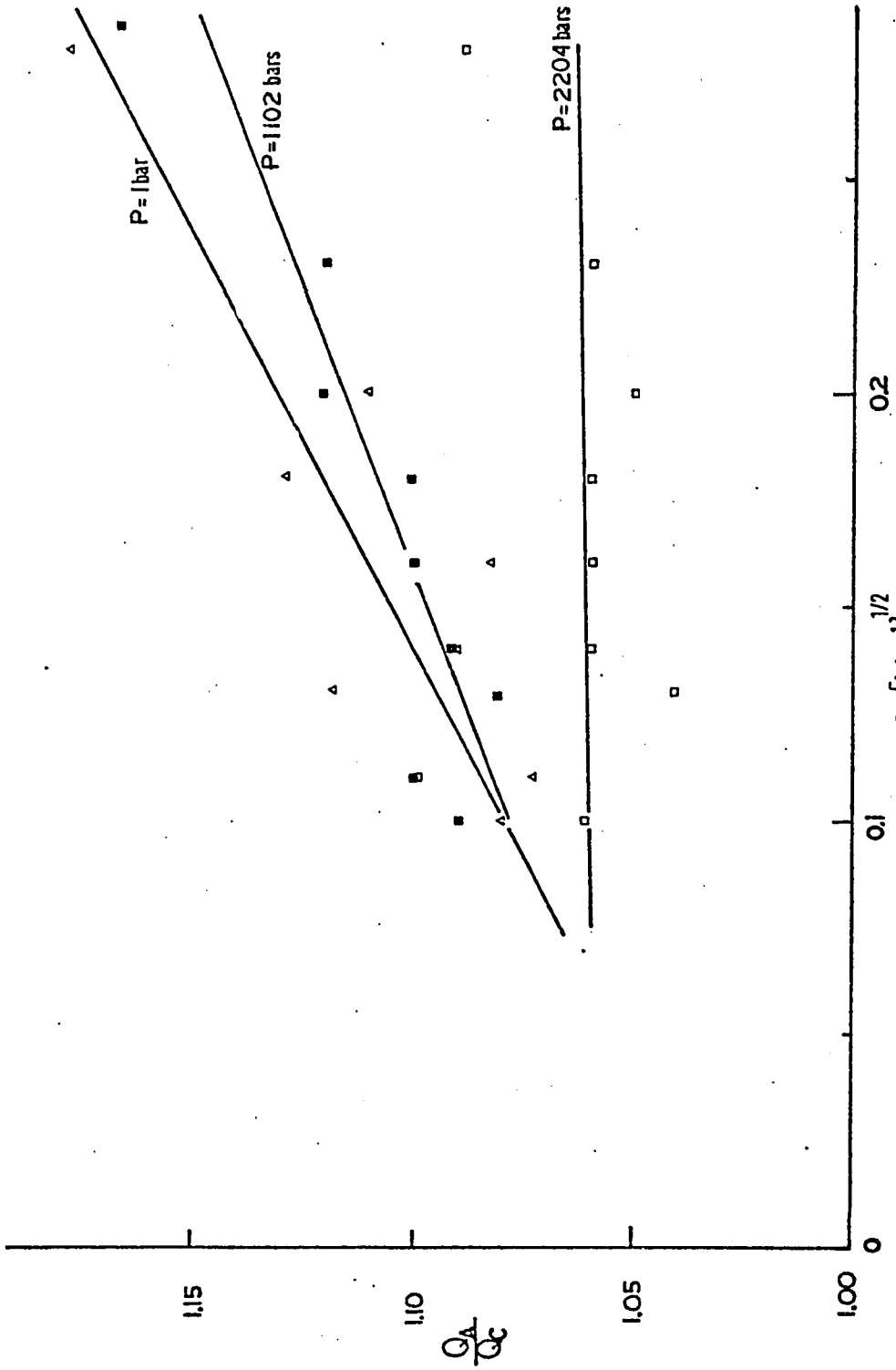

FIGURE 5.1.4 The variation of Q_A/Q_C with $s_C^{\frac{1}{2}}$ at 1, 1102 and 2204 bars.

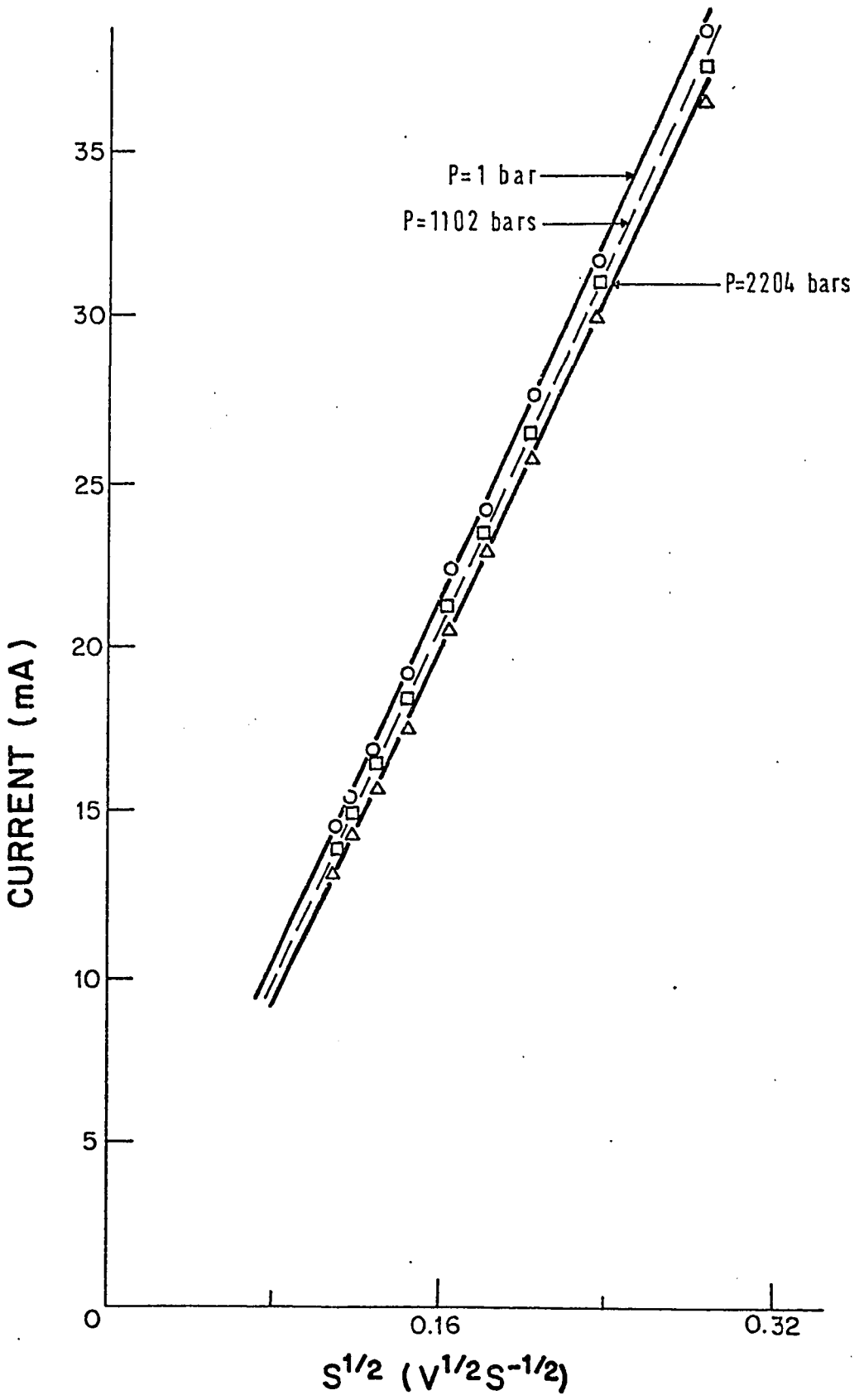

FIGURE 5.1.5 The variation of cathodic peak current, i_p, with $s_C^{\frac{1}{2}}$ at 1, 1102 and 2204 bars.

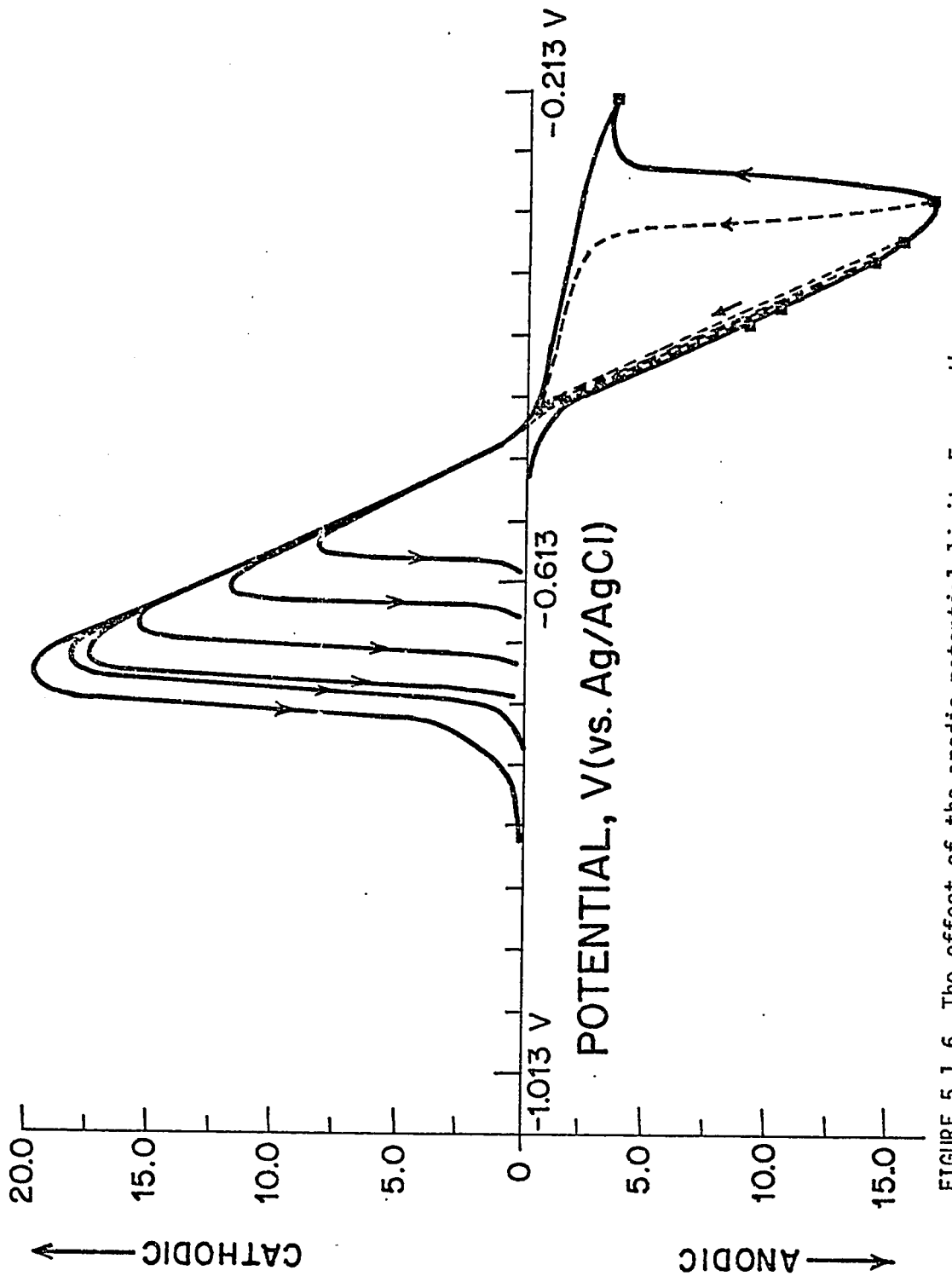

FIGURE 5.1.6 The effect of the anodic potential limit, E_A, on the form of the cathodic i-V profile. The E_A values are -0.403, -0.378, -0.353, -0.328, -0.288 and -0.213 V vs Ag, AgCl at P=1 bar.

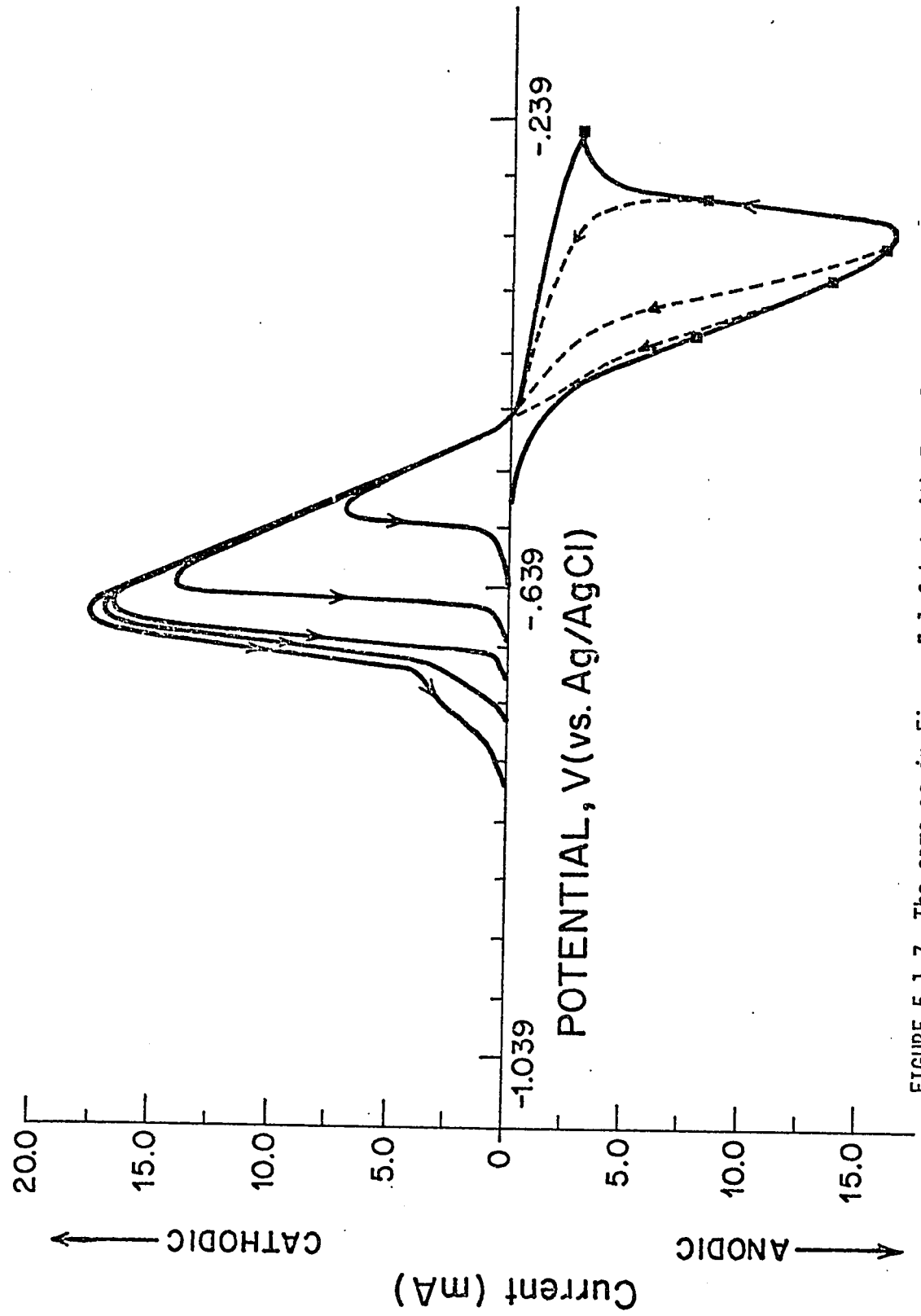

FIGURE 5.1.7 The same as in Figure 5.1.6 but with E_A values of -0.425, -0.379, -0.344, -0.299 and -0.239V vs Pt,H_2 at P=2204 bars.

TABLE 5.1.2

RELATIVE CHANGE OF Q_A AND Q_C WITH PRESSURE (A≃ 1 cm^2)

P(bars)	s ($mV\ s^{-1}$)	Q_A(mC)	Q_C(mC)	Q_A^P/Q_A^1	Q_C^P/Q_C^1
1	11	156	145	1.00	1.00
1102	11	121	111	0.78	0.76
2204	11	111	103	0.71	0.71

TABLE 5.1.3

EFFECT OF ANODIC POTENTIAL LIMIT, E_A (vs. Ag,AgCl), ON THE CATHODIC CHARGE, Q_C, AT 1 AND 2204 BARS. (A≃ 1 cm^2).

P = 1 bar			
E_A(V)	Q_A(mC)	Q_C(mC)	Q_A/Q_C
-0.403	30.7	31.0	0.99
-0.378	55.7	59.2	0.94
-0.353	100	105	0.95
-0.328	136	128	1.06
-0.288	141	133	1.06
-0.213	167	167	1.00
P = 2204 bars			
-0.425	28.8	24.0	1.20
-0.379	81.4	74.7	1.09
-0.344	122	114	1.07
-0.299	128	126	1.02
-0.239 V	145	139	1.04

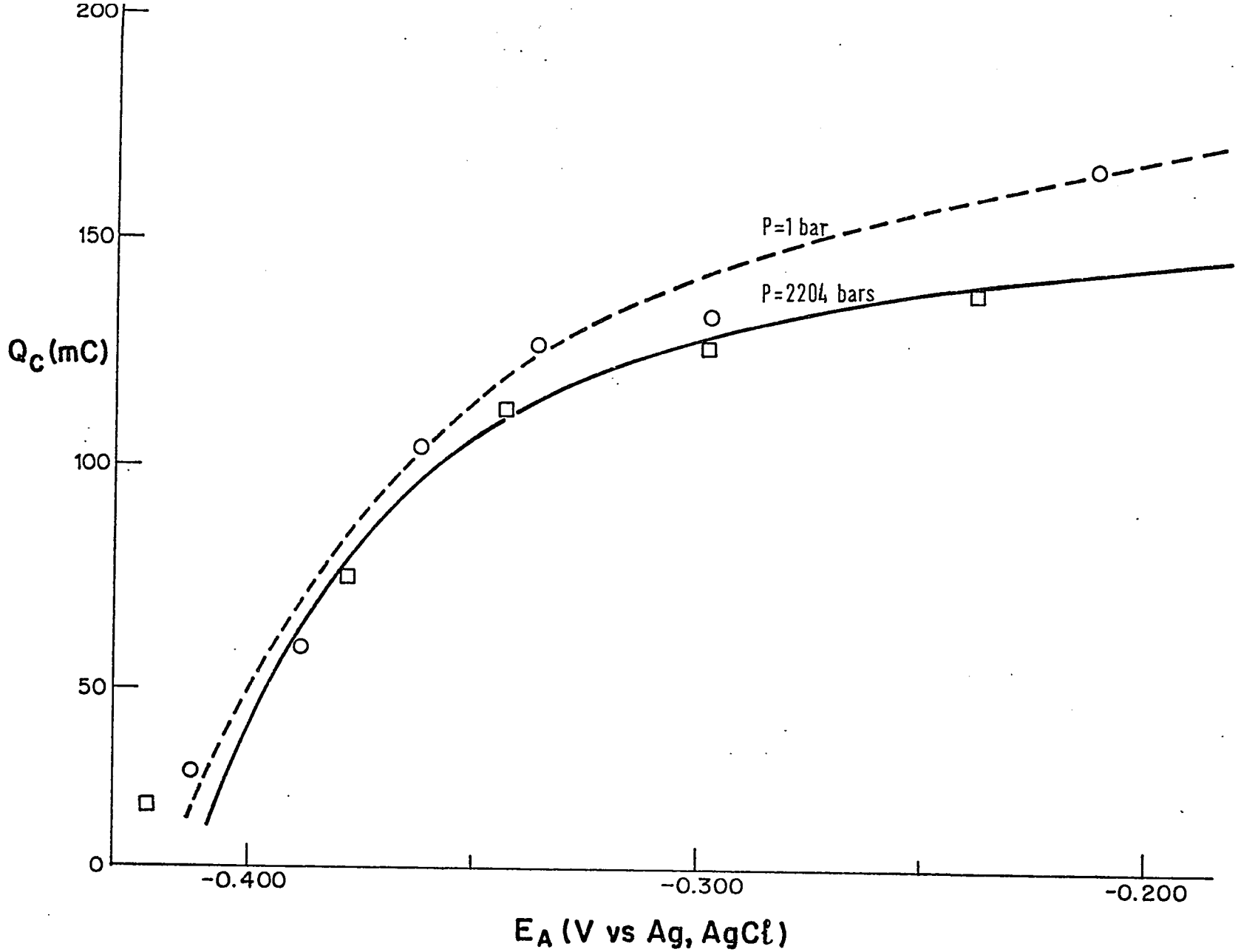

FIGURE 5.1.8 Cathodic charge, Q_C, recovered in a sweep after anodizing a Pb electrode in 1M KCl + 0.01 M HCl at various potentials E_A. The results are compared at 1 and 2204 bars.

The effect of pressure on the electrochemical formation of $PbCl_2$ and its chemical dissolution was studied by measuring the cathodic charge recovered as a function of the positive potential limit, E_A, in the anodic sweep. The i-V profiles for the Pb, $PbCl_2$ electrode for various E_A values are illustrated in Figure 5.1.6 for 1 bar pressure and in Figure 5.1.7 for a pressure of 2204 bars. The reference electrode was Ag, AgCl. The i-V profiles show the role of the (linear) ohmic contribution at all values of E_A. The basic difference between the form of the i-V profiles recorded at elevated pressure and those at ambient pressure is the more noticeable presence of a shoulder on the cathodic reduction profile at potentials more negative than that of the main peak. The magnitude of the shoulder increases as the positive potential limit of the preceding anodic sweep is extended into the trans-passive region (see Figure 5.1.7). This behaviour may be indicative of a chemical dissolution process involving the $PbCl_2$ surface film and chloride ions in solution, with subsequent reduction of solution-soluble $PbCl_n^{2-n}$ complex-ion species at potentials negative to the main cathodic peak. It may alternatively be due to the formation of basic lead salts at higher positive potentials with their reduction appearing as a distinguishable shoulder on the main peak.

The cathodic charges recovered, Q_C, and the charge balance values Q_A/Q_C, are recorded in Table 5.1.3 as a function of the positive limit E_A in the anodic sweep for P = 1 and P = 2204 bars. The variation of Q_C with E_A at each pressure is illustrated in Figure 5.1.8. For small excursions of potential in the anodic sweep, the values of Q_C are almost the same at each pressure, but as the potential limit becomes more positive in the anodic sweep, relatively less charge is recovered at elevated pressures than at ambient pressure. The charge recovered in the cathodic sweep

becomes virtually independent of E_A when E_A is more positive than the potential of the passivation peak.

5.2 Conductivity of $PbCl_2$ Solutions as a Function of Pressure

The current-potential profiles for formation and reduction of $PbCl_2$ at lead electrodes characterize a process of initial lead dissolution as Pb^{2+} (or other complex ions), precipitation and film growth of $PbCl_2$ while, in the cathodic direction, reduction of the film occurs with some redissolution. An electrochemical process of dissolution is thus followed by a physiochemical one of precipitation and crystal growth. It was surmised that since the dissolution-precipitation reaction with $PbCl_2$ must involve a substantial volume change in the reaction $Pb^{2+}_{aq.} + 2\ Cl^-_{aq.} \rightarrow PbCl_{2\,solid}$, the electrochemical behaviour of the $Pb/PbCl_2$ system would depend appreciably on pressure due to the anticipated volume change in such a reaction. Similar expectations apply to $PbSO_4$ precipitation (see p.244). It was considered that the only satisfactory method available for *in situ* (in a pressure bomb) determination of changes of solubility of $PbCl_2$ with pressure would be to measure changes of conductance of a $PbCl_2$-saturated solution.

5.2.1 Conductivity Cell Constants

The constants for conductivity cells 'R' and 'B' were evaluated in 0.01 m KCl from the data of Horne[43] for aqueous KCl solutions at elevated pressures. The small but significant effects of pressure on the conductivity cell constants are listed in Table A.1.1. The results indicate that the concentric electrode arrangement minimizes the deforming effect of elevated pressure. Therefore the mean value of the cell constant $\bar{k}$ was used to calculate the specific conductivity, κ, for the desired solutions at all pressures.

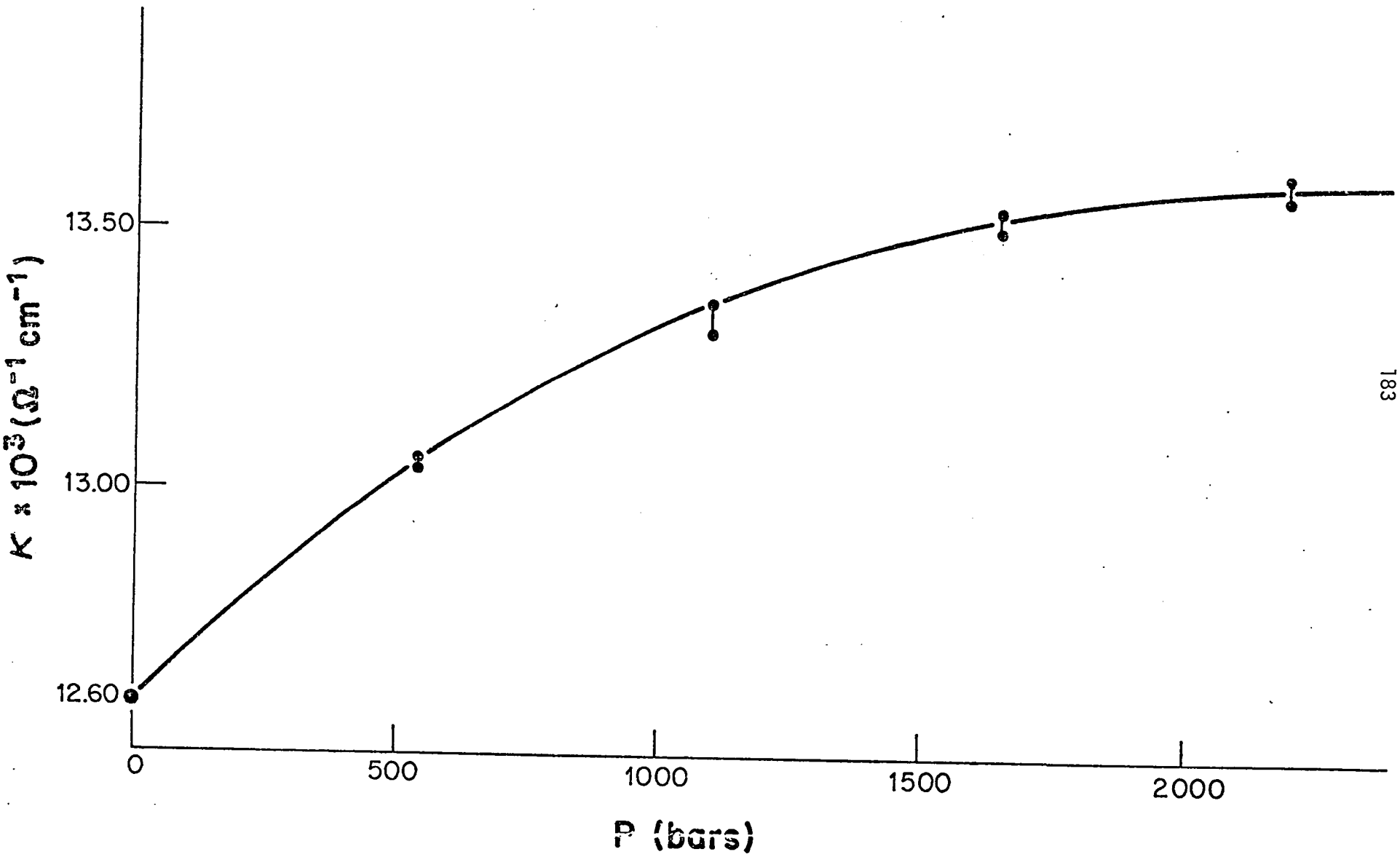

FIGURE 5.2.1 The variation of the specific conductivity, κ, with pressure for 0.10 m KCl at 298.0 K.

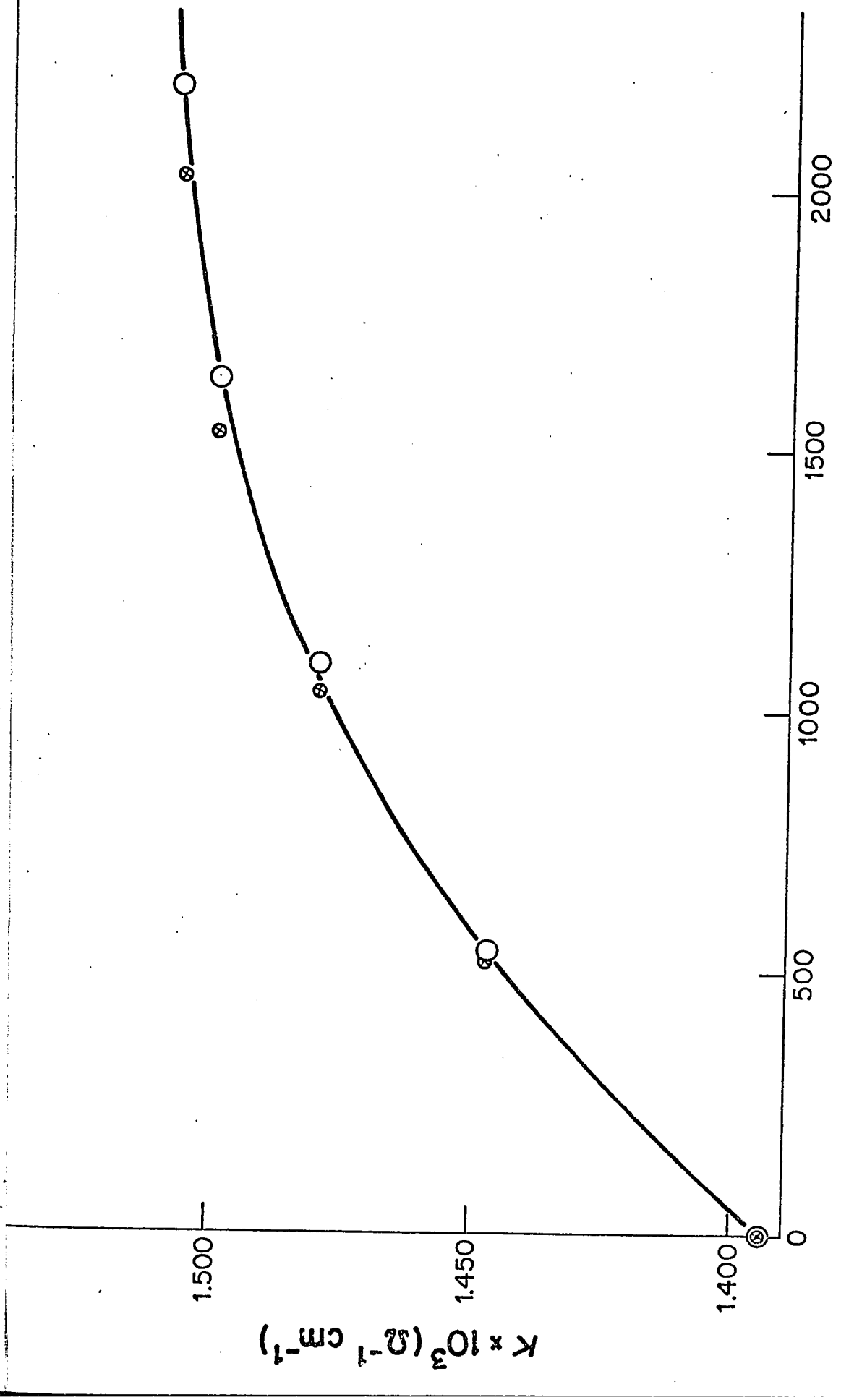

FIGURE 5.2.2 The same as in Figure 5.2.1 but for 0.01 m KCl.

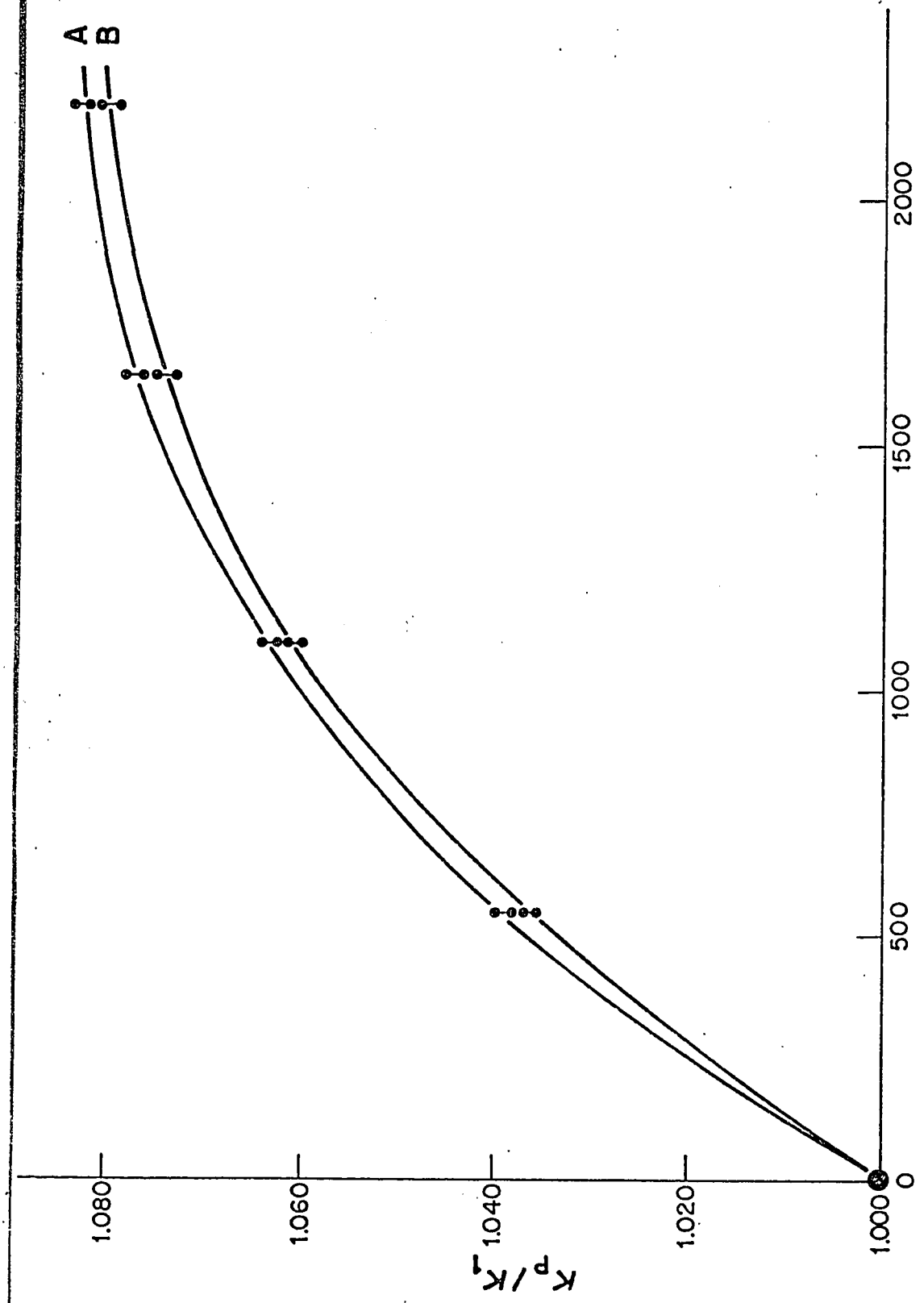

FIGURE 5.2.3 The effect of pressure in terms of the relative change of the specific conductivity, κ_p/κ_1 , for: A) 0.01 m KCl and
B) 0.10 m KCl.

The effects of pressure on the conductance of 0.10 and 0.01 molal KCl solutions are listed in Tables A.1.2 and A.1.3. The results are tabulated as the specific conductivity, κ, as well as the relative change of κ with pressure expressed as κ_{p/κ_1}, where κ_p is the value of κ at a pressure P and κ_1 that at a pressure of 1 bar. The variation of κ with pressure is illustrated in Figures 5.2.1 and 5.2.2. Figure 5.2.3 shows the effect of pressure in terms of the relative change of specific conductance, κ_p/κ_1.

These results are typical of the behaviour of strong electrolytes such as KCl. The specific conductivity of the solution exhibits a rapid increase with application of moderate hydrostatic pressures but approaches a maximum value in the region of 2000 bars. At higher pressures, although not utilized in the present work, the conductivity is expected to decrease until the solvent crystallizes out at approximately 10 kbars.

5.2.2 Conductivity of $PbCl_2$ Solutions

The solubility of $PbCl_2$ in pyro-distilled water as a function of applied pressure was evaluated from the conductivity of aqueous $PbCl_2$ solutions in the following manner: The specific conductivity of $PbCl_2$ solutions at molar concentrations of 0.001, 0.0025, 0.005, 0.01, 0.015, 0.0388 and in a saturated solution (0.0388 M at P = 1 bar) were measured as a function of hydrostatic pressure. The specific conductivity, κ, the specific conductivity ratio, κ_p/κ_1, the equivalent conductivity, Λ, and the equivalent conductivity ratio, Λ_p/Λ_1, at each pressure are listed in Table A.1.4. The results are illustrated in Figures 5.2.4-5.2.8. The specific conductivity ratio, κ_p/κ_1 at a given pressure increases with the ionic strength of the solution. The large relative increase in κ is to be attributed, in part, to the presence of the ion-pair $PbCl^+$.

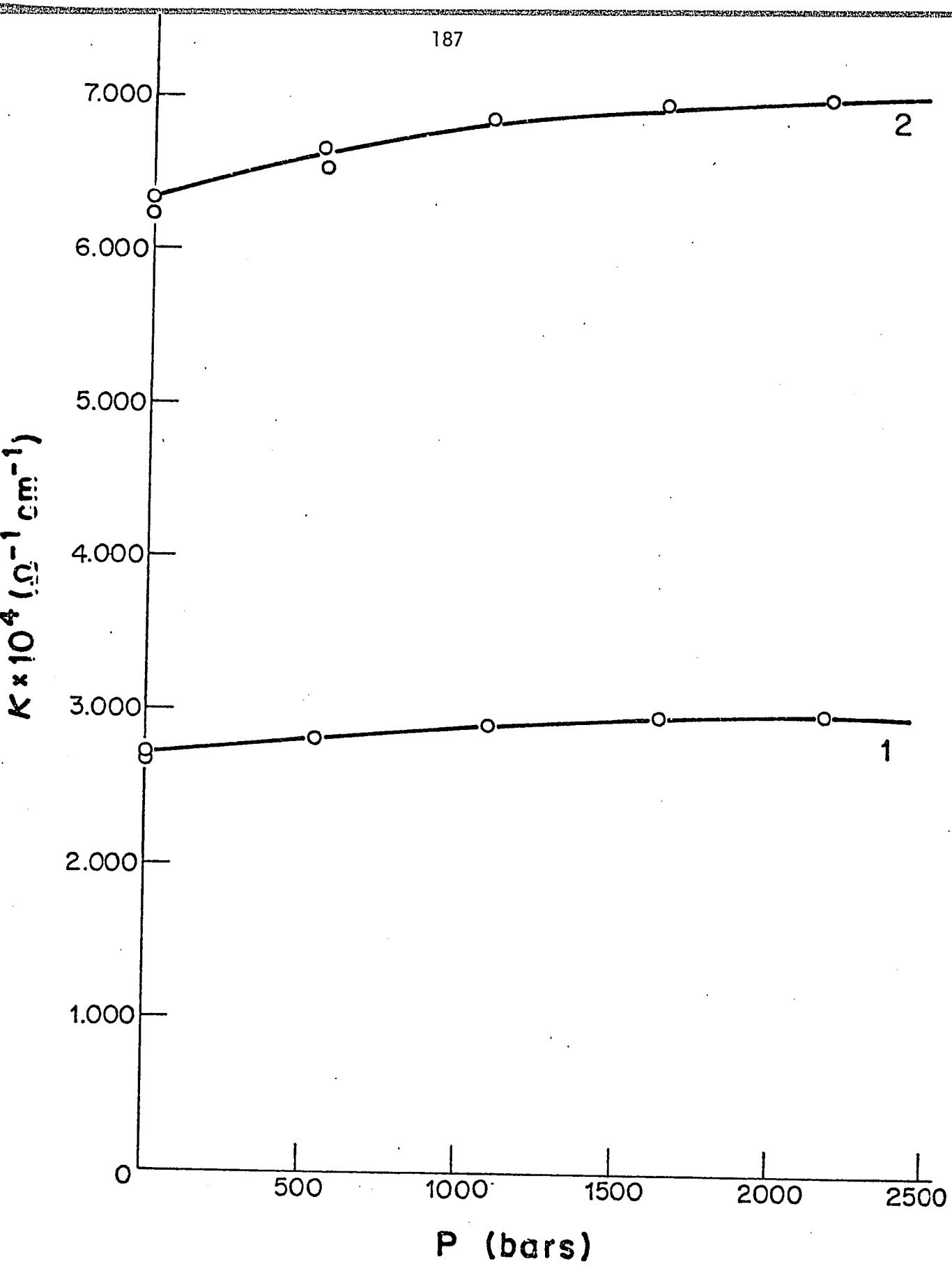

FIGURE 5.2.4 Variation of specific conductivity with pressure for:

1) 0.001 M $PbCl_2$ and

2) 0.0025 M $PbCl_2$.

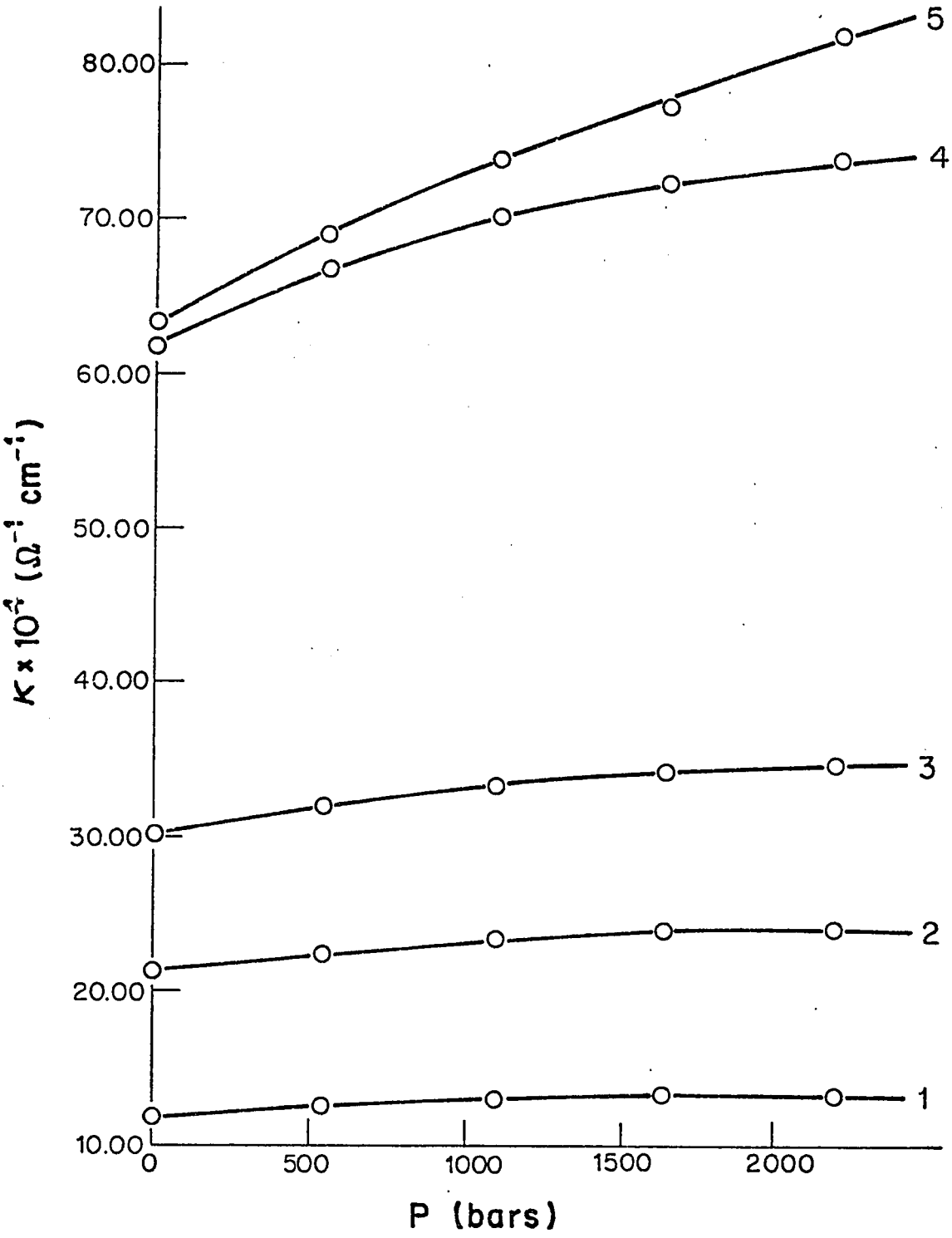

FIGURE 5.2.5 The variation of the specific conductivity with pressure for:

1) 0.005 M $PbCl_2$
2) 0.01 M $PbCl_2$
3) 0.015 M $PbCl_2$
4) 0.0388 M $PbCl_2$ and
5) a saturated solution of $PbCl_2$.

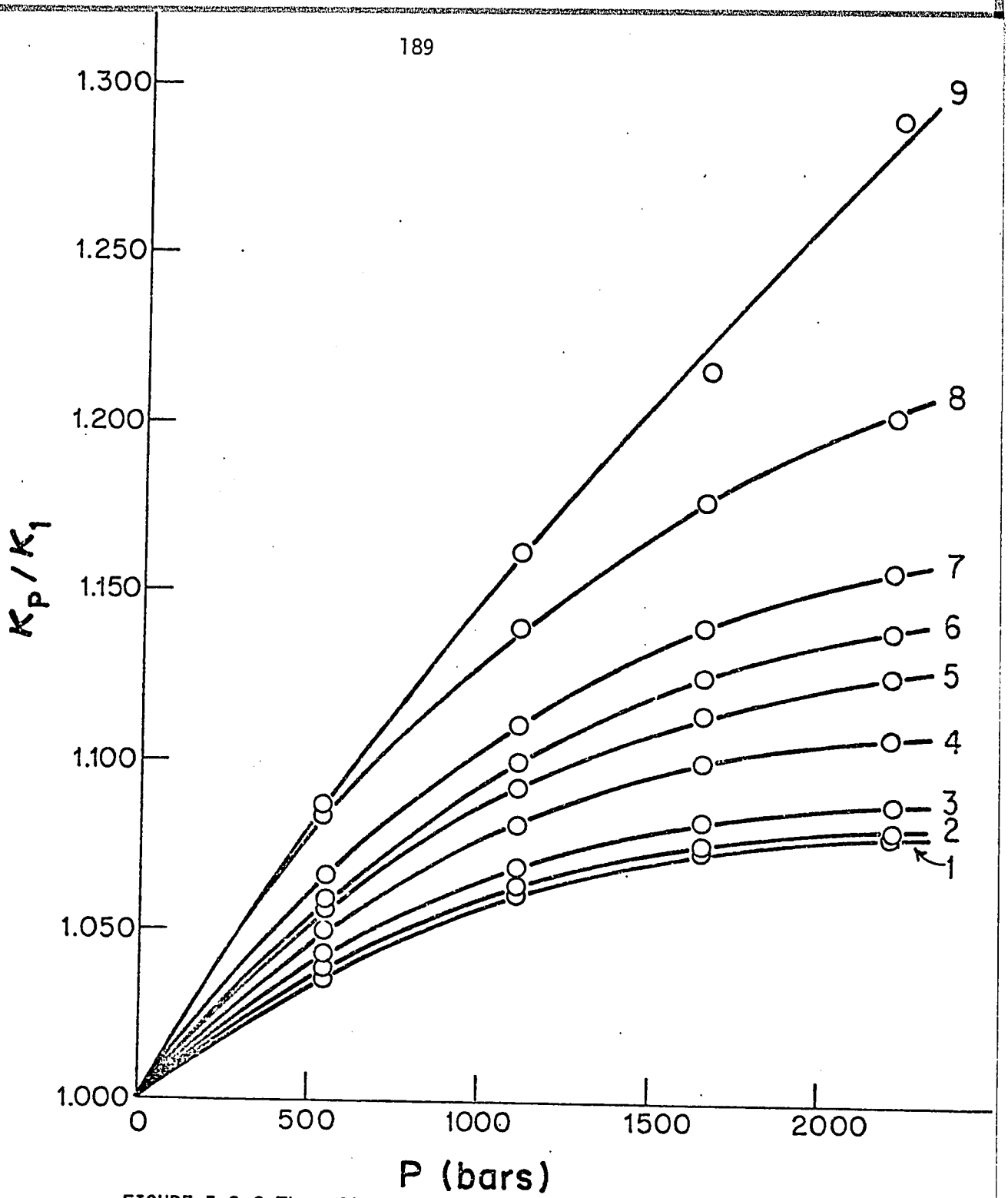

FIGURE 5.2.6 The effect of pressure in terms of the relative change of the specific conductivity, κ_p/κ_1 , for:

1) 0.10 m KCl
2) 0.01 m KCl
3) 0.001 M $PbCl_2$
4) 0.0025 M $PbCl_2$
5) 0.005 M $PbCl_2$
6) 0.01 M $PbCl_2$
7) 0.015 M $PbCl_2$
8) 0.0388 M $PbCl_2$ and
9) saturated solution of $PbCl_2$.

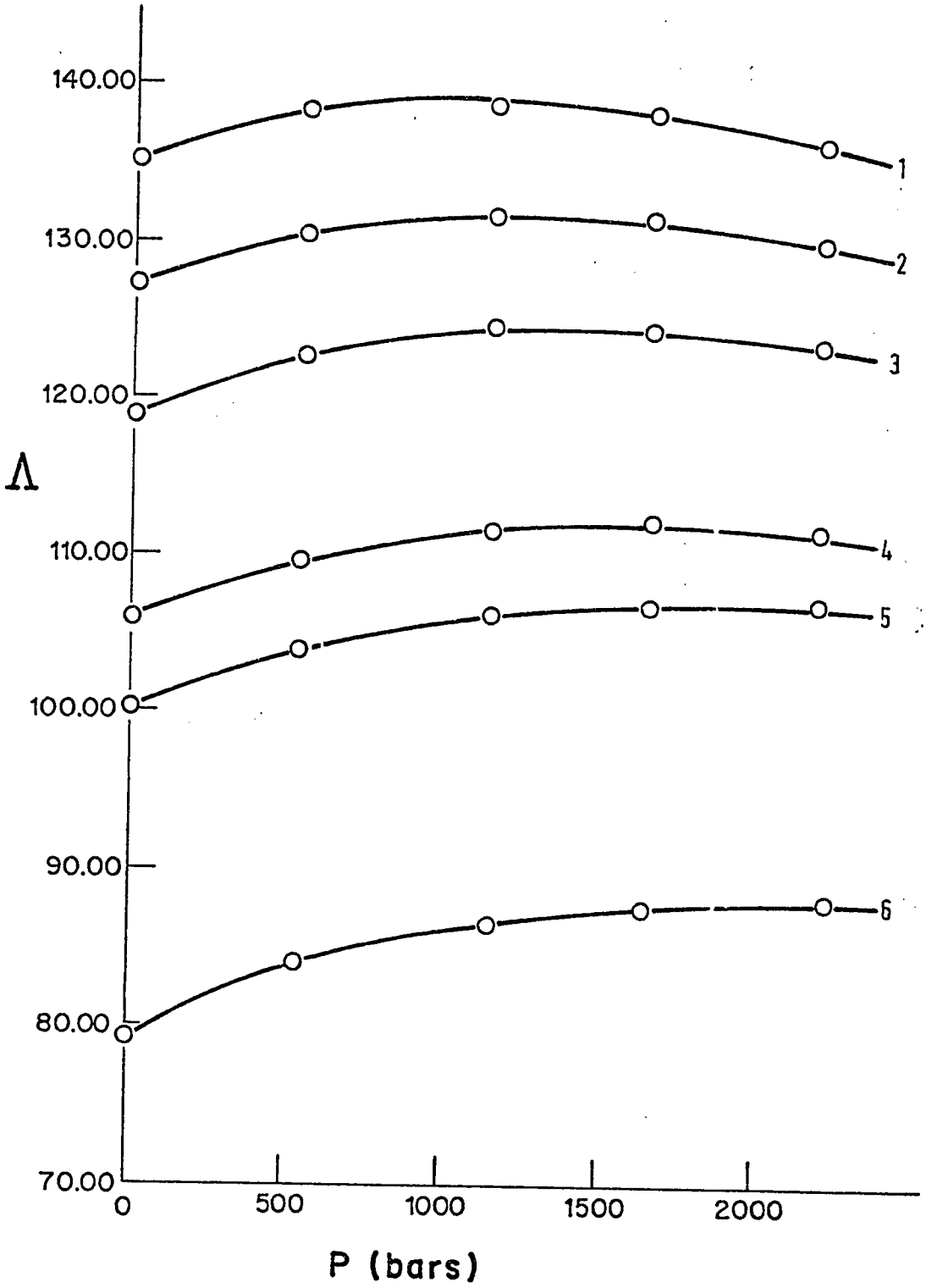

FIGURE 5.2.7 The variation of the equivalent conductivity with pressure for:

1) 0.001 M $PbCl_2$
2) 0.0025 M $PbCl_2$
3) 0.005 M $PbCl_2$
4) 0.01 M $PbCl_2$
5) 0.015 M $PbCl_2$ and
6) 0.0388 M $PbCl_2$

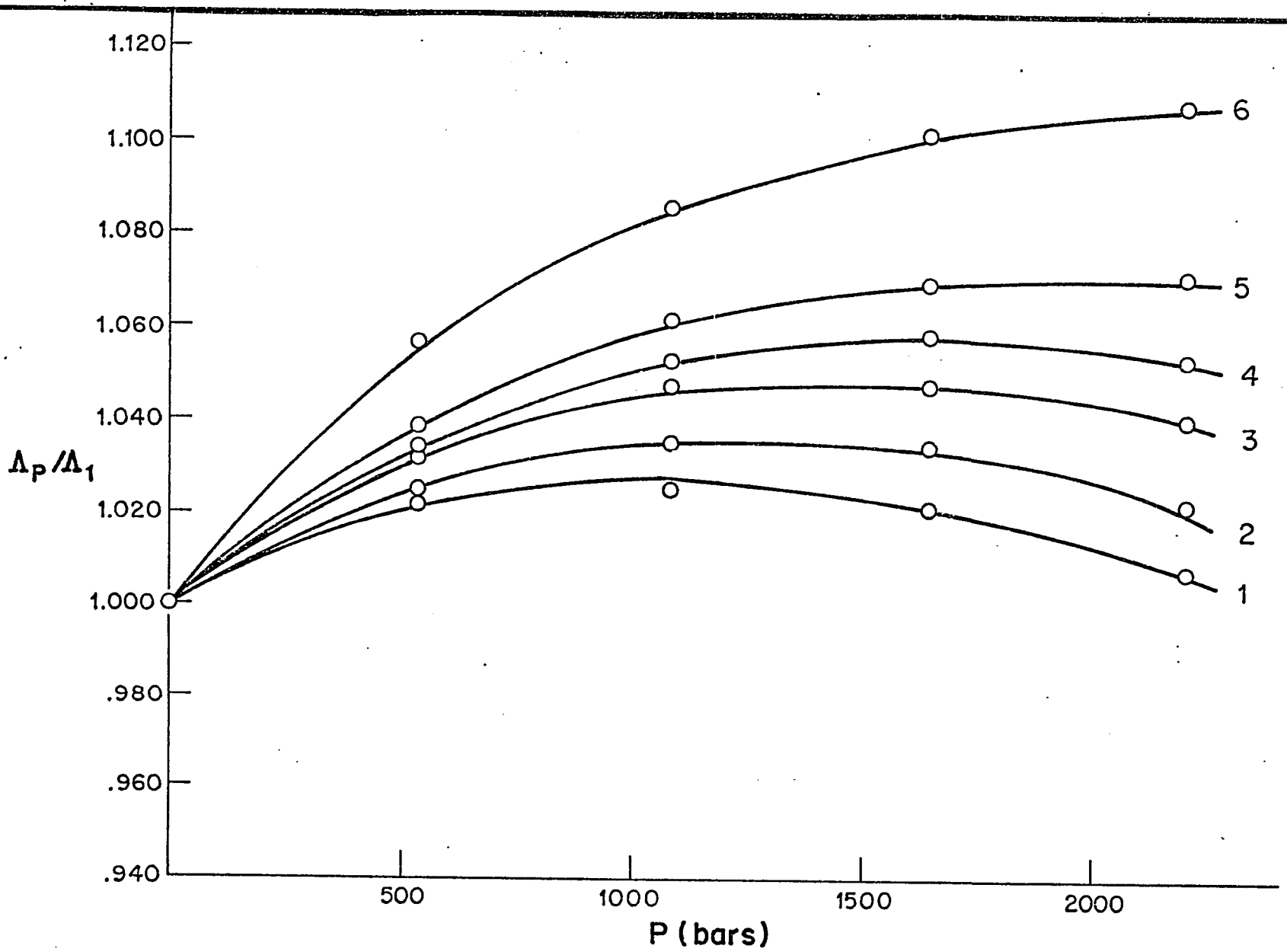

FIGURE 5.2.8 The relative change of equivalent conductivity, Λ_P/Λ_1 ,with pressure for $PbCl_2$

at concentrations: 1) 0.001 M $PbCl_2$ 4) 0.010

2) 0.0025 5) 0.015

3) 0.005 6) 0.0388

If dissociation of $PbCl^+$ occurs with a net volume decrease, then pressure will favour such a process. A saturated solution of $PbCl_2$ is known[139] to contain 6% of undissociated $PbCl_2$ salt; about one half of the remaining $PbCl_2$ undergoes the dissociation reaction

$$PbCl_2 \rightleftharpoons Pb^{2+} + 2Cl^-$$

and the other half, the dissociation process

$$PbCl_2 \rightleftharpoons PbCl^+ + Cl^-$$

Therefore, $PbCl^+$ is expected to make a significant contribution to the pressure-dependence of the conductivity data in dilute as well as in saturated $PbCl_2$ solutions. In order to evaluate the pressure-dependence of the solubility product of $PbCl_2$, it is necessary to determine the concentration of the various Pb species* in solution at each pressure. However, the solubility of $PbCl_2$ must be determined at each pressure.

The specific conductivity ratio κ_p/κ_1 (from Table A.1.4) is plotted as a function of $I^{1/2}$ (where I = 3C) as illustrated in Figure 5.2.9. A series of straight lines are observed whose slopes are pressure dependent. The best-fit straight lines are extrapolated at each pressure to the observed κ_p/κ_1 ratio for the saturated solution of $PbCl_2$ to give the pressure dependent concentration of dissolved $PbCl_2$. The concentration of dissolved $PbCl_2$ at each pressure is listed in Table 5.2.3. The method of representing

* Various species can be present in $PbCl_2$ solutions: complex ions, contact ion-pairs and solvent-separated ion-pairs. The first two types are probably not chemically distinguishable. From the point of view of the conductivity measurements involved here, it will be immaterial what is the actual chemical nature of the species of a given stoichiometric type. Only whether it is neutral, positively or negatively charged is of concern. We shall therefore generically refer to the various species as "ion-pairs".

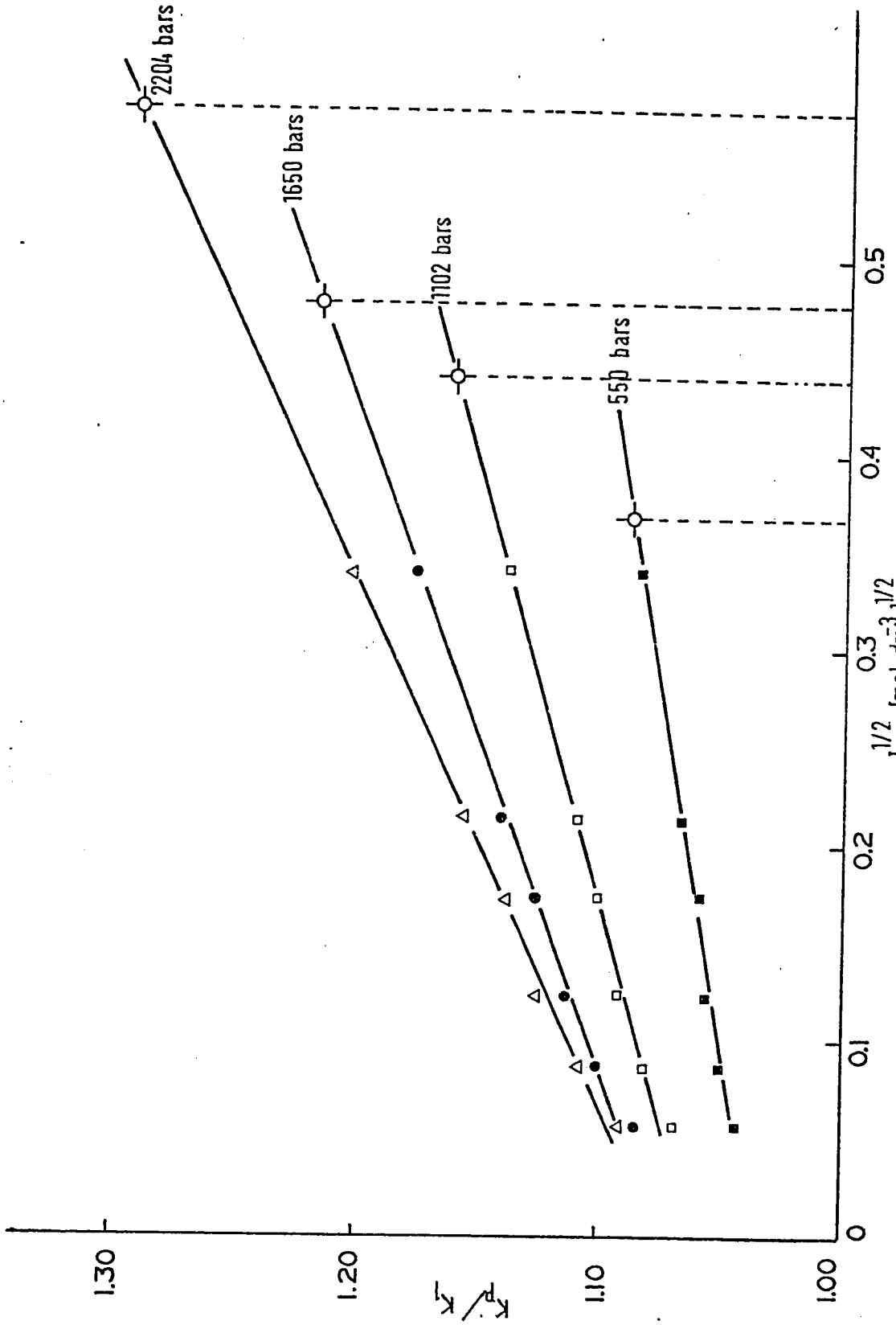

FIGURE 5.2.9 A plot of the specific conductivity ratio κ_p/κ_1 at 550, 1100, 1650 and 2204 bars versus the square root of ionic strength, $I^{\frac{1}{2}}$, for aq $PbCl_2$ at 298.0 K. The respective best-fit straight lines at each pressure are extrapolated to the κ_p/κ_1 values for the saturated solution of $PbCl_2$.

κ_p/κ_1 as a function of $C^{1/2}$ (or $I^{1/2}$) has been used successfully by Brummer and Gancy[66,71] in the determination of the limiting equivalent conductivity of a number of 1:1 salts as a function of applied pressure. The theoretical significance of such a procedure is discussed in reference 66.

The evaluation of the solubility product of $PbCl_2$ requires knowledge of the quantity of $PbCl^+$ present if the K_{sp} is defined in terms of the reaction

$$PbCl_2 \rightleftharpoons PbCl^+ + Cl^-$$

Therefore

$$K_{sp} = f_{PbCl^+} \; [PbCl^+] \; f_{Cl^-} \; [Cl^-]$$

5.2.3 Evaluation of $PbCl^+$ Concentration

The analysis of conductivity data for an unsymmetrical electrolyte in which ion-pair formation arises presents a problem in the choice of a suitable conductivity expression. The Debye-Hückel-Onsager equation does not recognize the presence of the $PbCl^+$ ion; therefore the expression cannot be used in its original form to evaluate the degree of dissociation.

The conductivity equation for relatively high concentrations can be written as

$$\Lambda = \Lambda^\infty - \left[\left(\frac{2.801\times10^6 |z_1 z_2| q\Lambda^\infty}{(\varepsilon T)^{3/2}(1+q^{1/2})(1+Ba\sqrt{I/2})}\right) + \left(\frac{41.25(|z_1|+|z_2|)}{\eta(\varepsilon T)^{1/2}}\right]\frac{I^{1/2}}{1 + BaI^{1/2}} \qquad (5.2.1)$$

The significance of each term was listed in Chapter 1, while the pressure-dependent terms are listed numerically in Table A.1.5. The equation can be written more concisely as

$$\Lambda = \Lambda^{\infty} - \left[\frac{R\Lambda^{\infty}}{1 + Ba\sqrt{I/2}} + E\right] \frac{I^{1/2}}{1 + BaI^{1/2}} \qquad (5.2.2)$$

where R and E are defined by comparison with eqn. 5.2.1.

The method for determining the degree of ion-pair dissociation for $PbCl^+$ will now be outlined. The ion-pair association can be written as

$$Pb^{2+} + Cl^- \rightleftharpoons PbCl^+$$

and if α is the degree of association, then the concentrations of $PbCl^+$ Pb^{2+}, and Cl^- are αC, $(1-\alpha)C$ and $(2-\alpha)C$, respectively. Therefore, the measured equivalent conductivity, Λ_m, (cf. equation 1.4.15) can be expressed in terms of the individual ionic mobilities and the degree of association as

$$\Lambda_m = (1-\alpha)\Lambda_{Pb^{2+}} + \frac{\alpha}{2}\Lambda_{PbCl^+} + \frac{(2-\alpha)}{2}\Lambda_{Cl^-}$$

$$= [(1-\alpha)\Lambda_{Pb^{2+}} + (1-\alpha)\Lambda_{Cl^-}] + \frac{\alpha}{2}\Lambda_{PbCl^+} + [\frac{(2-\alpha)}{2}\Lambda_{Cl^-} - (1-\alpha)\Lambda_{Cl^-}]$$

$$= (1-\alpha)\Lambda_{PbCl_2} + \frac{\alpha}{2}\Lambda_{(PbCl^+)(Cl^-)} \qquad (5.2.3)$$

The solution can thus be treated as a mixture of completely dissociated $(PbCl^+)(Cl^-)$ and completely dissociated $PbCl_2$, so that Λ_{PbCl_2} and $\Lambda_{(PbCl^+)(Cl^-)}$ are the calculated equivalent conductivity values for the completely dissociated species. This approach was first applied by Davies and Righelleto[73] in 1930 to the conductivity behavior of a number of uni-bivalent salts, including $PbCl_2$ at ambient pressure. More recently, Fisher and co-workers[45,47] have applied the same approach to determine the effect of pressure on the dissociation of $La(SO_4)^+$ and $NaSO_4^-$ ion-pairs.

The conductivity Λ_{1-1} (or $\Lambda_{(PbCl^+)(Cl^-)}$) of the uni-univalent salt $(PbCl^+)(Cl^-)$ at each concentration and pressure is evaluated from equation 5.2.2 in the form

$$\Lambda_{1-1} = \Lambda^{\infty}_{1-1} - \left[\frac{R_{1-1}\,\Lambda^{\infty}_{1-1}}{1 + B_{1-1}\,a_{1-1}\sqrt{I/2}} + E_{1-1}\right] \frac{I^{1/2}}{1 + B_{1-1}\,a_{1-1}(I)^{1/2}} \qquad (5.2.4)$$

The constants R_{1-1}, B_{1-1}, a_{1-1} and E_{1-1} for each pressure are listed in Table A.1.6. The limiting equivalent conductivity of the 1-1 salt, Λ^{∞}_{1-1}, is given by

$$\Lambda^{\infty}_{1-1} = \Lambda^{\infty}_{PbCl^+} + \Lambda^{\infty}_{Cl^-}$$

The limiting equivalent conductivity of $PbCl^+$ was assumed to be 0.60 $\Lambda^{\infty}_{Cl^-}$, as used earlier by Davies[73]. The variation of $\Lambda^{\infty}_{Cl^-}$, with pressure was evaluated from the combined data presented by Hamann (p.66-67, Tables 3 and 4 in reference 41). The pressure dependence of $\Lambda^{\infty}_{Cl^-}$ as treated by Hamann was determined from the transference number data of Wall and Berkowitz[140] and the limiting equivalent conductivity data of Gancy and Brummer[66,71] for KCl solutions as a function of applied pressure. The limiting equivalent conductivity[69] of Pb^{2+} ions at 1 bar is taken as 69.5; however, the variation of $\Lambda^{\infty}_{Pb^{2+}}$ with pressure is unknown. It has been assumed that the pressure-dependence of $\Lambda^{\infty}_{Pb^{2+}}$ is the same as that for $\Lambda^{\infty}_{La^{3+}}$ because the actual Λ^{∞} values at 1 bar are almost identical. The latter quantity has been evaluated by Fisher[47] and co-workers at pressures up to 2000 bars. The values of $\Lambda^{\infty}_{Cl^-}$ $\Lambda^{\infty}_{PbCl^+}$ and $\Lambda^{\infty}_{Pb^{2+}}$ as a function of pressure are listed in Table A.1.8. Also included in this Table are the limiting equivalent conductivities of the uni-univalent salt $(PbCl^+)(Cl^-)$

and the uni-bivalent salt, $PbCl_2$.

In a similar manner, the theoretical value of Λ_{1-2}, for the uni-bivalent salt, is calculated from the expression

$$\Lambda_{1-2} = \Lambda^{\infty}_{1-2} - \left[\frac{R_{1-2}\,\Lambda^{\infty}_{1-2}}{1 + B_{1-2}\,a_{1-2}\sqrt{I/2}} + E_{1-2}\right] \frac{I^{1/2}}{1 + B_{1-2}\,a_{1-2}(I)^{1/2}} \qquad (5.2.5)$$

The pressure-dependent terms are listed in Table A.1.7.

The measured equivalent conductivity, Λ_m can be related to Λ_{1-2} and Λ_{1-1} through equation 5.2.3 in the following manner:

$$\Lambda_m = (1-\alpha)\,\Lambda_{1-2} + 0.5\alpha\,\Lambda_{1-1} \qquad (5.2.6)$$

The degree of association, α, is evaluated by successive approximations (cf. the method of Davies[73]) Initially, the ionic strength, I, is assumed to be 3C; Λ_{1-1} and Λ_{1-2} are calculated by means of equations 5.2.4 and 5.2.5 and the value of α is determined from equation 5.2.6. This value of α is then used to calculate a new value for the ionic strength using the equation

$$I = C(3-2\alpha) \qquad (5.2.7)$$

Then Λ_{1-1} and Λ_{1-2} are recalculated to give a second value of α. Three iterations are generally required to achieve an almost constant value of α.

The molal dissociation constant, K_m, for the reaction

$$PbCl^+ \rightleftharpoons Pb^{2+} + Cl^-$$

is evaluated from the expression

$$K_m = \frac{f_{Pb^{2+}} \; f_{Cl^-} \; (1 + \beta)\beta_m}{f_{PbCl^+} \; (1-\beta)}$$

$$= \frac{f_{Pb^{2+}} \; f_{Cl^-} \; (2-\alpha)(1-\alpha)m}{f_{PbCl^+} \; \alpha} \qquad (5.2.8)$$

where m is the molality of the solution and β is the degree of dissociation, i.e. $1-\alpha$. The activity coefficients of the univalent ions are assumed to be equal and the activity coefficient for Pb^{2+} is calculated from the expression

$$\log f_{\pm} = - \frac{A|z_1 \; z_2|I^{1/2}}{1 + Ba \; I^{1/2}} \qquad (5.2.9)$$

In more exact terms, the stoichiometric activity coefficient, γ, should be used in equation 5.2.8; however, in dilute solutions when the rational activity coefficient, f, is employed, the resulting error will be negligible.

The values for Λ_m, Λ_{1-1}, Λ_{1-2}, β, $f_{Pb^{2+}}$, and K_m at concentrations 0.001, 0.0025, 0.005, 0.01, 0.015, 0.0388 M $PbCl_2$, and for a saturated solution, are listed in Table 5.2.1 as a function of pressure. The evaluations of equivalent conductivity, ionic strength and activity coefficient are based on molar concentrations corrected at each pressure for the compression of the solution, using the known[41] density and compressibility of water.

The values of K_m at each pressure exhibit a fluctuation over the entire concentration range, the discrepancies being greatest at the lowest and highest concentrations of $PbCl_2$. The mean values of K_m, neglecting those at the highest and lowest concentrations, are listed in Table 5.2.2. The variation of ln K_m with applied pressure is illustrated in Figure 5.2.10 and the limiting slope is found to be

TABLE 5.2.1

CONDUCTIVITY AND THERMODYNAMIC DATA FOR $PbCl_2$ SOLUTIONS AT ELEVATED PRESSURES

P(bars)	C($PbCl_2$)	0.001 M	0.0025 M	0.005 M	0.01 M	0.015 M	0.0388 M	Saturated Solution
1	Λ_m	134.93	127.09	118.84	105.97	100.07	79.33	81.87
	Λ_{1-1}	117.[illegible]	115.60	113.48	111.10	109.41	105.55	105.29
	Λ_{1-2}	138.91	135.90	133.16	130.30	128.42	124.53	124.29
	β	0.950	0.887	0.813	0.675	0.615	0.370	0.408
	$f_{Pb^{2+}}$	0.894	0.849	0.809	0.768	0.741	0.685	0.682
	K_m	0.033	0.032	0.032	0.027	0.029	0.022	0.026
550	Λ_m	137.84	130.24	122.67	109.59	103.86	84.04	75.05
	Λ_{1-1}	120.95	118.78	116.64	114.29	112.49	108.47	108.45
	Λ_{1-2}	140.74	137.66	134.84	131.98	129.94	125.82	125.80
	β	0.964	0.905	0.841	0.701	0.646	0.416	0.291
	$f_{Pb^{2+}}$	0.894	0.852	0.812	0.771	0.744	0.687	0.700
	K_m	0.047	0.039	0.040	0.031	0.034	0.027	0.017
1102	Λ_m	137.71	131.48	124.31	111.47	106.12	86.53	57.64
	Λ_{1-1}	122.14	120.01	117.90	115.53	113.82	109.86	110.50
	Λ_{1-2}	140.72	137.69	134.89	131.97	130.00	125.83	126.44
	β	0.962	0.920	0.861	0.724	0.673	0.446	0.034
	$f_{Pb^{2+}}$	0.899	0.856	0.816	0.774	0.747	0.689	0.687
	K_m	0.045	0.047	0.047	0.035	0.039	0.031	0.0016
1650	Λ_m	137.48	131.21	124.39	112.12	106.97	87.74	52.18
	Λ_{1-1}	121.86	119.75	117.63	115.23	113.46	109.37	-
	Λ_{1-2}	139.15	136.18	133.42	130.50	128.53	124.33	-
	β	0.979	0.935	0.879	0.748	0.700	0.475	~ 0
	$f_{Pb^{2+}}$	0.902	0.858	0.818	0.777	0.750	0.691	-
	K_m	0.083	0.060	0.056	0.040	0.045	0.036	-
2204	Λ_m	136.09	129.67	123.57	111.60	107.13	88.19	36.31
	Λ_{1-1}	120.71	118.85	116.58	114.23	112.50	108.42	-
	Λ_{1-2}	136.42	133.61	130.84	127.99	126.05	121.88	-
	β	0.996	0.947	0.900	0.769	0.729	0.502	~ 0
	$f_{Pb^{2+}}$	0.903	0.860	0.821	0.780	0.752	0.693	
	K_m	0.450	0.075	0.070	0.046	0.053	0.041	

TABLE 5.2.2

MEAN MOLAL DISSOCIATION CONSTANT FOR $PbCl^+$ AS A FUNCTION OF PRESSURE

P (bars)	$\overline{K}_m$ (mol dm^{-3})
1	0.030 ± 0.002
550	0.036 ± 0.004
1102	0.043 ± 0.005
1650	0.050 ± 0.009
2204	0.061 ± 0.010

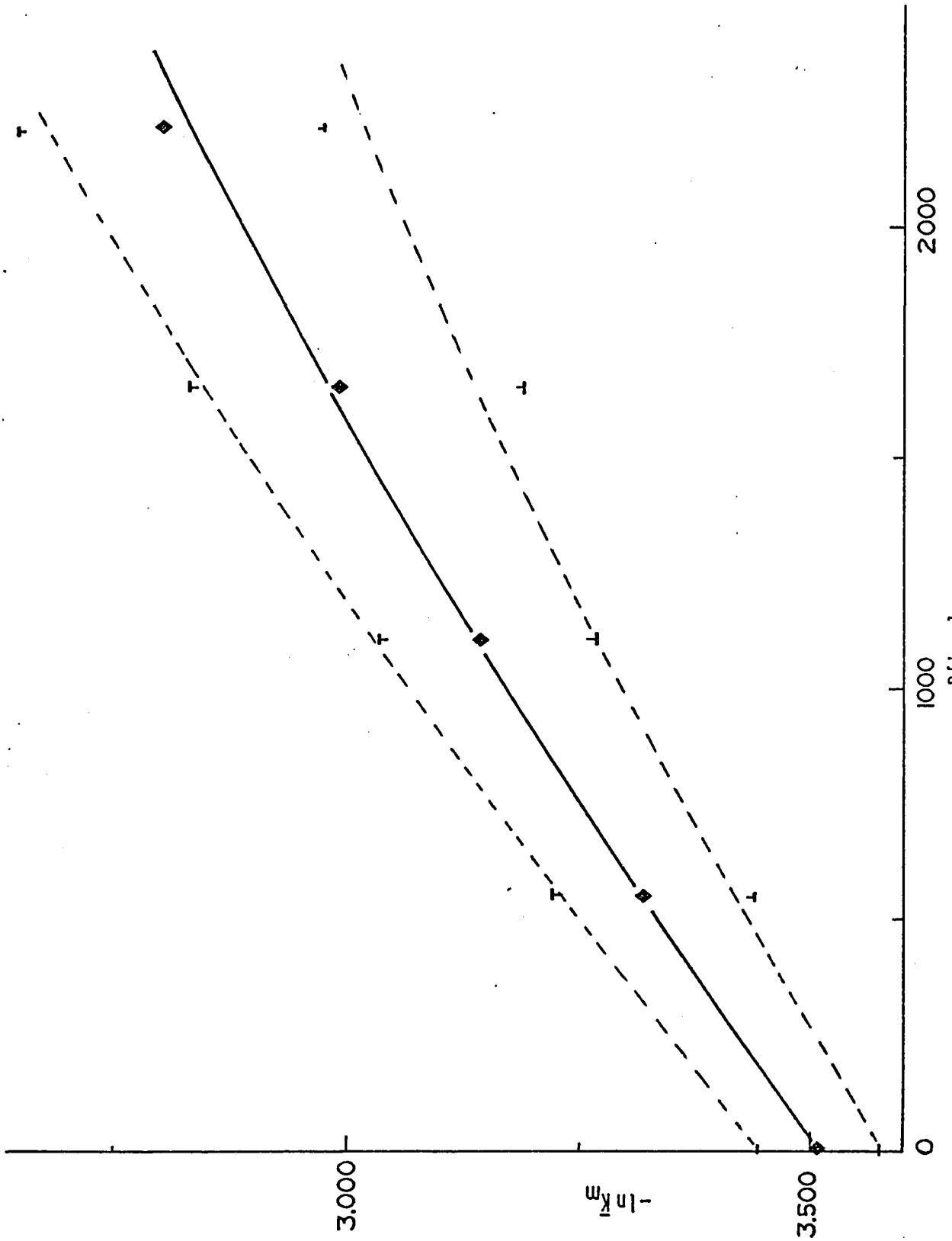

FIGURE 5.2.10 The variation of the natural logarithm of the molal dissociation constant for the ion - pair, $PbCl^+$, with pressure.

$$\left(\frac{\partial \ln K_m}{\partial P}\right) = -\frac{\Delta V}{RT} = 3.8 \times 10^{-4} \text{ bar}^{-1}$$

The corresponding partial molar volume change, ΔV, for the ion-pair dissociation is hence -9.3 $cm^3\ mol^{-1}$. The partial molar volume, V_{PbCl^+}, of the ion-pair $PbCl^+$, can be evaluated from the relationship

$$\Delta V = V_{Pb^{2+}} + V_{Cl^-} - V_{PbCl^+} = -9.3 \text{ cm}^3 \text{ mol}^{-1}$$

taking[110]

$$V_{Pb^{2+}} = -26.3 \text{ and } V_{Cl^-} = 23.23 \text{ cm}^3 \text{ mol}^{-1}$$

Therefore

$$V_{PbCl^+} = 6.3 \text{ cm}^3 \text{ mol}^{-1}$$

5.2.4 Evaluation of the Solubility Product of $PbCl_2$ as a Function of Pressure

It may be expected that the solubility will be affected owing to the volume change upon dissolution of the salt. The solubility product for the process

$$PbCl_2 \rightleftharpoons PbCl^+ + Cl^-$$

is defined as

$$K_{sp} = f_{PbCl^+} [PbCl^+] f_{Cl^-} [Cl^-]$$

where the activity coefficients at $I = C(3-2\alpha)$ can be calculated from equation 5.2.9. However, the ion-pair $PbCl^+$ undergoes a further pressure-dependent dissociation

$$PbCl^+ \rightleftharpoons Pb^{2+} + Cl^-$$

The concentrationsof $PbCl^+$ and Cl^- will therefore depend on the extent of this dissociation process. If C is the concentration of $PbCl_2$ dissolved in solution and β is the degree of ion-pair dissociation, then the concentrations of $PbCl^+$ and Cl^- are $C(1-\beta)$ and $C(1+\beta)$ respectively. The mean activity coefficients for the uni-univalent salt, $f_\pm$ and the calculated values of the solubility product of $PbCl_2$ are given in Table 5.2.3. The pressure-dependence of $\ln K_{sp}$ is shown in Figure 5.2.11 from which the pressure coefficient is found to be

$$\frac{\partial \ln K_{sp}}{\partial P} = -\frac{\Delta V}{RT} = 7.0 \times 10^{-4} \text{ bar}^{-1}$$

limitingly at P = 1 bar. Therefore the volume change accompanying the dissolution of $PbCl_2$ is $\sim$ -17 $cm^3\ mol^{-1}$.

5.2.5 General Comments on Ion-Pair Equilibria and Solubility Product Calculations

The evaluation of the molal dissociation constant for an unsymmetrical ion-pair involves several assumptions. In general, the lead chloride solution must be treated as a mixture of uni-univalent and uni-bivalent salt species. However, the two uncertainties which arise in this approach are the satisfactory assignments of limiting equivalent conductivities to a) the $PbCl^+$ ion-pair and b) to the Pb^{2+} ion. The value of $\Lambda^\infty_{PbCl^+}$ was taken as 0.6 $\Lambda^\infty_{Cl^-}$ at all pressures used following the approach of Righellato and Davies[73], based on the findings of Chandler[141]. Chandler, in treating the behaviour of dibasic organic acids, has reported that the intermediate univalent ion has a mobility of 0.6 times that of the acid anion. Davies[73] concluded that this leads to an error of less than 10%

TABLE 5.2.3

SOLUBILITY PRODUCT OF $PbCl_2$ AS A FUNCTION OF PRESSURE

P (bars)	C (mol dm^{-3})	$f_{\pm}$	$K_{sp} \times 10^4$ (mol dm^{-3})	ln K_{sp}
1	0.039	0.789	7.80	-7.155
550	0.046	0.793	12.2	-6.711
1102	0.064	0.803	26.3	-5.938
1650	0.074	0.803	35.3	-5.646
2204	0.113	0.777	77.7	-4.866

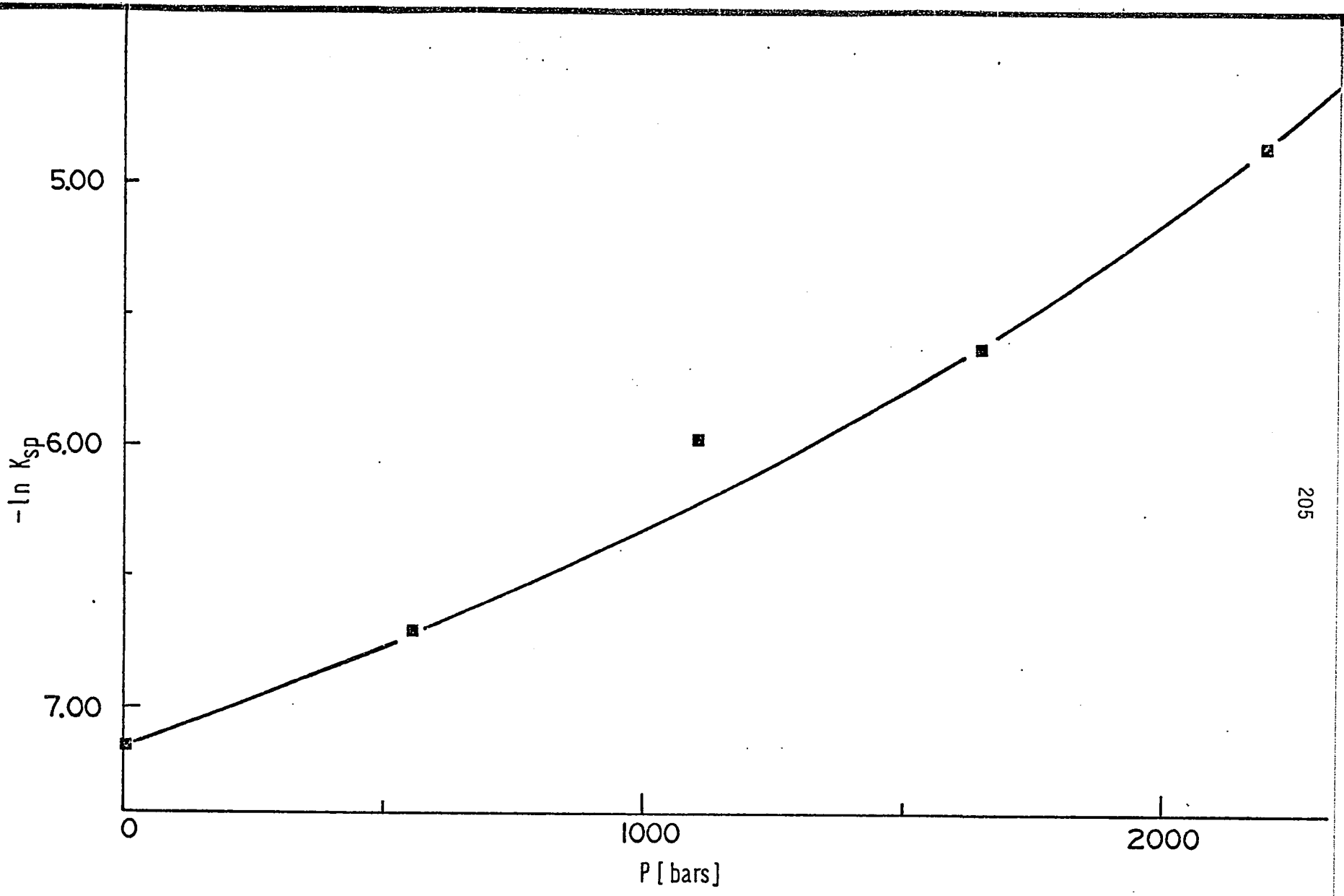

FIGURE 5.2.11 The variation of the natural logarithm of the solubility product for $PbCl_2$ with pressure.

in the derived degree of dissociation. Recently, Fisher[45] and co-workers have applied this method to the $NaSO_4^-$ ion-pair; however, the limiting equivalent conductivity of $NaSO_4^-$ was taken as 0.5 times that of the SO_4^{2-} ion. This assumption gave dissociation constants for the ion-pair $NaSO_4^-$ which were virtually independent of ionic strength.

Although there is an obvious variation of K_m with ionic strength in this work, the values of K_m at the lowest concentration (where experimental errors and errors arising from the various assumptions are expected to be relatively large) and the values of K_m at the high concentrations (where the Debye-Hückel-Onsager equation is not truly obeyed) are not included in the evaluation of the mean value of K_m at each pressure. The mean value of K_m at ambient pressure compares favourably with the values reported in the literature:

	Present Work	Righellato and Davies[73]	James[74]	Carmody[142]
$\overline{K}_m$(mol dm^{-3})	0.030 ± 0.002	0.030	0.026	0.029

In order to extend these calculations to elevated pressures, the limiting equivalent conductivities of Pb^{2+}, Cl^- and $PbCl^+$ must be known as a function of pressure. The values of $\Lambda^\infty_{Cl^-}$ have been determined[41] at pressures up to 2000 bars; therefore, based on the assumption that $\Lambda^\infty_{PbCl^+} = 0.6\ \Lambda^\infty_{Cl^-}$, the value of Λ_{PbCl^+} can be obtained as a function of pressure. The value of $\Lambda^\infty_{Pb^{2+}}$ has been assumed to be similar to that of $\Lambda^\infty_{La^{3+}}$ at all pressures studied. This assumption is based on the fact that both ions have identical limiting mobilities (Λ^∞ = 69.5) at 1 bar and the limiting equivalent conductivity of most ions varies with pressure in the same manner. That is Λ^∞ increases slightly with application

of low hydrostatic pressures but then reaches a maximum in the pressure range 500 to 1000 bars. At higher pressures, the values of Λ^{∞} then decrease quite rapidly to values below those at 1 bar. It is expected that the value chosen for $\Lambda^{\infty}_{Pb^{+2}}$ will be in error by less than 2 conductivity units. It will be shown below that any discrepancy between the true values of $\Lambda^{\infty}_{La}3+$ and $\Lambda^{\infty}_{Pb}2+$ will have little effect on the values of K_m, even in the most dilute solutions ($\sim$ 0.001 M).

At 1102 bars and C = 0.001 M $PbCl_2$, the value of $\Lambda^{\infty}_{Pb^{2+}}$ is taken as 68.45. This gives a value for the degree of association, α, of 0.038 and thus K_m = 0.045 mol dm^{-3} (see Table 5.2.1). However, if the value of $\Lambda^{\infty}_{Pb}2+$ is in error by 1 conductivity unit, that is $\Lambda^{\infty}_{Pb}2+ = 69.45$, then α = 0.038 and K_m = 0.045 mol cm^{-3}. This leads to negligible error in the calculated value of K_m. However, if any errors remain in the evaluation of K_m, the error in the derivative of ln K_m with respect to pressure will be relatively less than that in K_m itself.

The partial molar volume change for the ion-pair dissociation was evaluated above as -9.3 cm^3 mol^{-1}. The error in this value is determined by the accuracy of the experimental conductivity results and the choice of a suitable form of the conductivity equation for use at elevated pressures. The conductivity measurements at various $PbCl_2$ concentrations are reproducible to within 0.8%. However, at the lowest concentrations ($\sim$ 0.001 M) the accuracy of the results becomes questionable since a solvent correction was not applied; at higher concentrations, the effect of the pressure-dependent conductivity of H_2O on the measured conductivity of $PbCl_2$ is negligible. The error in ΔV has not been evaluated but is expected to be less than 1 cm^3 mol^{-1}. In fact, if the limiting slopes $\left(\frac{\partial \ln K_m}{\partial P}\right)_T$ are calculated using the standard deviations of K_m values at each pressure, a mean deviation for ΔV of $\pm$ 0.8 cm^3 mol^{-1} is obtained.

The evaluation of the solubility of $PbCl_2$ as a function of pressure depends on the reliability of the κ_p/κ_1 values at each concentration of $PbCl_2$ and at each pressure. The plots of κ_p/κ_1 versus $I^{1/2}$ (Figure 5.2.9) yield straight lines at each pressure with deviations only at the lowest ionic strength. The confidence limit for the best-fit straight lines (neglecting the lowest concentration of $PbCl_2$, 0.001M) is better than 99.6% at all pressures. The variation of ln K_{sp} with pressure (Figure 5.2.11) has a limiting slope of 7×10^{-4} bar^{-1} at P = 1 bar. The corresponding volume change for the dissolution of $PbCl_2$ is approximately -17 cm^3 mol^{-1}. This value is consistent with the value calculated from the known partial molar volumes of $PbCl^+$ and Cl^-, and the molar volume of $PbCl_2$:

$$\Delta V = V_{PbCl^+} + V_{Cl^-} - V_{PbCl_2}$$

$$= +6.3 + 23.2 - 47.5 \text{ cm}^3 \text{ mol}^{-1}$$

$$= -18 \text{ cm}^3 \text{ mol}^{-1}$$

5.3 Some Additional Observations on the Behaviour of the Pb, $PbCl_2$ Electrode at Ambient Pressure

It has been proposed by Barradas[28-31] that $PbCl_2$ formed as an anodic film on Pb is composed of two types of $PbCl_2$ surface species. It is supposed that a basal layer of $PbCl_2$ is formed initially, followed by chemical dissolution of $PbCl_2$, reactivation of the electrode surface and redeposition of a secondary layer of $PbCl_2$. The electrode was assumed to be passivated by the presence of the second type of $PbCl_2$ surface film. In order to relate the observed pressure effects on the electrochemical behaviour of $PbCl_2$ to a possible dissolution-redeposition mechanism, additional experiments were performed at ambient pressure utilizing cyclic voltammetry in conjunction with a rotating Pb disc electrode. However, the behaviour at a stationary electrode must first be described.

5.3.1 Cyclic Voltammetry Results at a Stationary Pb Electrode

The current-potential (i-V) profiles for the anodic formation of a film of $PbCl_2$ and its subsequent reduction in the cathodic sweep are illustrated in Figure 5.3.1. The anodic potential limit, E_A, is + 0.093V vs Pt, H_2. The cathodic sweep rate, s_c, was kept constant at 13 mV s^{-1} while the anodic scan rate, s_A, was varied from 13 to 117 mV s^{-1} in a series of consecutive sweeps.

The cathodic i-V profiles at low values of s_A (< 50 mV s^{-1}) exhibit a shoulder at potentials negative to the main peak. However, as the anodic sweep rate is increased, the shoulder disappears. This behaviour indicates that the time spent, $\Delta V/s_A$, during the anodic cycle over a potential range, ΔV, is an important factor in the development of the shoulder. A similar type of behaviour is observed if the anodic potential limit, E_A, is made progressively more positive on each successive voltage scan at a constant sweep rate ($s_A = s_C = 13$ mV s^{-1}). The value of E_A is varied from -0.105 V (pre-passive potential region) to + 0.161 V (approximately + 0.220 V w.r.t. the passivation peak potential, $E_P \simeq -0.060$V). As Figure 5.3.2 indicates, a shoulder on the cathodic i-V profile becomes evident when E_A is extended beyond the passivation potential. The process(es) responsible for the generation of the current shoulder appears to be dependent on the value of E_A as well as the time spent in the trans-passive potential region.

The factors responsible for the shape of the cathodic i-V profile can be investigated more thoroughly by examining the behaviour of the $PbCl_2$ film as a function of the time, t_A, spent at a given fixed anodic potential, E_A, as illustrated in Figures 5.3.3. (a), (b), (c), (d), and (e). The potential is held at various values on both sides of the passivation potential E_p. For E_A values negative to E_P (Figure 5.3.3(a)), the i-V profiles show that the cathodic charge recovered, Q_t, depends

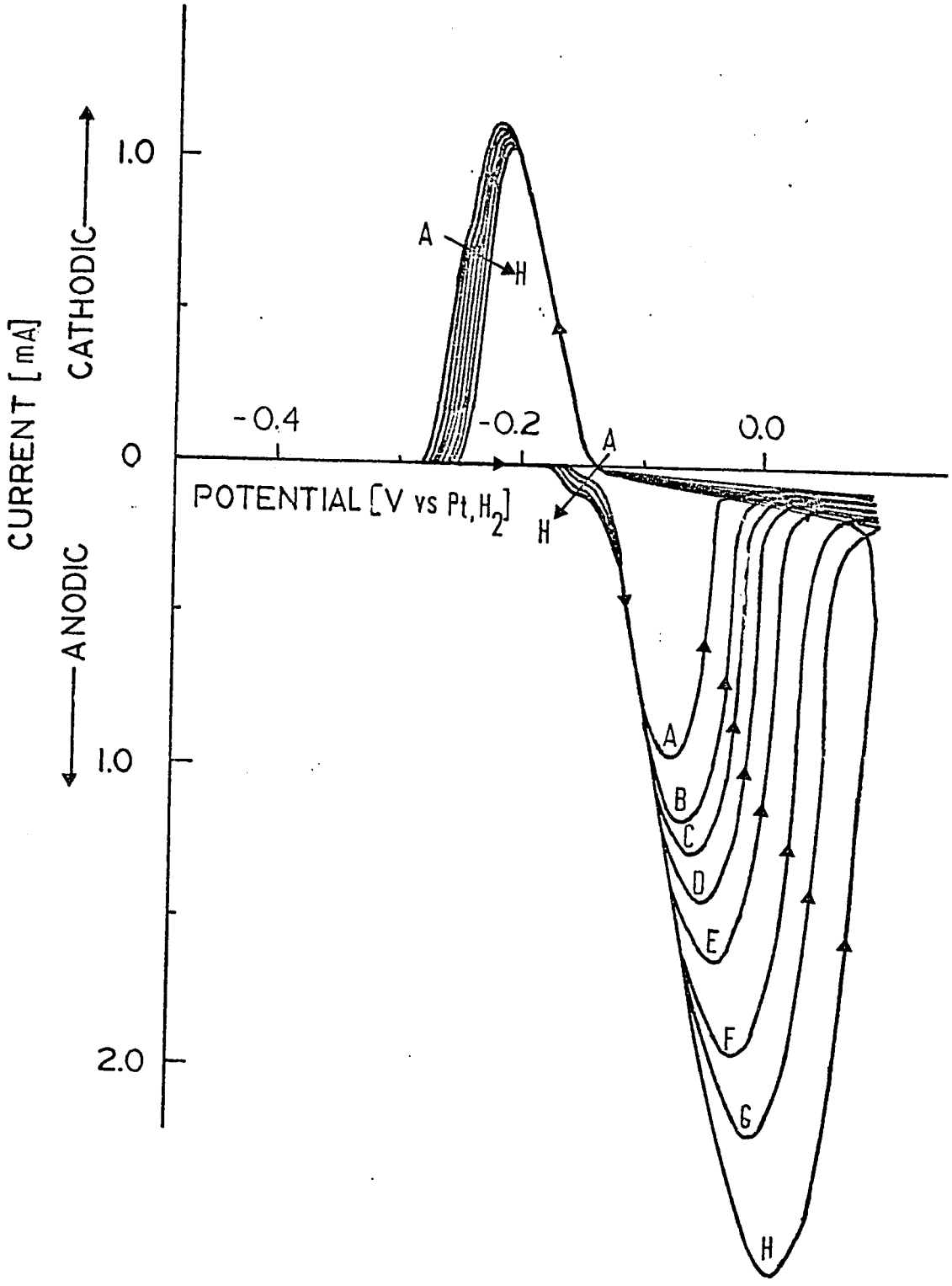

FIGURE 5.3.1 Cyclic voltammograms (i-V profiles) for the formation and reduction of $PbCl_2$ in 1.0 M KCl + 0.01 M HCl at P=1 bar. The cathodic sweep rate, s_C, is fixed at 13 mV s^{-1} and the anodic sweep rate, s_A, is varied in successive cycles. The i-V profiles labelled A,B,C,D,E,F,G and H refer to s_A values of 13,20,23,29,39,58,78 and 113 mV s^{-1}, respectively.

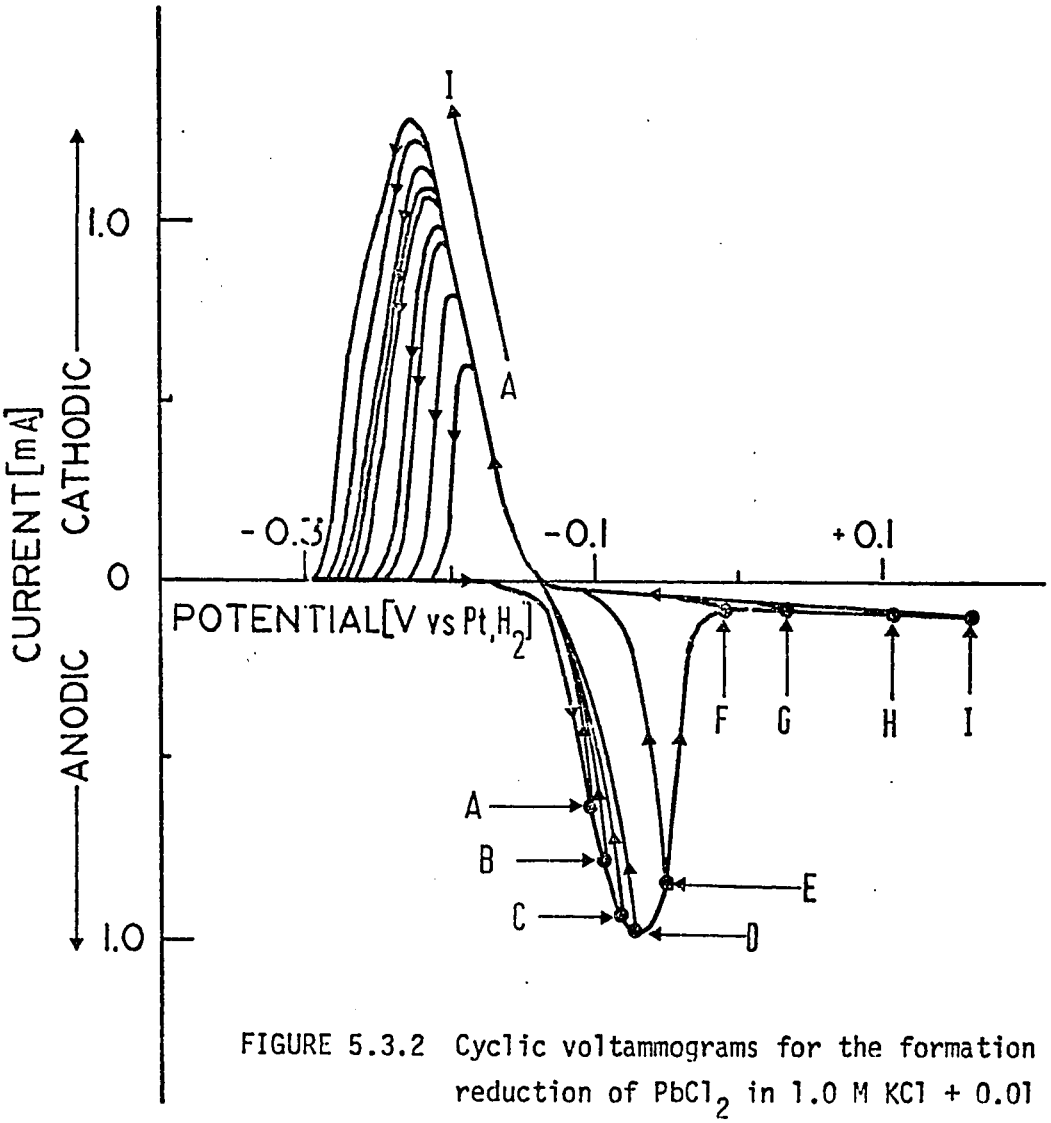

FIGURE 5.3.2 Cyclic voltammograms for the formation and reduction of $PbCl_2$ in 1.0 M KCl + 0.01 M HCl at fixed anodic and cathodic sweep rates of 13 mV s^{-1} but with different anodic potential limits for each successive cycle. The i-V profiles represented by A, B, C, D, E, F, G, H and I have E_A values of -0.105, -0.090, -0.085, -0.080, -0.050, 0.0, 0.031, 0.091 and 0.161 V versus Pt, H_2, respectively.

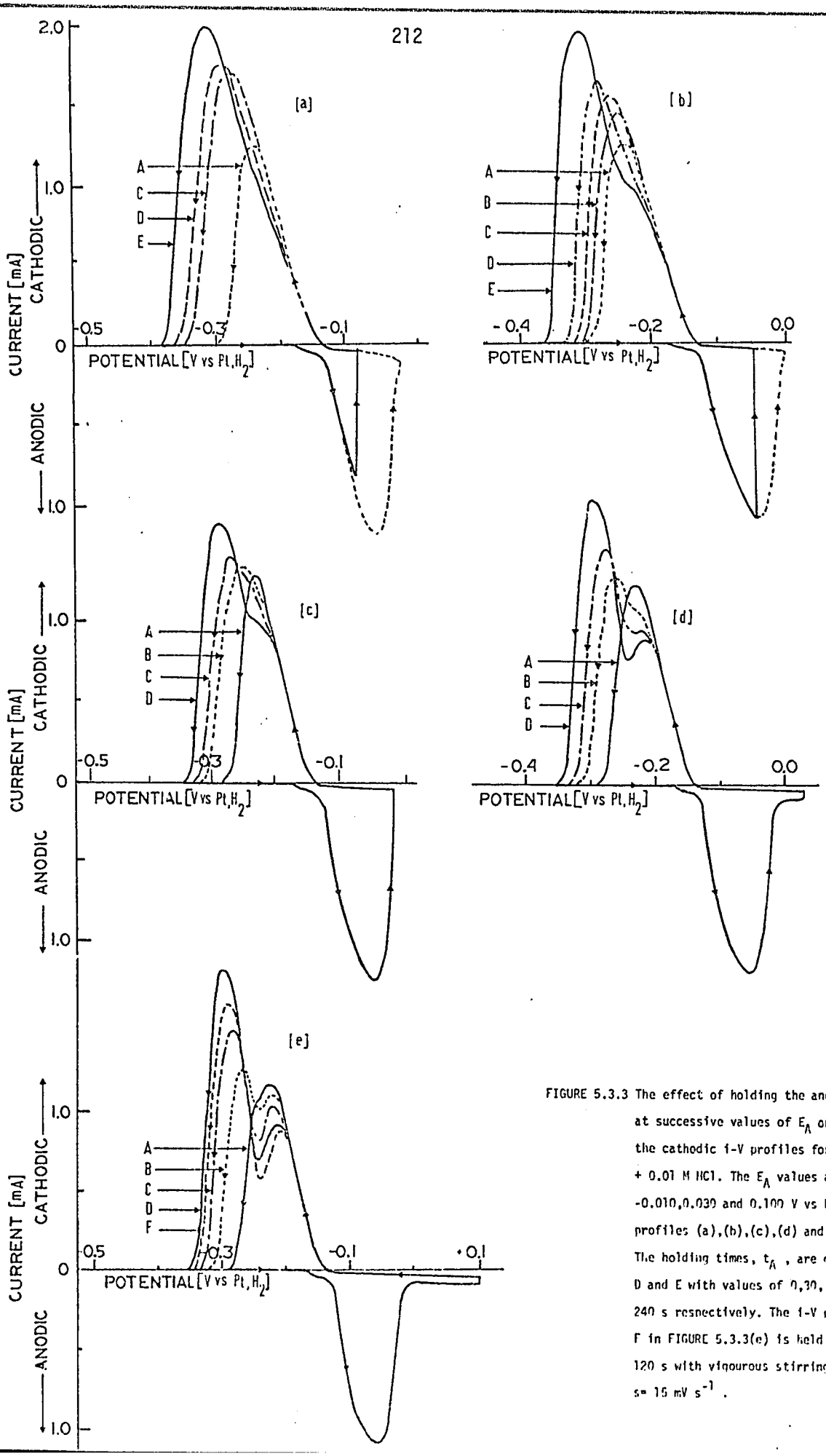

FIGURE 5.3.3 The effect of holding the anodic potential at successive values of E_A on the shape of the cathodic i-V profiles for Pb in 1.0 M KCl + 0.01 M HCl. The E_A values are -0.070,-0.040, -0.010,0.030 and 0.100 V vs Pt,H_2 for i-V profiles (a),(b),(c),(d) and (e) respectively. The holding times, t_A , are designated A,B,C, D and E with values of 0,30, 60,120 and 240 s respectively. The i-V profile labelled F in FIGURE 5.3.3(e) is held at 0.100 V for 120 s with vigourous stirring of the solution. $s = 15\ mV\ s^{-1}$.

markedly on the time spent at E_A. The general shape of the i-V profile for reduction does not appear to be affected by holding in the pre-passive region. However, the potential required for completion of the reductive removal of the $PbCl_2$ becomes more negative with increasing values of t_A (see Fig.5.3.2). This is mainly because more $PbCl_2$ is formed with increasing time t_A. The process(es) responsible for the growth of the reduction peak is (are) the continuing electrochemical dissolution of lead in the previous anodic cycle at the potential, E_A, followed by deposition of $PbCl_2$ and some accompanying redissolution of $PbCl_2$ into the bulk of solution from the exterior of the deposited phase.

As the value of E_A is extended from that of the passivation peak potential (Figure 5.3.3 (b)) to more positive values, the cathodic current-potential profiles exhibit a shoulder when t_A and E_A have low values. However, as E_A becomes more positive, two reduction peaks become clearly resolved (Figures 5.3.3 (c), (d) and (e)). The cathodic peak, P_1, decreases slightly with extended holding at E_A, while the peak, P_2, occurring at more negative potentials, continues to grow with increasing holding times. The resolution of the two reduction peaks is more apparent when film formation has been conducted at higher positive values of E_A, as is illustrated in Figure 5.3.4. The recovered charge, Q_C, for a given value of t_A (120 s) appears to be independent of E_A (Figure 5.3.4) but this result may be artificial due to variation of the electrode area during the course of the experiment.

The significance of the two peaks in the cathodic current-potential profile cannot be elucidated from the (i-V)profiles alone,e.g.Pb as chloride in two valence states is not possible at the potentials involved. However, it was initially thought that in 1MKCl + 0.01M HCl a basic lead chloride,Pb(OH)Cl, might be formed in addition to $PbCl_2$. In order to determine the validity of this idea, the behaviour of Pb was investigated in 1.0M HCl,where formation

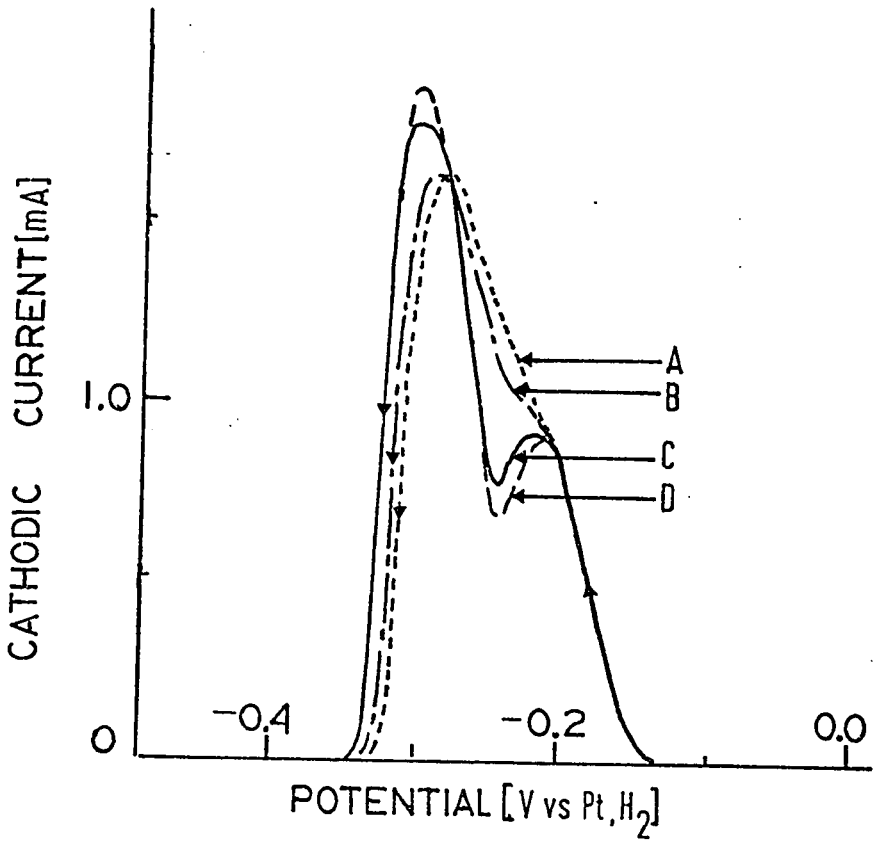

FIGURE 5.3.4 Cathodic i-V profiles for the reduction of $PbCl_2$ in 1.0 M KCl + 0.01 M HCl after the Pb electrode had been anodized at various anodic potentials, E_A, for a period of 120 s. The i-V profiles labelled A, B, C and D refer to values of E_A of +0.100, + 0.030,+ 0.010 and - 0.040 V versus Pt, H_2,respecitvely. s=15 mV s^{-1}.

of a basic chloride would be less significant.

The effect of holding the potential at a given E_A value after passivation has occurred was investigated to see if two peaks could be resolved, as in KCl. The results are illustrated typically in Figures 5.3.5 (a)-(e) for E_A = -0.135, + 0.046, + 0.107 + 0.154 and +0.186V (vs Pt, H_2), respectively. As E_A is made progressively more positive in the range -0.135V to + 0.046V, the cathodic i-V profiles exhibit only a single peak for all t_A values. However, at +0.107V and for $t_A \geq 120$ s, a shoulder appears in the cathodic sweep at potentials negative to the main i-V peak for reduction and becomes a separate peak when E_A = +0.150V and $t_A > 120$ s. For E_A = +0.186V and t_A = 240 s, the height of the second peak, P_2, resolved under these conditions exceeds that of the presiously designated "main" cathodic peak, P_1.

The behaviour of the $PbCl_2$ film in HCl at various holding potentials is thus significantly but not qualitatively different from that of the film formed in 1.0 M KCl. However, much more positive E_A values are required in HCl solution than in KCl for the second peak to be resolved. Also, in the latter solution, the second peak appears at potentials less positive relative to the passivation potential than in 1.0 M HCl. In fact, the process responsible for this behaviour on the cathodic sweep already commences in the potential region of the anodic passivation peak. In 1.0 M HCl, the second peak arises only when $E_A \geq$ +0.107V, i.e. approximately 0.3V more positive than the potential of the passivation peak ($\simeq$-0.210V). The main peak, P_1, continues to grow, as does the secondary peak, P_2, with increasing t_A. This is in contrast to the behaviour in 1.0 M KCl: in the latter case, the main peak (having the more positive peak potential) decreases slightly with increasing t_A while the secondary peak is enhanced after its respective holding period.

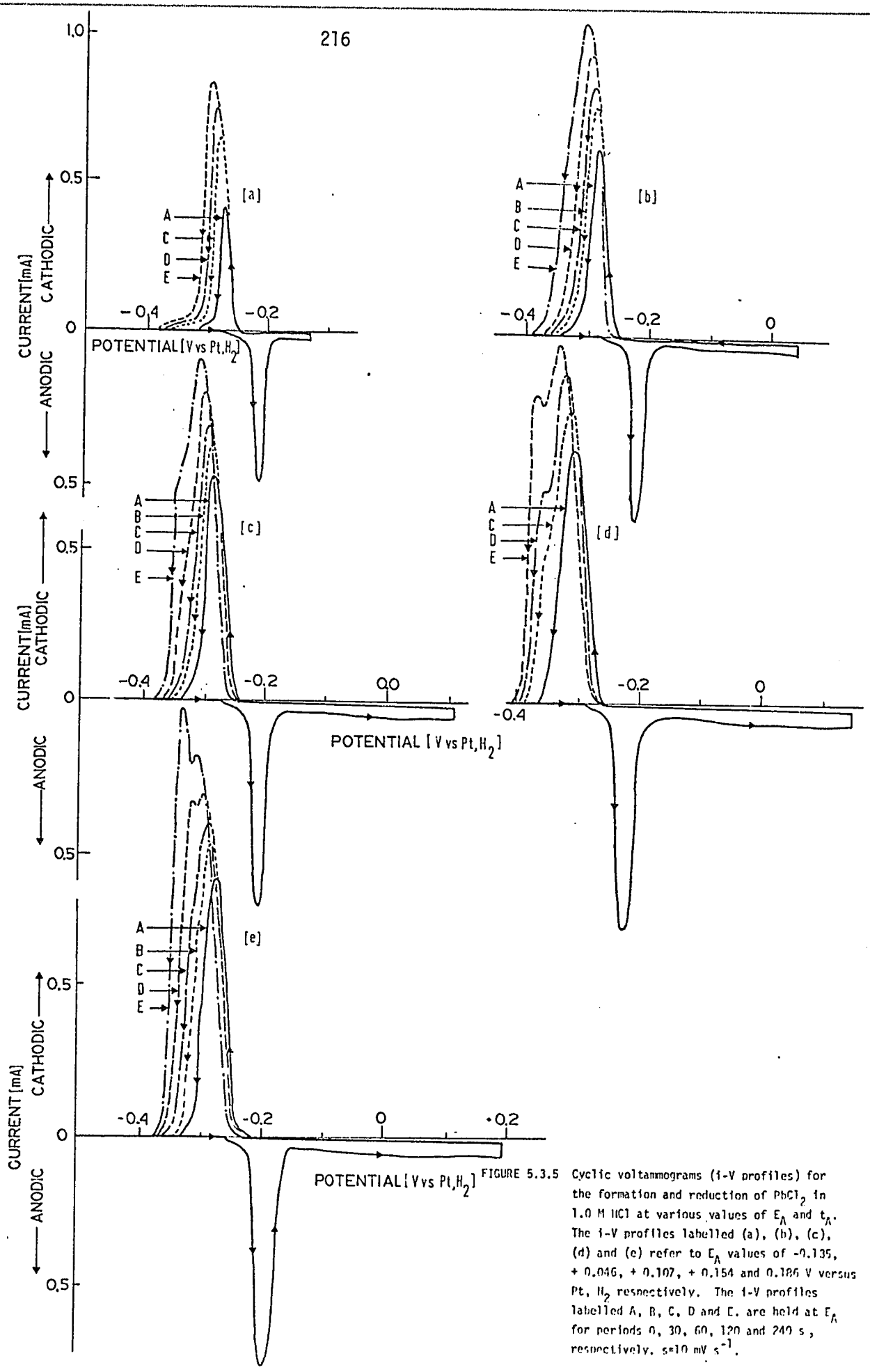

FIGURE 5.3.5 Cyclic voltammograms (i-V profiles) for the formation and reduction of $PbCl_2$ in 1.0 M HCl at various values of E_A and t_A. The i-V profiles labelled (a), (b), (c), (d) and (e) refer to E_A values of -0.135, + 0.046, + 0.107, + 0.154 and 0.186 V versus Pt, H_2 respectively. The i-V profiles labelled A, B, C, D and E, are held at E_A for periods 0, 30, 60, 120 and 240 s, respectively, set 0 mV s^{-1}.

5.3.2 Rotating-Disc Electrode (R D E) Studies

i) Significance of R D E Studies

It has been shown earlier that under certain conditions of holding at relatively positive values of potential in a sweep two reduction peaks can arise on the cathodic sweep. Such peaks could, for example, be described in terms of a solution-soluble lead species being reduced prior to the removal of the lead chloride film. The holding experiments previously described in Section 5.3.1 indicate that two species having apparently different reduction potentials are produced in the anodic potential region. Their relative amounts depend on the positive potential limit, E_A, as well as the time spent, t_A, at E_A.

In order to provide further information on the two peaks, it is necessary to compare the behaviour of the current-potential (i-V) profiles under conditions where the solution is quiescent or stirred (rotating-disc electrode). Use of a rotating electrode provides information on the contributions of solution-soluble species to the currents in, and hence the shape of, the i-V profiles for reduction. The rationale of experiments of this kind is that if a solution-soluble intermediate is produced, e.g. in the anodic sweep, it will be spun away into the bulk solution, so that it will no longer be available for reduction in the following cathodic sweep. Correspondingly, if passivation requires build-up of a critical concentration of Pb^{2+} ions prior to precipitation of a species such as $PbCl_2$ which blocks the surface, rotation should have a large effect on the charge required for onset of passivation.

ii) Effect of Electrode Rotation on the Anodic i-V Profile

A striking feature of the current-potential (i-V) profiles arising in the anodic sweep is that they are almost independent of rotation speed up to the maximum used, 10,000 rpm, as shown in Figure 5.3.6(a). Thus,

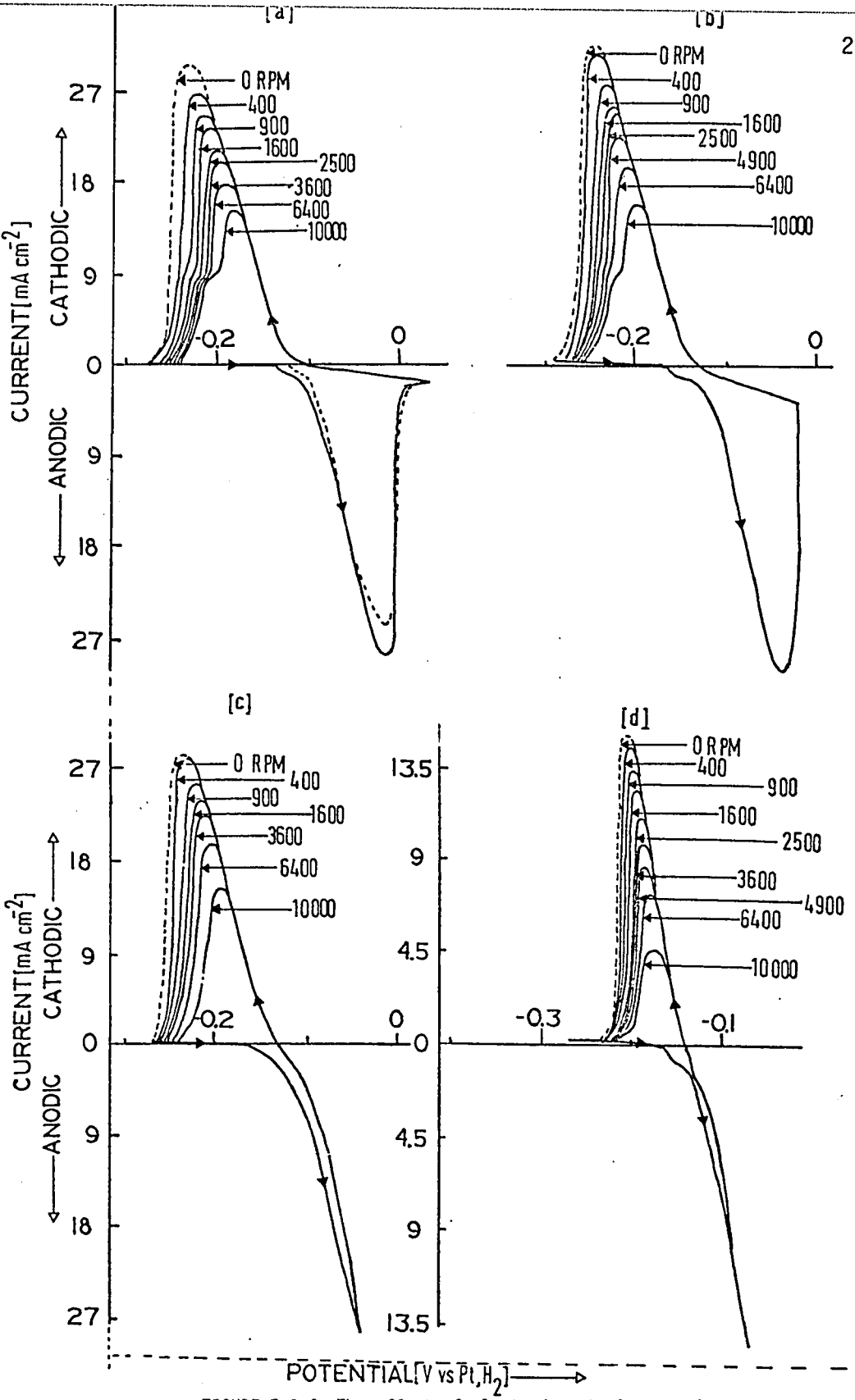

FIGURE 5.3.6 The effect of electrode rotation speed ω, on the form of the current - potential profile for the formation and reduction of $PbCl_2$ in 1.0 M KCl + 0.01 M HCl at different E_A values. The E_A values are + 0.037, -0.017 -0.038 and -0.070 V vs Pt, H_2 for the i-V profiles labelled (a), (b), (c) and (d), respectively. s=33 mV s^{-1}.

the charge $Q_{A,P}$ required for passivation to be attained is relatively independent ($\sim$ 10% variation) of rotation speed (Figure 5.3.7 and Table 5.3.1) in comparison with the corresponding cathodic i-V profiles for the reduction of the film. There is a decrease of Q_C by ca. 30% upon rotation at 2500 rpm.

This result is of considerable interest as it implies that the onset of passivation is not due primarily to build-up of a $PbCl_2$ film generated by precipitation from anodically dissolved Pb^{2+} ions but is caused by direct deposition of a film by discharge of the Cl^- anion. Relative reflectivity ($\Delta R/R$) measurements performed by Dr. F.C. Ho in our laboratory indicate that a surface film already appears well before the onset of passivation. Much of this film is evidently mechanically adherent (i.e., it is not completely spun away by electrode rotation) but does not appreciably inhibit passage of anodic current. Further information on the constitution of the film is gained from observation of the cathodic current-potential profiles for stationary and rotated electrode conditions.

5.3.2 (iii) Effect of Electrode Rotation on the Cathodic i-V Profile

In contrast to the effect of electrode rotation on the anodic current-potential profiles referred to above, the charge required to effect reduction of the film in the cathodic sweep is markedly diminished upon rotation. This behaviour is clearly evident when the i-V profiles recorded at various rotation speeds (ω = 0 to ω = 10,000 rpm) are compared, as shown in Figures (5.3.6 (a) - (d)). It is found that the shoulder which is usually observed on the cathodic i-V profile is dependent on both ω and E_A as is seen from Figures (5.3.6 (a)-(d)) where E_A is reduced from +0.037V (in the trans-passive potential region) to -0.070V (at the foot of the anodic i-V profile). For E_A values beyond the passivation potential and when $\omega \geq 2500$

TABLE 5.3.1

RESULTS OF ROTATING-DISC ELECTRODE STUDIES AT

Pb IN 1 M KCl (pH = 2)

ω(RPM)	s ($V\ s^{-1}$)	Q_A ($mC\ cm^{-2}$)	Q_C ($mC\ cm^{-2}$)	Q_A/Q_C
0	0.033	59.3	54.5	1.09
2500	0.033	62.7	36.3	1.73
		$\frac{Q_A^{2500}}{Q_A^o} = 1.06$	$\frac{Q_C^{2500}}{Q_C^o} = 0.67$	

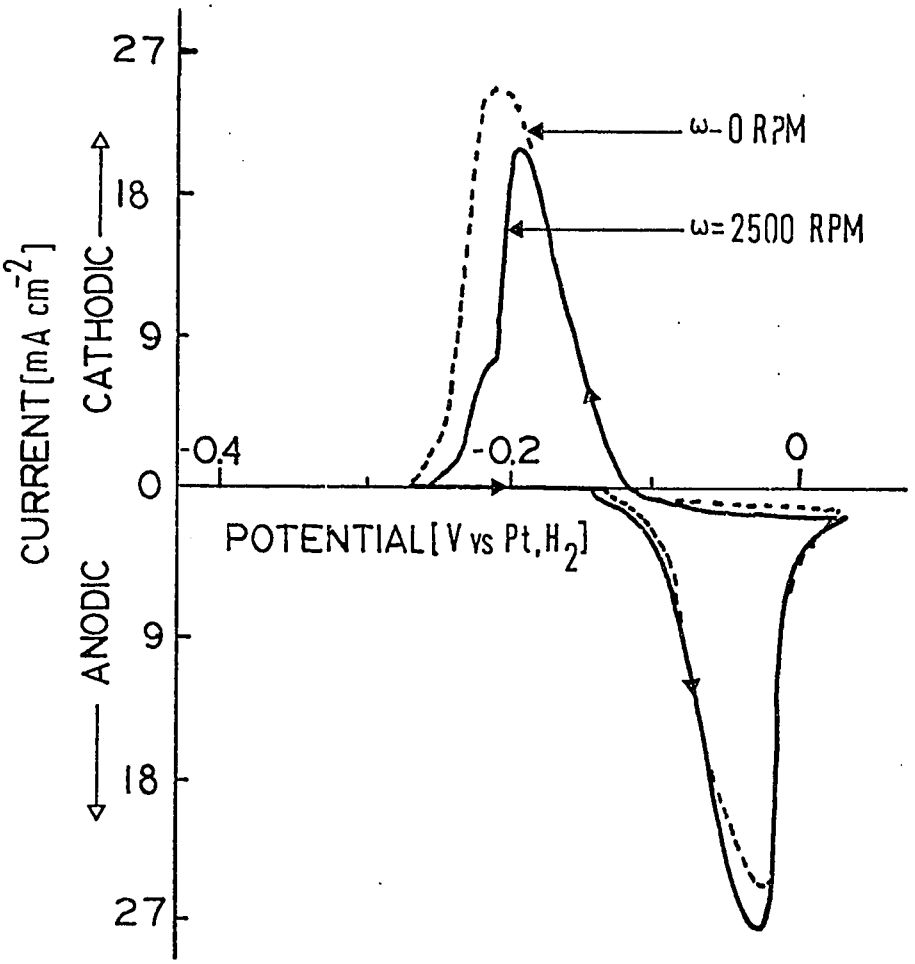

FIGURE 5.3.7 Current - potential profiles for the formation and reduction of $PbCl_2$ in 1.0 M KCl + 0.01 M HCl at rotation speeds of 0 and 2500 RPM. s=33 mV s^{-1}.

rpm, the shoulder is always present. However, when the potential limit E_A is restricted to the pre-passive region, only a single cathodic peak is observed at all rotation speeds and the peak current diminishes as ω is increased (Figure 5.3.6 (c), (d)). If the anodic i-V profile has been taken to sufficiently positive potentials for passivation to be observed, it is found that the magnitude of the shoulder in the cathodic i-V profile is almost independent of ω (Figure 5.3.6 (a), (b)) while the current in the first region of the cathodic i-V profile is steadily diminished with increasing ω. The latter behaviour is similar to that for cathodic curves taken from potentials in the pre-passive region.

These results serve to distinguish two types of surface species: (a) one that is formed in the pre-passive region (and probably also in the trans-passive region) but is extremely dependent on electrode rotation rate and (b) another species that is produced in the anodic region but whose extent of formation appears to be almost independent of the rate of rotation of the electrode. This latter species which is reduced in the ω - independent shoulder of Figure 5.3.6 (a), may be responsible for the passivation of the electrode ($Q_A \neq f(\omega)$).

5.3.2 (iv) Effect of Holding the Electrode Potential at Various E_A Values, with and without Rotation

Holding the potential at E_A at the termination of the anodic sweep allows continuing anodic oxidation to occur with a consequent time-dependent increase in the growth of the $PbCl_2$ film. If the potential is held at E_A = +0.07 V, i.e. just beyond the passivation peak, with the current on, the situation illustrated in Figs. 5.3.8 (a) and (b) results. In Figure 5.3.8 (b) the electrode potential is held for times of 0, 15,30,60 and 120 s with rotation at 2500 rpm. For holding times of 15 to 120 s, two

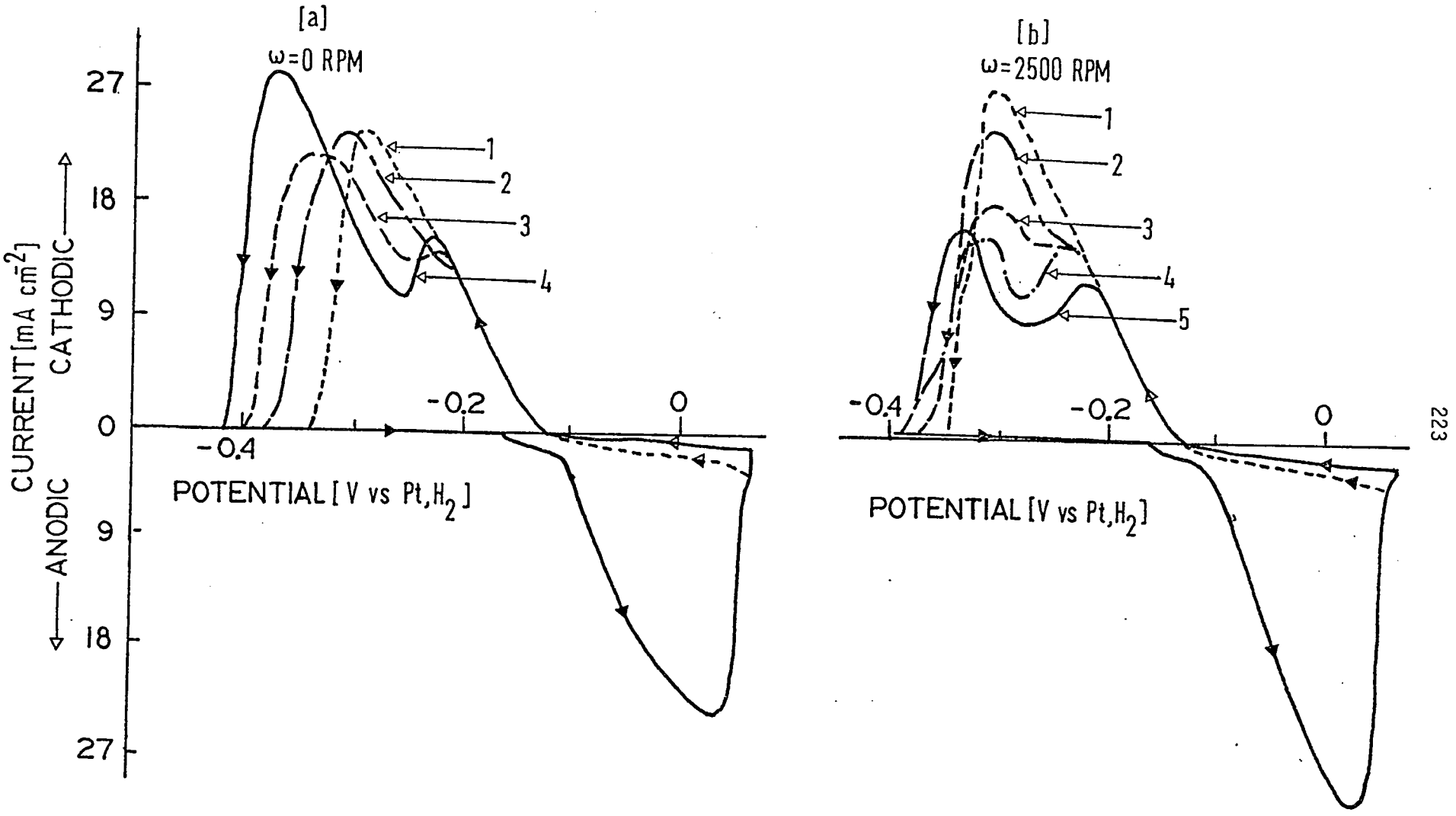

FIGURE 5.3.8 a) Current - potential profiles for Pb in 1.0 M KCl + 0.01 M HCl in a quiescent (ω=0) solution with E_A = 0.070 V vs Pt, H_2.

b) Same as in a) but ω = 2500 RPM. I-V profiles labelled 1, 2, 3, 4 and 5 refer to results obtained after holding at E_A for periods of 0, 15, 30, 60 and 120 s, respectively. s= 33 mV s^{-1}.

peaks are now clearly resolved: the first peak occurs on the rising part of the cathodic i-V profile and has an almost constant peak height for holding times of 15 to 60 s. The second, larger peak decreases with holding times of 15 to 60 s. For t_A = 120 s, the previously invariant first cathodic peak is now reduced in height while the larger peak is somewhat enhanced. A similar trend is observed if the solution is quiescent: (Figure 5.3.8 (a)) two cathodic reduction peaks are always resolved if the holding time $t_A \geq$ 30 s; the smaller peak at the lower cathodic potential has a height essentially independent of holding time while the main peak increases if $t_A >$ 30 s.

The situation when the electrode potential is held for various lengths of time near the base of the anodic i-V profile (E_A = -0.120V) is illustrated in Fig. 5.3.9 (ω = 2500). For t_A=0, the cathodic i-V profile exhibits a small spike which may be due to the reduction of an initial thin film of $PbCl_2$ or to reduction of solution-soluble lead species which are formed prior to and in parallel with formation of the $PbCl_2$ film. For t_A=15 and 30 s, the spike increases while a larger cathodic peak arises at more negative potentials. For t_A = 60 s the peak at less negative potentials becomes slightly larger than the second peak while for t_A = 120 s, a single large reduction peak is observed with a shoulder on the cathodic side of this main peak.

If the electrode is now treated as in the above case, but with the solution quiescent, the i-V profiles illustrated in Figure 5.3.10 are observed. As t_A is increased from 0 to 60 s, the cathodic i-V profile exhibits a single peak which increases with holding time.

The results described below (Figure 5.3.11) are obtained if the potential is held at the passivation peak (E_A = -0.030V) for 60 s under the following conditions:

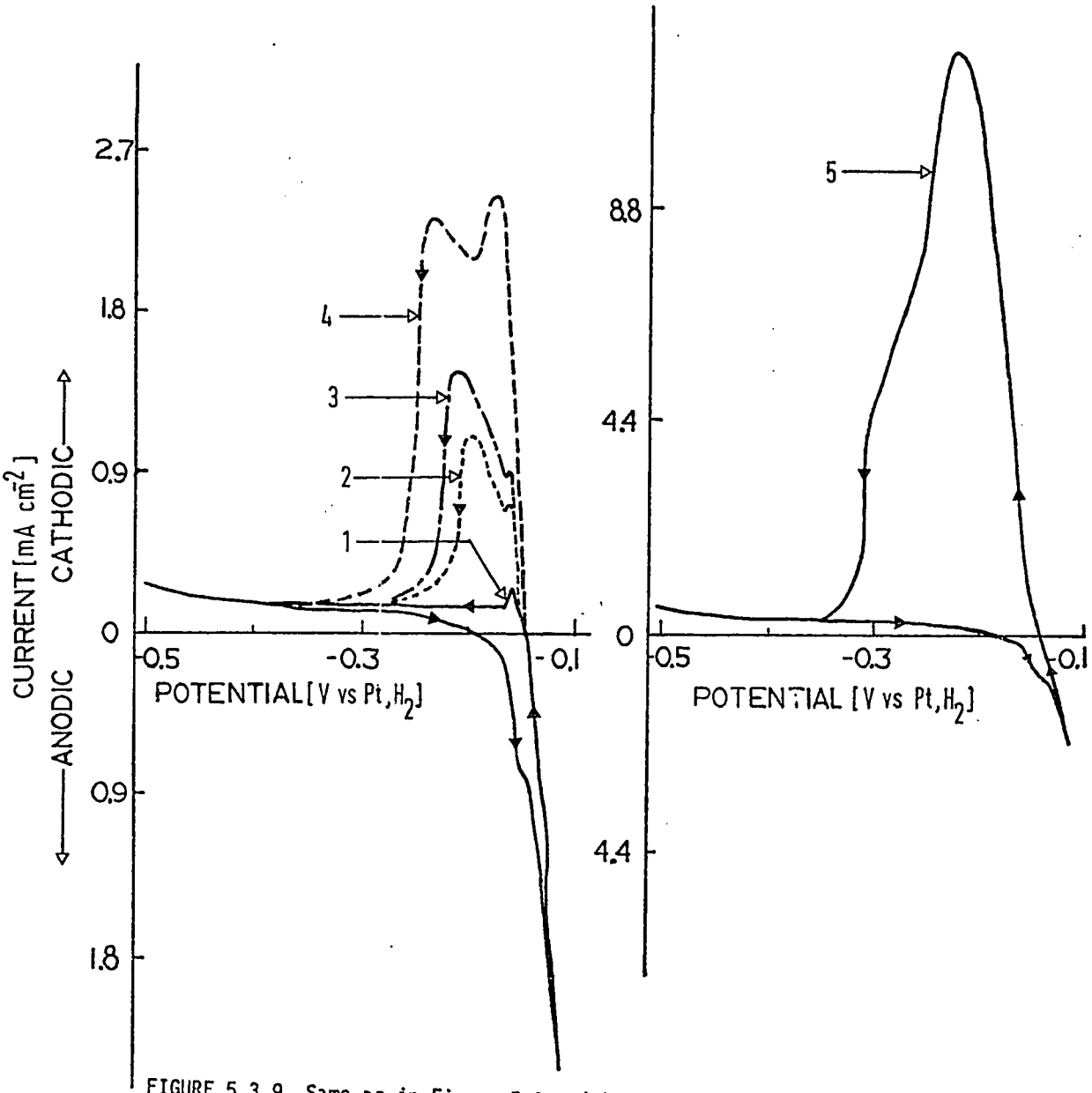

FIGURE 5.3.9 Same as in Figure 5.3.8 (b) but E_A = -0.120 V versus Pt, H_2.

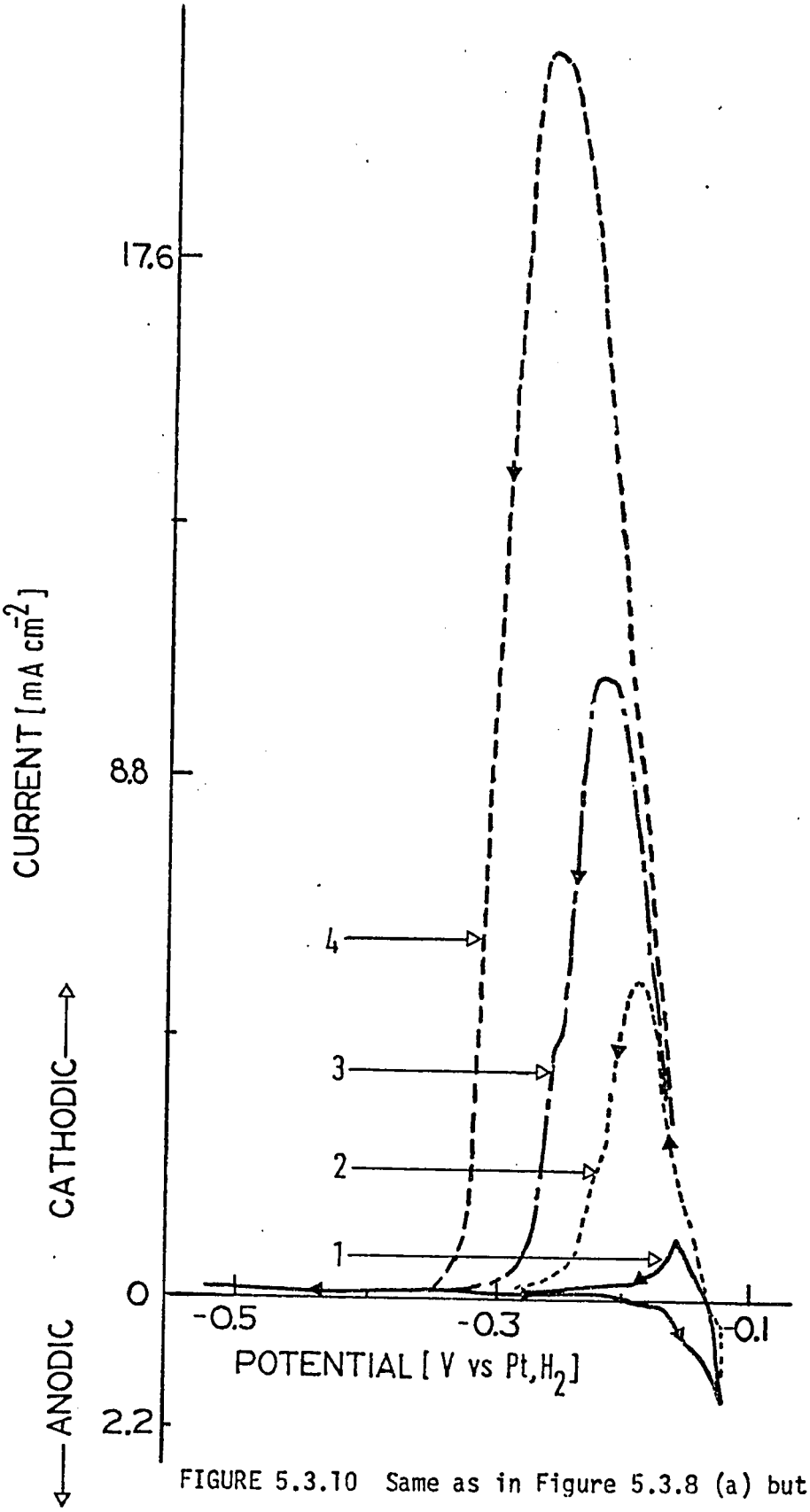

FIGURE 5.3.10 Same as in Figure 5.3.8 (a) but E_A= -0.120 V vs Pt, H_2.

1. the solution is quiescent (ω = 0) during a complete cycle with t_A = 0;

2. the solution is quiescent (ω = 0) during the holding time as well as during the subsequent cathodic sweep;

3. the electrode is rotated (ω = 2500 rpm) during the holding time only, but the cathodic sweep is taken without rotation;

4. the electrode is rotated during the holding time and during the cathodic sweep (ω = 2500 rpm).

The i-V profiles for reduction under the above conditions are illustrated in Figure 5.3.11 . The smaller cathodic peaks which appear at less negative potentials than those for the larger peaks are independent of hydrodynamic conditions as was mentioned with regard to Fig. 5.3.8 earlier. The second peak is largest for quiescent conditions but decreases when the electrode is rotated during holding; this decrease is larger if the electrode is rotated during the hold period as well as in the subsequent cathodic sweep.

5.3.2 (v) Effect of Holding the Electrode on Open-Circuit After Generation of the Anodic Film

The effect of holding the electrode potential on open-circuit (i=0) after the passivation has occurred (i.e. to allow time for any further crystallization of $PbCl_2$ to occur) is illustrated in Figures 5.3.12(a) and (b) . If the electrode is rotated (ω=2500 rpm), the charge recovered in the cathodic i-V profile is again considerably reduced. As the holding time, t_A, is increased from 0 to 75 s, the main peak is reduced relative to the shoulder but it is significant that the shoulder contribution in Figure 5.3.12(b) stays approximately constant at ω= 2500 rpm with increasing t_A. However, if ω=0, currents in the cathodic i-V profile are virtually independent of holding time on open circuit (i=0). This

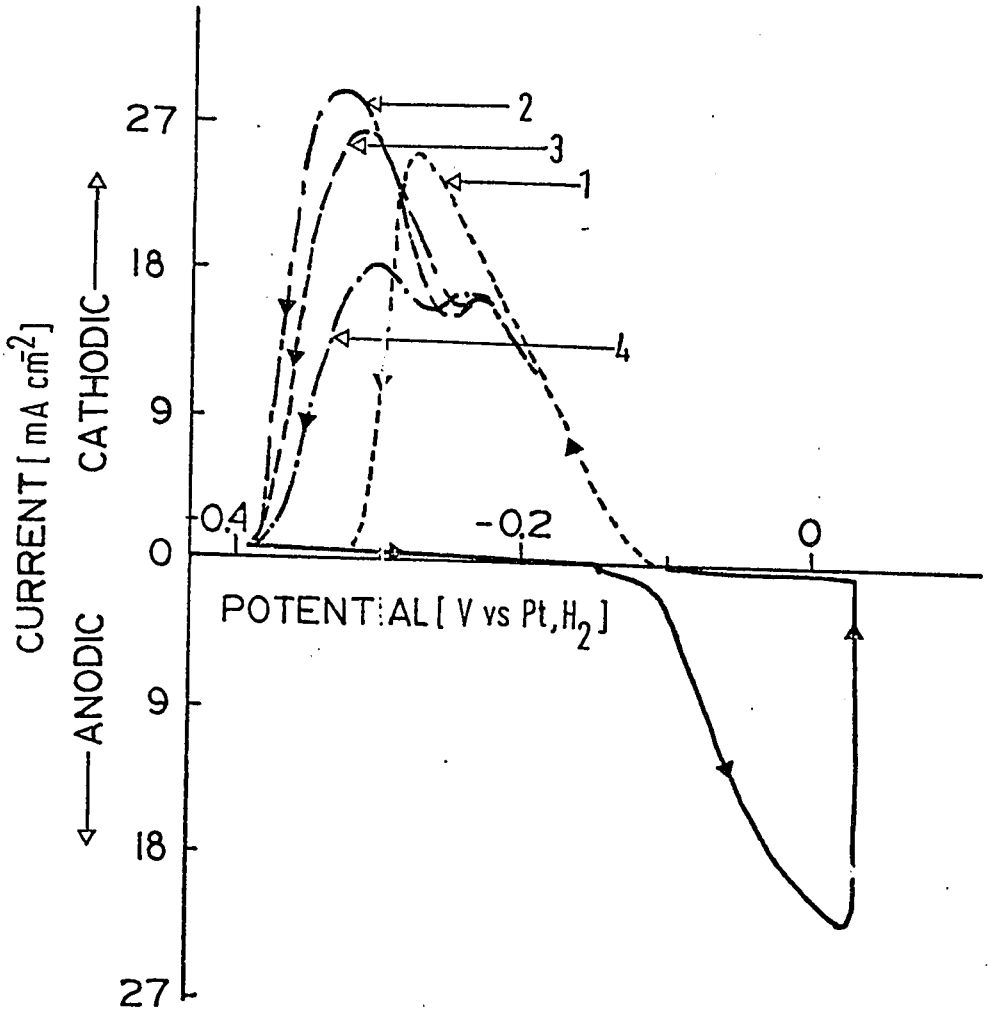

FIGURE 5.3.11 Current-potential profiles for Pb in 1.0 M KCl +0.01 M HCl. s=33 mV s^{-1}.

Conditions under which each i-V profile was measured:

1) ω=0, and t_A=0

2) ω=0 and t_A=60 s

3) ω=2500 RPM (during holding period, t_A, only.) and t_A =60 s.

4) ω=2500 RPM (during voltage sweep and holding period t_A.) and t_A=60 s.

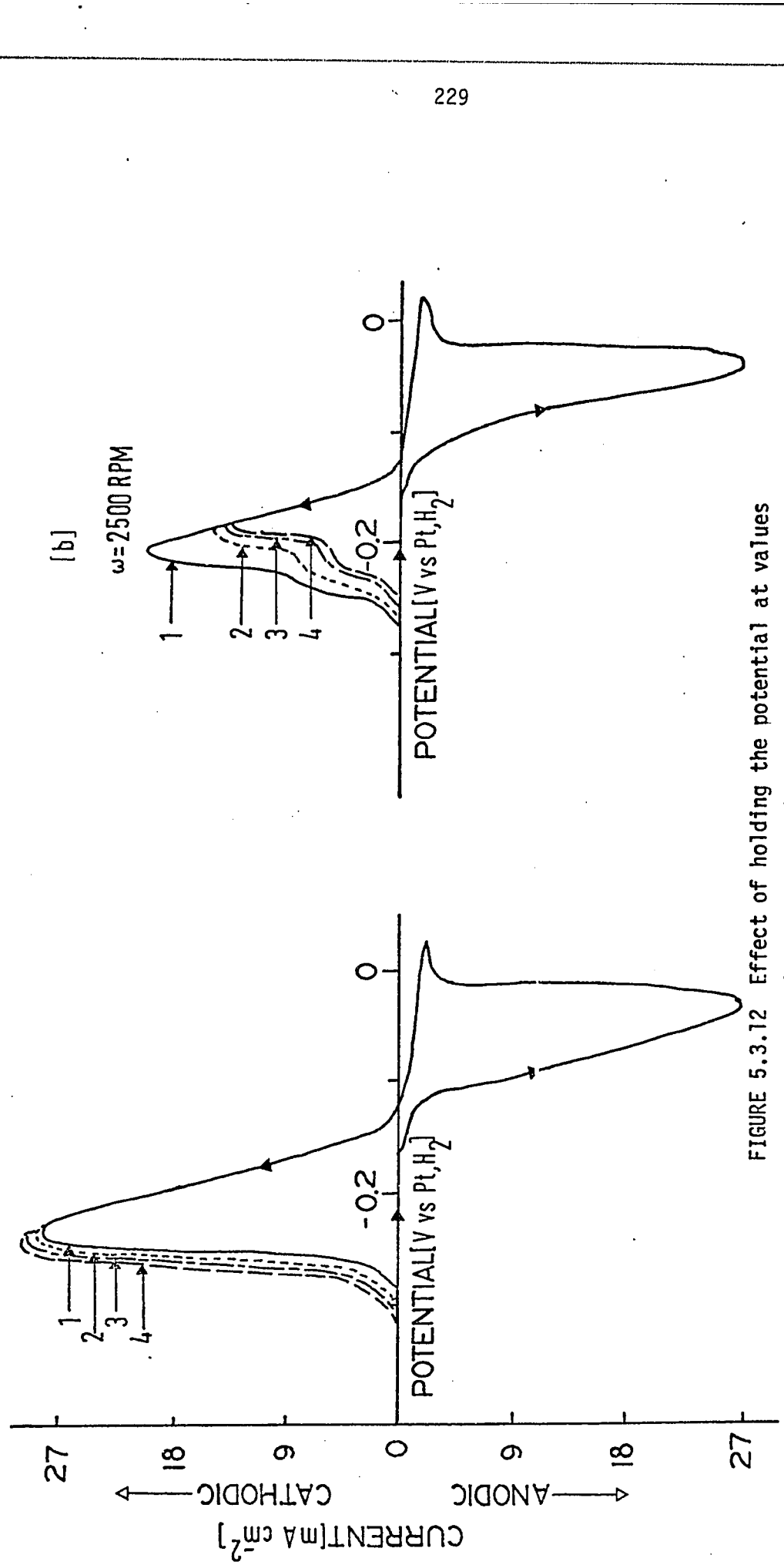

FIGURE 5.3.12 Effect of holding the potential at values (E_A = + 0.037 V) beyond the passivation peak under open circuit conditions (i=0).
The i-V profiles in (a) and (b) were obtained when ω=0 and ω=2500 RPM. respectively. The i-V profiles labelled 1, 2, 3 and 4 refer to holding periods, t_A, of 0, 25, 50 and 75 s, respectively. s=33 mV s^{-1}.

indicates that rotation of the electrode results in (a) an increase in the amount of chemical dissolution of the anodically generated $PbCl_2$ film and (b) a dispersal (spin-out effect) of any solution-soluble lead species generated in the anodic sweep.

5.4 Discussion

The electrochemical behaviour of Pb in Cl^- solutions involves a number of complex chemical and electrochemical processes. The RDE experiments, indicate that the formation of $PbCl_2$ occurs predominately by a nucleation and growth mechanism. However, the existence of two reduction peaks, under certain experimental conditions, implies a transformation of part of the passivating film into a second type of surface species, reducible at more negative potentials. The holding experiments indicate that film growth continues beyond the passivation potential. This behaviour appears to signify that some chemical dissolution of the passivating film occurs by a reaction such as $PbCl_2 + (n-2)\ Cl^- \rightleftharpoons PbCl_n^{2-n}$.

This process allows further anodic oxidation of the lead substrate and subsequent film formation to occur.

5.4.1 Effects of High Pressure

The volume change for dissolution of $PbCl_2$ in water which determines the pressure-dependence of its solubility has been evaluated from the conductivity measurements (Section 5.2.4) as $-17\ cm^3\ mol^{-1}$. If the amount of charge required to passivate the electrode surface is related to the Pb^{2+} ion concentration required to exceed the solubility product of lead chloride, then it is to be expected that Q_A (and Q_C) will increase with applied pressure. However, in 1 M KCl, it is observed that both Q_A and Q_C

are decreased with increasing hydrostatic pressure, indicating the apparent solubility of $PbCl_2$ to be inversely related to the applied pressure. Also the observed charge Q_A' measured to the current maximum of the anodic i-V profile decreases with applied pressure. This behaviour is illustrated clearly in Figure 5.4.1; (the i-V profiles at each pressure are superimposed in such a manner that the reversible potential for the Pb, $PbCl_2$ electrode occurs at the same value at each pressure) the charge Q_A', relative to its value at ambient pressure is 0.88 and 0.86 at 1102 and 2204 bars, respectively.

It is proposed that the following dissolution-precipitation reaction scheme applies during the initial stages of film formation at low over-potentials:

$$Pb \rightarrow Pb^{2+} + 2e \qquad (5.4.1)$$

$$Pb^{2+} + n\ Cl^- \overset{K_1}{\rightleftharpoons} PbCl_n^{2-n} \qquad (5.4.2)$$

$$Pb^{2+} + 2Cl^- \rightleftharpoons PbCl_2\downarrow \qquad (5.4.3)$$

The extent of the dissolution-precipitation mechanism occurring during the complete anodic cycle is quite small (probably only 6-15% of the passivating surface film is formed by this mechanism as was indicated by the RDE results (Figure 5.3.7)) but is significant in relation to pressure effects.

In order for precipitation of the $PbCl_2$ to occur, a critical concentration of Pb^{2+} ions must be generated in the vicinity of the electrode surface. This critical concentration of Pb^{2+} ion is related to the solubility product K_{sp}, of $PbCl_2$ in the usual way

$$[Pb^{2+}] = \frac{K_{sp}}{[Cl^-]^2} \qquad (5.4.4)$$

The concentration of Cl^- ions (1.01 M) is in excess so that the process of precipitation is not limited by solution-diffusion of Cl^- ions. Therefore

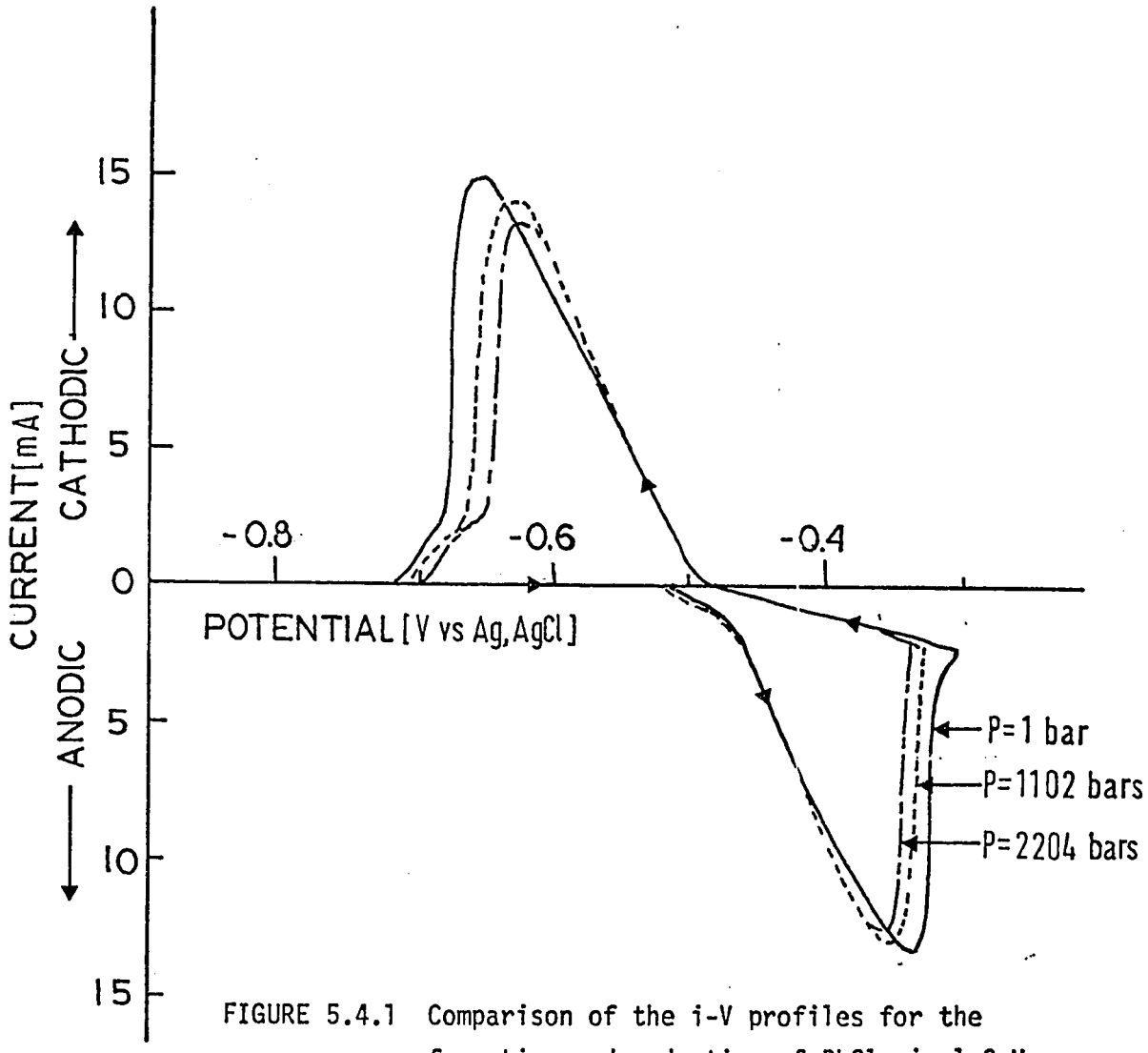

FIGURE 5.4.1 Comparison of the i-V profiles for the formation and reduction of $PbCl_2$ in 1.0 M KCl + 0.01 M HCl at 1, 1102 and 2204 bars. The respective anodic changes, Q'_A. as measured to the passivation peak are 94, 83 and 78 mC. s=10 mV s^{-1}.

the concentration of Pb^{2+} is a critical factor in generating the $PbCl_2$ film.

If it is assumed that the rate of the anodic dissolution of lead through reaction 5.4.1 is an activation controlled process, then the effect of pressure will be related to the volume of activation of reaction 5.4.1,viz.

$$\left(\frac{\partial \ln k}{\partial P}\right)_T = -\frac{\Delta V^{\ddagger}}{RT} \qquad (5.4.5)$$

The volume change, ΔV_o, for reaction 5.4.1 at equilibrium can be evaluated from the appropriate partial molar volumes and the relation

$$\Delta V_o = V_{Pb^{2+}} + 2\,V_e - V_{Pb}$$

so that

$$\Delta V_o = -26.3 + 6 - 18.3 \quad cm^3\ mol^{-1}$$
$$= -39\ cm^3\ mol^{-1}$$

Since ΔV_o is large and negative, it is expected that the volume of activation $\Delta V^{\ddagger}$, of reaction 5.4.1 will also be negative.

The rate of formation of Pb^{2+} ions at a given electrode potential is therefore expected to be larger at elevated pressures than at P = 1 bar. The concentration of Pb^{2+} necessary for precipitation of $PbCl_2$ will be generated earlier in the anodic sweep at high pressures.

However, the solubility product of $PbCl_2$ is expected to be pressure-dependent (cf. section 5.2.4). The volume change for reaction 5.4.3 has been previously evaluated as + 17.0 $cm^3\ mol^{-1}$ which includes the pressure dependence of the equilibrium process 5.4.2. It is assumed, for convenience, that the chemical equilibrium reaction 5.4.2 can be represented by

$$Pb^{2+} + Cl^- \rightleftharpoons PbCl^+.$$

The overall effect of an increase of pressure will be to increase the rate at which the solution is saturated but the actual charge to effect this condition is increased. Therefore the mechanism 5.4.1-5.4.3 does not appear to be realistic in relation to the experimental evidence.

In 1 M KCl solutions, the solubility of $PbCl_2$ is decreased due to the common-ion effect but there is a tendency for Pb^{2+} ions to form a variety of complex ions. In 1 M Cl^- ion solutions, the predominant species[143-145] are $PbCl_2$ and $PbCl_3^-$. Therefore, the following equilibria must be considered in elucidating the effect of pressure on the quantity of charge required for passivation of the electrode. The overall mechanism for $PbCl_2$ formation should be represented in terms of the complexation equilibria:

$$Pb \rightleftharpoons Pb^{2+} + 2e^- \qquad (5.4.1)$$

$$Pb^{2+} + Cl^- \rightleftharpoons PbCl^+ \qquad (5.4.2)$$

$$PbCl^+ + Cl^- \rightleftharpoons PbCl_{2aq.} \qquad (5.4.6)$$

$$PbCl_2 + Cl^- \rightleftharpoons PbCl_3^- \qquad (5.4.7)$$

and the solubility equilibrium

$$Pb^{2+} + 2Cl^- \rightleftharpoons PbCl_2\downarrow \qquad (5.4.4)$$

The effect of pressure on the equilibria represented by equations 5.4.2, 5.4.6 and 5.4.7 can be examined by determining the volume change for the overall equilibrium process

$$Pb^{2+} + 3Cl^- \rightleftharpoons PbCl_3^- \qquad (5.4.8)$$

This volume change can be estimated if the individual molar volumes of Pb^{2+}, Cl^- and $PbCl_3^-$ are known. The partial molar volume of Cl^- and Pb^{2+} are reliably known[110] to be 23.23 and -26.3 $cm^3\ mol^{-1}$. The partial molar volume of $PbCl_3^-$ is, however, unknown but an estimate can be made using the approach of Laidler and Couture[146,147], based on the following empirical equation for evaluating the partial molar volumes of oxy-anions:

$$V_- = 58.8 + 0.89\ (0.25\ nr)^3 - 26|z_-| \qquad (5.4.9)$$

The first two terms represent the intrinsic volume of the anion and the last term in 5.4.9 is the electrostriction contribution. The value of the radius of the $PbCl_3^-$ ion is taken as the sum of the ionic radii of Pb^{+2} and Cl^-, and the Van der Waals radius of the Cl^- ion. Therefore the effective radius $0.25n\ (r_{Pb^{2+}} + r_{Cl^-} + 1.8)$ is equal to 3.62 $\mathring{A}$ where n = 3. The partial molar volume $V_{PbCl_3^-}$ is then 75.1 $cm^3\ mol^{-1}$. Although this value is only an estimate, the partial molar volume of $PbCl_3^-$ is expected to be a large positive quantity.

The overall volume change of reaction 5.4.8 is represented by

$$\Delta V_o = V_{PbCl_3^-} - V_{Pb^{2+}} - 3\ V_{Cl^-}$$

$$= 75.1 + 26.3 - 69.7$$

$$= 32\ cm^3\ mol^{-1}$$

An increase in pressure will shift the equilibrium to the left in equation 5.4.8 since the volume change of reaction 5.4.8 is large and positive. Although the solubility product of $PbCl_2$, as defined by equation 5.4.5, is expected to increase with pressure, the effect of pressure on the dissociation of $PbCl_3^-$ is large enough to cause a decrease of the solubility of $PbCl_2$. This can be illustrated by evaluating the sum of

the volume changes for reactions 5.4.3 and 5.4.8:

$$PbCl_3^- \rightleftharpoons Pb^{+2} + 3\,Cl^- \qquad \Delta V_o = -32.0$$

$$Pb^{+2} + 2Cl^- \rightleftharpoons PbCl_2(s) \qquad \Delta V_o = 27.4$$

$$PbCl_3^- \rightleftharpoons PbCl_2(s) + Cl^- \qquad \Delta V_o \simeq -5 \text{ cm}^3 \text{ mol}^{-1} \qquad (5.3.10)$$

Thus, the overall volume change is negative, so that $PbCl_2$ is less soluble at elevated pressures. The charge required to saturate the solutions with respect to Pb^{2+} species is also expected to diminish with increasing pressure.

The experimentally observed decrease in the charge required to passivate the electrode surface as the pressure is increased is consistent with the interpretation of a pressure-induced decrease in the solubility of $PbCl_2$. Also, since a smaller quantity of complex ions is expected to be present in solution at elevated pressures, then the charge balance Q_A/Q_C at given sweep rate is expected to be closer to unity at elevated pressures. The values of Q_A/Q_C at elevated pressures are also expected to be less dependent on cathodic sweep rate. It is seen that this behaviour is confirmed experimentally in Figure 5.1.4 where Q_A/Q_C is plotted as a function of $s_C^{1/2}$ at 1, 1102 and 2204 bars.

Once the solution adjacent to the electrode surface reaches a super-saturated condition, $PbCl_2$ crystals can be formed in solution. As these crystals grow, their ability to escape from the vicinity of the electrode diminishes with time. The $PbCl_2$ crystals are then precipitated on the surface of the electrode, but the deposit is not of sufficient quantity or thickness to cause passivation. The anodic dissolution of the lead substrate continues but now Pb^{2+} is discharged directly as $PbCl_2$ on the electrode surface together with the existing $PbCl_2$ crystals. The film continues to

grow by a nucleation and growth mechanism until the deposit is sufficiently extensive to cause passivation.

The overall thickness of the $PbCl_2$ deposit can be calculated from the measured charge required to passivate the electrode and the known molar volume of $PbCl_2$. The charge required to passivate the electrode, $\simeq$ 60 mC cm^{-2} (see Table 5.3.1) at 1 bar, corresponds to 3×10^{-7} mol cm^{-2} of $PbCl_2$. Since the molar volume of $PbCl_2$ is 47.4 cm^3 mol^{-1}, the thickness of the passivating layer of $PbCl_2$ is 150 nm.

The mechanism of passivation can be visualized in terms of a model[148] in which islands of $PbCl_2$ crystals grow on the surface in the form of right circular cones or cylinders. The measured charge required to passivate the electrode and the corresponding thickness of the film show that oxidation to monolayer coverage (Q_{mono} = 440 μC cm^{-2}) is insufficient to account for the observed film growth and passivation. In fact the passivating film is produced predominantly by a three-dimensional nucleation and growth process[54,148]. The cones (or cylinders) (Figure 5.4.2) grow three-dimensionally with an increase in basal area and height. At a certain point in time, after initiation of film growth, the bases of some of the circular cones overlap resulting in passivation as overlapping becomes appreciable. However, Pb^{2+} ions will still be generated at unpassivated areas of the electrode surface until completion of overlap of the circular cones leads to the electrode surface becoming fully blocked. This results in a sudden decrease in the current passing during the anodic voltage sweep; hence the electrode is said to be passivated. Upon reductive removal, instead of islands of $PbCl_2$ crystals being formed, the removal of $PbCl_2$ results in the formation of so-called "lakes" in the film. The reduction of $PbCl_2$ occurs by the converse of the deposition mechanism.

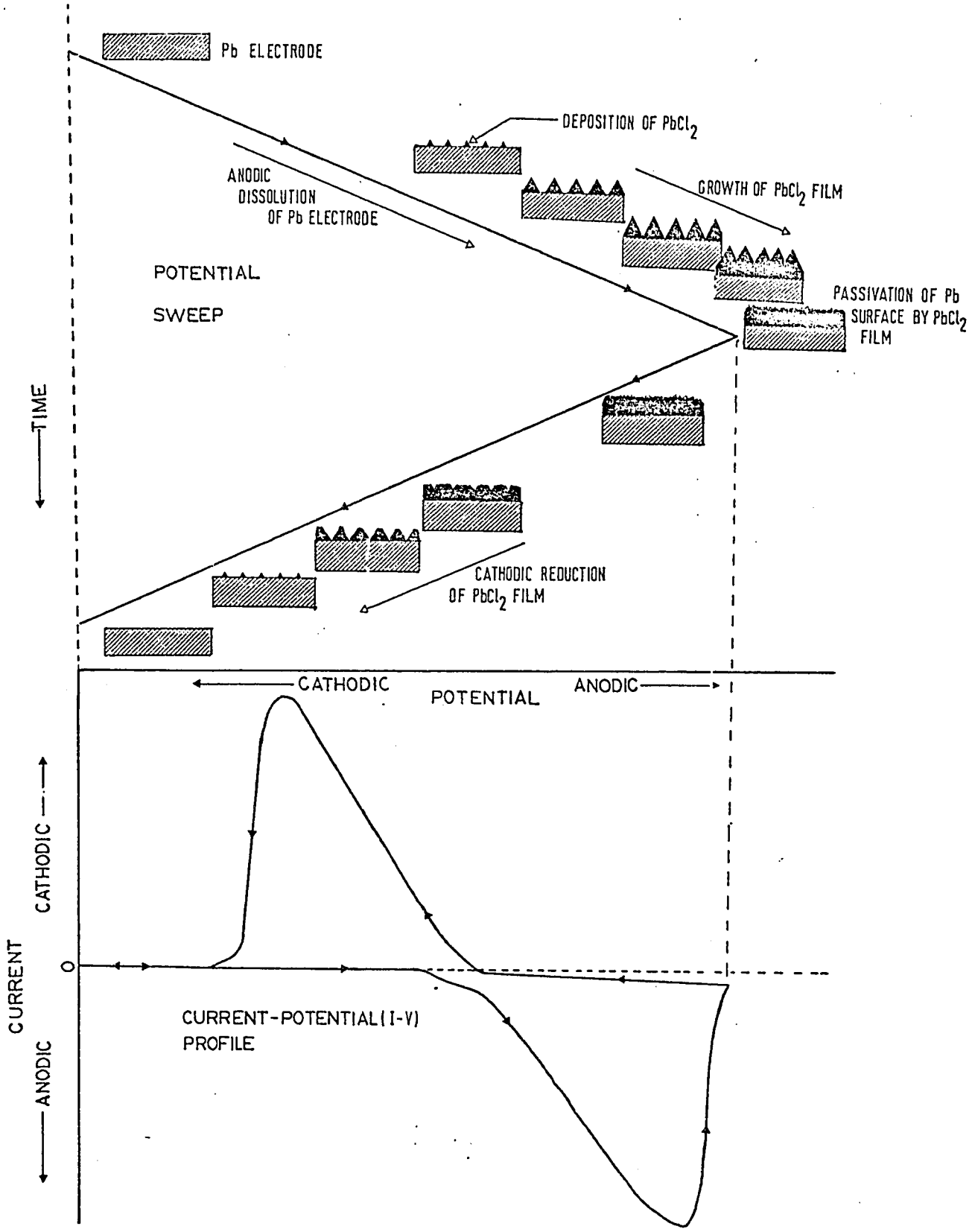

FIGURE 5.4.2 A schematic diagram illustrating the formation and reduction of a passivating film of $PbCl_2$ on Pb in relation to the observed current-potential profile.

This type of model for film formation and reduction is an idealized representation since electron micrographs of passivating films[148], e.g. of $PbCl_2$ or $PbSO_4$, show complex surface structures with micro-crystal formation. However, it is instructive in visualizing why such thick films are necessary to passivate an electrode surface.

5.4.2 Formation of Two Reducible Species

The formation of two reducible species is observed under certain experimental conditions such as when holding experiments are conducted at relatively high anodic potentials and when RDE experiments are performed. The mechanism responsible for the transformation of a single surface species to multiple species can only be inferred from existing data since the exact chemical composition of the anodic film was unknown in the present work. Two possible mechanisms will be discussed and supported by experimental data where possible.

i) Two Types of $PbCl_2$ Surface Species

The formation of two types of reducible $PbCl_2$ surface species has been advocated by Barradas[28-31]. The initially formed $PbCl_2$ deposit (basal layer) undergoes chemical dissolution via reaction 5.4.10 resulting in reactivation of the Pb electrode so that the process

$$Pb \rightleftharpoons Pb^{2+} + 2e^- \qquad (5.4.1)$$

can proceed. The occurrence of this process is supported by the current-potential profiles in Figure 5.3.12 which show that for additional film growth to occur, charge must be passed during the holding period at E_A. Thus the continuing anodic dissolution of the lead substrate maintains the solution near the electrode in a super-saturated condition. This is regarded as resulting in the formation of a second type of $PbCl_2$ deposit.

The height of the first reduction peak P_1 is independent of hydrodynamic conditions and the time spent ($t_A \leq 60$ s) at E_A (Figure 5.3.8). This is due to the growth of the second $PbCl_2$ layer on the so-called basal layer, resulting in an apparent decrease of the solubility of the initially formed $PbCl_2$ film. However, the extent of formation of the secondary layer (cathodic peak P_2) is dependent on hydrodynamic conditions as well as the time spent at E_A (Figure 5.3.8). The extent of formation of the secondary layer at an RDE decreases with increasing holding times up to $t_A = 60$ s. This is due to enhanced dissolution of the outer-layer of $PbCl_2$ when the electrode is rotated. When $t_A > 60$ s, the dissolution of the secondary layer is sufficiently extensive that chemical dissolution of the freshly exposed basal layer can occur. This is evident as a decrease in the first cathodic peak, P_1, and slight increase in the second current peak, P_2. At a stationary electrode, the secondary layer (the reduction current for which is associated with peak P_2) continues to grow with increasing t_A while the quantity of the basal layer remains essentially constant (Figures 5.3.3 (d), (e), and 5.3.8).

The generation of two peaks in the cathodic i-V profiles corresponding to different reduction potentials of the film is difficult to rationalize thermodynamically since both species are presumably $PbCl_2$. The particle size of the basal layer is, however, expected to be small because the rate of film growth occurs quite rapidly during the voltage sweep. This situation of increased surface-to-volume ratio makes the basal film more susceptible to chemical attack by Cl^- ions (reaction 5.4.10). The second layer is grown on the basal layer, most probably at a slower rate than in the primary layer itself; therefore the particle size of the deposit is expected to be large. The basal layer, due to its

proximity to the electrode surface, is reduced prior to the outer-layer. Also, the larger particle size of the secondary $PbCl_2$ film makes it inherently more stable than the primary layer; therefore the two layers are reduced at different potentials.

Although the formation of two types of $PbCl_2$ has been tentatively proposed, as above, the conditions under which they are generated are often extreme (RDE, high anodic potentials and long holding times). However, the study of the $Pb,PbCl_2$ electrode at ambient pressure under such conditions illustrates the importance of the chemical dissolution of $PbCl_2$. In the high pressure experiments, the electrochemical conditions were less severe so that no formation of a secondary layer could be detected. Nevertheless, the chemical dissolution of the primary layer is indicated by the determination of the values of Q_A, Q'_A and Q_C with increasing hydrostatic pressure.

5.4.2 (ii) Formation of Basic Lead Salts

Another mechanism for the appearance of two reduction peaks in the cathodic i-V profile could involve the formation of basic lead chlorides such as PbOHCl or $PbCl_2.Pb(OH)_2$. It is known[28-31] from x-ray diffraction studies on the structure of precipitated $PbCl_2$ from H_2O solutions (pH=7), that PbOHCl is present in the precipitate. This is due to an hydrolysis reaction such as

$$Pb^{2+} + H_2O + Cl^- \rightleftharpoons Pb(OH)Cl + H^+$$

The electrolyte used in the study of the $Pb,PbCl_2$ electrode was 1.0 M KCl + 0.01 M HCl; inclusion of a small concentration of acid was for the purpose of preventing hydrolysis of Pb^{2+} ions by the above process. However, at sufficiently positive potentials, an alkaline condition may still be produced in the pores of the anodically formed film. This process

can be understood by analogy with the situation where $PbSO_4$ is known[59] to be converted to PbO_2. The film will grow at sufficiently positive potentials where chemical dissolution permits continuing anodic production of Pb^{2+} ions. However, if transport of Cl^- ions from the bulk of the solution into the pores of the film towards the Pb surface (where Pb^{2+} ions are produced) is sluggish, charge-balance with respect to Pb^{2+} ions can only be maintained by dissociation of water in the pores of the film. The diffusion of the proton out of the pore maintains the charge balance but the electrolyte in in the pore becomes alkaline. If deposition continues in or around the pore, the film will be a basic lead chloride such as PbOHCl or in the extreme case, $Pb(OH)_2$, rather than $PbCl_2$. The solubility of $PbCl_2.Pb(OH)_2$ is 1.8×10^{-4} mol dm^{-3} in H_2O at 18°C. This is approximately 200 times smaller than that of $PbCl_2$.

The extent of formation of basic lead salts is expected to depend on both the solution pH and the anodic potential limit E_A. The influence of the value of E_A and t_A on the generation of the second type of reducible species is clearly illustrated in Figures 5.3.3 (a)-(e). The second cathodic peak, P_2, becomes more prominent when the film has been formed at higher positive potentials. The internal supply of Pb^{2+} is expected to be enhanced with increasing positive potential, thus tending to make the relative contribution of the supposed basic lead species more significant. Similar behaviour is observed in the RDE experiments (Figures 5.3.6 (a)-(d)); a second reduction process is evident when the anodic potential limit is equal to, or more positive than, the passivation potential. The magnitude of the shoulder (Figure 5.3.6(a)), P_2, is independent of electrode rotation speed which indicates that the species generated has a very low solubility. As mentioned above, a salt such as PbOHCl or $Pb(OH)_2$ is known to be much more insoluble than $PbCl_2$ itself.

In 1 M HCl, the positive potential limit, E_A (relative to the passivation potential) required to produce two surface species resolvable in the subsequent cathodic sweep, is considerably larger ($\sim$ 250 mV, Figure 5.3.5(d) vs 10-20 mV, Figure 5.3.3 (d)) than in 1 M KCl + 0.01 M HCl. This difference of behaviour is presumably the result of the difficulty of producing an alkaline condition in the pores of the anodic film when the supporting electrolyte is more acidic. At high positive potentials and with long holding periods, the $PbCl_2$ itself is the main component of the anodic film (Figures 5.3.5 (d) and(e)) but some formation of the supposed basic salt is still evident.

5.4.3 Concluding Remarks on the Behaviour of Pb in Cl^- Solutions

The formation of two types of lead salt surface species in both 1 M HCl and 1 M KCl + 0.01 M HCl solutions is clearly evident in the shape of the cathodic current-potential profiles. Two possible mechanisms of formation of an additional surface species have been proposed but in the absence of further knowledge of the exact chemical composition of the anodic film, such mechanisms are rather speculative. Although some of the results (cf. Figure 5.3.9) described in the preceding sections cannot be explained in terms of either mechanism, the mode of generation of the two species most likely involves the formation of a basic lead salt and/or the transformation of $PbCl_2$ to a basic lead salt.

The electrochemical behaviour of Pb in Cl^- ion solutions requires further investigation in order to resolve the origin of the multiple reduction peaks. These investigations should be applied to a) the elucidation of the morphology of the passivated surface (using Scanning Electron Microscopy); b) the determination of the chemical composition of the anodic film under varying conditions of pH and electrode potential (E_A)

and c) evaluation of the mode of chemical dissolution of the passivating film by identification of the complex ions present in solution near the electrode surface. This course has not been pursued in the present work since its main purpose was to provide a basic understanding of the effect of elevated pressure on certain electrochemical processes of practical ($PbCl_2$) and theoretical ($Fe(CN)_6^{3-}/Fe(CN)_6^{4-}$ redox couple) interest.

5.5 The Behaviour of the Pb, $PbSO_4$ Electrode at Elevated Pressures

The behaviour of the Pb, $PbSO_4$ electrode is of considerable practical importance in relation to its use in the lead-acid battery. The formation and reduction of $PbSO_4$ was briefly studied by cyclic voltammetry at elevated pressures in order to compare the anodic formation behaviour at elevated pressures of a highly insoluble lead salt, $PbSO_4$, with that of the more soluble $PbCl_2$.

5.5.1 Current-Potential Profiles

The current-potential profiles for the formation of $PbSO_4$ in 0.5 M H_2SO_4 (discharge reaction of the lead-acid battery) and its subsequent reduction in the cathodic sweep are illustrated in Figure 5.5.1 for pressures of 1, 1102 and 2204 bars. The form of the anodic i-V profile is again typical of a passivation process, as in the Pb,$PbCl_2$ system. However, the cathodic current-potential profile exhibits a characteristic tail beyond the current maximum. The reduction of $PbSO_4$ appears to be a slow process in contrast to the reduction of $PbCl_2$. In the latter case, the reductive removal of the film is almost complete at the cathodic current maximum.

In contrast to the behaviour of the Pb, $PbCl_2$ system, the charge passed in the anodic and cathodic cycles increases substantially with applied pressure. The change of the anodic and cathodic charges, Q_A^P/Q_A^1

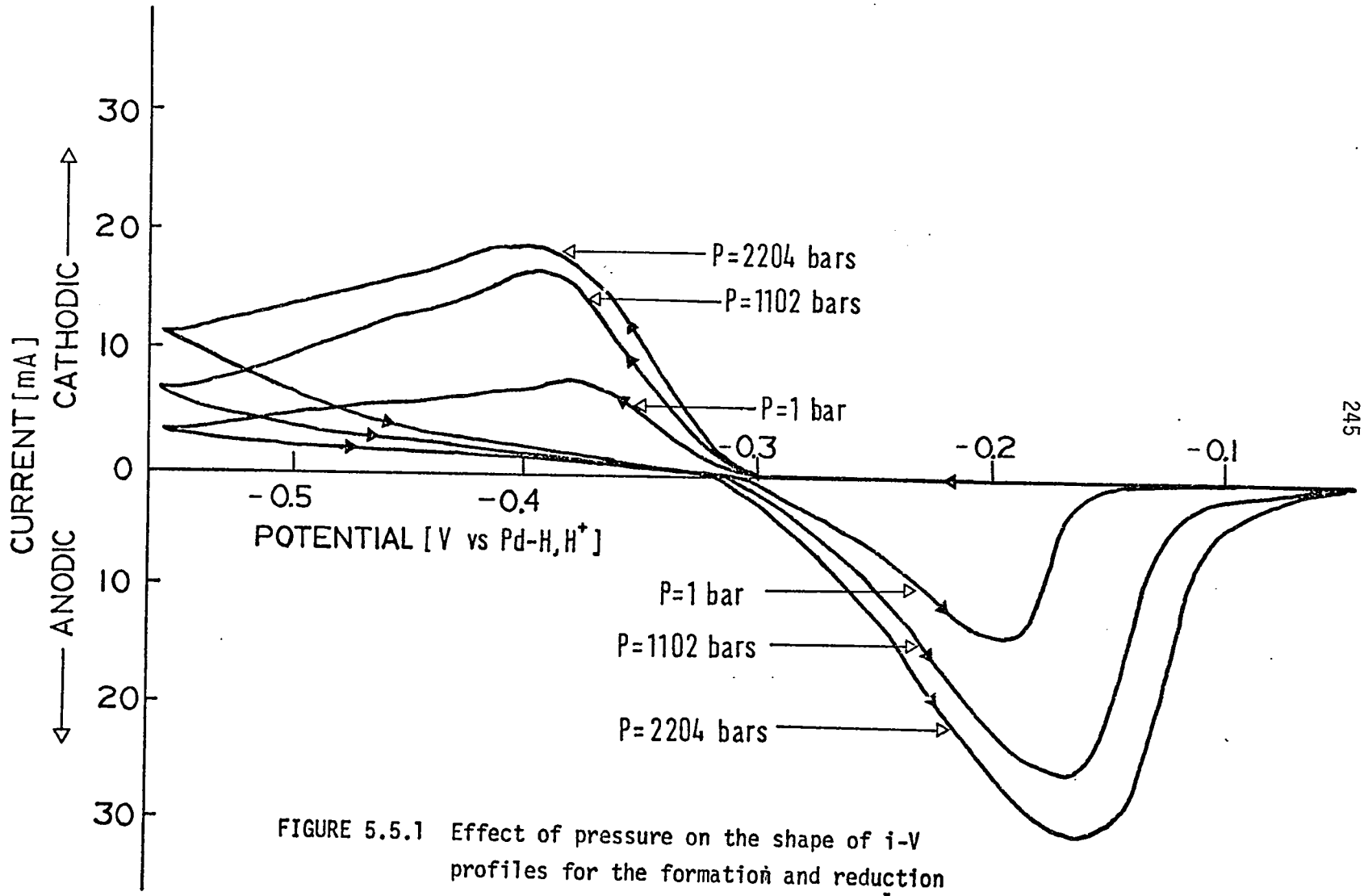

FIGURE 5.5.1 Effect of pressure on the shape of i-V profiles for the formation and reduction of $PbSO_4$ in 0.5 M H_2SO_4 s= 10 mV s^{-1}.

and Q_C^P/Q_C^1, i.e. relative to the values at P = 1 bar, are 2.8 and 2.6, respectively, at 2204 bars (see Table 5.5.1).

The effect of cathodic sweep rate on the charge-balance ratio, Q_A/Q_C, is presented in Table 5.5.2 as derived from the i-V profiles (in Figure 5.5.2) at 1, 1102 and 2204 bars. The change of Q_A/Q_C with cathodic sweep rate, s_c, is independent of applied pressure indicating that very little chemical dissolution of the film occurs.

Although pressure increases the charge required for passivation, the process responsible for removal of the $PbSO_4$ film is still quite slow, even at 2204 bars. This behaviour is to be contrasted with the effect of temperature on the reduction of $PbSO_4$ as illustrated in Figure 5.5.3. In 0.5 M H_2SO_4 at 78°C, the reduction of the surface film is virtually complete at potentials 75 mV more negative than the cathodic current maximum.

5.5.2 Comments on the Effect of Pressure on the Pb, $PbSO_4$ Electrode

The electrochemical behaviour of the Pb, $PbSO_4$ electrode as a function of applied pressure is markedly different from that of the Pb,$PbCl_2$ electrode. The large pressure-induced increase in anodic and cathodic charges is difficult to rationalize for this system since several pressure-dependent solution equilibria are likely to be involved. For example, the dissociation constant of HSO_4^- ion is known[41] to increase by a factor of 4.2 as the pressure is increased from 1 to 2204 bars. Also, equilibria involving sulphato-lead complex ions such as $Pb(HSO_4)^+$, $PbSO_4$ and $Pb(SO_4)^{2-}$ are expected to be pressure dependent.

The rate of anodic dissolution of lead by reaction 5.5.1 is expected to depend on pressure as in the case of reactions in the Pb,$PbCl_2$

TABLE 5.5.1

ANODIC AND CATHODIC CHARGE DATA FOR THE Pb, $PbSO_4$ ELECTRODE ($A \simeq 1\ cm^2$) IN 0.5 M H_2SO_4 AT VARIOUS PRESSURES

P (bars)	S($mV\ s^{-1}$)	Q_A^P (mC)	Q_C^P	Q_A/Q_C	Q_A^P/Q_A^1	Q_C^P/Q_C^1
1	10	131	137	1.0	1.0	1.0
1102	10	258	278	0.9	2.0	2.0
2204	10	371	350	1.1	2.8	2.6
1*	10	197	206	1.0	-	-

* Results obtained at P = 1 bar at the termination of the high pressure experiment.

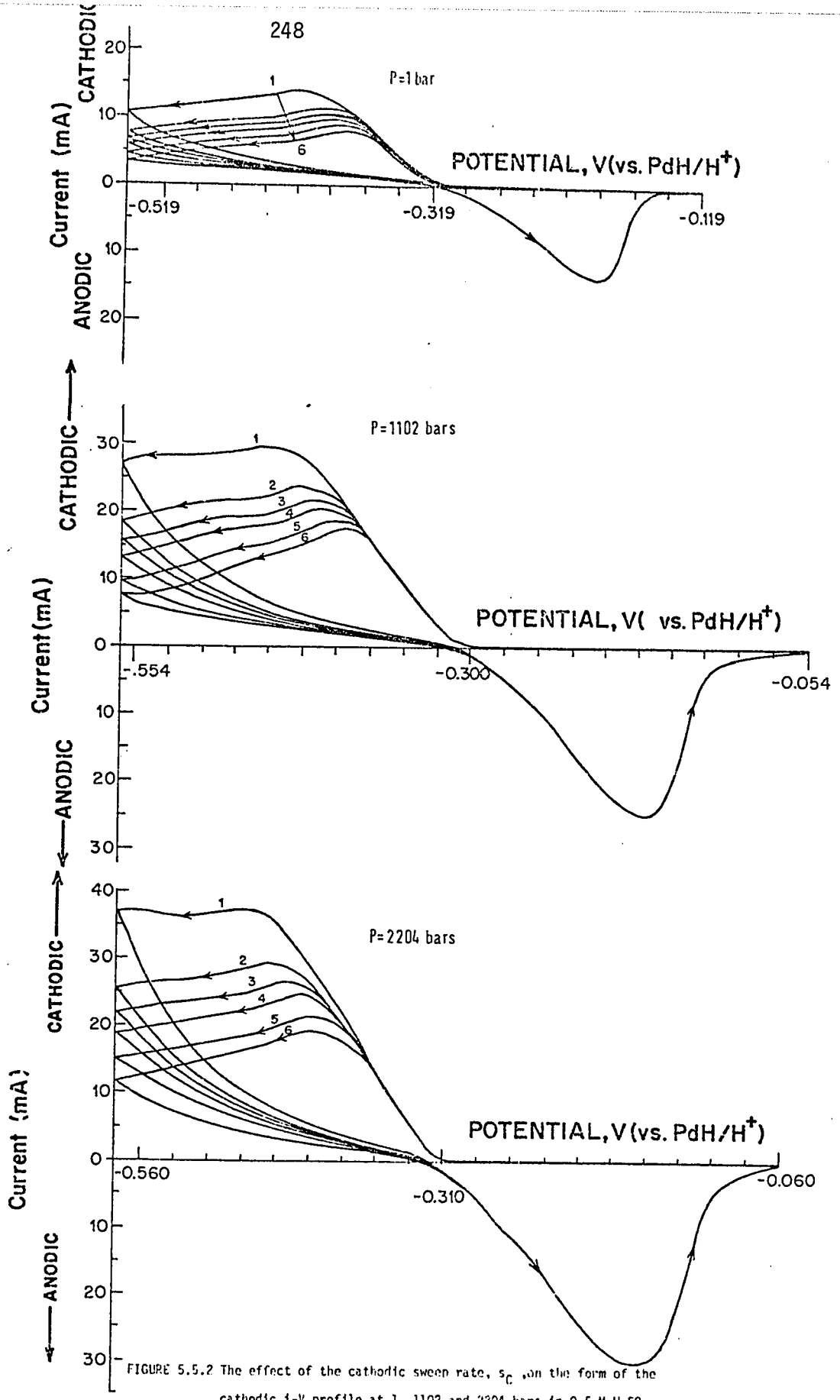

FIGURE 5.5.2 The effect of the cathodic sweep rate, s_C, on the form of the cathodic i-V profile at 1, 1102 and 2204 bars in 0.5 M H_2SO_4. At 1 bar, the cathodic sweep rate, s_C, is varied in successive cycles from 8 to 41 mV s^{-1}. At 1102 and 2204 bars, the values of s_C are varied from 10 to 50 mV s^{-1}. The corresponding i-V profiles are labelled 6 through 1.

TABLE 5.5.2

ANODIC AND CATHODIC CHARGE DATA FOR THE $Pb,PbSO_4$ ELECTRODE IN 0.5 M H_2SO_4 AS A FUNCTION OF PRESSURE AND CATHODIC SWEEP RATE

P (Bars)	$s_A(mV.s^{-1})$	s_C	$Q_A(mC)$	Q_C	Q_A/Q_C
1	8	8	131	137	1.0
	8	10	131	126	1.0
	8	14	131	112	1.2
	8	16	131	101	1.3
	8	21	131	89	1.5
	8	41	131	56	2.4
1102	10	10	258	278	0.9
	10	12	258	258	1.0
	10	17	258	222	1.2
	10	20	258	201	1.3
	10	25	258	178	1.5
	10	50	258	109	2.4
2204	10	10	371	350	1.1
	10	12	371	313	1.2
	10	17	371	275	1.4
	10	20	371	243	1.5
	10	25	371	221	1.7
	10	50	371	135	2.7
1 *	10	10	197	206	1.0
	10	12	197	198	1.0
	10	17	197	172	1.2
	10	20	197	152	1.3
	10	25	197	126	1.6
	10	50	197	80	2.5

* Results obtained at P = 1 bar at the termination of the high pressure experiment.

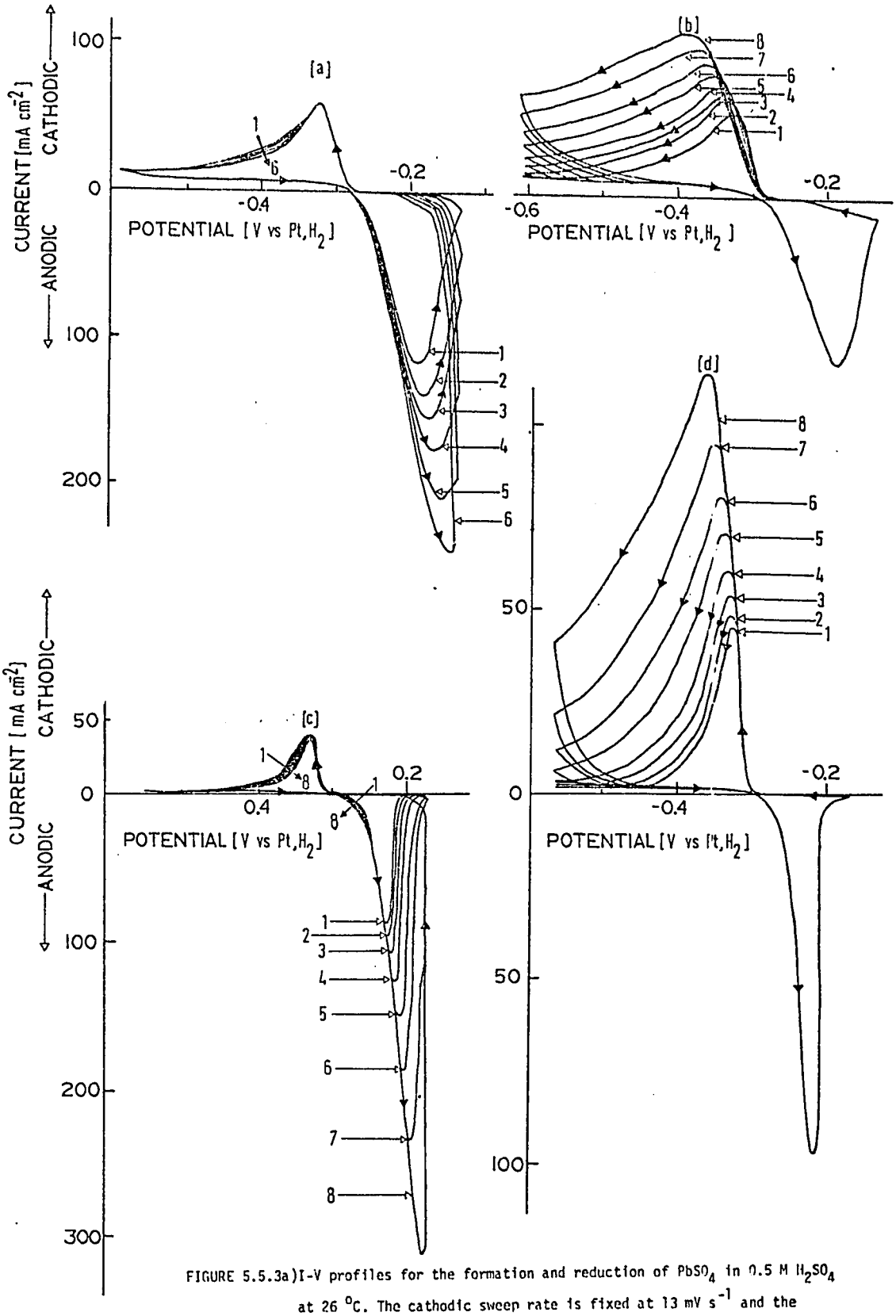

FIGURE 5.5.3a)I-V profiles for the formation and reduction of $PbSO_4$ in 0.5 M H_2SO_4 at 26 °C. The cathodic sweep rate is fixed at 13 mV s^{-1} and the anodic sweep rate is varied in successive cycles from 13 to 153 mV s^{-1}. The i-V profiles labelled from 1 to 8 refer to increasing sweep rate.

b) Same as in a) but s_c is varied from 13 to 153 mV s^{-1}.

c) Same as in a) but at 78 °C.

d) Same as in b) but at 78 °C.

system. The solubility reaction for $PbSO_4$ is written as

$$PbSO_4 \underset{}{\overset{K_{sp}}{\rightleftharpoons}} Pb^{2+} + SO_4^{2-} \qquad (5.5.1)$$

with a corresponding volume change of -47.8 $cm^3\ mol^{-1}$. Therefore, the solubility of $PbSO_4$ at 2200 bars would tend to be approximately 71 times greater than the value at 1 bar. However, the HSO_4^- dissociation process is also pressure-dependent. At 2200 bars, the concentration of SO_4^{2-}, in 0.5 M H_2SO_4 is expected to be 1.16 times as large as the value at ambient pressure.

If the formation of lead sulphate complexes were assumed to be negligible, then the net effect increase of pressure to 2200 bars would be to increase the solubility of $PbSO_4$ relative to that at 1 bar by a factor of 61. The solubility[149] of $PbSO_4$ in 0.5 M H_2SO_4 at P = 1 bar is known to be 7×10^{-6} mol dm^{-3} which corresponds to a charge of 0.14 mC required to saturate 0.10 cm^3 of solution adjacent to the electrode surface (electrode of area 1 cm^2 and a diffusion-layer thickness of 0.10 cm). At 2200 bars, the necessary charge for saturation is expected to be 61 x 0.14 or 8.5 mC, owing to the increased solubility of $PbSO_4$ at elevated pressures. However, this calculated increase of charge is not large enough to explain completely the observed pressure effects (see Table 5.5.1).

Van't Riet and Kolthoff[150] have observed supersaturated solutions of $PbSO_4$ at P = 1 bar in which the activity product of Pb^{2+} and SO_4^{2-} ions is approximately 260 times as large as that for the saturated solution. If this situation were to apply to the formation of $PbSO_4$, then the charge required to effect $PbSO_4$ crystal growth would be correspondingly large. The charges previously calculated are expected to be $(260)^{1/2}$ times larger when the solution is supersaturated to the extent proposed by Van't Riet and Kolthoff. The charges required for supersaturation are 2.3

and 137 mC at 1 and 2200 bars, respectively. The difference of these charges, ΔQ, of 135 mC is of the correct order of magnitude in relation to the experimentally observed increase in Q_A as the pressure is raised from 1 to 2200 bars (see Table 5.5.1).

Evaluation of the role of complex ions in the formation of $Pb/PbSO_4$ in H_2SO_4 is a formidable exercise, even at ambient pressure. The determination of the formation constants of complex ions of a sparingly soluble salt is often a difficult experimental problem as indicated by the variabilty of reported values for some of the formation constants. In the case of the association constant for $PbSO_4$(aq.), the values range from 5.5^{151} $dm^3\ mol^{-1}$ (ref.151) to 8.5×10^3 $dm^3\ mol^{-1}$ (ref.152), depending on the analytical method and the ionic strength.

However, in order to make some progress, it is useful to explore the consequences of assuming that the only relevant complex ion is the ion pair $Pb(SO_4)$. The effect of pressure on the extent of complex ion dissociation by the reaction

$$Pb(SO_4)_{\text{ion pair}} \rightleftharpoons Pb^{2+} + SO_4^{2-} \qquad (5.5.2)$$

is determined, as usual, by the equilibrium volume change in the reaction. However, the partial molar volume of the $Pb(SO_4)$ complex ion is unknown, but the volume change associated with reaction 5.5.2 can be estimated from the data of Fisher and Davis[46] for the reaction

$$Mn(SO_4) \rightleftharpoons Mn^{2+} + SO_4^{2-} \qquad (5.5.3)$$

The volume change for reaction 5.6.3 is -7.4 $cm^3\ mol^{-1}$. Therefore elevated pressure is expected to shift the equilibrium of reaction of 5.5.2 to the right. However, the contribution of reaction 5.5.2 to the overall pressure dependence of the solubility of $PbSO_4$ is expected to be

relatively insignificant compared with the effects previously discussed, e.g. the solubility product, and HSO_4^- ion dissociation.

Nevertheless the net effect of increasing hydrostatic pressure is to increase the solubility of $PbSO_4$. Hence, in order to passivate the lead electrode with $PbSO_4$ at elevated pressure, additional charge must be passed to supersaturate the solution adjacent to the electrode surface.

This is observed, as indicated from Figure 5.5.1, where the area under the anodic peak (i.e. the Q_A) becomes substantially larger as the pressure is increased. If the solubility of $PbSO_4$ were to be appreciably enhanced at elevated pressures, then the cathodic charge, Q_C, would be expected to be more dependent on sweep rate at elevated than at ambient pressure. Although Q_C is markedly dependent on the cathodic sweep-rate, s_C (Table 5.5.2), this dependence appears to be similar at all pressures. It may be that the solution is no longer supersaturated after the electrode is passivated, so that the concentration of solution-soluble lead species has then become greatly reduced.

APPENDIX

Tabulation of Conductivity Data for Aqueous Solutions of Lead Chloride Species

TABLE A.1.1

CONDUCTIVITY CELL CONSTANTS*

AS A FUNCTION OF PRESSURE AT 298.0K

P (bars)	CELL "B" k_B (cm^{-1})	CELL "R" k_R (cm^{-1})
1	0.6550	0.6417
550	0.6507	0.6368
827	0.6497	——
1102	0.6509	0.6379
1650	0.6588	0.6441
2204	data of Horne uncertain	
1	0.6550	0.6396
	$\bar{k}_B$= 0.6530±0.0038 cm^{-1}	$\bar{k}_R$=0.6400±0.0029 cm^{-1}

* Calculated from the data of Horne [43] for the conductivity of 0.01 m KCl as a function of pressure.

TABLE A.1.2

CONDUCTIVITY DATA FOR 0.10m KCl AT ELEVATED PRESSURES AT 298.0 K

P(bars)	$\kappa \times 10^3(\Omega^{-1}\ cm^{-1})$	κ_p/κ_1	$\kappa \times 10^3$	κ_p/κ_1
1	12.59	1.000	12.60	1.000
550	13.04	1.036	13.06	1.037
1102	13.30	1.061	13.36	1.060
1650	13.51	1.073	13.55	1.075
2204	13.58	1.079	13.62	1.081
	CELL B		CELL R	

TABLE A.1.3

CONDUCTIVITY DATA FOR 0.01m KCl AT ELEVATED PRESSURES AT 298.0 K

P(bars)	$\kappa \times 10^3(\Omega^{-1}\ cm^{-1})$	κ_p/κ_1	$\kappa \times 10^3$	κ_p/κ_1
1	1.394	1.000	1.392	1.000
550	1.447	1.038	1.448	1.040
1102	1.480	1.062	1.481	1.064
1650	1.499	1.075	1.500	1.078
2204	1.506	1.080	1.508	1.083
	CELL B		CELL R	

TABLE A,1,4

CONDUCTIVITY DATA FOR $PbCl_2$ SOLUTIONS

$C(PbCl_2)$	P(bars)	$\kappa \times 10^4 (\Omega^{-1}\ cm^{-1})$	κ_P/κ_1	Λ_m	Λ_P/Λ_1
0.001 M	1	2.705	1.000	135.25	1.000
	550	2.821	1.043	138.28	1.022
	1102	2.890	1.068	138.27	1.022
	1650	2.930	1.083	138.21	1.022
	2204	2.946	1.089	136.39	1.008
	1102	2.898	1.071	138.60	1.025
	1	2.711	1.000	135.56	1.000
0.0025	1	6.361	1.000	127.22	1.000
	550	6.677	1.050	130.41	1.025
	1102	6.875	1.081	131.70	1.035
	1650	6.996	1.100	131.50	1.034
	2204	7.048	1.108	130.04	1.022
	1	6.363	1.000	127.22	1.000
0.005	1	11.89	1.000	118.90	1.000
	550	12.57	1.057	122.75	1.032
	1102	12.99	1.092	124.43	1.047
	1650	13.25	1.114	124.53	1.047
	2204	13.39	1.126	123.75	1.041
	1102	13.06	1.090	125.10	1.052
	1	11.94	1.000	119.40	1.000
0.01	1	21.20	1.000	106.00	1.000
	550	22.43	1.058	109.63	1.034
	1102	23.31	1.100	111.53	1.052
	1650	23.86	1.126	112.12	1.058
	2204	24.15	1.139	111.60	1.053
	1102	23.37	1.102	111.82	1.055
	1	21.01	1.000	106.44	1.000
0.015	1	30.02	1.000	100.07	1.000
	550	31.99	1.066	103.86	1.038
	1102	33.32	1.110	106.12	1.061
	1650	34.23	1.140	106.97	1.069
	2204	34.71	1.156	107.13	1.071
	1102	33.39	1.112	106.34	1.063
	1	30.00	1.000	99.98	1.000
0.0388	1	61.56	1.000	79.33	1.000
	550	66.73	1.084	84.04	1.059
	1102	70.09	1.139	86.53	1.091
	1650	72.47	1.177	87.74	1.106
	2204	74.08	1.203	88.19	1.112
	1	61.16	1.000	78.81	1.000
Saturated solution of $PbCl_2$	1	63.53	1.000	81.87	1.000
	550	69.05	1.087	75.05	0.917
	1102	73.78	1.161	57.64	0.704
	1650	77.23	1.216	52.18	0.637
	2204	82.06	1.292	36.31	0.444
	1	63.41	-	-	-

TABLE A.1.5

PRESSURE DEPENDENCE OF CONSTANTS IN THE CONDUCTANCE EQUATION (5.2.1)

AT 298.0 K

P(bars)	ε	$(\varepsilon T)^{1/2}$	$(\varepsilon T)^{3/2} \times 10^{-6}$	η (Poise)	$-A\lvert z_+z_-\rvert$	
					$\lvert z_+\rvert=2, \lvert z_-\rvert=1$	$\lvert z_+\rvert=\lvert z_-\rvert=1$
1	78.54	152.99	3.581	0.00894	-1.018	-0.509
550	81.05	155.41	3.754	0.00902	-0.972	-0.486
1102	83.35	157.60	3.914	0.00917	-0.932	-0.466
1650	84.45	159.58	4.064	0.00940	-0.898	-0.449
2204	87.30	161.29	4.196	0.00974	-0.868	-0.434

TABLE A.1.6

CONDUCTIVITY PARAMETERS FOR THE UNI-UNIVALENT SALT $(PbCl^+)\ Cl^-$

AT 298.0 K

P(bars)	q	R	E	$a(\text{Å})^*$	B	$\Lambda^\infty_{1\text{-}1}$
1	0.500	0.2291	60.34	3.57	0.3287	122.16
550	0.500	0.2185	58.85	3.46	0.3236	125.33
1102	0.500	0.2096	57.09	3.37	0.3191	126.43
1650	0.500	0.2019	55.00	3.28	0.3152	126.07
2204	0.500	0.1955	52.52	3.21	0.3118	124.80

* Based on the Bjerrum distance of closest approach $\frac{\lvert z_+z_-\rvert e^2}{2\varepsilon kT}$

TABLE A.1.7

CONDUCTIVITY PARAMETERS FOR THE BI-UNIVALENT SALT $Pb^{++}2Cl^-$ AT 298.0 K

P(bars)	q	R	E	$a(\mathring{A})$ *	B	Λ^{∞}_{1-2}
1	0.4376	0.4119	90.05	7.14	0.3287	145.85
550	0.4357	0.4060	88.28	6.92	0.3236	147.73
1102	0.4341	0.3752	85.63	6.73	0.3191	147.47
1650	0.4327	0.3599	82.50	6.56	0.3152	145.72
2204	0.4311	0.3465	78.77	6.42	0.3118	142.78

* Based on the Bjerrum distance of closest approach $\frac{|z_+z_-|e^2}{2\varepsilon kT}$

TABLE A.1.8

LIMITING EQUIVALENT CONDUCTIVITIES OF SPECIES IN $PbCl_2$ SOLUTIONS AT 298.0 K

P(bars)	$\Lambda^{\infty}_{Cl^-}$	$\Lambda^{\infty}_{PbCl^+}$	$\Lambda^{\infty}_{Pb^{2+}}$	$\Lambda^{\infty}_{(PbCl^+)(Cl^-)}$	$\Lambda^{\infty}_{PbCl_2}$
1	76.35	45.81	69.50	122.16	145.85
550	78.33	47.00	69.40	125.33	147.73
1102	79.02	47.41	68.45	126.43	147.47
1650	78.80	47.27	66.93	126.07	145.72
2204	78.00	46.80	64.78	124.08	142.78

CLAIMS TO ORIGINAL RESEARCH

1) The influence of pressure on the EMF of three reversible electrode reactions is examined. The pressure coefficients of EMF of the electrochemical cells.

$Pt,H_2|0.5\ M\ H_2SO_4|Pd\text{-}H,Pd$

$Pt,H_2|1\ M\ HCl|Pd\text{-}H,Pd$

$Pd,Pd\text{-}H|AgCl,\ Ag$

are evaluated and related to volume changes for the respective overall cell reactions. The molar volume of Pd-H is estimated and the volume of H in Pd derived. It is shown that these electrodes are satisfactory for use as reference electrodes over a wide range of hydrostatic pressures.

2) The significance of effects of pressure on the rates of multistep electrochemical reactions, eg. cathodic H_2 evolution, is examined in detail for various conditions. In addition to the effect of the pressure-dependence of the reversible electrode potential, it is shown that the effect of the pressure dependence of surface coverage of intermediates must be taken into account and is an important factor required for the evaluation of the true volume of activation. The experimentally observed apparent volumes of activation (of Hills and co-workers, and of Heusler and Gaiser) are converted to the respective true volumes of activation for different conditions of surface coverage and reaction mechanism. The occurence of negative volumes of activation is discussed in terms of the hydrated proton in the state $H_9O_4^+$ becoming localized in the transition state on one of H_2O molecules, thus increasing

the electrostriction at H^+ temporarily in the act of discharge.

3) The nature of the activation process in a single electron transfer reaction is examined by the evaluation of the true volume of the activation for the redox reaction

$$Fe(CN)_6^{3-} + e \longrightarrow Fe(CN)_6^{4-}$$ at a Au electrode.

The experimentally observed apparent volume of activation is corrected for the pressure-dependence of the reference electrode potential. The relatively large true volume of activation is discussed in terms of the contributions of the respective volume changes due to electrostriction in the primary hydration shell and in the bulk of solution. Comparison of the measured true volume of activation and the calculated volume changes in the primary hydration shell and in the bulk of solution indicate that the activation process for electron transfer in the redox couple $Fe(CN)_6^{3-}$/ $Fe(CN)_6^{4-}$ is due mainly to solvent reorganization near the ions and not further into the bulk of the solution.

4) The effect of pressure on the reversible potential for deposition of species H and OH on noble metals provides useful information on the nature of these adsorbed species. The pressure coefficients of EMF for such processes are measured and related to the associated reaction volume change. The volume of H adsorbed on Pt is derived and the relatively large volume is discussed in terms of a covalently bonded H atom. The pressure - dependent potential for onset of Pt and Au surface oxidation is related to the volume of electrodeposited Pt-OH and Au-OH and the volume

change due to anion desorption.

5) The formation of $PbCl_2$ at a Pb electrode in Cl^- ion solutions is believed to occur in part by a dissolution - precipitation type mechanism and in principle should be markedly affected by application of elevated pressure. However, in reality, the observed behaviour is not as predicted. The small decrease of charge required to passivate the electrode surface as the pressure is elevated is discussed in terms of solution - soluble complex ions of the type $PbCl_n^{2-n}$. The partial molar volumes of these species are large enough to effect a decrease in the solubility of $PbCl_2$ at elevated pressures.

6) The charge required to effect precipitation of $PbCl_2$ is related in part to the solubility product of $PbCl_2$. The solubility of $PbCl_2$ in pyro-distilled H_2O is evaluated by conductivity measurements at pressures up to 2204 bars. The solubility product is evaluated at each pressure in terms of the existence of the ion-pair, $PbCl^+$. The pressure-dependence of the molal dissociation constant of $PbCl^+$ is determined and the partial molar volume of $PbCl^+$ estimated.

7) The pressure-dependent behaviour of the $Pb,PbSO_4$ electrode in 0.5M H_2SO_4 is determined and compared with that of $Pb,PbCl_2$. It is found that there is a large increase of the observed anodic and cathodic charges as the pressure is elevated. This is discussed in terms of the ability of $PbSO_4$ to form highly supersaturated solutions and the large increase in the solubility of $PbSO_4$ at elevated pressures.

REFERENCES

1. P. W. Bridgman, The Physics of High Pressure, Bell, London (1931).
2. Discussion of the Faraday Society, 22 (1956).
3. S. D. Hamann, Physico - chemical Effects of Pressure, Butterworths, London (1957).
4. K. J. Laidler, "Chemical Kinetics", McGraw - Hill (1965)
5. M. G. Evans and M. Polanyi, Trans. Faraday Soc., 31, 875 (1935).
6. M. W. Perrin, Trans. Faraday Soc., 34, 144 (1938).
7. K. J. Laidler and D. T. Y. Chen, ibid., 54, 1026 (1958)
8. K. J. Laidler and R. Martin, International Journal of Chemical Kinetics, Vol. 1, 113 (1969).
9. B. T. Baliga and E. Whalley, J. Phys., Chem., 73, 654 (1969).
10. G. J. Hills and R. Payne, Trans. Faraday Soc., 61, 316 (1965).
11. G. J. Hills and R. Payne, Ibid, 61, 326 (1965).
12. G. J. Hills and P. J. Ovenden, in Advances in Electrochemistry and Electrochemical Engineering, Vol. 4, Eds. P. Delahay and C. W. Tobias, Interscience, New York (1966).
13. G. J. Hills and D. R. Kinnibrugh, J. Electrochem. Soc., 113, 1111 (1966).
14. G. J. Hills in Advances in High Pressure Research, Vol. 2, Ed. R. S. Bradley, Academic Press, London - New York (1969).
15. K. E. Heusler and L. Gaiser, Ber Bunsenges, 72, 1059 (1969).

16. E. M. L. Valeriote and L. D. Gallup, J. Electrochem., Soc., 121, 1245 (1974).

17. B. E. Conway and J. C. Currie, in course of publication.

18. S. Barnartt, Electrochimica Acta, 13, 901 (1968).

19. G. J. Hills, B. E. Conway, L. I. Kristalik and R. Parsons (discussions on ref. 13) J. Electrochem., Soc., 113, 1117 (1966).

20. R. A. Marcus, Ann. Rev. Phys. Chem., 15, 155 (1964); J. Chem. Phys., 24, 966 (1956).

21. N. Hush, J. Chem. Phys., 28, 962 (1958).

22. V. G. Levich, Chapter 12 in Vol. IX B, Physical Chemistry, an Advanced Treatise, Eds. H. Eyring et al., Academic Press, N.Y. (1970).

23. E. Sacher and K. J. Laidler in Modern Aspects of Electrochemistry, Vol. 3, Ed. J. O'M. Bockris and B. E. Conway, Butterworths, London (1964).

24. G. Archdale and J. A. Harrison, J. Electroanal. Chem., 34, 21 (1972).

25. G. Archdale and J. A. Harrison, J. Electroanal. Chem., 39, 357 (1972).

26. G. Archdale and J. A. Harrison, J. Electroanal. Chem., 43, 321 (1973).

27. G. Archdale and J. A. Harrison, J. Electroanal. Chem., 47, 93 (1973).

28. J. Ambrose, R. G. Barradas, K. Belinko and D. W. Shoesmith, J. Colloid Interface Sci., 47, 441 (1974).

29. R. G. Barradas, K. Belinko and J. Ambrose, Can. J. Chem., 53, 389 (1975).

30. R. G. Barradas, K. Belinko and E. Ghibaudi, Can. J. Chem., 53, 407 (1975).

31. R. G. Barradas, K. Belinko and W. Shoesmith, Electrochim. Acta, 21, 357 (1976).

32. M. J. Temkin, Zh. Fiz. Khim., 22, 1081 (1948).

33. B. E. Conway and D. J. MacKinnon, J. Electrochem. Soc., 116, 1665 (1969).

34. B. E. Conway, Theory and Principles of Electrode Processes. Ronald Press, New York (1965).

35. M. Fleischmann, W. B. Gara and G. J. Hills, J. Electroanal. Chem., 60, 313 (1975).

36. R. Zana and E. Yeager, J. Phys. Chem., 70, 954 (1966).

37. R. Zana and E. Yeager, J. Phys. Chem., 71, 521 (1967).

38. R. Zana and E. Yeager, J. Phys. Chem., 71, 4241 (1967).

39. B. E. Conway, pp. 577-578, in Chemical Physics of Ionic Solutions, Eds. B. E. Conway and R. G. Barradas, John Wiley and Sons, New York (1966).

40. W. J. le Noble, Prog. Phys. Org. Chem., 5, 207 (1967).

41. S. D. Hamann, in Modern Aspects of Electrochemistry, Vol. 9, Eds. J. O'M. Bockris and B. E. Conway, Butterworths, London (1974).

42 S. D. Hamann, P. J. Pearce and W. Strauss, J. Phys. Chem., 68, 375 (1964).

43. R. A. Horne, in Adv. High Pressure Research Vol. 2, Ed. R. S. Bradley, Academic Press, London (1969).

44. F. H. Fisher, J. Phys. Chem., 66, 1607 (1962).

45. F. H. Fisher and A. P. Fox, J. Solution Chem., 4, 225 (1975).

46. F. H. Fisher and D. F. Davis, J. Phys. Chem., 69, 2595 (1965).

47. F. H. Fisher and D. F. Davis, J. Phys. Chem., 71, 819 (1967).

48. W. R. Hainsworth, H. J. Rowley and D. A. MacInnes, J. Am. Chem., Soc., 46, 1437 (1924).

49. A. Disteche, Rev. Sci. Instr. 30, 474 (1959).

50. A. Disteche, J. Electrochem. Soc., 109, 1084 (1962).

51. J. O'M. Bockris and A. K. N. Reddy, Modern Electrochemistry Vol. 2, Plenum Press, New York (1970).

52. a) S. Hsieh, Ph. D. Thesis, University of Southampton (1969).
b) G. J. Hills and S. Hsieh, Chem. Ing. Tech., 44, 216 (1972).

53. E. W. Tiepel and K. E. Gubbins, J. Phys. Chem., 76, 3044 (1972).

54. D. A. Vermilyea in Advances in Electrochemistry and Electrochemical Engineering, Vol. 3, Eds. P. Delahay and C.W. Tobias, John Wiley and Sons (1963).

55. J. R. Coleman, J. Appl. Electrochem. 1, 65 (1971).

56. C. W. D. Briggs and W. F. K. Wynne - Jones, J. Chem. Soc., 2966 (1956.

57. P. Jones and R. Lind and W. F. K. Wynne-Jones. Trans. Faraday Soc., 50, 972 (1954).

58. M. Fleischmann and H. R. Thirsk, Trans. Faraday Soc., 51, 71 (1955)

59. D. Pavlov, Electrochim. Acta, 13, 2051 (1968).

60. D. Pavlov, V. Iliev, G. Papazoy, and E. Bashtavelova, J. Electrochem. Soc., 121, 854 (1974).

61. J. Burbank, J. Electrochem. Soc., 118, 525 (1971).

62. T. Chiku and K. Nakajima, J. Electrochem. Soc., 118, 1395 (1971).

63. D. Pavlov, G. Papazov and V. Iliev, J. Electrochem. Soc., 119, 8 (1972).

64. R. Ruetschi, J. Electrochem. Soc., 120, 331 (1973).

65. J. Weininger, J. Electrochem. Soc., 121, 1454 (1974).

66. S. B. Brummer and A. B. Gancy in Water and Aqueous Solutions, Ed. R. A. Horne, Wiley - Interscience, New York (1972).

67. See references, 3, 40 and 41 for references to early high pressure research.

68. H. S. Harned and B. B. Owen, Physical Chemistry of Electrolyte Solutions, 3rd ed., Reinhold, New York (1957).

69. R. A. Robinson and R. H. Stokes, Electrolyte Solutions, 2nd Ed. Butterworths, London (1959).

70. J. Buchanan and S. D. Hamann, Trans. Faraday Soc., 49, 1425 (1953).

71. A. B. Gancy and S. B. Brummer, J. Phys. Chem. 73, 2429 (1969).

72. C. W. Davies, Ion Association, Butterworths, Washington (1962).

73. E. C. Righellato and C. W. Davies, Trans. Faraday Soc., 26, 592 (1930).

74. J. C. James, J. Am. Chem. Soc., 71, 3283 (1949).

75. G. H. Nancollas, J. Chem. Soc., 1458 (1955).

76. R. M. Garrels and F. T. Gucker, Chem. Rev., 44, 117 (1949).

77. H. Fromherz and K. H. Lih, Z. Physik. Chem., 153A, 321 (1931).

78. W. G. Davies, R. J. Otter and J. E. Prue, Disc. Faraday Soc., 24, 103 (1957).

79. W. A. Adams, Ph. D. Thesis, University of Ottawa (1967).

80. B. E. Conway, H. Angerstein-Kozlowska, W. B. A. Sharp and E. E. Criddle, Anal. Chem., 45, 1331 (1973).

81. M. Breiter, J. Electrochem. Soc., 112, 845 (1965).

82. M. Breiter in Proc. Symposium on Electrode Processes, Ed. E. Yeager, the Electrochemical Society (1958), Wiley, New York (1960).

83. B. V. Tilak, R. S. Perkins, H. A. Kozlowska and B. E. Conway, Electrochem. Acta., 17, 144 (1972).

84. S. Schuldiner, J. P. Hoare and G. W. Castellan, J. Chem. Physics, 28, 16, 20, 22 (1958).

85. T. B. Flanagan and F. A. Lewis, Trans. Faraday Soc., 55, 1409 (1959).

86. P. C. Aben and W. G. Burgers, Trans. Faraday Soc., 58, 1989 (1962).

87. W. Beck, J. O'M. Bockris, J. McBreen and L. Nanis, Proc. Roy. Soc., 290: 220 (1966).

88. H. A. Wriedt and R. A. Oriani, Acta Metallurgica, 18, 753 (1970).

89. H. S. Frank and M. W. Evans, J. Chem. Phys., 13, 507 (1945).

90. E. g. see R. Parsons, Trans. Faraday Soc., 47, 1332 (1951).

91. G. J. Hills, Disc. Faraday Soc., 39, 207 (1965).

92. B. E. Conway and J. C. Currie, in course of publication.

93. A. Bewick, B. E. Conway and A. Tuxford, J. Electroanal. Chem., 42, App. 11-15 (1973).

94. E. Wicke, M. Eigen and Th. Ackermann, Zeitt. phys. Chem., N.F., 1, 340 (1956).

95. A. J. Cunningham, J. D. Paysant and P. Kebarle, J. Amer. Chem., Soc., 94, 7627 (1972); See also J. Amer. Chem. Soc., 89, 6393 (1967).

96. See ref. 41, Chapter 2 (Tables 17 and 18).

97. D. H. Angell and T. Dickinson, J. Electroanal. Chem., 35 55 (1974).

98. R. Parsons and E. Passeron, J. Electroanal. Chem., 12, 524 (1966).

99. J. O'M. Bockris, R. J. Mannan and A. Damjanovic, J. Chem. Phys., 48, 1898 (1968).

100. A. J. Appelby, J. O'M. Bockris, R. K. Sen and B. E. Conway, Chapter 1, MTP Int. Rev. of Sci., Series 1, Vol. 6, Ed. J. O'M. Bockris, Butterworths, London (1973).

101. J. O'M. Bockris, R. K. Sen and B. E. Conway, Nature (physical science) 240, 143 (1972).

102. J. E. B. Randles, Disc. Faraday Soc., 1, 11 (1947).

103. J. E. B. Randles and K. W. Somerton, Trans. Faraday Soc., 48, 937 (1952).

104. A. M. Bond, J. Electroanal. Chem., 50, 285 (1974).

105. A. M. Bond, Anal. Chem., 44, 315 (1972).

106. M. Rehbach and J. H. Sluyters, Recueil, 80, 469 (1961).

107. J. O'M. Bockris and B. E. Conway, J. Chem. Phys., 28, 707 (1958).

108. P. Delahay, New Instrumental Methods in Electrochemistry, Interscience, New York (1954).

109. L. G. Hepler, J. M. Stokes and R. H. Stokes, Trans. Faraday Soc., 61, 20 (1965).

110. F. J. Millero, in Water and Aqueous Solutions, Ed. R. A. Horne, Wiley - Interscience, New York (1972).

111. B. E. Conway, R. E. Verrall and J. E. Desnoyers, Trans. Faraday Soc., 62, 2738 (1966).

112. H. C. Brown, J. Phys. Chem., 56, 868 (1952).

113. See ref. 20 at pp. 156 and 159.

114. R. G. Shulman and S. Sugano, J. Chem. Phys., 42, 39 (1965).

115. W. E. Bailey, R. J. Williams and W. O. Milligan, Acta Cryst., B29, 1365 (1973).

116. M. Pierrot, R. Kern and R. Weiss, Acta Cryst., 20, 425 (1966).

117. J. G. Mathieson, Ph. D. thesis, 1972, University of Newcastle, N.S.W., Australia; in course of publication with R. Curthoys.

118. G. S. Hartley and G. W. Donaldson, Trans. Faraday Soc., 33, 457 (1937).

119. G. Jones and F. C. Jelen, J. Amer. Chem. Soc., 59, 1760 (1937).

120. C. W. Davies, J. Amer. Chem. Soc., 58, 2581 (1936).

121. Th. Ackermann, Disc. Faraday Soc., 24, 180 (1957).

122. J. E. Desnoyers, R. E. Verrall and B. E. Conway, J. Chem. Phys., 43, 243 (1965).

123. H. S. Frank, J. Chem. Phys., 23, 2023 (1955).

124. B. E. Conway, J. E. Desnoyers and A. C. Smith, Phil. Trans. Roy. Soc., London A256, 389 (1964).

125. D. C. Grahame, J. Chem. Phys., 21, 1054 (1951).

126. F. Booth, J. Chem. Phys., 19, 391; 1327; 1615 (1951).

127. L. Hepler, J. Phys. Chem., 61, 1426 (1957).

128. B. E. Conway, Elektrokhimiya, (Frumkin memorial issue) in press, 1977.

129. J. Horiuti and T. Toya, Solid State Surface Science, Ed. M. Green, Marcel Dekker, N. Y. (1969).

130. B. E. Conway, H. Angerstein-Kozlowska and F. C. Ho, J. Vac. Sci. Technol., 14, 351 (1977).

131. B. E. Conway, H. Angerstein-Kozlowska, W. B. A. Sharp, B. MacDougall and J. Klinger, Faraday Discussions Chem. Soc., London, 56, 199 (1973).

132. L. G. Hepler, J. Phys. Chem., 69, 965 (1965).

133. H. Angerstein-Kozlowska, B. E. Conway and W. B. A. Sharp, J. Electroanal. Chem., 43, 9 (1973).

134. B. E. Conway and J. C. Currie, in course of publication.

135. W. B. A. Sharp, Ph. D. thesis, University of Ottawa (1976).

136. J. W. Schultze, Electrochim. Acta, 21, 327 (1976).

137. H. Angerstein-Kozlowska and B. E. Conway, in press; see also ref. 130.

138. F. C. Ho, B. E. Conway and H. Angerstein-Kozlowska, in course of publication.

139. H. Remy, Treatise on Inorganic Chemistry, Vol. 1, p. 550, Elsevier Publishing Co. (1956).

140. F. T. Wall and J. Berkowitz, J. Phys. Chem., 62, 87 (1958). see also reference 41, p. 66-67.

141. G. Chandler, J. Amer. Chem. Soc., 30, 694 (1908).

142. W. R. Carmody, J. Amer. Chem. Soc., 51, 2905 (1929).

143. G. P. Haight, Jr. and J. R. Peterson, Inor. Chem., 4, 1073 (1965).

144. F. Vierling, G. Schorsch and J. Bye, Revue, Chim. Min., 3, 875 (1966).

145. Stability Constants, Chem. Soc., London (1964).

146. A. M. Couture and K. J. Laidler, Can. J. Chem., 34, 1209 (1956).

147. A. M. Couture and K. J. Laidler, Can. J. Chem., 35, 207 (1957).

148. H. R. Thirsk and J. A. Harrison, A. Guide to the Study of Electrode Kinetics, Academic Press, London and New York, (1972).

149. H. D. Crockford and D. J. Brawley, J. Amer. Chem. Soc., 56, 2600 (1934)

150. B. van't Riet and I. M. Kolthoff, J. Amer. Chem. Soc., 64, 1045 (1960).

151. A. M. Bond and G. Hefter, J. Electroanal. Chem., 34, 227 (1972).

152. I. M. Korenman, Izvet VUZ Khim., 4, 554 (1961).

153. Results of Kopp quoted by S. Glasstone, Textbook of Physical Chemistry, MacMillan and Co., London (1940)

154. B.E. Conway, E. Gileadi and M. Dzieciech, Electrochimica Acta, 8, 143 (1963).